

# Field Induced Orientation of Semicrystalline and Non-crystalline Block Copolymer Microdomain Patterns

by

Cheolmin Park

M.S., Fiber and Polymer Science  
Seoul National University, 1995

Submitted to the Department of Materials Science and Engineering in  
Partial Fulfillment of the Requirement for the Degree of

Doctor of Philosophy in Polymers

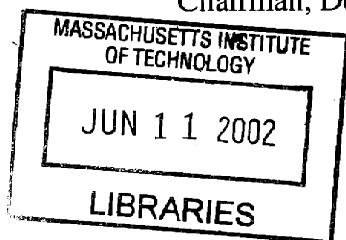
at the  
Massachusetts Institute of Technology  
June 2001

©2001 Massachusetts Institute of Technology  
All right reserved

Signature of Author .....  
Department of Materials Science and Engineering  
April 17, 2001

Certified by.....  
Edwin L. Thomas  
Morris Cohen Professor of Materials Science and Engineering  
Thesis Supervisor

Accepted by.....  
Harry L. Tuller  
Professor of Ceramics and Electronic Materials  
Chairman, Department Committee on Graduate Students



# **Field Induced Orientation of Semicrystalline and Non-crystalline Block Copolymer Microdomain Patterns**

by

Cheolmin Park

Submitted to the Department of Materials Science and Engineering  
on April 17, 2001 in Partial Fulfillment of the Requirement for the  
Degree of Doctor of Philosophy of Materials Science and  
Engineering

## **ABSTRACT**

Various block copolymer microdomain structures are controlled in bulk as well as in thin film by employing flow fields, directional solidification, and substrates. In bulk systems, flow fields generated by the 'roll casting' process orient amorphous cylindrical microdomains along the flow direction in a semicrystalline block copolymer. Subsequent crystallization of the crystalline block is significantly influenced by the pre-existing oriented amorphous cylindrical microdomains. The orientation of crystalline lamellae is achieved parallel to the cylinder axis, completely suppressing spherulite formation.

Microdomain structures of block copolymers are also controlled in thin films by directional solidification of a crystallizable solvent. This new method is based on the use of crystalline organic materials, which are solvents for the block copolymers above their melting temperatures. The directional crystallization of the solvent induces the directional microphase separation of the block copolymer. Furthermore, the flat (001) crystal face of benzoic acid or anthracene provides both a surface for epitaxy of a semicrystalline polyethylene block as well as a confining surface for the thin polymer film which forms between the crystallizing solvent and the glass or silicon wafer substrate.

Several semicrystalline and non-crystalline block copolymers were directionally solidified using a crystallizable solvent. A bi-axially ordered edge-on crystalline lamellar structure is obtained due to the epitaxy between a melt-compatible semicrystalline block copolymer and benzoic acid single crystal. Directional solidification generates vertically aligned lamellar and cylindrical microdomain structures of conventional non-crystalline block copolymers such as PS/PMMA and PS/PI. The combination of epitaxy and directional solidification with a strongly segregated cylinder forming semicrystalline block copolymer produces a perpendicularly aligned cylindrical microstructure with each cylinder containing precisely one crystalline lamella. In addition, the utilization of the degenerate epitaxy between anthracene and the polyethylene block in a semicrystalline block terpolymer alters the classic block copolymer microstructure into a new pattern structure. This new process was also performed on a topographically pre-patterned silicon oxide substrate and produced two types of spatially patterned cylinders (vertical and in-plane), depending on the local film thickness. The selective removal of the diene domains by reactive ion etching points the way towards a host of nano-technological applications such as high density magnetic storage media and photonic crystals.

Thesis Supervisor: Edwin L. Thomas

Title: Morris Cohen Professor of Materials Science and Engineering

## **Table of Contents**

<b>LIST OF TABLES.....</b>	<b>7</b>
<b>LIST OF TABLES.....</b>	<b>17</b>
<b>ACKNOWLEDGEMENTS.....</b>	<b>18</b>
<b>FOREWORD: .....</b>	<b>20</b>
Introduction .....	20
Thesis Structure .....	21
<b>CHAPTER 1: Background and Motivation .....</b>	<b>23</b>
1.1 Nanotechnology .....	23
1.1.1 Nanoscale pattern structure .....	24
1.1.2 Self assembly: natural materials .....	26
1.1.3 Biomimetic materials .....	28
1.1.4 Block copolymers.....	30
1.1.5 Nanotechnologies with block copolymers .....	30
1.1.6 Limitations and opportunities.....	35
1.1.7 Brief outline of the thesis.....	36
1.1.8 References .....	37
1.2 Orientation of Block Copolymer Microdomains .....	41
1.2.1 Mechanical flow fields .....	41
1.2.1.1 Shear flow fields .....	41
1.2.1.2 Compression flow fields .....	43
1.2.1.3 Roll casting: shear and elongational flow fields .....	43
1.2.2 Temperature gradient .....	44
1.2.3 Electric fields .....	44
1.2.4 Homogeneous substrate interactions .....	45
1.2.5 Special block copolymers: architecture, liquid crystallization, crystallization .....	47
1.2.6 Solvent control .....	48
1.2.7 Patterned substrates.....	48
1.2.8 Summary.....	50
1.2.9 References .....	53
1.3 New Approaches .....	60
1.3.1 Eutectic directional solidification .....	60
1.3.1.1 Lamellar eutectics .....	61

1.3.1.2 Polymer diluent eutectics .....	65
1.3.1.3 Block copolymer diluent eutectics .....	68
1.3.1.4 References .....	71
1.3.2 Epitaxy .....	72
1.3.2.1 Epitaxy of polymers .....	72
1.3.2.1.1 Epitaxy on inorganic substrates .....	75
1.3.2.1.2 Epitaxy on organic substrates .....	76
1.3.2.1.3 Epitaxy on polymer substrates .....	78
1.3.2.2 References .....	80
1.3.3 Summary .....	83
1.4 Summary .....	83
<b>CHAPTER 2: Materials and Experimental Methods .....</b>	<b>85</b>
2.1 Materials .....	85
2.1.1 Semicrystalline block copolymers .....	85
2.1.2 Amorphous block copolymers .....	88
2.2 Experimental Methods .....	89
2.2.1 Solution cast films .....	89
2.2.2 Roll cast films .....	89
2.2.3 Transmission electron microscope (TEM) and atomic force microscope (AFM) .....	90
2.2.4 X-ray scattering .....	91
2.2.5 Directional solidification and/or epitaxy .....	92
2.3 References .....	94
<b>PART I</b>	
<b><u>Orientation of Block Copolymer Microdomains in Bulk</u> .....</b>	<b>95</b>
<b>CHAPTER 3: Spherical to Cylindrical Microdomain Transformation by Application of a Flow Field .....</b>	<b>96</b>
3.1 Introduction .....	96
3.2 Results and Discussion .....	99
3.3 Conclusions .....	108
3.4 References .....	109
<b>CHAPTER 4: Influence of an Oriented Glassy Cylindrical Microdomain Structure on the Morphology of Crystallizing Lamellae in a Semicrystalline Block Terpolymer .....</b>	<b>112</b>
4.1 Introduction .....	112
4.2 Results and Discussion .....	115
4.3 Conclusions .....	130
4.4 References .....	131



<b>PART II</b>	
<b><u>Orientation of Block Copolymer Microdomains in Thin Films</u></b> .....	133
<b>CHAPTER 5: Epitaxy: Control of Molecular and Microdomain Orientation in a Semicrystalline Block Copolymer Thin Film by Epitaxy</b> .....	134
5.1 Introduction .....	134
5.2 Results and Discussion .....	137
5.2.1 Bulk samples .....	137
5.2.2 Thin films .....	138
5.3 Conclusions .....	145
5.4 References .....	147
<b>CHAPTER 6: Directional Solidification: Orientation of Block Copolymer Microdomains via Directional Solidification</b> .....	150
6.1 Introduction .....	150
6.2 Results and Discussion .....	153
6.3 Conclusions .....	161
6.4 References .....	162
<b>CHAPTER 7. Directional Solidification and Epitaxy</b> .....	164
7.1 Microdomain Patterns via Directional Eutectic Solidification and Epitaxy .....	164
7.1.1 Introduction .....	164
7.1.2 Results and Discussion .....	165
7.2 Control of Molecular and Micropattern Orientation in Semicrystalline Block Copolymer Thin Films by Directional Solidification and Epitaxy .....	176
7.2.1 Introduction .....	176
7.2.2 Results and Discussion .....	178
7.2.2.1 PS/PEP/PE block terpolymer .....	178
7.2.2.2 PS/PE diblock copolymer .....	185
7.2.2.2.1 Benzoic acid .....	185
7.2.2.2.2 Anthracene .....	188
7.2.3 Conclusions .....	190
7.3 References .....	193
<b>CHAPTER 8: New Micropattern structure: Alteration of Classical Microdomain Patterns by Degenerate Epitaxy</b> .....	195
8.1 Introduction .....	195
8.2 Results and Discussion .....	196
8.3 References .....	206
<b>CHAPTER 9: Conclusions and Future Work</b> .....	207

9.1 Summary: PART I .....	207
9.2 Future Work: PART I .....	208
9.3 Summary: PART II .....	210
9.4 Future Work: PART II .....	212
9.4.1 Orientation of block copolymer microdomains on topographically patterned substrate via directional solidification: Preliminary results .....	213
9.4.2 Directionally solidified microdomain modifications via ozone and oxygen plasma reactive ion etching methods .....	218
9.5 References .....	222
<b>BIOGRAPHICAL NOTE .....</b>	<b>223</b>

## LIST OF FIGURES

<b>Figure 1.1</b> Microstructures of A/B diblock copolymer.....	31
<b>Figure 1.2</b> Bright field TEM micrograph of PS/PI (45/12) block copolymer thin film. The film was cast on a glass substrate and annealed at 120 °C for 2 days. OsO <sub>4</sub> was used to stain the cylindrical PI microdomains which appear dark.....	35
<b>Figure 1.3</b> (a) Hypothetical schematic phase diagram of A/B mixtures. See the text for detailed definitions of parameters (b) Optical micrograph of directionally solidified Pb/Cd crystals. Alloy Pb/Cd forms a eutectic structure with the composition of 17.4 wt% of Pb. (c) Schematic diagram of advancing front of directionally solidified $\alpha/\beta$ eutectic crystals.....	62
<b>Figure 1.4</b> Experimental phase diagrams of (a) PE/1,2,4,5-tetrachlorobenzene, (b) PE/1,3,5-tribromobenzene and (c) paraffin (nC <sub>36</sub> H <sub>74</sub> )/benzoic acid determined by DSC. All diagrams show eutectic points.....	67
<b>Figure 1.5</b> (a) Experimental phase diagram of BA and PS/PE block copolymer mixtures determined by DSC with the cooling rate of 60 °C/min. (b) Experimental phase diagram of BA and PS/PEP/PE block copolymer mixtures determined by DSC with the cooling rate of 30 °C/min.....	70
<b>Figure 1.6</b> Schematic of a polymer epitaxy on a crystalline substrate.....	73
<b>Figure 2.1</b> Schematic diagram of roll casting apparatus. A typical radius of roll is 20 mm and a film with the thickness of 2 mm is obtained after process.....	90
<b>Figure 2.2</b> (a) photograph and (b) polarized optical microscope image of directionally crystallized BA crystals. The large, flat and elongated BA crystals are aligned with the <i>b</i> axis parallel to growth front direction. BA single crystals with various thicknesses lead to different colors under polarized light.....	93
<b>Figure 3.1</b> (a) Bright field TEM micrograph for the simple cast PS/PEP/PE (15/70/15) film. The film was stained with RuO <sub>4</sub> for 20 min so that the PS domains appear dark. Poorly ordered PS spheres are shown. (b) SAXS profiles at 140 °C for the simple cast PS/PEP/PE film .....	101
<b>Figure 3.2</b> (a) 2-dimensional SAXS pattern with the incident beam along the flow direction, normal to the YZ plane. (b) SAXS patterns with different threshold cut off to emphasize 6-fold symmetry. (c)Azimuthal averaged SAXS profile shows peaks in the ratio of 1.0, 3 <sup>1/2</sup> , 4 <sup>1/2</sup> , 7 <sup>1/2</sup> , 9 <sup>1/2</sup> .....	102
<b>Figure 3.3</b> (a) 2-dimensional SAXS pattern with the incident beam along the normal to the XZ plane. Several strong reflections are shown perpendicular to the flow direction. (b) SAXS profile along the vertical direction of (a) also shows peaks in the	

ratio of 1.0,  $3^{1/2}$ ,  $4^{1/2}$ ,  $7^{1/2}$  etc. confirming the structure is hexagonal packing..... 103

**Figure 3.4** (a) Bright field TEM micrograph for the roll cast PS/PEP/PE (15/70/15) film: view normal to YZ. The film was stained with RuO<sub>4</sub>. Circular regions of PS are evident. Inset of the selected area magnified from (a) shows a hexagonally ordered structure but with many regions without PS domains.  
(b) Bright field TEM micrograph for the roll cast PS/PEP/PE (15/70/15) film: view normal to XZ. Needle shape and prolate spherical PS domains are shown parallel to the roll casting direction. Inset of the selected area magnified from (b) shows an elongated PS domains.....105

**Figure 3.5** Schematic diagram of the proposed mechanism of cylinder formation under the flow field with solvent evaporation. (a) Microphase separation is initiated at a certain concentration of polymer solution during the evaporation of solvent in roll casting process. Solvent swollen PS spheres are formed. (b) The PS spheres become prolate and align along the flow direction. (c) The development of needle shape PS cylinders. (d) PS cylinders arrange to form a hexagonally packed structure..... 107

**Figure 4.1** (a) 2-dimensional SAXS pattern of the roll cast sample taken at 150 °C with the incident beam perpendicular to the flow direction, normal to the XZ plane. Several strong reflections are shown perpendicular to the flow direction. (b) SAXS profile along the horizontal (equatorial) direction of (a) shows peaks in the ratio of  $1:\sqrt{3}:\sqrt{4}:\sqrt{7}:\sqrt{9}:\sqrt{12}$  etc., implying the structure is characterized by a hexagonal packing of cylinders. (c) 2-dimensional SAXS pattern of the roll cast sample at 150 °C with the incident beam along the flow direction, normal to the YZ plane. (d) SAXS pattern with different threshold cut off to emphasize the 6-fold symmetry of the first and second order reflection..... 117

**Figure 4.2** (a) 2D SAXS pattern of the slowly cooled sample taken at 50 °C when the incident beam perpendicular to the XZ plane. The pattern with a different threshold cut off to emphasize the first order reflection is shown in the inset. It confirms that the oriented structure of the PS microdomains formed by the applied flow field is preserved after the crystallization of PE.  
(b) Comparison between the SAXS profiles along the horizontal (equatorial) direction ( $\pm 10^\circ$  sector slice) at 150 °C and at 50 °C. The increase of the scattering intensity at the high  $q$  region ( $q = 0.4 \sim 0.5 \text{ nm}^{-1}$ ), due to the presence of the crystalline PE lamellae is apparent in the 50 °C pattern.  
(c) 2D SAXS pattern of the slowly cooled sample at 50 °C when the incident beam along the flow direction normal to YZ plane. The same pattern with a different threshold cut off to emphasize the 6 fold symmetry of the first  $\sqrt{1}$  reflection, is shown in the inset. The  $\sqrt{3}$  reflection is only observed as a weak, broad continuous ring. It indicates that the lateral packing of the PS microdomain structure developed during the roll cast was perturbed by the crystallization of PE..... 119

**Figure 4.3** The equatorial azimuthal intensity distribution profiles of the  $(10\bar{1}0)$  reflection at 150 °C in Figure 4.1a and at 50 °C in Figure 4.2a. Two highly oriented

peaks appear at  $0^\circ$  and  $180^\circ$  at both temperatures. The FWHM value of the peak is approximately  $45^\circ$  in both cases, indicating that the crystallization of the PE block does not disturb the orientation of the cylindrical PS microdomains along the flow Direction..... 122

**Figure 4.4** (a) 2-dimensional WAXS patterns, obtained simultaneously with the SAXS pattern of Figure 4.2a, of the slowly cooled sample with the incident beam normal to the XZ plane. The diffuse inner ring is the unoriented amorphous halo. The first crystalline reflection corresponds to (110) reflection of orthorhombic PE crystals and displays four off-axis regions of high intensity. The (200) and (020) reflections are preferentially located on the equator and on the meridian respectively. These features indicate that the PE lamellae are oriented with the *b* axis normal to the X-ray beam, therefore parallel to the flow direction.

(b) Schematic diagram of the WAXS pattern with indexed reflections.

(c) 2-dimensional WAXS pattern, obtained simultaneously with SAXS pattern of Figure 4.2c, of the slowly cooled sample with the incident beam normal to the YZ plane. The isotropic (110) and (200) diffraction rings indicate uniaxial symmetry around the *b* axis of the PE crystals..... 123

**Figure 4.5** Bright field TEM images of the microtomed sections of the slowly cooled roll cast films stained with RuO<sub>4</sub>.

(a) Transverse view showing PS cylinders aligned parallel to the flow direction. The orientation of PS cylinders is still preserved after the crystallization of PE.

(b) Axial view showing circular cross sections of PS cylinders. The hexagonally packed structure, observed in the SAXS pattern taken at  $150^\circ\text{C}$ , is disrupted by the crystallization of PE in the matrix..... 126

**Figure 4.6** Underfocus phase contrast bright field TEM images of the microtomed sections of the unstained roll cast films slowly cooled to room temperature.

(a) Transverse view showing crystalline PE lamellae (seen edge-on) (dark region), oriented along the roll casting direction. The thickness of lamellae ranges from 10 nm to 20 nm.

(b) Axial view showing crystalline PE lamellae (seen edge-on) oriented in various directions..... 127

**Figure 4.7** Schematic diagram of the microdomain structure of the slowly cooled roll cast sample. The crystallization of PE is confined between the preformed hexagonally packed PS cylinders, and *b* and *c* axes of the PE crystals are preferentially parallel and perpendicular to the axes of the PS cylinders respectively. Various orientations of the crystalline PE lamellae develop on the view of the YZ plane not only due to the hexagonal symmetry of the cylindrical PS microdomains but also due to many defects and misaligned PS cylinders in the roll cast microstructure. In addition, random nucleation of the PE crystals in the matrix generates various other orientations..... 129

**Figure 5.1.** (a) Small angle X-ray diffraction patterns and (b) wide angle X-ray diffraction patterns of a bulk sample of the PE/PEP/PE block copolymer recorded at

the indicated temperatures during cooling from a homogeneous melt..... 139

**Figure 5.2** TEM bright-field image of a thin film of PE/PEP/PE block copolymer obtained by casting from a xylene solution. Radially oriented lamellar PE microdomains, characterized by crystalline spherulites having size of 5-10  $\mu\text{m}$ , are imaged through the diffraction contrast..... 140

**Figure 5.3** Selected area electron diffraction pattern of a thin film of PE/PEP/PE block copolymer epitaxially crystallized onto BA. The pattern presents mainly the  $0kl$  reflections of PE, hence it indicates that the (100) plane of PE is normal to the electron beam and parallel to the (001) exposed face of the BA crystals. A small tilting of the lamellae around the  $b$  axis, or progressive tilting of successive stacks of lamellae, accounts for the presence of arced reflections as well as the  $1kl$  and  $2kl$  type reflections (in particular, 121 and 112 reflections) and the weak 110 and 200 reflections..... 141

**Figure 5.4** Schematic diagram of the epitaxial relationship between PE and BA crystals..... 142

**Figure 5.5** (a) Under-focused TEM bright-field image of a thin film of PE/PEP/PE block copolymer epitaxially crystallized onto BA corresponding to an area similar to that of Figure 5.3. The light noncrystalline regions appear bright due to phase contrast. The dark regions correspond to the denser crystalline PE phase, which form long lamellae standing edge-on on the substrate surface. The lamellae are preferentially oriented with the  $b$  axis of PE parallel to the  $b$  axis of the BA. (b) TEM (110) dark-field image of a thin film of PE/PEP/PE block copolymer epitaxially crystallized onto BA corresponding to an area similar to that of Figure 5.3. Long thin, highly parallel alternating regions of bright/dark contrast are evident over the field of view. The bright regions correspond to the crystalline PE lamellae in the Bragg condition. Dark regions crossing the lamellar structure correspond to crystalline areas where the crystals are tilted or twisted out of the Bragg condition..... 144

**Figure 5.6** Schematic model showing the crystalline and amorphous microdomains in the PE/PEP/PE block copolymer epitaxially crystallized onto BA. Epitaxial relationship shows the relative orientation of the polyethylene lamellae on the benzoic acid.  $(100)_{\text{PE}} // (001)_{\text{BA}}$ , and  $c_{\text{PE}} // a_{\text{BA}}$ ,  $b_{\text{PE}} // b_{\text{BA}}$ . The orientation of the PE molecular chains perpendicular to the lamellar plane  $\hat{c} // \hat{n}$  is also shown..... 146

**Figure 6.1** (a) TEM bright-field image of a thin film of PS/PMMA(26/32) block copolymer, directionally solidified with BA, and stained with  $\text{RuO}_4$ . The dark regions correspond to the stained PS microdomains. The lamellae are well aligned along the fast growth direction of the BA crystals (crystallographic  $b$  axis). Inset shows the FFT power spectrum of the TEM micrograph. Spot-like first reflection located on the meridian shows the nearly single crystal-like microstructure. (b) Schematic model of the microstructure of PS/PMMA processed with BA. Alternating lamellae of PS and PMMA microdomains are aligned along the  $b$  axis of

**Figure 6.2** (a) TEM bright-field image of a thin film of PS/PI(45/12) block copolymer, directionally solidified with BA, and subsequently stained with OsO<sub>4</sub>. The dark regions correspond to the stained PI cylinders, while the white regions correspond to the PS matrix. The cylindrical PI microdomains are well aligned along the fast growth direction of the BA crystals. No grain boundaries are evident. A few dislocation defects are seen.

Inset shows the Fast Fourier Transform (FFT) power spectrum of the TEM micrograph. Spot-like reflections located on the equator at  $q_0$  and  $2q_0$  indicate a nearly single crystal-like microstructure. In particular absence of the  $\sqrt{3}q_0$  reflection in this FFT power spectrum demonstrates that there is no rotation and tilting of microdomain lattice along the cylinder axis. (b) Schematic model of the microstructure of PS/PI processed with BA. Cylindrical PI microdomains are edge-on to the crystalline substrate and aligned along the  $b$  axis of BA crystal..... 156

**Figure 6.3** TEM bright-field image of a thin film of PS/PI(45/12) block copolymer, directionally solidified with AN, and stained with OsO<sub>4</sub>. The dark regions correspond to the stained PI cylinders, while the white regions corresponds to the PS domains. The cylindrical PI microdomains are not so well aligned along the same direction, which corresponds to the fast growth direction of the AN crystals. Many dislocation defects are observed. Inset is the FFT power spectrum of the TEM micrograph. The arced first order reflection perpendicular to  $b$  axis of AN crystals demonstrates the orientation of the PI microdomains observed in TEM, which is not as good as when the PS/PI copolymer is processed with BA..... 158

**Figure 6.4** TEM bright-field images of a thin film of PS/PI(45/12) block copolymer, directionally solidified with AN, and stained with OsO<sub>4</sub>. (a) Block copolymer has dewetted on the AN crystals. Low magnification image shows that directional solidification occurred macroscopically. (b) The magnified image of certain area of (a) shows that cylindrical PI microdomains are aligned parallel to the macroscopic solidification direction. The dark regions correspond to the stained PI cylinders, while the white regions corresponds to the PS domains..... 159

**Figure 6.5** TEM bright-field images of a thin film of PS/PI(45/12) block copolymer, directionally solidified with BA, and stained with OsO<sub>4</sub>. The dark regions correspond to the stained PI cylinders, while the white regions corresponds to the PS domains. (a) Cylindrical PI microdomains are aligned along the fast growth direction of BA crystal. Vertically undulated PI microdomains are observed (b) Due to very thin film thickness, vertically undulated PI cylinders transform into hexagonally packed cylinders oriented perpendicular to the BA substrate Inset shows the FFT power spectrum of the TEM micrograph. Spot-like first reflections with 6-fold symmetry shows the nearly hexagonally packed microstructure. .... 160

**Figure 7.1.1** TEM micrographs of simple cast and directionally solidified and epitaxially crystallized block copolymers.

(a) Solvent cast thin film of PS/PE block copolymer stained with RuO<sub>4</sub>. The bright field TEM image shows a poorly ordered microphase separated structure. The lighter regions correspond to the PE cylindrical domains, the gray regions to the PS matrix. Darker regions appear due to island areas of greater film thickness.

(b) Uniform thickness well ordered thin film of PS/PE block copolymer formed by directional solidification of a solution of the block copolymer in BA. The PE component forms cylinders oriented perpendicular to the film surface and packed in a pseudo-hexagonal lattice. The interdomain spacing is 40 nm along the b-axis direction of BA, and about 10-15% smaller along the other 2 directions. Inset:

Magnified region showing the noncircular shape of the PS-PE interface..... 166

**Figure 7.1.2** Diffraction patterns and dark field image of directionally solidified and epitaxially crystallized block copolymer.

(a) Selected area electron diffraction pattern of an unstained film of PS/PE block copolymer crystallized from BA demonstrating epitaxy. The pattern exhibits only *Ok* reflections of PE, which indicates that the (100) plane of PE is normal to the electron beam and parallel to the (001) face of the BA crystals. The *c* and *b* axes of the PE crystals are parallel to the *a* and *b* axes of the BA crystal.

(b) Diffraction pattern from a similar sample after tilting 34° about the chain axis direction of PE. The strong (110) diffraction peaks of PE are prominent.

(c) Dark field image of the PS/PE film using the (110) diffraction spot. Small rectangular PE crystals are observed well aligned along the b axis direction of the BA crystals and packed on a pseudo-hexagonal lattice whose size and orientation is the same as seen in Figure 7.1.1b. The PE crystals are 7nm thick by 20nm long with their longest dimension parallel to [110]\*..... 169

**Figure 7.1.3** Hypothetical phase diagram of the BA-PS/PE block copolymer system showing the melting points of benzoic acid ( $T_m$  (BA)) and polyethylene ( $T_m$  (PE)) as well as the microphase separation transition temperature of the PS/PE block copolymer (MST) and the eutectic point and eutectic temperature ( $T_e$ ). The dilute polymer solution is cooled from location 1 to 3 during the film formation process..... 171

**Figure 7.1.4** Schematics depicting the evolution of the structure during the directional eutectic solidification and epitaxial crystallization of the block copolymer from the crystallizable solvent.

(a) Homogeneous solution of PS/PE in BA between two glass substrates.

(b) Directional solidification forms  $\alpha$  crystals of BA coexisting with a liquid layer of more concentrated polymer.

(c) Second directional solidification showing the eutectic liquid layer transforming into BA crystal (which grows on the pre-eutectic BA- $\alpha$  crystal) and an ordered lamellar block copolymer ( $\beta$ ).

(d) Due to the highly asymmetric composition of the block copolymer and the epitaxial crystallization of the PE in contact with the BA substrate, the flat interfaces



of vertically oriented lamellae are unstable and spontaneously deform in order to achieve a more preferred interfacial curvature and allow epitaxial growth of PE.  
 (e) The layers transform into an array of vertically oriented, pseudo-hexagonally packed semicrystalline PE cylinders. A single chain folded PE lamella is formed in each cylinder. The PE crystals have their (100) planes contacting the (001) plane of the BA crystal with  $a_{BA} // c_{PE}$  and  $b_{BA} // b_{PE}$ ..... 174

**Figure 7.2.1** SAD pattern and TEM images of a thin film of PS/PEP/PE terpolymer directionally solidified and epitaxially crystallized onto BA.

- (a) SAD pattern of a thin film of PS/PEP/PE terpolymer. The pattern presents the  $0kl$  reflections of PE, hence it indicates that the (100) plane of PE is normal to the electron beam and parallel to the (001) exposed face of the benzoic acid crystals. The  $c$  and  $b$  axes of the PE crystals are parallel to the  $a$  and  $b$  axes of the benzoic acid, respectively.
- (b) TEM Bright-field image of the unstained thin film of PS/PEP/PE terpolymer corresponding to an area similar to that of (a). The image contrast is enhanced by underfocus of the objective lens. The dark regions correspond to the crystalline PE phase, which form long lamellae oriented edge-on, and aligned along the  $b$  axis of PE, parallel to the  $b$  axis of BA.
- (c) TEM bright-field image of the stained thin film of PS/PEP/PE terpolymer with  $RuO_4$ . The dark regions correspond to the PS phase, which form cylinders aligned parallel to the crystalline lamellae..... 180

**Figure 7.2.2** Schematic model showing the development of the microstructure in thin films of the PS/PEP/PE terpolymer epitaxially crystallized onto BA.

- (a) Homogeneous solution of PS/PEP/PE in BA between two glass substrates.
- (b) Directional solidification forms crystals of BA coexisting with a liquid layer of more concentrated polymer.
- (c) Second directional solidification showing the eutectic liquid layer transforming into BA crystal (which grows on the pre-eutectic BA crystal) and an ordered lamellar block copolymer.
- (d) Due to the highly asymmetric composition of the block copolymer, the flat interfaces of vertically oriented lamellae are unstable and spontaneously deform in order to achieve a more preferred interfacial curvature.
- (e) Epitaxial crystallization of PE blocks onto the BA crystals occurs resulting in the formation of long, thin crystalline PE lamellae in between the PS cylinders. The PE crystals have their (100) planes contacting the (001) plane of the BA crystal with  $a_{BA} // c_{PE}$  and  $b_{BA} // b_{PE}$ ..... 183

**Figure 7.2.3** Small angle X-ray diffraction patterns of a bulk sample of the PS/PE block copolymer recorded at the indicated temperatures during the cooling from the melt. The ratios ( $q_n/q_1$ ) of the diffraction vectors  $q_n$ , with respect to that of the first peak at  $q = q_1 = 0.15 \text{ nm}^{-1}$ , are also shown. The ratios 1,  $\sqrt{3}$ ,  $\sqrt{7}$ ,  $\sqrt{9}$ ,  $\sqrt{11}$  indicates the presence of a microstructure characterized by a hexagonal packing of PE cylinders. The expected peak at  $q/q_1 = \sqrt{4}$  is probably concealed by the broad peak at  $q/q_1 = \sqrt{3}$ .. 186

**Figure 7.2.4** SAD pattern and TEM image of a thin film of PS/PE block copolymer directionally solidified and epitaxially crystallized onto BA.

(a) SAD pattern of a thin film of PS/PE block copolymer. The pattern presents only the  $0kl$  reflections of PE. This indicates that the (100) plane of PE is normal to the electron beam and parallel to the (001) exposed face of the BA crystals. The  $c$  and  $b$  axes of the PE crystals are parallel to the  $a$  and  $b$  axes of the BA, respectively.

(b) TEM Bright-field image of a thin film of PS/PE block copolymer stained with  $\text{RuO}_4$ . The darker regions correspond to the stained PS matrix, while the light regions correspond to the crystalline PE microdomains, which form hexagonally packed

cylinders oriented perpendicular to the substrate surface..... 187

**Figure 7.2.5** SAD pattern and TEM image of a thin film of PS/PE block copolymer directionally solidified and epitaxially crystallized onto AN.

(a) SAD pattern of a thin film of PS/PE block copolymer. The pattern presents the  $0kl$  reflections of PE, hence indicates that the (100) plane of PE is parallel to the (001) exposed face of the AN crystals. The  $c$  axis of the PE crystals is parallel to the  $[110]$  and  $[\bar{1}\bar{1}0]$  directions of AN crystal. Therefore, two diffraction patterns rotated by an angle of  $70^\circ$  and oriented symmetrically relative to the  $a^*$  axis of the AN crystals is shown along the  $[110]$  and  $[\bar{1}\bar{1}0]$  directions of AN crystals.

(b) TEM Bright-field image of a thin film of PS/PE block copolymer stained with  $\text{RuO}_4$ . The darker regions correspond to the stained PS matrix, while the light regions correspond to the crystalline PE microdomains, which form hexagonally packed

cylinders oriented perpendicular to the substrate surface..... 189

**Figure 7.2.6** Schematic models of the microstructures in thin films of the PS/PE block copolymer directionally solidified and epitaxially crystallized onto BA (a) or AN (b).

(a) Vertically oriented PE cylinders are packed on a hexagonal lattice and contain one crystalline PE lamella oriented edge-on on the substrate with the  $b$  axis parallel to the  $b$  axis of BA crystal.

(b) Vertically oriented PE cylinders are packed on a hexagonal lattice and contain one crystalline PE lamella oriented edge-on on the substrate with two different

orientations in which the  $c$  axis of PE lamella is parallel to either  $[110]$  or  $[\bar{1}\bar{1}0]$

directions of AN crystals..... 191

**Figure 8.1.** (a) Selected area electron diffraction pattern of a thin film of PS/PEP/PE block terpolymer epitaxially crystallized onto AN. The pattern presents the  $0kl$  reflections of PE, and hence indicates that the (100) plane of PE is normal to the electron beam and parallel to the (001) exposed face of the AN crystals. The  $c$  axis of the PE crystals is normal to the lamellar surface and parallel to the  $[110]$  and  $[\bar{1}\bar{1}0]$

directions of AN crystal due to the matching between  $b_{\text{PE}}$  and  $d_{110}$  inter-row spacing as well as due to the matching of the  $2c_{\text{PE}}$  with  $(1/2)d_{110}$  of AN. Therefore, two diffraction patterns rotated by an angle of  $70^\circ$  and oriented symmetrically relative to the  $a^*$  axis of the AN crystals is shown along the  $[110]$  and  $[\bar{1}\bar{1}0]$  directions of AN

crystals. (b) Schematic of epitaxy between PE and AN.....197

**Figure 8.2** TEM bright-field and AFM images of a thin film of PS/PEP/PE epitaxially crystallized on AN corresponding to an area similar to that of Figure 8.1.

a) TEM bright-field image of the unstained sample. The phase contrast is enhanced by underfocus of the objective lens. The dark regions correspond to the crystalline PE phase, which forms cross oriented PE lamellae standing edge-on. Inset shows FFT spectrum of the TEM image, confirming the two orientations of crystalline PE lamellae.

b) Tapping mode AFM image of the unstained sample. The contrast results from the height difference. The cross oriented PE lamellae are shown to protrude on the surface.

c) TEM bright-field image of the sample stained with RuO<sub>4</sub>. Image contrast is mass thickness amplitude contrast. The dark regions correspond to the PS phase, which forms a similar double oriented structure to that of the PE microdomains..... 200

**Figure 8.3** Schematic model showing the relationship between the orientation of the crystalline phase and the alignment of the microdomains in a semicrystalline block copolymer. (a) The cylindrical PS microdomains are initially aligned along the fast growth direction of AN crystals (*b* axis) via the directional solidification prior to the crystallization of the PE. (b) The orientation of the molecular chains in the crystalline phase is induced by the epitaxial crystallization on the surface of AN crystal. The 2 dimensional orientation of the crystalline PE lamellae standing edge-on on the substrate surface, and oriented parallel to the  $[110]$  and  $[\bar{1}\bar{1}0]$  directions of AN crystal is obtained. The epitaxy of the PE on the AN crystal reorganizes the pre-oriented PS microdomains. (c) Schematic model showing the crystalline and amorphous microdomains in the PS/PEP/PE block terpolymer epitaxially crystallized onto AN. Epitaxial relationship shows the relative orientation of the polyethylene lamellae on AN.  $(100)_{PE} // (001)_{AN}$ , and  $c_{PE} // [110]_{AN}$ . The PS microdomain is shown in between the edge-on PE crystalline lamellae aligned into two different directions..... 203

**Figure 9.1** Schematic of topographically pre-patterned silicon substrate..... 214

**Figure 9.2** TEM bright-field image of a thin film of PS/PI(45/12) block copolymer, directionally solidified with BA on the pre-patterned substrate, and stained with OsO<sub>4</sub>. The dark regions correspond to the stained PI microdomains. The cylindrical PI microdomains perpendicular and parallel to the substrate are shown in the square mesa (light) and matrix dark regions respectively..... 215

**Figure 9.3** (a) Tapping mode AFM image of a thin film of PS/PI(45/12) block copolymer, directionally solidified with BA on the pre-patterned substrate. The amplitude contrast image is shown. The cylindrical PI microdomains with two different orientations with respect to the substrate are well aligned along the fast growth direction of the BA crystals. The square shape mesa regions show the PI cylinders perpendicular to the substrate. The thicker matrix regions show the in-plane PI cylinders.

(b) Higher magnification AFM image of (a). Hexagonally packed PI cylinders vertically aligned to the substrate are observed. In addition, smooth transition is clearly seen from perpendicular to parallel orientation of PI cylinders..... 216

**Figure 9.4** Schematic of the PS/PI block copolymer orientations between top glass substrate and bottom pre-patterned substrate. The block copolymer films confined between BA crystal and the bottom pre-patterned substrate undergo thickness variation, leading to two different orientations..... 217

**Figure 9.5** TEM bright-field images of a thin film of PS/PI(45/12) block copolymer, directionally solidified with BA, and exposed to ozone. Void microdomain structure after removal of the PI cylinders by ozone appears brighter. (a) Thinner block copolymer film shows vertically ordered cylindrical microdomains to the substrate (b) Thicker block copolymer film shows directionally solidified PI microdomains oriented parallel to the substrate..... 219

**Figure 9.6** TEM bright-field images of a thin film of PS/PI(45/12) block copolymer, directionally solidified with BA, and treated via O<sub>2</sub>-RIE. Void microdomain structure after removal of the PI cylinders by O<sub>2</sub>-RIE appears brighter. (a) Thinner block copolymer film shows vertically ordered cylindrical microdomains to the substrate (b) Thicker block copolymer film shows directionally solidified PI microdomains oriented parallel to the substrate..... 220

## LIST OF TABLES

<b>Table 1.1:</b> Characteristics of nanometer scale patterning techniques.....	27
<b>Table 1.2:</b> Characteristics of block copolymer nanotechnologies.....	34
<b>Table 1.3:</b> Summary of techniques for controlling block copolymer microdomains.....	52
<b>Table 2.1:</b> Molecular characteristics of the three semicrystalline block copolymers.....	87
<b>Table 2.2:</b> Melting and crystallization properties of high density polyethylene and the three semicrystalline block copolymers.....	88

## ACKNOWLEDGEMENTS

The last five years at MIT were a most exciting and fruitful time in my life. Getting a PhD in a foreign country involves many difficulties besides the research itself – there are issues such as a different language, culture, food and so on to deal with. Sometimes they came to me as adventures, which I was willing to face, but sometimes they were huge mountains I would never climb. I have kept asking myself if a PhD is worth obtaining with all these hurdles. Now I found a right answer. *Yes it is*. It is worthier than I have imagined. I have gotten so many things through this period, not only scientific knowledge, research skills, but also friendship, love and life with great people. Constant accumulation of time, effort and hope finally offers me one of the most valuable in my life, PhD. It doesn't mean just academic achievement. It does mean much more than that. It means something which can elevate a human being one step higher to someone who has deeper and broader knowledge, someone who can solve problems even not related to his areas, someone who knows how to help others, how to appreciate others' help and how to love someone else. My destiny allowed me to have great luck to meet the most wonderful people in the world. Without them, all of these would have never been possible. Here I express my unlimited thanks to those people from the bottom of my heart.

First of all, I would really like to thank Prof. Thomas my advisor. The knowledge, ideas and motivations he gave me to guide my research are countless. More valuably I learned from him ways of finding problems, organizing complicated thoughts and solving those problems. In addition, I saw through him what a good educator would be.

I have several other mentors. One of them is Prof. W. H. Jo of Seoul National University, my masters' thesis advisor, who first introduced to me this fascinating world of polymer science. Another person is Dr. Y. S. Kang of the Korea Institute in Science and Technology who also showed me how wonderful polymer science is. The others include Prof. C. De Rosa of the University of Naples, Italy and Prof. B. Lotz of the CNRS in Strasbourg, France. I have been fortunate enough to know them and spend time together here at MIT. Their visit two years ago provided me a great opportunity to work with world best researchers in polymer crystals. And it resulted in a breakthrough for my research. I really appreciate their enormous help as well as their education, which made me one step closer to a PhD.

I am grateful to my committee members Prof. A. M. Mayes and Prof. S. M. Allen for giving me a lot of useful advice on my thesis. Even in a short time, working with Prof. Mayes on the patterned substrate project enabled me to experience a different style of education.

A good research environment can not be achieved without good people in the group. First of all, I would like to thank Mr. C. Osuji, my classmate for helping me almost every step in graduate school. I am thankful to Dr. Y. Zhang of Cornell University and Prof. Y. Cohen of Technion University for spending a lot of time to discuss and interpret my data. I extend my thanks also to Dr. A. Avgeropoulos for teaching me microtoming and

transmission electron microscopy when I first joined the group at MIT. I cannot mention all the names of the many great lab-mates with whom I have had the opportunity to work and interact over my tenure here at MIT, but my deep thanks to them will be always in my heart.

I have also wonderful collaborators outside of MIT - Dr. L. J. Fetters kindly provided me with block copolymer materials he made personally. I am grateful to Prof. B. Hsiao and Dr. F. Yeh at the State University of New York in Stony Brook for their help at Brookhaven National Laboratory's National Synchrotron Light Source. I am thankful to Dr. M. J. Fasolka of the National Institute of Standard and Technology for his help.

Research is not possible without financial support. This work was supported by National Science Foundation DMR98-07591, ACS PRF-300350-AC7 and US-France NSF-CNRS, INT 9726544.

I have so many wonderful Korean friends who always encourage and support me. I really appreciate my friends at MIT. I extend my thanks to my lifetime friends: middle, high school and collage mates including Young-Mook, Sung-Ho, Kang-taek, Joung-Yup, Hea-Jun, Sung-Min, Jin-Hyun, Yang-Suk, Jin-Ho and Jeong-Yul for sharing my sadness, difficulties and happiness all together through my life.

I am eternally grateful to my parents, Hae-Sung and Jung-Un for unconditionally supporting and encouraging me, and for always believing in me in every path I have chosen in my life. They showed me how small and trivial things could turn out unexpected happiness to our family when shared together. Furthermore, they have always taught me not to be selfish and to be modest. My two brothers, Jae Min and Jun Min have always been my supporters. I especially thank them. I would also like to thank my grandmother who passed away last year for always believing in me. I am deeply indebted to my lovely wife, Hyejin. She endlessly encourages and supports me but sometimes corrects me to right direction with her warmest and deepest heart. I must admit that I learned so many things from her not just as my wife but as my closest friend, as my senior PhD and as my lifetime colleague.

I dedicate this small piece of achievement to my greatest family.

## FOREWORD

### Introduction

Nanometer scale patterns based on self assembly have been considered as alternatives to replace high resolution lithographic technologies such as X ray, electron beam and interference lithography. In particular block copolymers have recently received attention not only thanks to the scale of the microdomains (tens of nanometers) but also due to the convenient size tuneability of microdomains by simply changing their molecular weights.

Many potential usages of block copolymers for different nanotechnologies have been proposed. However the main drawback of using block copolymers lies in difficulty of their microstructure control. Achievement of microdomain orientation and further control of the microstructures of block copolymers requires introduction of external fields. Mechanical, electrical, magnetic and surface interactions have been proposed to manipulate the microstructures of block copolymers.

In this thesis microdomain structures of various block copolymers are controlled in the bulk state as well as in thin films. An initiate study used the roll cast process to manipulate the microstructure of a semicrystalline lamellar-glassy cylinder block copolymer in bulk. The crystallization of the crystalline block was significantly guided, completely avoiding the spherulite growth, by the pre-aligned microphase separated cylindrical domain structure.

Two new approaches and their combination, involving new types of interactions with block copolymer microdomains (epitaxy and directional solidification) are introduced. *Epitaxy* between a crystalline block and a crystalline substrate whereby a crystallizable organic solvent (such as benzoic acid and anthracene) serves as a solvent for a semicrystalline block copolymer at temperatures above the solvent melting temperature and becomes a substrate onto which the crystallizable block can orient when the block is cooled below the solvent's melting point is shown to be an excellent way to form highly aligned edge-on lamellae in both lamellar and cylindrical microdomains. *Directional solidification* of the crystallizable solvent induces an overall orientation of the block copolymer Inter-Material Dividing Surface (IMDS) parallel to the temperature gradient.



When a block copolymer which contains a crystallizable block is used, one can also utilize epitaxy in combination with directional solidification to control the microdomain pattern. When the process is conducted on a film confined to have various thickness (topographically patterned substrate), 2 types of microdomain orientation can be accessed.

## **Thesis Structure**

This thesis is an experimental study of the nanometer scale texture of several types of block copolymers. The thesis consists of two parts. Part I describes the control of semicrystalline block copolymer domains in bulk. In part II, various examples of control of microdomains of block copolymers in thin films are presented.

Chapter 1 introduces and describes the broad background related to the current study. Various nanotechnologies are discussed with a particular focus on those utilizing self assembled block copolymers. Previous methods used to control the block copolymer microdomain structures, a most important step for industrial applications are reviewed. Two new types of interactions which can strongly couple to the block copolymer domains and lead to controlled pattern structures are identified. These are epitaxy and directional solidification.

Materials and various experimental methods used in this thesis are discussed in chapter 2. Synthesis and characterization of semicrystalline and amorphous block copolymers are presented. In particular the experimental procedures to prepare directionally and/or epitaxially solidified thin block copolymer films are dealt with in chapter 2.

Flow field facilitated equilibrium microdomain structure and its orientation of the microstructure is presented in chapter 3. A cylindrical microdomain structure is formed to occur at volume fraction as low as 12 % minority component. Chapter 4 describes the induced alignment of the lamellar microdomains due to their crystallization in the presence of a pre-oriented glassy amorphous cylindrical microdomain structure.

Chapter 5 demonstrates that epitaxy of a melt-compatible semicrystalline block copolymer onto a crystalline organic substrate is a good way to manipulate the microdomain structure. Directional solidification induced by eutectic phase separation

between a crystallizable organic solvent and a block copolymer is also discussed as another method for controlling microstructures in chapter 6. Microdomain structures such as a vertically aligned lamellar structure and thickness dependent ordered cylindrical structures oriented parallel or perpendicular to the substrate are presented. In addition the combination of these two types of interactions allows for better control of semicrystalline block copolymer textures as discussed in chapter 7. A vertically oriented hexagonally packed cylindrical microdomain structure with each cylinder containing precisely one crystalline lamellae epitaxially oriented with respect to the crystalline substrate is produced by directional solidification of a crystallizable solvent which also possesses an epitaxial relationship to the crystallizable block. Not only orientation of microdomains but also alteration of block copolymer micropattern structure by degenerate epitaxy is demonstrated in chapter 8. A double oriented cylindrical microdomain structure is induced by the crystallization texture.

Chapter 9 collects the various principal conclusions and suggests directions for future work. In particular an in-progress study using the new directional solidification and a topographically patterned substrate method is described in detail in section 9.3 and 9.4. In addition, the directionally solidified microdomain structure is modified via chemical and physical etching methods such as ozone and oxygen plasma reactive ion etching.

# CHAPTER 1: Background and Motivation

## 1.1 Nanotechnology

Condensed-matter physics addresses the various properties that describe solid and liquid substances, including their thermal, elastic, electrical, chemical, magnetic, and optical characteristics.<sup>1</sup> Theoretical advances in solid state physics have been made in recent years to study crystalline materials, whose properties are described in terms of quantum mechanics. Crystalline and amorphous semiconductors and insulators, as well as properties of the liquid state matter (for example, liquid crystals and quantum liquids) are also examined in condensed-matter physics.

Nanometer size structures in materials draw attention for their interesting size dependent physical properties, and therefore their potential for nanotechnologies. The need for smaller electronic, optical and mechanical devices has created the new field of nanotechnology. The underlying principles for nanoscale devices are remarkably different because the systems are so small that quantum effects often govern their behavior. Nanotechnology involves the fabrication of functional structures in the 1 to 100 nanometer range. Nanometer scale systems exhibit particularly peculiar and interesting characteristics: quantized excitation,<sup>2</sup> single-electron tunneling (SET),<sup>3</sup> and metal-insulator transition.<sup>4</sup> Other interesting physical processes that can be observed in similar structures—for example, near-field optical behavior<sup>5</sup> and interaction of light with photonic band-gap crystals<sup>6</sup> represent nanoscopic manifestations of processes. Recent developments in surface microscopy, physical chemistry, and computational engineering have come together to help scientists better understand, fabricate, and manipulate structures at this level.

Various approaches to nanotechnology have been described as top-down by the engineering disciplines and bottom-up by the physical disciplines. People working from the bottom up are attempting to create a new understanding and structure from the dynamics of the basic molecules. Those working from the top down seek to improve existing devices, such as transistors, and to make them smaller and therefore faster.

### 1.1.1 Nanoscale pattern structure

Fabrication of nanoscale structures is essential for nanotechnology. The ability to fabricate on the nanometer scale guarantees a continuation in the miniaturization of functional devices. New advanced fabrication technologies have enabled the lateral dimensions of devices to be shrunk well below 100 nm. Lithography is usually the most critical procedure for successfully defining structures with such dimensions. Photolithographic methods all share the same operational principle.<sup>7</sup> Exposure of an appropriate material to electromagnetic radiation (ultra violet (UV), deep ultra violet (DUV) or X-ray) introduces a latent image (usually a difference in solubility) into the material as a result of a set of chemical changes in its molecular structure; this latent image is subsequently developed into 1D or 2D relief structures through etching.

Methods based on writing with particles (electrons or ions) usually accomplish the same task using a scanned beam or projected image of energetic particles rather than photons. Exposure is usually patterned either by interposing a mask between the source of radiation (or particles) and the material or by scanning a focused spot of the source across the surface of the material. When masks are used, the lithographic process yields a 1D or 2D replica of the pattern on the mask.

Electron beam nanolithography is well suited for generating patterns on the submicron scale.<sup>8-12</sup> However, it is not the best method for accurately manipulating structures which are less than approximately 30 nanometers wide. 50 nm period structures have so far been obtained by various state of the art direct e-beam lithography approaches in which proximity effects (the dose delivered by the electron beam tool is not confined to the shapes that the tool writes, resulting in pattern specific linewidth variations) can be minimized. Recently by optimizing the exposure and development conditions Scherer's group generated a nanostructure array of 12 nm dots with 25 nm period and 20 nm lines with 40 nm period.<sup>11</sup>

X-ray lithography has also been used to create sub micron size features.<sup>13</sup> Combined with electron beam lithography to make a mask, X ray source replicated features as small as 25 nm in size in a practical reproducible way. Moreover, interferometric lithography, using interactions between two or more coherent laser beams, has been well matched to create sub-micron features in an inexpensive way.<sup>14,15</sup> Generally periodic and quasi-

periodic 2D pattern structures were easily fabricated with interferometric lithography. Recently Smith et al. developed a new technique, Zone-Plate Array Lithography in which array of Fresnel zone plates focus the X-ray beam source and directly pattern on the resist surface without a mask.<sup>16</sup>

A shadow-mask evaporation or nanostencil method has also been used to define sub-micron single layer material patterns.<sup>17</sup> In this approach, the nanostencil, a perforated ultra-thin silicon nitride membrane with various sub-micron size apertures, is in contact with the surface during deposition. This technique which does not involve photoresist processing steps, successfully created a periodic 2 D array of metal dots having lateral dimension of 100 – 750 nm on substrates. The combination of shadow mask (nanostencil) and scanning probe methods such as atomic force microscope (AFM), scanning tunneling microscope (STM) provided better and faster control of the pattern structures.

With scanning probes, a sharp tip (< 50 nm) induces local change in a resist or causes local deposition. Methods that involve scanning or writing can generate arbitrary 2D patterns and therefore be used for master writing. Advantages of scanning probe methods include resolution that, for AFM and STM methods, approaches the atomic level, the ability to generate features with nearly arbitrary geometries, and the capability to pattern over surface topography that deviates significantly from planarity.<sup>18</sup> These methods are serial techniques, however, and have writing speeds that are typically limited by the mechanical resonances of the tips and the piezoelectric elements that maintain constant separation between the tips and the sample.

Direct patterning on self assembled monolayers (SAMs) using atomic force microscope (AFM) was developed to study selective protein absorption on patterned area. The method, called nanografting<sup>19,20</sup>, combined the displacement of selected resist molecules by an AFM tip and the adsorption of new adsorbate. Nanografting allows a more precise control over the size and geometry of patterned features and their locations on surfaces.

Another technology using scanning probes is dip-pen nanolithography (DPN) developed in Mirkin's group.<sup>21</sup> DPN uses an AFM tip as a "nib," a solid-state substrate (in this case, Au) as "paper," and molecules with a chemical affinity for the solid-state substrate as "ink." Capillary transport of molecules from the AFM tip to the solid

substrate is used in DPN to directly "write" patterns consisting of a relatively small collection of molecules in submicrometer dimensions. However, these methods pattern the substrate sequentially, and therefore the patterning time scales linearly with the area to be patterned. The characteristics of various nanolithographic techniques mentioned above are summarized in Table 1.1.

### **1.1.2. Self assembly: natural materials**

Nature uses self-assembling materials for nanostructures as the components for living cells.<sup>22</sup> The structures of biological systems are hierarchically organized in discrete levels or scales. Several levels of structure can be distinguished in proteins.<sup>23</sup> The primary structure of the sequence of amino acid groups along the polypeptide chain is developed into various secondary structural motifs, such as coils, sheets and ribbons. The motifs are packed together to give the overall molecule a distinctive shape, the tertiary structure. The association of several sub tertiary units corresponds to the protein's quaternary structure. Another example of self assembly of biomaterials is tobacco mosaic virus which is a self-assembling replication machine.<sup>23</sup> It contains a core of coiled RNA surrounded by a coat of protein subunits. The self assembly of these subunits takes place spontaneously in slightly acidic or near neutral solution. Another hierarchical biomaterial structure is found in spider silk (*Nephila clavipes*).<sup>23</sup> The structure of dragline silk contains regions of largely crystalline protein, about 50 nm across, embedded in a disordered tangle of protein chains. Again within the fully disordered matrix, there are much smaller crystallites, about 2 nm across of stacked polyalanine  $\beta$  sheets.

Most of biocomposite systems also exhibit hierarchy and at least one distinct structural feature that lies within each length scale and is defined by the molecular, nanoscopic, microscopic and macroscopic regions. Examples such as bones and shells demonstrate how nature can assemble different materials into a variety of useful composites at the cellular level. In general biocomposites achieve design at the nanoscale through the self-assembly of organic structures. The inorganic structures then form via directed or template-assisted self assembly, during which the self assembled organic materials (e.g. proteins and/or lipid) first build the scaffolding which in turn regulates the nucleation, growth morphology and orientation of the inorganic compounds. For example

Technique	Resolution (nm)	Source Material	Nature of Patterns	Intrinsic Limitations	Advantages	Ref.
UV photo lithography	250	248 nm KrF excimer laser	2D	Diffraction Depth of focus	Easy replication	7
Electron Beam Lithography	10 ~ 30	Focused electron beam	2D	Electrostatic interaction Serial writing Small field writing	Writing pattern	8-12
X-ray lithography	25	Soft X-ray with $\lambda$ near 1 nm	2D	Diffraction Depth of focus	Easy replication	13
Interferometric lithography	> 100	Halographic interactions between two or more lasers	2D	Diffraction Depth of focus Limited patterns	No mask Easy replication	14,15
Zone plate array lithography	> 100	Fresnel zone plates X-ray beam	2D	Zone plate fabrication	No mask	16
Nanostencil	< 100 ~ 750	Perforated ultra thin SiN membrane	2D	Fabrication of mask Relatively low resolution	No photoresist	17
Nanografting	5 ~ 50	Modified AFM tip	2D	Serial patterning Limited writing speed	High resolution Arbitrary geometries Chemical patterns	19,20
Dip-pen lithography	5 ~ 50	Modified AFM tip	2D	Serial patterning Limited writing speed	High resolution Arbitrary geometries Chemical patterns	21

**Table 1.1:** Characteristics of nanometer scale patterning techniques

an abalone shell consists of layered platelets of  $\text{CaCO}_3$  (~ 400 nm thick) that are held together by much thinner (< 30 nm) organic polymer materials. The organic materials not only bind the platelets together, but also act as a template to induce the growth of these epitaxially oriented, chemically distinct components.<sup>24</sup> Another example is found in a spine from the sea mouse *Aphrodita*,<sup>25</sup> which consists of an array of hollow cylinders, with the long axis of the cylinders along the spine. This structure reflects visible light to create various colors. The spine normally appears to be deep red in color, but when light is incident perpendicular to the axis of the spine, different colors are seen.

However, human attempts at similar structures are limited to building self-assembling nanoscale materials a few atoms or molecules at a time. Various examples can be observed in biology, in the field of embryology and morphogenesis<sup>22</sup>; in chemistry, where groups of molecules form supramolecular structures.<sup>26</sup> In achieving nanostructures and nanoelectronic devices, chemical self-assembly has become an important factor in building supramolecular nanostructures.

### 1.1.3 Biomimetic materials

The field of biomimetics is based on the supposition that nature can provide models for processing at the submicrometer scale. Artificial nanoscale structures can be fabricated with similarity to biological materials, through the application of self assembly coupled with lamination and patterning methods. Originally the biological processes that create the mineralized tissues (e.g. bone, teeth, and shell) inspired the directed synthesis of ceramic materials through the use of organic molecules.<sup>27</sup>

Sellinger et al. fabricated a laminated hierarchical organic-inorganic composite structures similar to the structure of narce of abalone shell, using a self assembly process.<sup>28</sup> A solution of silica, surfactant and organic monomers was evaporated on a silicon substrate via dip-coating to induce the formation of surfactant micelles with organic monomers and silica. Subsequent self assembly of nanolayers created a laminated organic-inorganic composite structure. Additional polymerization of organic monomers fixed the structure, completing the nanocomposite assembly process.<sup>28</sup>

In addition to laminated biomimetic composite structures, many other organic-inorganic hybrid nanoscale structures have been demonstrated.<sup>29,30</sup> For example, bacterial



S-layers, self assembled, two dimensionally ordered films of proteins that feature in many bacterial cell walls, were used as templates for the in situ nucleation of ordered two dimensional arrays of cadmium sulfide nanocrystals.<sup>29</sup> Another example is an inorganic macroporous structure fabricated using a colloidal crystal, comprised of monodisperse polystyrene spheres.<sup>30</sup> An inorganic precursor, like a metal alkoxide, was infiltrated into the octahedral and tetrahedral interstitial void spaces of a latex colloidal crystal. Hydrolytic polycondensation of the metal alkoxide forms a composite metal oxide-polymer colloidal crystal. Subsequent solvent extraction facilitated the removal of the polymer spheres to leave behind an inorganic shell with the structure of an inverted opal.<sup>30</sup>

Polymer films can be grown directly on inorganic surfaces that have been functionalized with a self-assembled monolayer of polymerizable monomer.<sup>31</sup> In this strategy an alkylalkoxysilane or alkanethiol with a terminal olefinic moiety may be anchored to a silicon, silica or gold substrate. Platinum catalyzed hydrosilation of a hydrosiloxane polymer facilitates the chemical attachment of the polymer to the substrate. “Hairy” polymer-SiO<sub>2</sub> nanoparticles may self-assemble into densely packed arrays of inorganic nanoparticles with controlled packing dimensions.

A similar approach has been pursued by Boal et al., using monolayer-functionalized gold nanoparticles.<sup>32</sup> To provide a general means for the controlled self-assembly of nanoparticles, a “brick and mortar” method was developed in which colloidal gold particles functionalized with recognition elements serve as bricks, while polymer bearing complementary functionality serves as the mortar, holding together the colloidal particles. Using this strategy, the conformational flexibility of the polymer compensates for irregularities in the size and shape of the aggregate structure.

Block copolymers have also been used as hosts for inorganic materials.<sup>33</sup> A film of poly(*tert*-butylacrylate)-*b*-poly(2-cinnamoyl ethylmethacrylate) (PtBA-*b*-PCEMA) assembled to give hexagonally packed cylinders of PtBA inside the PCEMA matrix. Subsequent hydrolysis removed the tBu groups to leave loosely packed poly(acrylic acid) inside the channels. These nanochannels could then be filled with solid state materials such as CdS and Fe<sub>2</sub>O<sub>3</sub>. Other various examples using block copolymers for templating are discussed in the section of 1.1.5.

#### 1.1.4 Block copolymers

Block copolymers satisfy the size requirement for many nanotechnologies.<sup>34</sup> Block copolymers consist of chemically distinct macromolecules covalently linked to form a single chain. Owing to their mutual repulsion, dissimilar blocks tend to segregate into different domains, the spatial extent of the domains being limited by the constraint imposed by the chemical connectivity of the blocks. Area minimization at the interface of two blocks takes place due to the interfacial energy difference of two blocks. As a result of these competing effects, self-organization of periodic microstructures occurs on the nanoscopic length scale. Various microstructures are achieved, depending on relative volume ratio between two blocks.

In the simplest case of AB diblock copolymers, the composition of the AB diblock (i.e., the volume fraction  $f$  of block A) controls the geometry of the structure (see Figure 1.1). For nearly symmetric diblocks ( $f \sim 1/2$ ), a lamellar (LAM) phase occurs. For moderate asymmetries, a complex bicontinuous state, known as the double gyroid (DG) phase, has been observed in which the minority blocks form domains consisting of two interweaving threefold-coordinated networks. At yet higher compositional asymmetry, the minority component forms hexagonally packed cylinders (CYL) and then spheres (SPH) arranged on a body-centered cubic lattice. Eventually, as  $f \rightarrow 0$  or 1, a homogeneous phase results.<sup>35</sup> A schematic diagram of various microstructures of AB diblock copolymer, depending on relative volume fraction ratio between A and B blocks, is shown in Figure 1.1

#### 1.1.5. Nanotechnologies with block copolymers

Until recently, most industrial applications of block copolymers were as adhesives or as mechanical property modifiers (e.g. thermoplastic elastomers). Only in the past 10 years have researchers taken block copolymers into the “high technology” area, to the so called “nanotechnologies”.

Many attempts have been made to utilize block copolymers in nanotechnology. One dimensional photonic crystal was made with high molecular weight block copolymer.<sup>36-38</sup> Layer-by-layer stacked alternating block copolymer lamellae structure in between two glass substrates showed nearly perfect normal incidence photonic band gap property.

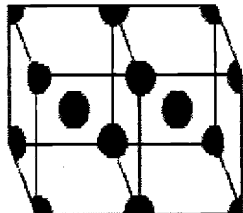

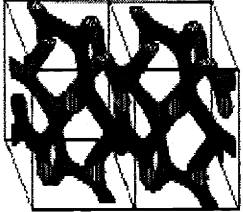


Nature of patterns	Spheres (SPH) (3D)	Cylinders (CYL) (2D)	Double gyroid (DG) (3D)	Double diamond (DD) (3D)	Lamellae (LAM) (1D)
Blue domains: A block					
Volume fraction of A block	0-21%	21-33%	33-37%	37-50%	

Figure 1.1: Microstructures of A/B diblock copolymer

Variation of microdomain size to vary the band gap was successfully controlled by adding homopolymers.

A low dielectric constant silicon based material was obtained by ozoneolysis of a silicon containing block copolymer precursor.<sup>39</sup> A self assembled double gyroid microdomain structure was developed from spin casting, annealing and ozoneolysis to create a nanoscale bicontinuous ceramic (SiO<sub>2</sub>) channel structure.

Mesostructured silicates have been prepared through the use of block copolymers as structure-directing agents. The processing of ceramics with block copolymers is similar to that of surfactant molecules at a longer length scale as discussed in section 1.1.3. Mesoporous silica films have been fabricated using amphiphilic block copolymers as the structure directing agent.<sup>40,41</sup> The aqueous silica cations partition within the hydrophilic regions of the self assembled system and subsequent sol-gel polymerization of the silica precursor produces a densely cross-linked silica network exhibiting the microphase separated block copolymer structure. An approach that is more obviously biomimetic uses synthetic cysteine-lysine block “copolypeptides” that mimic the properties of silicatein, a protein found to direct silica growth in certain sponges.<sup>42</sup> The morphology of the silica mesostructure, spheres and columns of amorphous silica, are produced by using the reduced and the oxidized forms of the copolymer, respectively.

Block copolymers have also been utilized not only as surfactants to inhibit coalescence of nanoscale particles such as metal, metal oxide, inorganics, molecular chromophore and quantum dots but also to spatially pattern the particles.<sup>43-57</sup> The selective dispersion of quantum dots in microdomains within functionalized polynorborene block copolymers was achieved by controlling the affinity between the selective block and quantum dot surface.<sup>47,48</sup> In addition, the block copolymer microstructure has been used as “nano-reactors” where nanoscale particles grow through the chemical reactions.<sup>43-47,49-56</sup> For example, nanometer scale platinum and palladium catalysts were generated and stabilized within the polystyrene core of polystyrene-*b*-ethylene oxide block copolymer micelles.<sup>49</sup> Electroless deposition of metals into selected microdomains has been recently performed to provide continuous material loading.<sup>51,55,56</sup>

The periodic nanostructures of block copolymers are very useful in thin films as templates for nanolithography.<sup>58-63</sup> By removing one polymer chemically, the patterns

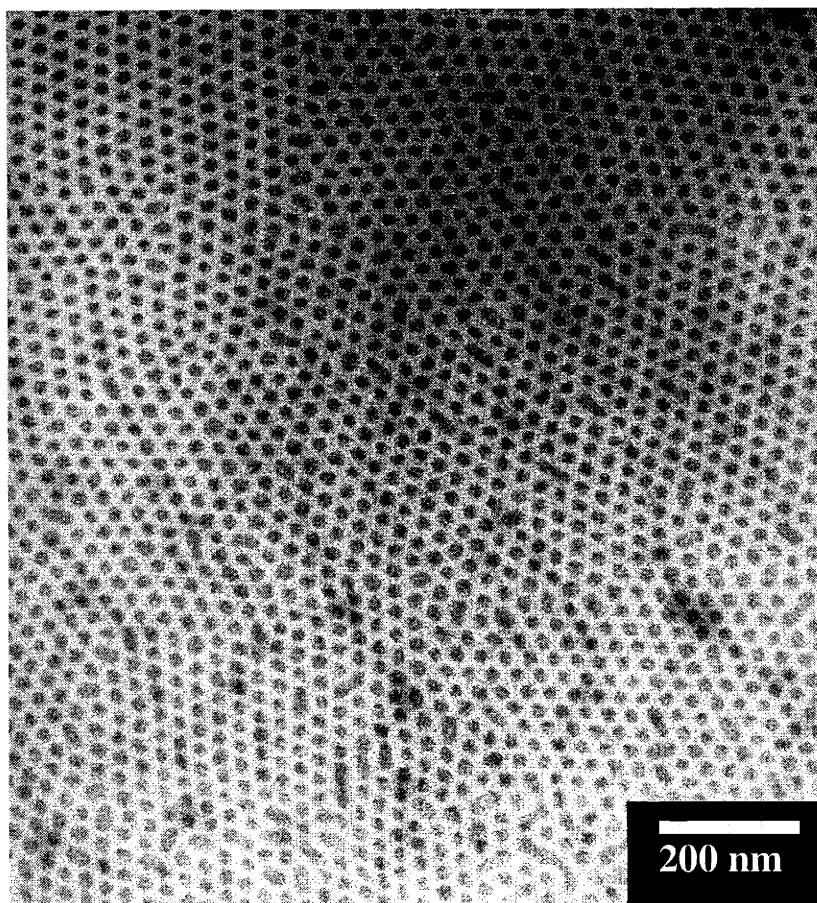
may be transferred to a substrate through either reactive etching or by thermal evaporation or electroplating of a component into the previously removed regions. Dense, periodic arrays of holes and troughs have been fabricated in silicon, silicon nitride, and germanium. Domains approximately 20 nm wide, 20 nm deep, and spaced 40 nm apart, yielding a pattern with  $3 \times 10^{12}$  holes/in<sup>2</sup> were obtained on a three inch wafer.<sup>61</sup> In addition, GaAs nanoparticles have been grown in a hexagonally ordered array of nanometer scale holes with a density as high as  $\sim 10^{11}$ /cm<sup>2</sup> by metal-organic chemical vapor deposition.<sup>63</sup> This array of holes was created using a block copolymer as the etching mask.

High density storage media can be made by transferring the block copolymer pattern into a magnetic substrate. A block copolymer-hard mask-magnetic layer scheme was recently used for creating single bit magnetic media storage.<sup>64</sup> One set of domains of the block copolymer were selectively removed by oxygen reactive ion etching (RIE) to create the nanopattern structure. The pattern was subsequently transferred into the hard mask used for better surface adhesion among the layers. The following ion milling process transferred the pattern structure of the hard mask into a magnetic layer and developed a nanoscale magnetic pattern structure. Thurn-Albrecht et al. have recently demonstrated a way to fabricate a high density ferromagnetic cobalt nanowire structure with the density as high as  $1.9 \times 10^{11}$  wires per square centimeter using a block copolymer template.<sup>65</sup> Enhanced coercivities were observed, proposing a new route to ultrahigh density storage media.

Furthermore, a potential display device application for side chain ferroelectric liquid crystalline polymer films has been considered.<sup>66</sup> Mao et al. examined a side chain liquid crystal block copolymer with a ferroelectric smectic C\* liquid crystal block.<sup>67</sup> They found that the block copolymer exhibits bistable switching behavior in electric fields and provides the possibility of a microphase stabilized ferroelectric liquid crystal device. The characteristics of various block copolymer nanotechnologies mentioned above are summarized in Table 1.2.

Technology	System Materials	Patterns	Key functions	Ref.
Photonic Band Gap Crystals	PS/PI + homo PI High $M_w$ BCPs	LAM, CYL	Total Reflection of Visible Light by Tunable BCP Microdomains	36-38
Ceramic Precursor Low Dielectric Materials	PPMDSS/PI	DG	Ozone etch and SiO <sub>2</sub> Formation	39
Organic/inorganic Biomimetic Agents	PEO/PPO/PEO, PI/PEO, P <sub>7</sub> BA/PCEMA	LAM, CYL, SPH	Sol/gel transition	33, 40-42
Nanoparticle Pattern Structures	PS/PEO, PS/PMMA, PMTD/PMORCOOH, PMTD/PNORPHOS, PS/PB/PS	DG, LAM, CYL, SPH	Sequestration Particle Growth	43-57
Nanolithographic Templates	PS/PB, PS/PI	SPH	RIE and Pattern Transfer	58-63
High Density Magnetic Media Structures	PS/PFS, PS/PMMA	SPH, CYL	Pattern Transfer and Ferromagnetic Bit Formation	64,65
Display	PS/PI-LC	LAM/ smectic C*	Bistable switching under E field	66,67

**Table 1.2:** Characteristics of block copolymer nanotechnologies



**Figure 1.2** Bright field TEM micrograph of PS/PI (45/12) block copolymer thin film. The film was cast on a glass substrate and annealed at 120 °C for 2 days. OsO<sub>4</sub> was used to stain the cylindrical PI microdomains which appear dark.

### **1.1.6. Limitations and opportunities**

The chief limitation to using block copolymers to form periodic patterns lies with the fact that the self assembled structure is hard to control. Indeed, the microdomains composed of the different blocks, having sizes of several tens of nanometers, typically nucleate randomly and grow as a polygranular texture, with periodic ordering maintained only over distances of several tens of lattice constant (i.e., a grain size of only 1 ~ 2 microns). For example, Figure 1.2 shows a bright field TEM micrograph of a cylinder forming PS/PI block copolymer thin film. The cylindrical PI microdomains look dark due

to OsO<sub>4</sub> staining for 4 hours. Most of PI cylinders are ordered perpendicular to the substrate due to thin film thickness (see the chapter 6). Laterally several grain boundaries are observed. The typical size of a grain is approximately 1 μm. A few point dislocation defects are also seen where one PI cylinder is surrounded by 7 or by 5 other PI ones instead of 6. In these cases, the center PI cylinder looks a little bigger than others. A greater range of engineering applications demands control over the orientation and position of the microdomains.

Several techniques are currently used for inducing alignment of the microdomains in block copolymers. They rely on the ability to couple an externally applied field to somemolecular and/or supermolecular feature in the polymer, and thus achieve directional properties, such as transport, optical and mechanical properties.

In the next section, various approaches used in this thesis to control the microstructures of block copolymers, which should help make these potential nanotechnologies work, will be reviewed.

### **1.1.7 Brief outline of the thesis**

The thesis deals with methods to induce global order of block copolymer microdomains resulting in oriented microdomain structures. Mechanically generated flow fields in the “roll casting” process are utilized to develop an orientation of amorphous as well as crystalline microdomains in a semicrystalline block copolymer. New types of interactions between crystallizable organic solvent and block copolymer: epitaxy and directional solidification are introduced and applied to manipulate the various block copolymer microdomain structures in thin films of semicrystalline and non-crystalline block copolymers. A combination of the two types of interaction provides more precisely controlled hierarchical microdomain structure. Spatial control of microdomain structure and orientation is achieved via directional solidification on a topographically patterned substrate. The double microdomain texture is modified using ozone and RIE methods further demonstrating technological applications.



### 1.1.8 References

1. Marder, M. P. *Condensed Matter Physics* **1960**, John Wiley, New York.
2. Kastner, M. A. "Artificial atoms" *Phys. Today* **1993**, 24-31.
3. Likharev, K. K. "Correlated discrete transfer of single electrons in ultrasmall tunnel junctions" *IBM J. Res. Dev.* **1988**, 32, 144-158.
4. Vijayakrishnan, V.; Chainani, A.; Sarma, D. D.; Rao, C. N. R. "Metal insulator transitions in metal clusters-a high energy spectroscopy study of Pd and Ag clusters" *J. Phys. Chem.* **1992**, 96, 8679-8682.
5. Girard, C.; Dereux, A. "Near field optics theories" *Rep. Prog. Phys.* **1996**, 59, 657-699.
6. Joannopoulos, J. D.; Villeneuve, P. R.; Fan, S. "Photonic band gap microcavities in optical waveguides" *Nature* **1997**, 390, 143-149.
7. Moreau, W. M. *Semiconductor Lithography: Principles and Materials*; Plenum: New York, 1988.
8. Chou, S. Y.; Wei, M. S.; Krauss, P. R.; Fischer, P. B. "Single domain magnetic pillar array of 35 nm diameter and 65 Gbits/in<sup>2</sup> density for ultrahigh density quantum magnetic storage" *J. Appl. Phys.* **1994**, 76, 6673.
9. Dobisz, E. A.; Brandow, S. L.; Bass, R.; Shirey L. M. "Nanolithography in polymethylmethacrylate: an atomic force microscopy study" *J. Vac. Sci. Technol. B.* **1998**, 16, 3695.
10. Goodberlet, J.; Carter, J.; Smith H. I. "Scintillating global-fiducial grid for electron-beam lithography" *J. Vac. Sci. Technol. B* **1998**, 16, 3672.
11. Dial, O.; Cheng, C. C.; Scherer, A. "Fabrication of high-density nanostructures by electron beam lithography" *J. Vac. Sci. Technol. B* **1998**, 16, 3887.
12. Nicolau, D. V.; Taguchi, T.; Taniguchi, H.; Yoshikawa, S. "Negative and positive tone protein patterning on e-beam/deep-UV resists" *Langmuir* **1999**, 15, 3845.
13. Smith, H. I.; Schattenberg, M. L.; Hector, S. D.; Ferrera, J.; Moon, E. E.; Yang, I. Y.; Burkhardt, M. "X-ray nanolithography: Extension to the limits of the lithographic process" *Microelectron Eng.* **1996**, 32, 143.
14. Choi, J. O.; Jeong, H. S.; Pflug, D. G.; Akinwande, A. I.; Smith, H. I. "Fabrication of 0.1  $\mu\text{m}$  gate aperture Mo-tip field-emitter arrays using interferometric lithography" *Appl. Phys. Lett.* **1999**, 74, 3050.
15. Farhoud, M.; Hwang, M.; Smith, H. I.; Schattenberg, M. I.; Bae, J. M.; Youcef-Toumi, K.; Ross, C. A. "Fabrication of large area nanostructured magnets by interferometric lithography" *IEEE T Magn.* **1998**, 34, 1087.
16. Djomehri, I. J.; Savas, T. A.; Smith, H. I. "Zone-plate-array lithography in the deep ultraviolet" *J. Vac. Sci. Technol. B* **1998**, 16, 3426.
17. Luthi, R.; Schlittler, R. R.; Brugger, J.; Vettiger, P.; Welland, M. E.; Gimzewski, J. K. "Parallel nanodevice fabrication using a combination of shadow mask and scanning probe methods" *Appl. Phys. Lett.* **1999**, 75, 1314.
18. Minne, S. C.; Manalis, S. R.; Atalar, A.; Quate, C. F. "Contact imaging in the atomic force microscope using a higher order flexural mode combined with a new sensor" *Appl. Phys. Lett.* **1996**, 68, 1427.
19. Wadu-Mesthrige, K.; Xu, S.; Amro, N. A.; Liu, G. "Fabrication and imaging of nanometer-sized protein patterns" *Langmuir* **1999**, 15, 8580.

20. Xu, S.; Miller, S.; Laibinis, P. E.; Liu, G. "Fabrication of nanometer scale patterns within self-assembled monolayers by nanografting" *Langmuir* **1999**, 15, 7244.
21. Piner, R. D.; Zhu, J.; Xu, F.; Hong, S.; Mirkin, C. A. "Dip-pen nanolithography" *Science* **1999**, 283, 661.
22. Hyde, S.; Andersson, S.; Larsson, K.; Blum, Z.; Landh, T.; Lidin, S.; Ninham B. W. *The Language of Shape* **1997** Elsevier, New York.
23. Ball, P. *Made to Measure, Chapter 4 Only natural, Biomaterials* NY 1997.
24. Zaremba, C. M.; Belcher, A. M.; Fritz, M.; Li, Y. L.; Mann, S. "Critical transitions in the biofabrication of abalone shells and flat pearls" *Chem. Mater.* **1996**, 8, 679.
25. Parker, A. R.; McPhedran, R. C.; McKenzie, D. R.; Botten, L. C.; Nicorovici, N. P. "Aphrodite's iridescence" *Nature* **2001**, 409, 36.
26. Zubarev, E. R.; Pralle, M. U.; Li, L. M.; Stupp, S. I. "Conversion of supramolecular clusters to macromolecular objects" *Science* **1999**, 283, 523.
27. Sarikaya, M.; Aksay, I. A.; *Biomimetics: design and processing of materials* NY: Am. Inst. Phys. 352 pp.
28. Sellinger, A.; Weiss, P. M.; Nguyen, A.; Lu, Y.; Assink, R. A.; Gong, W.; Brinker, C. J. "Continuous self assembly of organic-inorganic nanocomposite coatings that mimic nacre" *Nature* **1998**, 394, 256.
29. Shenton, W.; Pum, D.; Sleytr, U. B.; Mann, S. "Synthesis of cadmium sulfide superlattices using self-assembled bacterial S-layers" *Nature* **1997**, 389, 585
30. Wijnhoven, J. E. G. J.; Vos, W. L. "Preparation of photonic crystals made of air spheres in titania" *Science* **1998**, 281, 802
31. von Werne, T.; Patten, T. E. "Preparation of structurally well defined polymer nanoparticle hybrids with controlled/living radical polymerizations" *J. Am. Chem. Soc.* **1999**, 121, 7409
32. Boal, A. K.; Lihan, F.; DeRouchey, J. E.; Thurn-Albrecht, T.; Russell, T. P.; Rotello, V. M. "Self-assembly of nanoparticles into structured spherical and network aggregates" *Nature* **2000**, 404, 746.
33. Liu, G.; Ding, J.; Hashimoto, T.; Kimishima, K.; Winnik, F. M.; Nigam, S. "Thin films with densely, regularly packed nanochannels: preparation, characterization and applications" *Chem. Mater.* **1999** 11, 2233
34. Muthukumar, M.; Ober, C. K.; Thomas, E. L. "Competing interactions and levels of ordering in self-organizing polymeric materials" *Science* **1997**, 277, 1225.
35. Matsen, M. W.; Bates, F. S. "Origins of complex self assembly in block copolymers" *Macromolecules* **1996**, 29, 7641.
36. Fink, Y.; Urbas, A. M.; Bawendi, B. G.; Joannopoulos, J. D.; Thomas, E. L. "Block copolymers as photonic bandgap materials" *J. Lightwave Tech.* **1999**, 17, 1963.
37. Urbas, A.; Fink, Y.; Thomas, E. L. "One-dimensionally periodic dielectric reflectors from self-assembled block copolymer-homopolymer blends" *Macromolecules* **1999**, 32, 4748.
38. Urbas, A.; Sharp, R.; Fink, Y.; Thomas, E. L.; Xenidou, M. L. J. Fetters, "Tunable block copolymer/homopolymer photonic crystals" *Adv. Mater.* **2000**, 12, 812.
39. Chan, V. Z-H.; Hoffman, J.; Lee, V. Y.; Latrou, H.; Avgeropoulos, A.; Hadjichristidis, N.; Miller, R. D.; Thomas, E. L. "Ordered bicontinuous nanoporous and nanorelief ceramic films from self assembling polymer precursors" *Science* **1999**, 286, 1716.

40. Zhao, D.; Yang, P.; Melosh, N.; Feng, J.; Chmelka, B. F.; Stucky, G. D. "Continuous mesoporous silica films with highly ordered large pore structures" *Adv. Mater.* **1998**, *10*, 1380.
41. Melosh, N. A.; Lipic, P.; Bates, F. S.; Wudl, F.; Stucky, G. D.; Fredrickson, G. H.; Chmelka, B. F. "Molecular and mesoscopic structures of transparent block copolymer-silica monoliths" *Macromolecules*, **1999**, *32*, 4332.
42. Cha, J. N.; Stucky, G. D.; Morse, D. E.; Deming, T. J. "Biomimetic synthesis of ordered silica structures mediated by block copolypeptides" *Nature* **2000**, *403*, 289
43. Yue, J.; Sankaran, V.; Cohen, R. E.; Schrock, R. R. "Interconversion of ZnF<sub>2</sub> and ZnS nanoclusters within spherical microdomains in block copolymer films" *J. Am. Chem. Soc.* **1993**, *115*, 4409.
44. Moller, M.; Spatz, J. P. "Mineralization of nanoparticles in block copolymer micelles" *Curr. Opin. Polym. Interface. Sci.* **1997**, *2*, 177.
45. Sohn, B. H.; Cohen, R. E. "Processible optically transparent block copolymer films containing superparamagnetic iron oxide nanoclusters" *Chem. Mater.* **1997**, *9*, 264.
46. Lee, T.; Yao, N.; Askay, I. A. "Nanoscale patterning of barium titanate on block copolymers" *Langmuir* **1997**, *13*, 3866.
47. Fogg, D. E.; Radzilowski, L. H.; Dabbousi, B. O.; Schrock, R. E.; Thomas, E. L. Bowendi, M. G. "Fabrication of quantum dot-polymer composites: Semiconductor nanoclusters in dual-function polymer matrices with electron-transporting and cluster-passivating properties" *Macromolecules* **1997**, *30*, 8433.
48. Fogg, D. E.; Radzilowski, L. H.; Blanski, R.; Schrock, R. E.; Thomas, E. L.; Bowendi, M. G. "Fabrication of quantum dot/polymer composites: Phosphine-functionalized block copolymers as passivating hosts for cadmium selenide nanoclusters" *Macromolecules* **1997**, *30*, 417.
49. Mayer, A. B. R.; Mark, J. E. "Transition metal nanoparticles protected by amphiphilic block copolymers as tailored catalyst systems" *Colloid Polym. Sci.* **1997**, *275*, 333.
50. Templin, M.; Frank, A.; Du Chesne, A.; Leist, H.; Zhang, Y.; Ulrich, R.; Schadler, V.; Wiesner U. "Organically modified aluminosilicate mesostructures from block copolymer phases" *Science* **1997**, *278*, 1795.
51. Hashimoto, T.; Tsutsumi, K.; Funaki, Y. "Nanoprocessing based on bicontinuous microdomains of block copolymers: Nanochannels coated with metals" *Langmuir* **1997**, *13*, 6869.
52. Zehner, R. W.; Lopes, W. A.; Morkved, T. L.; Jaeger, H.; Sita, L. R. "Selective decoration of a phase-separated diblock copolymer with thiol-passivated gold nanocrystals" *Langmuir* **1998**, *14*, 241.
53. Lin, B. H.; Morkved, T. L.; Meron, M.; Huang, Z. Q.; Viccaro, P. J.; Jaeger, H. M.; Williams, S. M.; Schlossman, M. L. "X-ray studies of polymer/gold nanocomposites" *J. Appl. Phys.* **1999**, *85*, 3180.
54. Kane, R. S.; Cohen, R. E.; Silbey, R. "Synthesis of doped ZnS nanoclusters within block copolymer nanoreactors" *Chem. Mater.* **1999**, *11*, 90.
55. Zehner, R. W.; Sita, L. R. "Electroless deposition of nanoscale copper patterns via microphase-separated diblock copolymer templated self-assembly" *Langmuir* **1999**, *15*, 6139.
56. Boontongkong, Y.; Cohen, R. E.; Rubner, M. F. "Selective electroless copper deposition within block copolymer microdomains" *Chem. Mater.* **2000**, *12*, 1628.

57. Evans, C. C.; Bates, F. S.; Ward, M. D. "Control of hierarchical order in crystalline composites of diblock copolymers and a molecular chromophore" *Chem. Mater.* **2000**, 12, 236.
58. Mansky, P.; Chaikin, P.; Thomas, E. L. "Monolayer films of diblock copolymer microdomains for nanolithographic applications" *J. Mat. Sci.* **1995**, 30, 1987.
59. Mansky, P.; Harrison, C. K.; Chaikin, P. M.; Register, R. A.; Yao, N. "Nanolithographic templates from diblock copolymer thin films" *Appl. Phys. Lett.* **1996**, 68, 2586.
60. Park, M.; Harrison, C.; Chaikin, P. M.; Register, R. A.; Adamson, D. H. "Block copolymer lithography: Periodic arrays of similar to 10(11) holes in 1 square centimeter" *Science* **1997**, 276, 1401.
61. Harrison, C.; Park, M.; Chaikin, P. M.; Register, R. A.; Adamson, D. H. "Lithography with a mask of block copolymer microstructures" *J. Vac. Sci. Technol. B* **1998**, 16, 544.
62. Lammertink, R. G. H.; Hempenius, M. G.; Van den Enk, J. E.; Chan, V. Z.-H.; Thomas, E. L.; Vancso, G. J. "Nanostructured thin films of organic-organometallic block copolymers: One-step lithography with poly(ferrocenylsilanes) by reactive ion etching" *Adv. Mater.* **2000**, 12, 98.
63. Li, R. R.; Dapkus, P. D.; Thompson, M. E.; Jeong, W. G.; Harrison, C.; Chaikin, P. M.; Register, R. A.; Adamson, D. H. "Dense arrays of ordered GaAs nanostructures by selective area growth on substrates patterned by block copolymer lithography" *Appl. Phys. Lett.* **2000**, 76, 1689.
64. Cheng, J. Y.; Ross, C. A.; Chan, V. Z. H.; Thomas, E. L.; Rob G. H. Lammertink, R. G. H.; Vancso, G. J. "Formation of a Cobalt Magnetic Dot Array via Block Copolymer Lithography" *Adv. Mater.* submitted.
65. Thurn-Albrecht, T.; Schotter, J.; Kastle, G. A.; Emley, N.; Shibauchi, T.; Krusin-Elbaum, L.; Guarini, K.; Black, C. T.; Tuominen, M. T.; Russell, T. P. "Ultra-high-density nanowire arrays grown in self assembled diblock copolymer templates" *Science* **2000**, 290, 2126.
66. Blackwood, K. M. "Device applications of side-chain ferroelectric liquid crystalline polymer films" *Science* **1996**, 273, 909.
67. Mao, G.; Wang, J.; Ober, C.; Brehmer, M.; O'Rourke, M.; Thomas, E. L. "Microphase-stabilized ferroelectric liquid crystals (MSFLC): Bistable switching of ferroelectric liquid crystal-coil diblock copolymers" *Chem. Mater.* **1998**, 10, 1538.

## **1.2 Orientation of Block Copolymer Microdomains**

Microstructural control of block copolymers can be achieved by the choice of molecular weight, composition and chain architecture. Coupling of external forces via a mechanical flow field, an electrical field or by the influence of surface interactions or temperature gradient can create preferred orientations of the microdomains. Block copolymer microdomain orientation is also affected by film thickness variation. Additionally by using solvent/block interactions and kinetics of the structure formation process, one can access non-equilibrium microdomain structures. The modification of block copolymers themselves by chemistry provides specific interactions to control the microstructures. Various surface patterning techniques, such as soft lithography, holography, and the silicon crystal miscut method, enable researchers to better control the microdomain structures of block copolymers. The numerous approaches which have been used to control block copolymer microstructures in bulk systems as well as in thin films are reviewed next.

### **1.2.1 Mechanical flow fields**

Various mechanical flow fields, involving steady shear, oscillatory shear, elongational flow, bi- or uni-directional compression and stretching, have successfully developed the alignment of microdomains of block copolymers in solution and/or in melt states. Keller and co-workers were first to apply melt extrusion of an already microphase separated copolymer to orient a cylinder forming styrene-butadiene-styrene triblock copolymer.<sup>1,2</sup> The shear gradient developed as the molten material was squeezed through an orifice into a heated glass capillary, resulted in well ordered microstructure with near “single crystal” texture.

#### **1.2.1.1 Shear fields**

After the pioneering work of the Keller group, other types of flows were utilized to develop highly textured microdomain samples. Oscillating a pair of parallel plates with an adjustable gap, provides great advantages for controlling the experimental variables such as film thickness, shear rate, and strain amplitude.<sup>3-6</sup> Shear flow experiments allowed comparison of the experimental observations with theory.<sup>7</sup> Parallel plate type

rheometers have been used extensively to study the development of orientation of microdomains in the microphase separated molten state.<sup>8-28</sup> By careful choice of shear rate and strain amplitude and temperature well ordered microstructures can be formed. In particular large amplitude oscillatory shear at different frequencies and temperatures produced two different types of orientations of lamellar-forming block copolymers: parallel (the normal to the lamellae is aligned along the velocity gradient direction) and perpendicular (the normal to the lamellae is aligned along the vorticity axis).<sup>11-26</sup> The detailed conditions for obtaining the two different microstructured orientations are now well documented in the literature.<sup>23</sup> In-situ X-ray scattering as well as birefringence measurements combined with rheological measurements of structural changes during shearing allowed study of the kinetics of the evolution as well as the mechanism for the appearance of different orientations.<sup>13,14,16-18,22,28</sup> The effect of surface anchoring on orientation developed under shear was also investigated by Winey et al.<sup>26</sup> They found that a parallel orientation of a lamellar forming PS/PI block copolymer persists up to 2  $\mu\text{m}$  into the bulk regardless of the orientation of interior region of the sample.

In addition to the microphase separated molten block copolymers, gels of solvent swollen microdomains in a closed sample holder which prevents evaporation of the solvent were subjected to shear flow to study the orientation of cylindrical as well as spherical microdomains.<sup>29-33</sup> Initially Mortensen and co-workers<sup>29,30</sup> used oscillatory shear to prepare aligned cubic spherical microdomains of a poly(oxyethylene)-poly(oxypropylene)-poly(oxyethylene) triblock copolymer. Recently several studies have been done to control micellar block copolymer structures, using a shear flow field.<sup>31-33</sup>

Coupling of liquid crystalline mesogens selectively attached on one of the blocks to oscillatory shear flow induced not only the global orientation of cylindrical microdomains but also the transition of orientation from parallel to transverse (the normal to the cylinders is aligned along the shear direction). The novel transverse structure is a compromise orientation due to the strong homogeneous boundary condition of the mesogens with respect to the IMDS.<sup>34</sup> This work suggests that the presence of hierarchical structure (i.e. smectic layers of the liquid crystal and the cylindrical microdomains of the block copolymer) could provide opportunities for manipulating the antagonistic or cooperative actions that occur when the material is placed in a field

interacting with both structures. This notion of using multiple interaction to better control pattern formation is indeed the main theme of this thesis.

#### **1.2.1.2 Compression fields**

Compression of microphase separated molten block copolymers can also induce orientation of microdomains.<sup>35,36</sup> Press molding to a desired thickness produces a biaxial flow field, resulting in the orientation of lamellar and cylindrical microdomains.<sup>35,36</sup> In addition, Cohen et al. developed the channel die apparatus similar to press molding but with flow constrained to a single direction.<sup>37-41</sup> The block copolymers confined in a deep channel area are compressed along the direction at elevated temperature and allowed to flow along one direction while being constrained in the other. Ordered lamellar and cylindrical microstructures have been observed in many different types of block copolymers using this method.<sup>37-41</sup>

#### **1.2.1.3 Roll casting: shear and elongational flow fields**

Another orientation technique called “roll-casting” has been developed by Albalak and Thomas.<sup>42-51</sup> Block copolymer solutions were applied between two counter rotating rolls. The flow field is complex, involving shear and elongational flows. The important difference from other flow field orientation techniques is that the flow field is applied to a solution and the solvent is allowed to evaporate so that the disorder to order transition occurs under a biasing field, resulting in global microdomain orientation. Roll casting permits the processing of higher molecular weight block copolymers below their degradation temperatures. Use of heated rollers, also offers the possibility to roll cast crystallizable block copolymers.

The global orientation of lamellar,<sup>42,49</sup> cylindrical,<sup>45</sup> spherical,<sup>46</sup> and bicontinuous<sup>47,48</sup> microdomains has been achieved by the roll cast method. Moreover a semicrystalline block copolymer subjected to flow fields on a heated roll cast apparatus not only developed the cylindrical microdomain orientation but also a strong molecular chain orientation of the crystalline block when the film was subsequently cooled below the crystallization temperature.<sup>50,51</sup> The aligned microdomain structures created via roll casting permitted the study of the anisotropic deformation behavior of lamellar,

cylindrical, spherical and double gyroid microstructures.<sup>45-49</sup> Recently Ha et al. have investigated the orientation and deformation behavior of block copolymer-nano clay composite materials using the roll cast method.<sup>52</sup>

### 1.2.2. Temperature gradient

A selective area temperature gradient apparatus somewhat analogous to the zone refining process used to purify semiconductor materials was utilized to align the block copolymer microstructures. Samples were prepared in a “zone heating device” which consists of a pair of central heating blocks, surrounded by two parts of cooling blocks. The centers of each pair of heating blocks and cooling blocks are aligned to form a sandwich, with the polymer film sample in the center.<sup>53</sup> A temperature gradient established along moving direction of temperature controller was on the order of about 30 °C/mm. Bodycomb et al. achieved vertically ordered lamellar microdomain structure of a millimeter thick film on the glass substrate with the rate of 2.16 mm/day of the temperature gradient.<sup>54</sup>

### 1.2.3. Electric fields

Block copolymers comprised of segments with different dielectric properties have been found to orient under an applied electric field.<sup>55-61</sup> Electric fields can be readily applied to bulk block copolymer films<sup>55-57</sup> as well as thin films.<sup>59-61</sup> Although previously used to control the morphology in multiphase systems including polymer blends and polymer solutions,<sup>62</sup> use of an electric field to induce microdomain orientation was not done until 1991 when Amundson et al.<sup>55-57</sup> used an electric field to order PS/PMMA melt. A theoretical determination of phase behavior of a block copolymer under electric field was done by Gurovich.<sup>58</sup> Shortly afterward, an in-plane electric field was applied to a cylinder forming polystyrene-polymethylmethacrylate block copolymer thin film patterned with electrode to induce local microdomain orientation parallel to the field lines.<sup>59</sup> By orienting the electric field across a thick (~ 1 mm) PS/PMMA block copolymer film, the cylindrical microdomains became oriented perpendicular to the electrode surface.<sup>60,61</sup> A vertically aligned cylindrical microstructure can be very useful in nanolithographic applications.<sup>61</sup> Recently an electric field was used to generate a



micropattern structure of a single homopolymer.<sup>63</sup> The combination of air-polymer interface instability and electric field allowed the development of a hexagonally arrayed PS cylindrical microstructure aligned vertically with respect to the electrode surface.

#### **1.2.4. Homogeneous substrate interactions**

Growing interest in thin film block copolymers has spurred researchers to develop new types of methods to control thin film block copolymer microstructures.<sup>64</sup> As opposed to bulk, thin films involve additional variables such as thickness of the film and two types of surface interactions: block copolymer/superstrate (often air), block copolymer/substrate. Manipulation of these additional parameters could generate diverse microstructures.

In thin films, the behavior of block copolymers depends primarily on two factors: interfacial interactions and commensurability of the period of the block copolymer and the film thickness. In most cases, there is a preferential wetting of one block at an interface to minimize interfacial and surface energies. Consequently a parallel orientation of the microdomains such as lamellae and cylinders is often induced at the interface and this orientation leads to propagate throughout the entire film.<sup>65-74</sup> In lamellar-forming block copolymers, the conditions of commensuration-incommensuration are given by the relation between the film thickness and the natural period of block copolymer microdomains.<sup>69-74</sup> Thin films with thicknesses which are incommensurate with the natural period of the block copolymer undergo quantization of the film thickness to discrete integer or half-integer values of repeat period, leading to the formation of terraces (i.e. islands and holes) at the polymer/air interface.<sup>69-74</sup> When one of the blocks preferentially interacts with both the substrate and the air surface in a substrate supported thin film, symmetric boundary conditions<sup>70</sup> are established while asymmetric conditions pertain when one block is preferentially wetted by the substrate and the other block by the superstrate.<sup>72</sup>

The experimental evidence shows that the variation of film thickness on the preferential substrate altered the microstructure.<sup>73,74</sup> In particular Fasolka et al. recently studied the extensive morphological phase behavior of the lamellar forming block copolymer thin film whose thicknesses are less than the period of the block copolymer.<sup>75</sup>

Adding a superstrate to a substrate supported block copolymer film, i.e. confinement of a block copolymer thin film in between two surfaces increases the possible ways to develop interesting microstructures.<sup>76-79</sup> Confinement of thin films between two surfaces, which have a specific interaction to one of the blocks, prohibits terracing formation and block copolymer chains experience either chain stretching or chain compression, depending on the deviation of the thickness from an integer or half integer multiple of the natural period.<sup>76,77</sup> By providing a neutral surface (i.e. by using a random copolymer of the same average composition as the confined lamellar block copolymer), the lamellar microdomains rearrange themselves into perpendicular orientation to a substrate.<sup>78</sup> In addition, severe frustration imposed by decreasing a confined film thickness creates a heterogeneous in-plane structure where both parallel and perpendicular lamellae are located near the confining substrate.<sup>79</sup> Theoretical studies are consistent with experimental work and predict the behavior of block copolymer thin films in confined geometry.<sup>80-87</sup>

The effects of film thickness and surface interaction on the orientations of block copolymers were also investigated with cylinder-forming asymmetric block copolymers.<sup>65, 88-93</sup> A parallel to vertical transition of cylindrical PB microdomains was observed in a PS/PB block copolymer, depending on film thickness.<sup>65</sup> Strong preferential surface interactions between one block and the substrate in a substrate supported thin film as well as a confined thin film was shown to induce a microstructural transition from cylindrical microdomain to a layered structure near the substrate surface both experimentally<sup>88</sup> and theoretically.<sup>89</sup> In addition, reducing the film thickness in an asymmetric PS/PB block copolymer created vertically oriented cylindrical PS microdomains.<sup>90</sup> Theoretical calculation of thickness effects in a cylinder forming block copolymer supports the presence of vertical cylinder microstructure.<sup>91,92</sup> Recently Konrad et al.<sup>93</sup> demonstrated, using stepwise erosion in a radio-frequency plasma, that the vertical cylindrical microdomain structure observed on the thin PS/PB/PS triblock copolymer film converted to parallel cylinders at some distance underneath the film surface.

Surface modification in addition to film thickness to tune the specific interaction between block copolymer and substrate has also generated alignment of microdomains in

both substrate supported films and confined films.<sup>94-99</sup> Application of a random copolymer brush anchored on the substrate was useful to control the surface interaction with the corresponding block copolymer. Systematic change of the amount of one of the components in the random copolymer permitted observation of the morphological transition from parallel to perpendicular or vice and versa. In addition, providing surface treatment with a PS homopolymer brush reduced the surface pinning of the PB block molecules which are supposed to wet the silicon surface, leading to less defective microstructures when a PS/PB block copolymer with cylindrical PB microdomains was spun cast.<sup>100</sup>

### **1.2.5 Special block copolymers: architecture, liquid crystallization, crystallization**

Chain architecture, liquid crystallization and crystallization of specially designed block copolymers can all lead to specific interactions between block copolymers and substrates, resulting in useful thin film orientations such as a vertically ordered lamellar structure with respect to a substrate.<sup>101-104</sup>

The architecture of block copolymers has been known to modify the surface interaction between the block copolymer and the air surface.<sup>101,102</sup> A short polybutadiene block attached between long PS and PMMA blocks in an ABC type block terpolymer interacted specifically with the air surface, resulting in a vertically ordered A-C lamellar microdomain structure on a glass substrate after a long time annealing.<sup>101,102</sup>

Wong et al. observed lamellar microdomains vertically ordered on a glass substrate in a thin film of coil block/side chain liquid crystal block copolymer.<sup>103</sup> They explained that the microstructure obtained results from block copolymer-interface wetting and configurational frustration induced by the incommensurability between the smectic spacing of liquid crystals within the LC domains and the block copolymer periodicity.

Slow crystallization at the rate of 1 nm/sec in a microphase separated structure allowed formation of a lamellar microdomain structure perpendicular to a non-crystalline silicon oxide substrate in a thin film of hydrogenated PB (amorphous)/PEO (semicrystalline) block copolymer.<sup>104</sup> Moreover the crystallization of the PEO block occurring at wetting-dewetting boundaries generated lateral alignment of the perpendicular lamellae over short distance.

### 1.2.6. Solvent control

The preparation of block copolymer thin films under various solvent evaporation conditions turned out to be a good way to manipulate the microstructures.<sup>105-107</sup> The solvent evaporation speed is one of the factors to determine the final kinetically trapped microstructures. Kim and Libera demonstrated that vertically aligned cylindrical PS microdomains were obtained in a PS/PB block copolymer thin film of the thickness of ~ 100 nm when intermediate evaporation (~ 5 nL/s) was used.<sup>105</sup> Fast (~ 200 nL/s) and slow (~ 1.5 nL/s) evaporation rates developed a microphase separated structure with no long range order and a duplex microstructure of PS cylinders with domains of either vertical or in-plane cylinders respectively.<sup>105</sup> A perpendicular lamellar microstructure was observed on fast solvent extraction process where a sample in a saturated solvent vessel was removed and brought in contact with a hot plate kept at 60 °C in a polystyrene/vinylpyridine/butyl methacrylate block copolymer.<sup>106</sup> The mechanical strain field observed on shear alignment of diblock copolymer melts present during the drying process was discussed for the observed microdomain structures.

Prewetting of the silicon oxide substrate with a minor polar solvent such as methanol or acetone before spin casting of the PS/PMMA block copolymer generated micron-scale annular structures with unique alignment of cylindrical microdomains.<sup>107</sup> The cylindrical PMMA microdomains were aligned radially on a micron size rim created during spin coating. Even though these approaches provided some interesting results in microdomain structures, more carefully controlled temperature, vapor pressure, vapor extraction speed and so on are required for more quantitative control and understanding of microstructure formation.

### 1.2.7. Patterned substrates

Introduction of lithographic technologies to modify the substrate surface properties provided ways for better control of block copolymer microdomains. Control of the nano-scale microdomains can be achieved by confining them into a lithographically patterned micro-scale structure. In particular the development of soft lithography<sup>108,109</sup> allowed easy preparation of chemically modified surface pattern structure in micron-scales with

the combination of self assembled monolayers (SAM).<sup>110,111</sup> Techniques which yield homogeneous substrate interactions were again applied to the PS/PVP block copolymers deposited on a SAM modified substrate. Heier et al.<sup>110,111</sup> showed that the local domain orientation for lamellar copolymers depended on the local chemistry of the substrate. The preferential wetting capability of the PVP block on a polar selective region can create a patterned structure comprised of a mixture of parallel and perpendicular lamellar microdomains. In addition, they demonstrated that the patterned chemistry affects the topography of the film surface. The energy required to form islands was different for each substrate domain, leading to the preferential formation of islands over the less energetically costly domain.

Another topographic technique to create a chemically patterned substrate was developed, using an off-cut silicon single crystal substrate.<sup>112,113</sup> In this technique, a one dimensional groove pattern is prepared from Si single crystal wafers miscut by a certain angles with respect to the (001) crystal plane. The period and amplitude of the grooves on the surface are determined by the miscut angle of the surface, the annealing temperature and time. The typical period and amplitude of the grooves are tens of nanometers and several nanometers respectively. The subsequent evaporation of metal atoms at a low incidence angle successfully generated a chemically and topographically modified nanoscale pattern substrate. The preferential wetting on each patterned domain and commensuration of substrate period and block copolymer period provided a vertically ordered lamellar microstructure of a PS/PMMA block copolymer.<sup>114</sup>

Theoretical predictions of block copolymer morphologies on chemically patterned substrates have also been made analytically and numerically.<sup>115-117</sup> With one dimensional striped patterns whose dimensions vary from a smaller to a larger length scale than the lamellar periodicity of a block copolymer, Chakrabarti et al. found that the morphology of the block copolymer thin film is strongly influenced by the commensurability between the bulk unconstrained lamellar periodicity and the period of the pattern. Various microdomain orientation was obtained with different combinations of the two factors.<sup>115,116</sup> In addition, Pereira et al. specifically modeled the case where a lamellar periodicity is larger than a width of striped pattern. The periodic striped surface induced a lamellar structure with unequal spacings and this striped potential developed an inverted

bilayers, i.e., an AB, AB pattern of AB diblock copolymer rather than the more usual AB, BA one.<sup>117</sup>

As opposed to chemically patterned substrates, topographically patterned substrates whose patterns consist of height variations on a chemically homogeneous non-crystalline substrate have also been fabricated to control the microdomain structures of block copolymers.<sup>118,119</sup> A one dimensional groove pattern, used for chemically modified pattern substrate previously<sup>114</sup> was prepared without the subsequent metal atom evaporation process to investigate the thickness effect of block copolymer thin film. The lamellar forming block copolymer thin film with two different film thicknesses (~ a half lamellar periodicity and less than a half lamellar periodicity in trough and peak regions respectively) overlaid on the patterned substrate exhibits a laterally patterned ordering.<sup>118</sup> Parallel and perpendicular orientation of lamellar microdomains with respect to the substrate were achieved in trough and peak regions respectively.<sup>118</sup>

Holographic method and subsequent chemical etching techniques<sup>120</sup> fabricated the silicon grating substrates with micron scale periodicity and various heights. PS/PVP block copolymer thin films with lamellar or cylindrical microdomain structure, cast and annealed on the patterned substrates, experienced the surface modulation of either in phase (conformal) or out of phase (anticonformal),<sup>121</sup> relying upon the periodicity of block copolymer microdomains with respect to the height of gratings.<sup>119</sup>

Recently Segalman et al. used a method “graphoepitaxy” with a topographically alternating mesa and well pattern to align spherical PVP microdomains of a PS/PVP block copolymer. Careful selection of material and pattern dimensions created a large area single crystal of the PVP spheres not only on the mesas but also on the wells.<sup>122</sup>

### 1.2.8 Summary

Various methods were presented to manipulate microdomain structures of block copolymers in bulk as well as in thin films. Mechanically driven flows such as shear, elongation and compression successfully created microdomain orientation in bulk. Temperature gradient and electric field were also utilized to align various types of microdomains. In thin films, the effect of thickness and/or surface interactions (substrate and superstrate) on microdomain orientation were extensively reviewed. In addition,

special block copolymers with multiple interactions such as liquid crystallization and crystallization were demonstrated for developing useful microdomain structures. Solvent control including evaporation rate, co-solvent was also a way for this purpose. Combination with lithographic techniques permitted better control of microdomain orientation. Chemically and/or topographically patterned substrates were used to alter microdomain orientation. The techniques mentioned in this section are summarized in Table 1.3. The next two sections will describe general background of new types of interactions such as eutectic directional solidification and epitaxy which are main topics of Part II in the thesis.

Interactions	Driving Forces	Methods	Characteristics	Type of Sample	Ref.
Mechanical Flow Fields	Shear and Elongation	Extrusion	Easy control, large sample	Bulk	1,2
	Shear	Rheometer	Easy control of parameters		3-34
	Compression	Channel Die	Simple apparatus		35-41
	Shear and Elongation	Roll Casting	Ordering from solution		42-52
Temperature Gradient	Temperature Gradient	Zone Refining Cell	High degree of orientation Slow process	Bulk	53,54
Electric Field	Dielectric Constant	In-Plane Vertical	Low degree orientation Lack of lateral orientation	Thin film and Bulk	55-61,63
	Commensurability	Thickness Control	Parallel/Vertical Lam. Cyl.	Thin film	64-93
Preferential Wetting	Confinement	Only parallel ordering			
Neutral Substrate	Random Copolymer	Vertical Lam. w/o lateral order			
Special Block Copolymers	Architecture	Spin Coating	Vertical Lam. w/o lateral order	Thin Films	101,102
	Liquid Crystallization		Vertical Lam. w/o lateral order		
	Crystallization and Wetting/Dewetting		Vertical Lam. w lateral order near wet./dewet. boundary		
Solvent Control	Evaporation Rate	Spin Coating	Vertical Cyl. w slow rate	Thin Films	105,106
	Prewetting		In-plane Cyl. near rims		
Patterned Substrates	Chemical Pattern	Soft Lithography	Vertical/parallel Lam.	Thin Films	110,111
	Combination of Both	Silicon Miscut/Metal Deposition	Vertical Lam.		
		Silicon Miscut	Vertical/parallel lamellae		
	Topographic Pattern	Holographic Pattern	Conformal/Anticonformal		
		Photolithography	Graphoepitaxy		

**Table 1.3:** Summary of techniques for controlling block copolymer microdomains



## 1.2.9 References

1. Folkes, M. J; Keller, A.; Scalisi, F. P. "An extrusion technique for the preparation of "single crystals" of block copolymers" *Colloid Polym. Sci.* **1973**, 251, 1.
2. Keller, A.; Pedemonte, E.; Willmouth, F. M. "Macro-lattice from segregated amorphous phases of a three block copolymer" *Nature* **1970**, 225, 538.
3. Skoulios, A. *J. Polym. Sci. Polym. Symp.* **1977** 58, 369.
4. Hadziioannou, G.; Mathis, A.; Skoulios, A. "Obtention de monocristaux de copolymères trisequences styrene/isoprene/styrene par cisaillement plan" *Colloid Polym. Sci.* **1979**, 257, 136.
5. Hadziioannou, G.; Mathis, A.; Skoulios, A. "Single crystals of triblock copolymer styrene/isoprene/styrene presenting cylinder structure. I. Study of orientation by small angle X ray diffraction" *Colloid Polym. Sci.* **1979**, 257, 15.
6. Okamoto, S.; Saijo, K.; Hashimoto, T. "Real time SAXS observations of lamella forming block copolymers under large oscillatory shear deformation" *Macromolecules* **1994**, 27, 5547.
7. Fredrickson, G. H. *J. Rheol.* **1994**, 38, 1045.
8. Morrison, F.; Bourvellec, G. L.; Winter, H. H. "Flow induced structure and rheology of a triblock copolymer" *J. Appl. Polym. Sci.* **1987**, 33, 1585.
9. Morrison, F. A; Winter, H. H. "Effect of unidirectional shear on the structure of triblock copolymers.1. polystyrene polybutadiene polystyrene" *Macromolecules* **1989**; 22: 3533.
10. Morrison, F. A; Winter, H. H; Gronski W.; Barnes, J. D. "Effect of unidirectional shear on the structure of triblock copolymers. 2. Polystyrene polyisoprene polystyrene" *Macromolecules* **1990**; 23: 4200.
11. Winey, K. I.; Patel, S. S.; Larson, R. G.; Watanabe, H. "Interdependence of shear deformations and block copolymer morphology" *Macromolecules* **1993**, 26, 2542.
12. Winey, K. I.; Patel, S. S.; Larson, R. G.; Watanabe, H. "Morphology of a lamellar diblock copolymer aligned perpendicular to the sample plane-transmission electron microscopy and small angle X ray scattering" *Macromolecules* **1993**, 26, 4373.
13. Kannan, R. M.; Kornfield, J. A. "Evolution of microstructure and viscoelasticity during flow alignment of a lamellar diblock copolymer" *Macromolecules* **1994**, 27, 1177.
14. Koppi, K. A.; Tirrell, M.; Bates, F. S.; Almdal, K.; Mortensen, K. "Epitaxial growth and shearing of the body centered cubic phase in diblock copolymer melts" *J Rheo* **1994**; 38: 999.
15. Patel, S. S.; Larson, R. G.; Winey, K. I.; Watanabe, H. "Shear orientation and rheology of a lamellar polystyrene-polyisoprene block copolymer" *Macromolecules* **1995**, 28, 4313.
16. Gupta, V. K.; Krishnamoorti, R.; Kornfield, J. A.; Smith, S. D. "Evolution of microstructure during shear alignment in a polystyrene polyisoprene lamellar diblock copolymer" *Macromolecules* **1995**, 28, 4464.
17. Gupta, V. K.; Krishnamoorti, R.; Kornfield, J. A.; Smith S. D. "Role of strain in controlling lamellar orientation during flow alignment of diblock copolymers" *Macromolecules* **1996**, 29, 1359.

18. Gupta, V. K.; Krishnamoorti, R.; Chen, Z-R.; Kornfield, J. A.; Smith, S. D.; Satkowski, M. M.; Grothaus, J. T. "Dynamics of shear alignment in a lamellar diblock copolymer: interplay of frequency, strain amplitude, and temperature" *Macromolecules* **1996**, *29*, 875.
19. Zhang, Y.M.; Wiesner, U.; Spiess, H. "Frequency dependence of orientation in dynamically sheared diblock copolymers" *Macromolecules*, **1995**, *28*, 778.
20. Zhang, Y.M.; Wiesner, U. "Symmetrical diblock copolymers under large amplitude oscillatory shear flow entanglement effect" *J. Chem. Phys.* **1995**, *103*, 4784.
21. Chen, Z-R; Issaian, A. M.; Kornfield, J. A.; Smith, S. D.; Grothaus, J. T.; Satkowski, M. M. "Pathways to macroscale order in nanostructured block copolymers" *Science* **1997**, *277*, 1248.
22. Chen, Z-R; Issaian, A. M.; Kornfield, J. A.; Smith, S. D.; Grothaus, J. T.; Satkowski, M. M. "Dynamics of shear induced alignment of a lamellar diblock: a rheo optical, electron microscopy and X-ray scattering study" *Macromolecules* **1997**, *30*, 7096.
23. Chen, Z-R; Kornfield, J. A. "Flow induced alignment of lamellar block copolymer melts" *Polymer*, **1998**, *39*, 4679.
24. Pinheiro, B. S.; Winey, K. I. "Mixed parallel-perpendicular morphologies in diblock copolymer systems correlated to the linear viscoelastic properties of the parallel and perpendicular morphologies" *Macromolecules* **1998**, *31*, 4447.
25. Polis, D. L.; Smith, S. D.; Terrill, N. J.; Ryan, A. J.; Morse, D. C.; Winey, K. I. "Shear induced lamellar rotation observed in a diblock copolymer by in situ small angle X ray scattering" *Macromolecules* **1999**, *32*, 4668.
26. Laurer, J. H.; Pinheiro, B. C.; Polis, D. L.; Winey, K. I. "Persistence of surface induced alignment in block copolymers upon large amplitude oscillatory shear processing" *Macromolecules* **1999**, *32*, 4999.
27. Vigild, M. E.; Almdal, K.; Mortensen, K.; Hamley, I. W.; Fairclough, J. P. A.; Ryan, A. J. "Transformations to and from the Gyroid Phase in a Diblock Copolymer" *Macromolecules* **1998**; *31*: 5702.
28. Wang, H.; Newstein, M. C.; Chang, M. Y.; Balsara, N. P.; Garetz, B. A. "Birefringence and depolarized light scattering of an ordered block copolymer melt under shear flow" *Macromolecules*, **2000**, *33*, 3719.
29. Mortensen, K.; Brown, W.; Norden, B. "Inverse melting transition and evidence of 3 dimensional cubatic structure in a block copolymer micellar system" *Phys. Rev. Lett.* **1992**, *68*, 2340.
30. Mortensen, K.; Pedersen J. S. "Structural study on the micelle formation of poly(ethylene oxide) poly(propylene oxide)poly(ethylene oxide) triblock copolymer in aqueous solution" *Macromolecules*, **1993**, *26*, 805.
31. Pople, J. A.; Hamley, I. W.; Fairclough, J. P. A.; Ryan, A. J.; Booth, C. "Orientational ordering of a poly(oxyethylene)-poly(oxybutylene) diblock copolymer gel under steady shear flow" *Macromolecules* **1998**, *31*, 2952.
32. Hamley, I. W.; Pople, J. A.; Fairclough, J. P. A.; Ryan, A. J.; Booth, C.; Yang Y. W. "Shear induced orientational transitions in the body centered cubic phase of a diblock copolymer gel" *Macromolecules* **1998**, *31*, 3906.
33. Daniel, C.; Hamley, I. W.; Mingvanish, W.; Booth C. "Effect of shear on the face centered cubic phase in a diblock copolymer gel" *Macromolecules* **2000**, *33*, 2163.

34. Osuji, C.; Zhang, Y. M.; Mao, G. P.; Ober, C.; Thomas E. L. "Transverse cylindrical microdomain orientation in an LC diblock copolymer under oscillatory shear" *Macromolecules* **1999**, *32*, 7703-7706.
35. Pakula, T.; Saijo, K.; Kawai, H.; Hashimoto, T. "Deformation behavior of styrene butadiene styrene triblock copolymer with cylindrical morphology" *Macromolecules* **1985**, *18*, 1294.
36. Yamaoka, I.; Kimura, M. "Effects of morphology on mechanical properties of a SBS triblock copolymer" *Polymer* **1993**, *34*, 4399.
37. Douzinas, K.C.; Cohen, R.E.: "Chain folding in EBEE semicrystalline diblock copolymers": *Macromolecules* **1992**, *25*, 5030.
38. Kofinas, P.; Cohen, R.E.: "Morphology of highly textured poly(ethylene)/poly(ethylene-propylene) (E/EP) semicrystalline diblock copolymers." *Macromolecules* **1994**, *27*, 3002.
39. Cohen, R.E.; Bellare, A.; Drzewinski, M.A.: "Spatial organization of polymer chains in a crystallizable diblock copolymer of polyethylene and polystyrene." *Macromolecules* **1994**, *27*, 2321.
40. Kofinas, P.; Cohen, R. E. "Melt processing of semicrystalline E/EP/E triblock copolymers near the order-disorder transition" *Macromolecules* **1995**, *28*, 336.
41. Quiram, D. J.; Register, R. A.; Marchand, G. R.; Adamson, D. H. "Chain orientation in block copolymers exhibiting cylindrically confined crystallization" *Macromolecules* **1998**, *31*, 4891.
42. Albalak, R. J.; Thomas, E. L. "Microphase separation of block copolymer solutions in a flow field" *J Polym Sci Part B Polym Phys* **1993**; *32*: 37.
43. Albalak, R. J.; Thomas, E. L. "Roll casting of block copolymers and of block copolymer homopolymer blends" *J Polym Sci Part B Polym Phys* **1994**; *32*: 341
44. Albalak, R. J.; Thomas, E. L.; Capel, M. S. "Thermal annealing of roll cast triblock copolymer films" *Polymer* **1997**; *38*: 3819.
45. Honeker, C. C.; Thomas, E. L. "Impact of morphological orientation in determining mechanical properties in triblock copolymer systems" *Chem. Mater.* **1996**, *8*, 1702.
46. Prasman, E.; Thomas, E. L. "High-strain tensile deformation of a sphere-forming triblock copolymer mineral oil blend" *J Polym Sci Part B Polym Phys* **1998**; *36*: 1625.
47. Dair, B. J.; Avgeropoulos, A.; Hadjichristidis, N.; Honeker, C. C.; Capel, M.; Thomas, E. L. "Oriented double gyroid films via roll casting" *Polymer* **2000** *41* 6231.
48. Dair, B. J.; Honeker, C. C.; Alward, D. B.; Avgeropoulos, A.; Hadjichristidis, N.; Fetters, L. J.; Capel, M.; Thomas, E. L. "Mechanical properties and deformation behavior of the double gyroid phase in unoriented thermoplastic elastomers" *Macromolecules* **1999**, *32*, 8145.
49. Cohen, Y.; Albalak, R. J.; Dair, B. J.; Capel, M. S.; Thomas, E. L. "Deformation of oriented lamellar block copolymer films" *Macromolecules*, **2000**, *33*, 6502.
50. Park, C.; Simmons, S.; Fetters, L. J.; Hsiao, B.; Yeh, F.; Thomas E. L. "Spherical to cylindrical microdomain transformation by application of a flow field" *Polymer* **2000**, *41*, 2971.
51. Park, C.; De Rosa, C.; Fetters, L. J.; Thomas E. L. "Influence of an oriented glassy cylindrical microdomain structure on the morphology of crystallizing lamellae in a semicrystalline block terpolymer" *Macromolecules* **2000**, *33*, 7931.

52. Ha S. and Thomas, E. L. Unpublished data
53. Hashimoto, T.; Bodycomb, J.; Funaki, Y.; Kimishima, K. "The effect of temperature gradient on the microdomain orientation of diblock copolymers undergoing an order-disorder transition" *Macromolecules* **1999**, *32*, 952.
54. Hashimoto, T.; Bodycomb, J.; Funaki, Y.; Kimishima, K. "Single grain lamellar microdomain from a diblock copolymer" *Macromolecules* **1999**, *32*, 2075.
55. Amundson, K.; Helfand, E.; Davis, D. D.; Quan, X.; Patel, S.; Smith, S. D. "Effect of an electric field on block copolymer microstructure" *Macromolecules* **1991**; *24*:6546.
56. Amundson, K.; Helfand, E.; Davis, D. D.; Quan, X.; Smith, S. D. "Alignment of lamellar block copolymer microstructure in an electric field. 1.alignment kinetics" *Macromolecules* **1993**; *26*: 2698.
57. Amundson, K.; Helfand, E.; Davis, D. D.; Quan, X.; Hudson, S. D.; Smith, S. D. "Alignment of lamellar block copolymer microstructure in an electric field. 2.mechanisms of alignment" *Macromolecules* **1994**; *27*: 6559.
58. Gurovich, E. "Copolymers under a monomer oriented field" *Macromolecules* **1994**, *27*, 7063.
59. Morkved, T. L.; Lu, M.; Urbas, A. M.; Ehrichs, E. E.; Jaeger, H. M.; Mansky, P.; Russel, T. P. "Local control of microdomain orientation in diblock copolymer thin films with electric fields" *Science* **1996**, *273*, 931.
60. Mansky, P.; DeRouchey, J.; Russell, T. P.; Mays, J.; Pitsilalis, M.; Morkved, T.; Jaeger, H. "Large area domain alignment in block copolymer thin films using electric fields" *Macromolecules* **1998**, *31*, 4399.
61. Thurn-Albrecht, T.; DeRouchey, J.; Russell, T. P.; Jaeger, H. M. "Overcoming interfacial interactions with electric fields" *Macromolecules* **2000**, *33*, 3250.
62. Xi, K.; Krause, S. "Droplet deformation and structure formation in two-phase polymer/polymer/toluene mixtures in an electric field" *Macromolecules* **1998**; *31*: 3974.
63. Schaffer, E.; Thurn-Albrecht, T.; Russell, T. P.; Steiner U. "Electronically induced structure formation and pattern transfer" *Nature*, **2000**, *403*, 874.
64. Matsen, M. W. "Self assembly of block copolymers in thin films" *Curr. Opin. Colloid Interface Sci.* **1998**, *3*, 40.
65. Henke, S. S.; Thomas, E. L.; Fetters L. J. "Effect of surface constraints on the ordering of block copolymer domains" *J. Mat. Sci.* **1988**, *23*, 1685.
66. Anastasiadis, S. H.; Russell, T. P.; Satija, S. K.; Majkrzak, C. F. "The morphology of symmetric diblock copolymers as revealed by neutron reflectivity" *J. Chem. Phys.* **1990**, *92*, 5677.
67. Coulon, G.; Deline, V. R.; Russell, T. P.; Green, P. F. "Surface induced orientation of symmetric, diblock copolymers: a secondary ion mass spectrometry study" *Macromolecules* **1989**, *22*, 2581.
68. Anastasiadis, S. H.; Russell, T. P.; Satija, S. K.; Majkrzak, C. F. "Neutron reflectivity studies of the surface induced ordering of diblock copolymer films" *Phys. Rev. Lett.* **1989**, *62*, 1852.
69. Collin, B.; Chatenay, D.; Coulon, G.; Ausserre, D.; Gallot, Y. "Ordering of copolymer thin films as revealed by atomic force microscopy" *Macromolecules* **1992**, *25*, 1621.

70. Russell, T. P.; Coulon, G.; Deline, V. R.; Miller, D. C. "Characteristics of the surface induced orientation for symmetric diblock PS/PMMA copolymers" *Macromolecules* **1989**, *22*, 4600.
71. Russell, T. P.; Menelle, A.; Anastasiadis, S. H.; Satija, S. K.; Majkrzak C. F. "Unconventional morphologies of symmetric, diblock copolymers due to film thickness constrains" *Macromolecules* **1991**, *24*, 6269.
72. Coulon, G.; Dailant, J.; Collin, B.; Benattar, J. J.; Gallot, Y. "Time evolution of the free surface of ultrathin copolymer films" *Macromolecules* **1993**, *26*, 1582.
73. Mayes, A. M.; Russell, T. P.; Bassereau, P.; Baker, S. M.; Smith G. S. "Evolution of order in thin block copolymer films" *Macromolecules* **1994**, *27*, 749.
74. Carvalho, B. L.; Thomas, E. L. "Morphology of steps in terraced block copolymer films" *Phys. Rev. Lett.* **1994**, *73*, 3321.
75. Fasolka, M. J.; Banerjee, P.; Mayes, A. M.; Pickett, G.; Balazs, A. C. "Morphology of ultrathin supported diblock copolymer films: Theory and experiment" *Macromolecules* **2000**, *33*, 5702.
76. Lambooy, P.; Russell, T. P.; Kellogg, G. J.; Mayes, A. M.; Gallagher, P. D.; Satija, S. K. "Observed frustration in confined block copolymers" *Phys. Rev. Lett.* **1994**, *72*, 2899.
77. Koneripalli, N.; Singh, M.; Levicky, R.; Bates, F. S.; Gallagher, P. D.; Satija, S. K. "Confined block copolymer thin films" *Macromolecules* **1995**, *28*, 2897.
78. Kellogg, G. J.; Walton, D. G.; Mayes, A. M.; Lambooy, P.; Russell, T. P.; Gallagher, P. D.; Satija, S. K. "Observed surface energy effects in confined diblock copolymers" *Phys. Rev. Lett.* **1996**, *76*, 2503.
79. Koneripalli, N.; Levicky, R.; Bates, F. S.; Ankner, J.; Kaiser, H.; Satija, S. K. "Confinement induced morphological changes in diblock copolymer films" *Langmuir* **1996**, *12*, 6681.
80. Turner, M. S. "Equilibrium properties of a diblock copolymer lamellar phase confined between flat plates" *Phys. Rev. Lett.* **1992**, *69*, 1788.
81. Shull, K. R. "Mean field theory of block copolymers: bulk, melts, surfaces, and thin films" *Macromolecules*, **1992**, *25*, 2122.
82. Kikuchi, M.; Binder, K. "Microphase separation in thin films of the symmetric diblock-copolymer melt" *J. Chem. Phys.* **1994**, *101*, 3367.
83. Pickett, G. R.; Witten, T. A.; Nagel S. R. "Equilibrium surface orientation of lamellae" *Macromolecules* **1993**, *26*, 3194.
84. Walton, D. G.; Kellogg, G. J.; ; Mayes, A. M.; Lambooy, P; Russell, T. P. "A free energy model for confined diblock copolymers" *Macromolecules*, **1994**, *27*, 6225.
85. Pickett, G. T.; Balazs, A. C. "Equilibrium orientation of confined diblock copolymer films" *Macromolecules* **1997**, *30*, 3097.
86. Matsen, M. W. "Thin films of block copolymer" *J. Chem. Phys.* **1997**, *106*, 7781.
87. Tang, W. H.; Witten T. A. "Quenched degrees of freedom in symmetric diblock copolymer thin films" *Macromolecules* **1998**, *31*, 3130.
88. Liu, Y.; Zhao, W.; Zheng, X.; King; A.; Singh, A.; Rafailovich, M. H.; Sokolov, J.; Dai, K. H.; Kramer, E. J.; Schwarz, S. A.; Gebizlioglu, O.; Sinha, S. K. "Surface induced ordering in asymmetric block copolymers" *Macromolecules* **1994**, *27*, 4000.
89. Turner, M. S.; Rubinstein, M.; Marques, C. M. "Surface induced lamellar ordering in a hexagonal phase of diblock copolymers" *Macromolecules* **1994**, *27*, 4986.

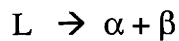
90. van Dijk, M. A.; van den Berg R. "Ordering phenomena in thin block copolymer films studied using atomic force microscopy" *Macromolecules* **1995**, 28, 6773.
91. Suh, K. Y.; Kim, Y. S.; Lee, H. H. "Parallel and vertical morphologies in block copolymers of cylindrical domain" *J. Chem. Phys.* **1998**, 108, 1253.
92. Huinink, H. P.; Brokken-Zijp, J. C. M.; van Dijk, M. A.; Sevink, G. J. A. "Asymmetric block copolymers confined in a thin film" *J. Chem. Phys.* **2000**, 112, 2452.
93. Konrad, M.; Knoll, A.; Krausch, G.; Maglerle, R. "Volume imaging of an ultrathin SBS triblock copolymer film" *Macromolecules* **2000**, 33, 5518.
94. Mansky, P.; Russell, T. P.; Hawker, C. J.; Pitsikalis, M.; Mays J.; "Ordered diblock copolymer films on random copolymer brushes" *Macromolecules* **1997**, 30, 6810.
95. Mansky, P.; Liu, Y.; Huang, E.; Russell, T. P.; Hawker, C. "Controlling polymer surface interactions with random copolymer brushes" *Science* **1997**, 275, 1458.
96. Huang, E.; Russell, T. P.; Harrison, C.; Chaikin, P. M.; Register, R. A.; Hawker, C. J.; Mays, J. "Using surface active random copolymers to control the domain orientation in diblock copolymer thin films" *Macromolecules* **1998**, 31, 7641.
97. Huang, E.; Rockford, L.; Russell, T. P.; Hawker, C. J. "Nanodomain control in copolymer thin films" *Nature* **1998**, 395(6704), 757.
98. Huang, E.; Pruzinsky, S.; Russell, T. P.; Mays, J.; Hawker, C. J. "Neutrality conditions for block copolymer systems on random copolymer brush surfaces" *Macromolecules* **1999**, 32, 5299.
99. Huang, E.; Mansky, P.; Russell, T. P.; Harrison, C.; Chaikin, P. M.; Register, R. A.; Hawker, C. J.; Mays, J. "Mixed lamellar films: evolution, commensurability effects, and preferential defect formation" *Macromolecules* **2000**, 33, 80.
100. Harrison, C.; Chaikin, P. M.; Huse, D. A.; Register, R. A.; Adamson, D. H.; Daniel, A.; Huang, E.; Mansky, P.; Russell, T. P.; Hawker, C. J.; Egolf, D. A.; Melnikov, I. V.; Bodenschatz, E. "Reducing substrate pinning of block copolymer microdomains with a buffer layer of polymer brushes" *Macromolecules* **2000**, 33, 857.
101. Stocker, W.; Bechmann, J.; Stadler, R.; Rabe, J. P. "Surface reconstruction of the lamellar morphology in a symmetric poly(styrene-*b*-butadiene-*b*-methylmethacrylate) triblock copolymer: a tapping mode scanning force microscope study" *Macromolecules* **1996**, 29, 7502.
102. Stocker, W. "Lamellar orientation at the surface of thin block copolymer films" *Macromolecules* **1998**, 31, 5536.
103. Wang, G. C. L.; Commandeur, J.; Fischer, H.; de Jeu, W. H. "Orientational wetting in hybrid liquid crystalline block copolymers" *Phys. Rev. Lett.* **1996**, 77, 5221.
104. Reiter, G.; Castelein, G.; Hoerner, P.; Riess, G.; Blumen, A.; Sommer, J. "Nanometer scale surface patterns with long range order created by crystallization of diblock copolymers" *Phys. Rev. Lett.* **1999**, 83, 3844.
105. Kim, G.; Libera M. "Morphological development in solvent cast polystyrene polybutadiene polystyrene (SBS) triblock copolymer thin film" *Macromolecules* **1998**, 31, 2569.
106. Fukunaga, K.; Elbs, H.; Maerle, R.; Krausch, G. "Large scale alignment of ABC block copolymer microdomains via solvent vapor treatment" *Macromolecules* **2000**, 33, 947.

107. Hahm, J.; Sibener, S. J. "Cylinder alignment in annular structure of microphase separated polystyrene b poly(methylmethacrylate)" *Langmuir* **2000**, 16, 4766.
108. Kumar, A.; Whitesides, G. M. "Features of gold having micrometer to centimeter dimensions can be formed through a combination of stamping with an elastomeric stamp and an alkanethiol ink followed by chemical etching" *Appl. Phys. Lett.* **1993**, 63, 2002.
109. Xia, Y.; Whitesides, G. M. "Soft lithography" *Annu. Rev. Mater. Sci.* **1998**, 28, 153.
110. Heier, J.; Kramer, E. J.; Walheim, S.; Krausch, G. "Thin diblock copolymer films on chemically heterogeneous surfaces" *Macromolecules* **1997**, 30, 6610.
111. Heier, J.; Genzer, J.; Kramer, E. J.; Bates, F. S.; Krausch, G. "Transfer of a chemical substrate pattern into an island forming diblock copolymer film" *J. Chem. Phys.* **1999**, 111, 11101.
112. Song, S.; Mochrie, S. G. J. "Attractive step interactions, tricriticality and faceting in the orientational phase diagram of silicon surfaces between [113] and [114]" *Phys. Rev. B* **1995**, 51, 10068.
113. Song, S.; Mochrie, S. G. J.; Stephenson, G. B. "Faceting kinetics of stepped Si(113) surfaces- a time resolved X ray scattering study" *Phys. Rev. Lett.* **1995**, 74, 5240.
114. Rockford, L.; Liu, Y.; Mansky, P.; Russell, T. P. "Polymers on nanopericodic, heterogeneous surfaces" *Phys. Rev. Lett.* **1999**, 82, 2602.
115. Chakrabarti, A.; Chen, H. "Block copolymer films on patterned surfaces" *J. Polym. Sci. Polym. Phys.* **1998**, 36, 3127.
116. Brown, G.; Chakrabarti, A. *J. Chem. Phys.* **1995**, 102, 1440
117. Pereira, G. G.; Williams, D. R. M. "Diblock copolymer thin films on heterogeneous striped surfaces: commensurate, incommensurate and inverted lamellae" *Phys. Rev. Lett.* **1998**, 80, 2849..
118. Fasolka, M. J.; Harris, D. J.; Mayes, A. M.; Yoon, M.; Mochrie, S. G. J. "Observed substrate topography mediated lateral patterning of diblock copolymer films" *Phys. Rev. Lett.* **1997**, 79, 3018.
119. Li, Z.; Qu, S.; Rafailovich, M. H.; Sokolov, J.; Tolan, M.; Turner, M. S.; Wang, J.; Schwarz, S. A.; Lorenz, H.; Kotthaus, J. P. "Confinement of block copolymers on patterned surfaces" *Macromolecules*, **1997**, 30, 8410.
120. Hansen, W.; Kotthaus, J. P.; Merkt, U. *Semiconductors and Semimetals 35; Nanostructured Systems; Academic Press, Inc.: New York, 1992*, p279.
121. Turner, M. S.; Joanny, J. F. "Diblock copolymer lamellae at rough surfaces" *Macromolecules*, **1992**, 25, 6681.
122. Segalman, R. A.; Yokoyama, H.; Kramer, E. J. *Advanced Materials* submitted.

## 1.3 New Approaches

### 1.3.1 Eutectic directional solidification

The word eutectic is derived from the Greek and means 'most fusible'. A typical binary phase diagram with a eutectic transformation is given in Figure 1.3a. Two distinctive features characterize the diagram: (i) there is complete miscibility in the liquid state and incomplete miscibility in the solid state; (ii) the slopes of both pairs of liquidus and solidus lines are negative, taking the pure materials as reference points. In the diagram, there are two solid solutions formed from the liquid, one rich in A and the second rich in B (denoted  $\alpha$  and  $\beta$  respectively). The liquidus lines meet at E, the composition of the equilibrium eutectic. At this composition, two phases separate from the liquid. At  $T_E$ , the equilibrium is a unique one between the L,  $\alpha$  and  $\beta$  phases. It is expressed as:



below  $T_E$  the equilibrium is between solid phases  $\alpha$  and  $\beta$ .

A variety of microstructures exists in eutectic alloys. Generally, these complicated microstructures are categorized into 3 different groups.<sup>1</sup>

(i) Continuous microstructures. Continuous in this sense means that both phases can be traced along some unbroken path from the beginning of the solidification process to the region of its completion, i.e. both phases are continuous along the growth direction. The lamellar structures and the rod-like structures fulfill this criterion. There are few discontinuous lamellae that result from 'faulted' regions or 'mismatched' surfaces which give the impression that the lamellae have undergone a shearing movement normal to their length.

(ii) Discontinuous microstructures. In this group, one of the phases of the alloy is dispersed in the second phase as discrete particles, and there is no continuity of one phase in any direction. Probably the outstanding example of this type of structure is the Al-Si eutectic system, in which the silicon is finely dispersed in the aluminium matrix.

(iii) Spiral structures. Only a few examples of this type are known. Mg-Zn eutectic alloys show hexagonal spirals.



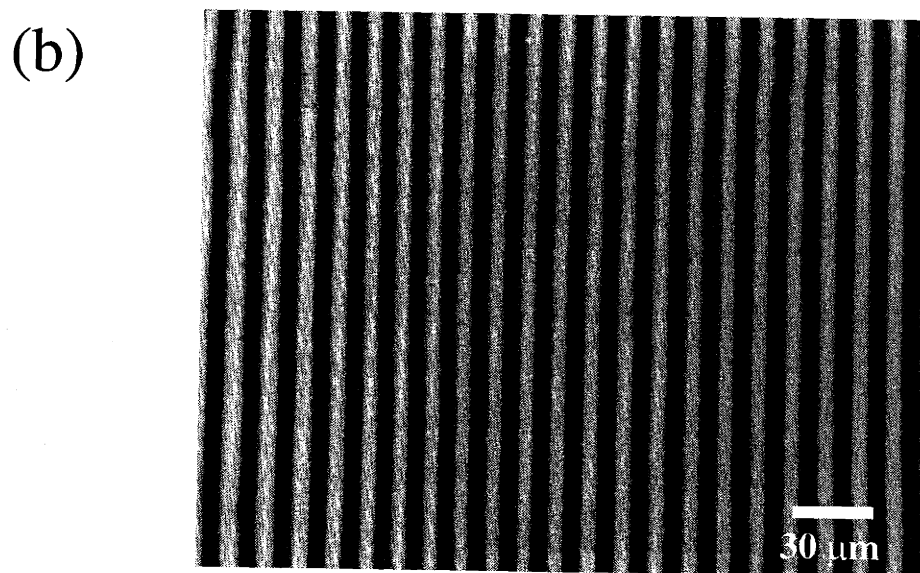
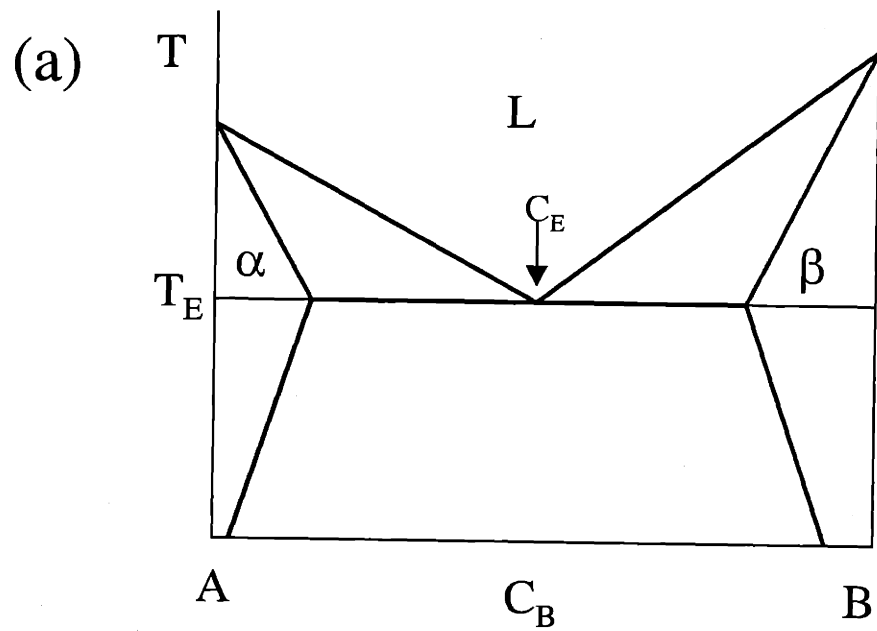
These finely structured composites can be used in a variety of applications, for example, as high-temperature materials or as superconductors.<sup>2</sup> In addition, similarly appearing composite structure can be made in alloys of noneutectic composition, thus permitting control to be exercised over the volume fraction of constituents present.

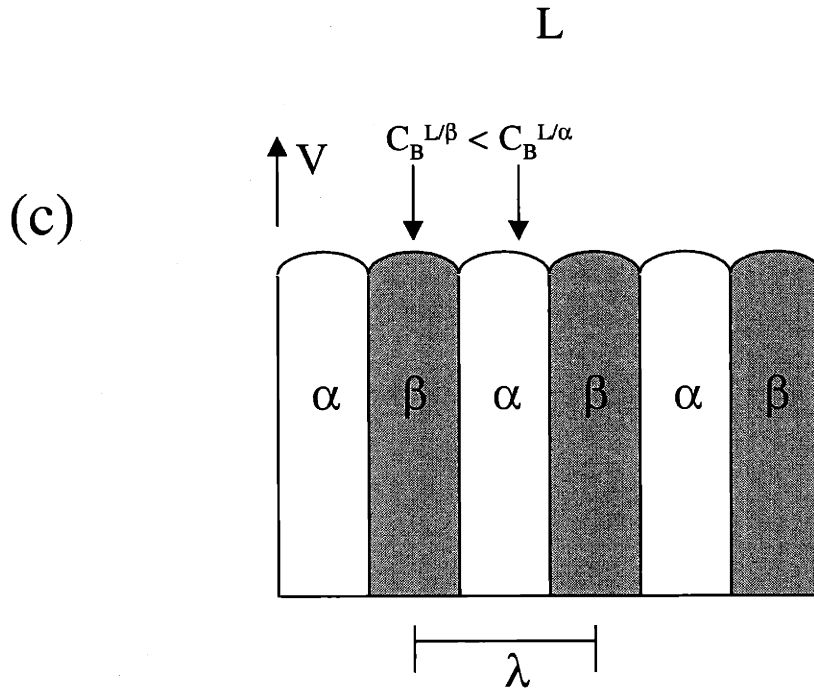
The common, lamellar eutectic microstructures are reviewed in the next section.

### **1.3.1.1 Lamellar eutectics**

An experimental example and a schematic drawing representing the growth of a lamellar eutectic alloy are given in Figure 1.3b and c respectively.<sup>3</sup>

The first theory of lamellar eutectic solidification appears to have been given by Tammann<sup>4</sup> (1908), who proposed that the two phases crystallized alternately; first a plate of one of the phases would grow, enrich the adjacent liquid in the second component, which would then nucleate and grow on the surface of the first phase, and so on. The solidification of the eutectic crystal was thus envisaged as the progressive build up of alternate lamellae. Vogel<sup>5</sup> (1912) expressed a different opinion of the growth mechanism, as he considered that the eutectic alloy of Cd-Zn solidified by the simultaneous crystallization of both phases. Lamplough and Scott<sup>6</sup> (1914) repeated Vogel's experiments and supported Vogel's view of simultaneous growth of the two phases, and also observed that increasing the growth rate (larger undercooling) led to a finer eutectic structure. Staumanis and Brakss<sup>7</sup> (1935) later verified that the mechanism of growth of lamellar eutectic alloys was by the simultaneous edgewise growth of both phases by conducting experiments in which the heat flow direction was controlled.





**Figure 1.3** (a) Hypothetical schematic phase diagram of A/B mixtures. See the text for detailed definitions of parameters (b) Optical micrograph of directionally solidified Pb/Cd crystals. Alloy Pb/Cd forms a eutectic structure with the composition of 17.4 wt% of Pb. (c) Schematic diagram of advancing front of directionally solidified  $\alpha/\beta$  eutectic crystals.

The average composition of the solid is exactly the same as the composition of the liquid from which it freezes, although the component phases  $\alpha$  and  $\beta$  of the solid can be of widely different compositions. During solidification the  $\alpha$  phase rejects atoms of B and the  $\beta$  phase rejects atoms of A. Under steady state growth conditions, the rate of rejection of B atoms by the  $\alpha$  phase is equal to the rate of rejection of A atoms by the  $\beta$  phase. For any particular growth rate, lateral concentration gradients are set up ahead of the interface in Figure 1.1c to give the required amount of diffusion of the two species of atoms to stabilize the steady state interlamellar spacing.

The following development is based on the Chapter 4 “Solidification” of Porter and Esterling’s book “Phase transformations in metals and alloys”.

For an interlamellar spacing,  $\lambda$ , there is a total of  $(2/\lambda)$  m<sup>2</sup> of  $\alpha/\beta$  interface per m<sup>3</sup> of eutectic. Thus the free energy change<sup>8</sup> associated with the solidification of 1 mol of liquid is given by

$$\Delta G(\lambda) = -\Delta G(\infty) + \frac{2\gamma_{\alpha\beta}V_m}{\lambda} \dots\dots\dots(1.1)$$

where  $V_m$  is the molar volume of the eutectic and  $\Delta G(\infty)$  is the free energy decrease for very large values of  $\lambda$ . Since solidification will not take place if  $\Delta G(\lambda)$  is positive,  $\Delta G(\infty)$  must be large enough to compensate for the interfacial energy term, i.e. the eutectic/liquid interface must be undercooled below the equilibrium eutectic temperature  $T_E$ . If the total undercooling is  $\Delta T_0$  it can be shown that  $\Delta G(\infty)$  is then given approximately by

$$\Delta G(\infty) = \frac{\Delta H \Delta T_0}{T_E} \dots\dots\dots(1.2)$$

where  $\Delta H$  is an enthalpy term. The minimum possible spacing ( $\lambda^*$ ) is obtained by using the relation  $\Delta G(\lambda^*) = 0$ , whence

$$\lambda^* = \frac{2\gamma_{\alpha\beta}V_mT_E}{\Delta H \Delta T_0} \dots\dots\dots(1.3)$$

When the eutectic has this spacing the free energy of the liquid and solid eutectic is the same, i.e. all three phases are in equilibrium. In order to balance the interfacial tension at the  $\alpha/\beta/L$  interface, interface,  $\alpha/L$  and  $\beta/L$  interfaces have appropriate curvature resulting in increase of total free energy.

If solidification is to occur at a finite rate there must be a flux of atoms between the tips of the  $\alpha$  and  $\beta$  lamellae and this requires a finite composition difference. For example, the concentration of B must be higher ahead of the  $\alpha$  phase than ahead of the  $\beta$  phase so that B rejected from the  $\alpha$  layer can diffuse to the tips of the growing  $\beta$ . If  $\lambda =$

$\lambda^*$  growth will be infinitely slow because the liquid in contact with both phases has the same composition,  $C_E$  in Figure 1.1a. However if the spacing is greater than  $\lambda^*$  the interfacial energy is lower. Under these circumstances the liquid in local equilibrium with the  $\alpha$  has a composition  $C_B^{L\alpha}$  which is richer in B than the composition in equilibrium with the  $\beta$  phase,  $C_B^{L\beta}$ . (see Figure 1.3c)

### 1.3.1.2 Polymer diluent eutectics

Eutectic-like behavior has been also observed in polymer-diluent binary mixtures. In addition to the two classical conditions required for the existence of a eutectic as explained in the previous section, the Flory-Huggins theory of freezing point depression in concentrated polymer solutions predicts a well defined eutectic point if the melting temperatures of both polymer and diluent are close together. However, since the kinetically induced folded chain polymer crystals have lower dissolution temperatures in comparison with the thermodynamically more stable extended chain polymer crystals, solvent-polymer eutectics are experimentally found at compositions and temperatures that deviate markedly from those predicted from thermodynamics.

Calculation of the liquidus curves for both solvent and polymer was made using the simplified Flory-Huggins lattice model. The liquidus curves are given by<sup>9-14</sup>

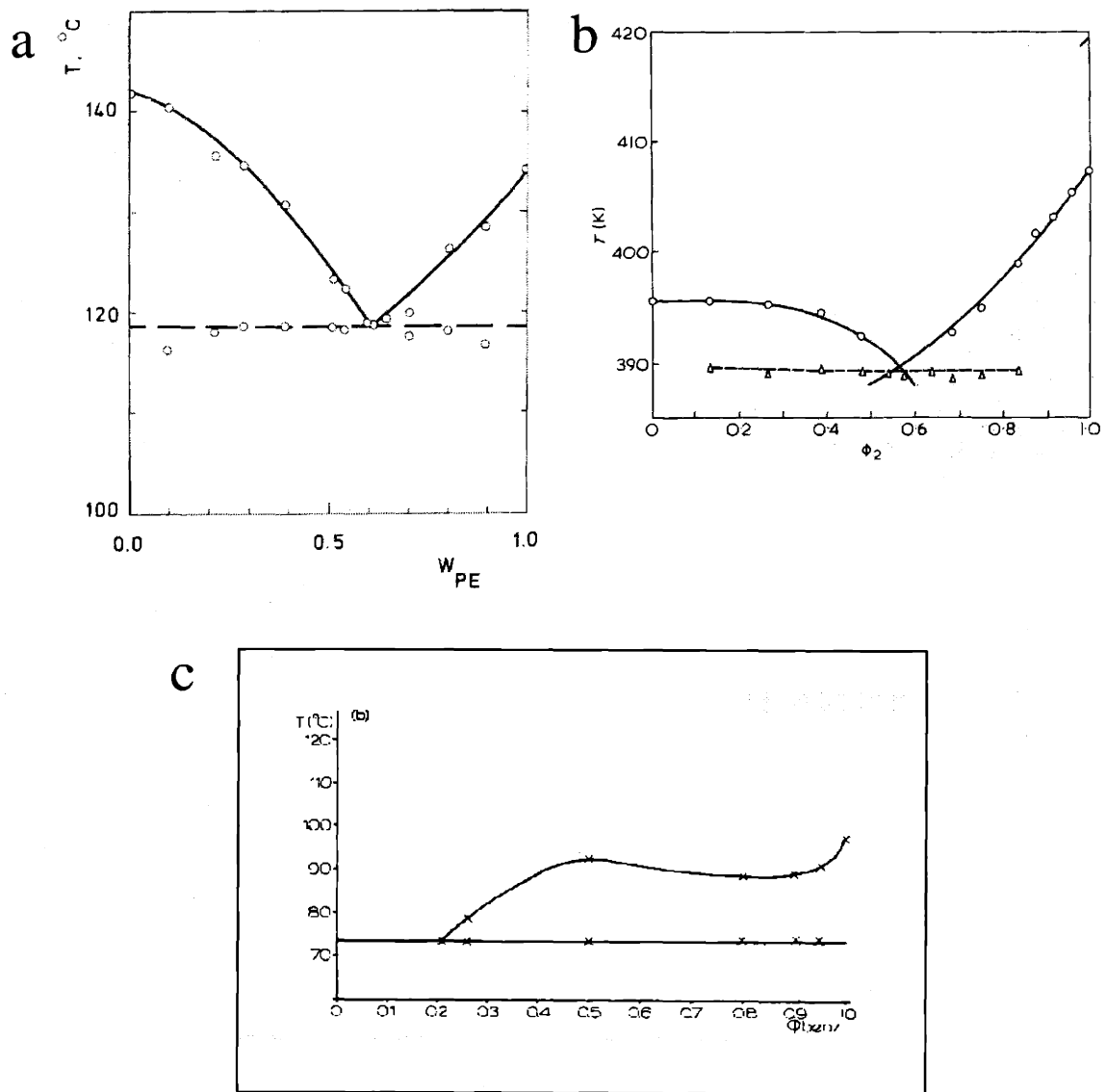
$$\frac{1}{T} - \frac{1}{T_1} = \frac{R}{\Delta H_1} [\ln \phi_1 + 1 - \phi_1 + \chi(1 - \phi_1)^2] \dots \dots \dots (1.4)$$

$$\frac{1}{T} - \frac{1}{T_2} = \frac{R}{\Delta H_2} \frac{V_2}{V_1} [-\phi_1 + \chi\phi_1^2] \dots \dots \dots (1.5)$$

where  $T_1$  and  $T_2$  are the melting temperatures of the solvent and the polymer respectively, and  $\Delta H_1$  and  $\Delta H_2$  are the heat of fusion of the solvent and the polymer respectively. Additionally  $\phi_1$  is a volume fraction of solvent and  $V_1$  and  $V_2$  are the molar volumes of the solvent and the polymer.  $\chi$  is the usual Flory-Huggins interaction parameter between the solvent and the polymer.

Eutectic crystallization in polymeric systems was at the first time studied by Smith and Pennings not only to achieve unique physical mechanical properties but also to

obtain information about the solidification mechanism. They found that the mixtures of polyethylene and 1,2,4,5-tetrachlorobenzene form a pseudo-eutectic solid with a melting point depressed by about 15 °C compared with that of the pure polymer.<sup>9,10</sup> Similar results were obtained by Wittmann and St. John Manley for other polymer-solvent eutectic systems, namely poly( $\epsilon$ -caprolactone)-trioxane, polyethylene oxide (PEO)-trioxane and polyethylene-1,3,5, tribromobenzene.<sup>11-13</sup> They also observed that in the hypoeutectic mixtures, the polymer crystals deposit epitaxially on the freshly grown diluent crystal surfaces, thus providing the examples of polymer epitaxy on organic substrates. Experimental phase diagrams of polyethylene and 1,2,4,5-tetrachlorobenzene and polyethylene-1,3,5, tribromobenzene mixtures obtained by differential scanning calorimetry (DSC) are shown in Figure 1.4 a and b.<sup>10,13</sup> The problems from the polydispersity and chain folding of polymer molecules hindering the formation of pure binary mixture and polymer diffusion respectively were addressed by Dorset et al. using monodisperse low molecular paraffin-n-hexatriacontane with organic solvents.<sup>14</sup> Anthracene, naphthalene, acridine and benzoic acid formed eutectic structures with paraffin and those eutectics were interpreted with various theoretical models.<sup>14</sup> In particular the paraffin-benzoic acid system clearly showed eutectic behavior which is closely related to this thesis. Experimental phase diagram of this system obtained by DSC is shown in Figure 1.4 c.<sup>14</sup>



**Figure 1.4** Experimental phase diagrams of (a) PE/1,2,4,5-tetrachlorobenzene, (b) PE/1,3,5-tribromobenzene and (c) paraffin ( $\text{nC}_{36}\text{H}_{74}$ )/benzoic acid determined by DSC. All diagrams show eutectic points.

### 1.3.1.3. Block copolymer diluent eutectics

The presence of solvent in a noncrystalline A/B block copolymer depresses the order-disorder temperature of block copolymer in certain ways depending on the solvent quality. In spite of diversity of theories to explain the phase behaviors of block copolymer-organic solvent mixtures, in general those agree with the depression of order-disorder transition (ODT) with solvent.<sup>15-17</sup> For example, in the simplest theory, the so-called dilution approximation, the primary role of added nonselective good solvent is to reduce the number of unfavorable A-B monomer contacts in a spatially uniform manner. The order-disorder transition is then given by<sup>15</sup>

$$(\phi_2 \chi N)_{ODT} = F(f) \dots \dots \dots (1.6)$$

where  $\phi_2$  is total polymer volume fraction and  $f$  is the volume fraction of one of the blocks and  $F$  is a weak function of  $f$ .

Since  $\chi$  is inversely proportional to  $T$ , the ODT temperature of block copolymer is predicted to decrease linearly with solvent concentration.

The freezing temperatures of organic diluents drop when they are mixed with block copolymers.<sup>18</sup> Bates et al.<sup>18</sup> demonstrated that the addition of a poly(ethylene oxide) (PEO)-*b*-poly(styrene) (PS) copolymer to a crystalline 2-chloro-4-nitroaniline (CNA) resulted in the freezing temperature depression of CNA. Selective partitioning of CNA into the polar PEO microdomains created a crystalline molecular complex, comprising two ethylene oxide repeat units per one CNA ( $\alpha$  phase). The phase diagram exhibits a eutectic point at approximately 40 % CNA between PEO crystalline phase and  $\alpha$  phase.<sup>18</sup>

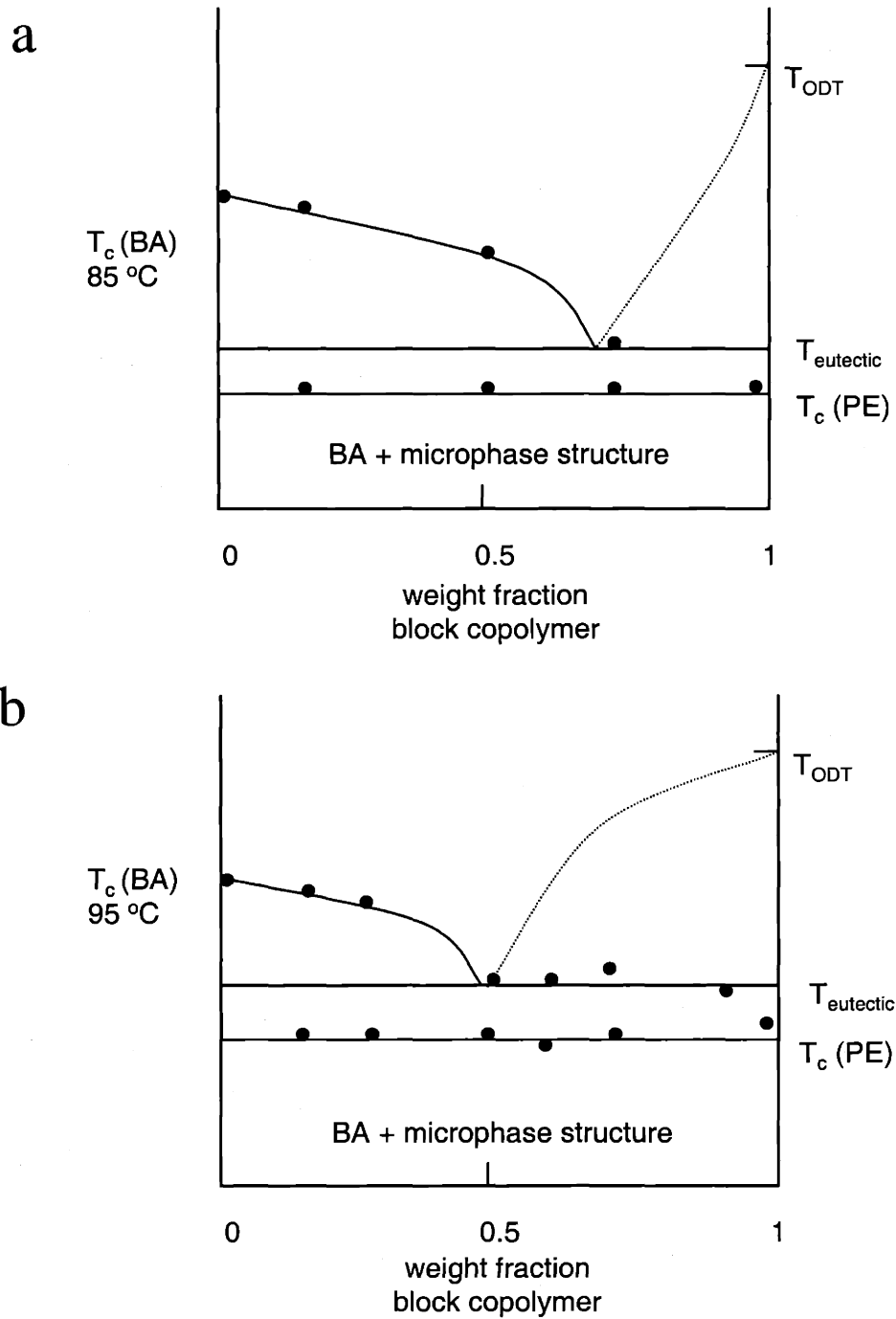
When the solvents are crystallizable, i.e. organic diluents, the mixtures of block copolymers and diluents can be expected to become eutectics. The two liquidus lines of the binary mixture of a block copolymer and an organic diluent: the freezing point depression curve of the organic diluent and the order-disorder temperature depression curve of the block copolymer can meet each other at a certain composition (the eutectic point) and induce a liquid to two solids phase transition. Since the order-disorder transition in a block copolymer is weak first order transitions, the phase separated block copolymer at the triple point can have some diluent inside as seen in the mixtures of



block copolymers and solvents.<sup>17</sup> If this is the case, the phase separation at the triple point would be from homogeneous liquid to pure solid (diluent) and another solid (solvent swollen microdomains).

The phase behaviors of two different block copolymers: polystyrene-block-poly(ethylene) (PS/PE) and polystyrene-*block*-(polyethylene-*alt*-propylene)-*block*-polyethylene (PS/PEP/PE) (see Chapter 2 for detailed material characteristics), were examined with a diluent, benzoic acid (BA) by differential scanning calorimetry (DSC). The mixtures of block copolymer and diluent of various compositions were heated up to 160 °C and held for 2 min to assume a complete homogeneous single phase mixture. The samples were then cooled to room temperature at the rate of 60 and 30 °C/min for BA and PS/PE mixtures and BA and PS/PEP/PE mixtures respectively. The crystallization of BA and block copolymer mixtures during fast cooling determined the non-equilibrium experimental phase behaviors of mixtures to minimize the loss of BA crystals caused by fast sublimation of BA crystals.

The phase diagrams of PS/PE and PS/PEP/PE with BA are shown in Figure 1.5a and 1.5b respectively. In both cases, the crystallization of BA is significantly affected by the block copolymers at higher diluent content, resulting in depression of the crystallization temperature. The crystallization temperatures of pure BA crystals in both cases are different due to the different cooling rates (60°C/min and 30°C/min for PS/PE and PS/PEP/PE respectively) . The second crystallization of BA expected in eutectic mixtures at the eutectic temperature was not observed due to the fast cooling rate. Since the heat involved on microphase separation of the block copolymers is hardly detected by DSC, only second crystallization of BA is observed at the eutectic temperature in higher block copolymer composition ranges. The eutectic temperatures determined in these samples both vary with cooling rate in DSC. The crystallization of PE in both block copolymers is independent of the presence of BA, occurring constantly at approximately 50 and 60 °C for PS/PE and PS/PEP/PE with the cooling rate of 60 °C/min and 30 °C/min respectively. It indicates that in both cases the crystallization of BA and the microphase separation of block copolymer are coupled to form a eutectic-like phase.



**Figure 1.5** (a) Experimental phase diagram of BA and PS/PE block copolymer mixtures determined by DSC with the cooling rate of 60 °C/min. (b) Experimental phase diagram of BA and PS/PEP/PE block copolymer mixtures determined by DSC with the cooling rate of 30 °C/min.

### 1.3.1.4 References

1. Chadwick, G. A. *Eutectic Alloy Solidification*, 1963, 12, The Macmillan Com. New York.
2. Galasso, F. S. "Unidirectionally solidified eutectics for optical, electronic, and magnetic applications" *J. Metals*, 1967, 19,17.
3. Stefanescu, D. M.; Abbaschian, G. J.; Bayuzick, R. J. *Solidification Processing of Eutectic Alloys* 1987 The Metallurgical Society, Inc. Chap. 1.
4. Tammann, G. *A Textbook of Metallography*, 1925, The Chem. Cat. Co., New York.
5. Vogel, R. Z. *Anorg. Chem.* 1912, 76, 425.
6. Lamplough, F. E. E.; Scott, J. T. *Proc. Roy. Soc.* 1914, 90A, 600.
7. Straumanis, W.; Brakss, N. Z. *Phys. Chem.* 1935, 30B, 117.
8. Porter, D. A.; Easterling, K. E. *Phase Transformations in Metals and Alloys*, 1992, Chapman & Hall, New York. Chap.4.
9. Smith, P.; Pennings, A. J. "Eutectic crystallization of pseudo binary systems of polyethylene and high melting diluents" *Polymer* 1974, 15, 413.
10. Smith, P.; Pennings, A. J. "Eutectic solidification of the pseudo binary system of polyethylene and 1,2,4,5-tetrachlorobenzene" *J. Mater. Sci.* 1976, 11, 1450.
11. Wittmann, J. C.; John Manley R. ST., "Polymer-monomer binary mixtures. I. Eutectic and epitaxial crystallization in poly( $\epsilon$ -caprolactone)-trioxane mixtures" *J. Polym. Sci. Polym. Phys. Ed.* 1977, 15, 1089.
12. Wittmann, J. C.; John Manley, R. ST. "Polymer-monomer binary mixtures. Eutectic crystallization of poly(ethylene oxide)-trioxane mixtures" *J. Polym. Sci. Polym. Phys. Ed.* 1977, 15, 2277.
13. Hodge, A. M.; Kiss, G.; Lotz, B.; Wittmann, J. C. "Eutectic solidification and oriented growth in mixtures of polyethylene and 1,3,5-tribromobenzene" *Polymer* 1982, 23, 985.
14. Dorset, D. L.; Hanlon, J.; Karet, G. "Epitaxy and structure of paraffin-diluent eutectics" *Macromolecules*, 1989, 22, 2169.
15. Fredrickson, G. H.; Leibler, L. "Theory of block copolymer solutions-nonselective good solvents" *Macromolecules*, 1989, 22, 1238.
16. Lodge, T. P.; Pan, C.; Jin, X.; Liu, Z.; Zhao, J.; Maurer, W. W.; Bates, F. S. "Failure of the dilution approximation in block copolymer solutions" *J. Polym. Sci. Polym. Phys.* 1995, 33, 2289.
17. Hamley, I. W.; Fairclough, J. P. A.; Ryan, A. J.; Ryu, C. Y.; Lodge, T. P.; Gleeson, A. J.; Pedersen, J. S. "Micellar ordering in concentrated solutions of di and triblock copolymers in a slightly selective solvent" *Macromolecules*, 1998, 31, 1188.
18. Evans, C. C.; Bates, F. S.; Ward, M. D. "Control of hierarchical order in crystalline composites of diblock copolymers and a molecular chromophore" *Chem. Mater.* 2000, 12, 236.

### 1.3.2 Epitaxy

Epitaxy is defined as the growth of one phase on the surface of a crystal of another phase in one or more strictly defined crystallographic orientations. The resulting mutual orientation is explained by a two dimensional or, less frequently, a one dimensional structural matching in the plane of contact of the two species. The oriented deposition of a solid phase upon another single crystal was discovered in 1817<sup>1</sup>; epitaxial single crystals were grown in the laboratory soon afterward. The organized study of possible epitaxial combinations began in the early 1900s using mainly optical microscopy. The development of X-ray crystal structure analysis permitted a detailed molecular description of epitaxy, that is, the periodic atomic arrangement of deposited crystal with respect to the substrate crystal structure.

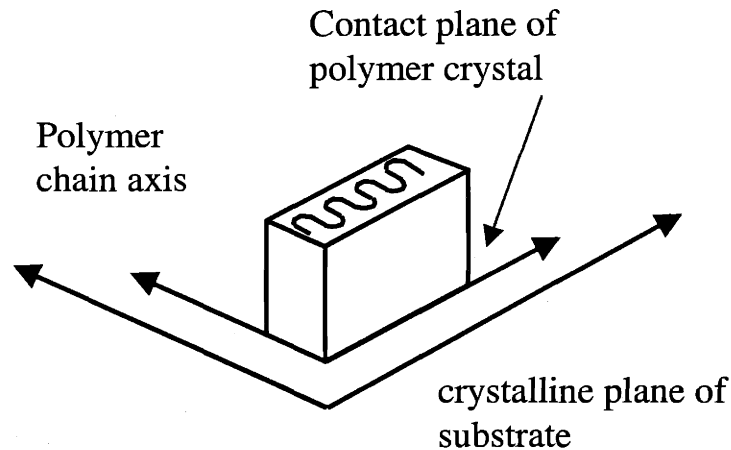
The term epitaxy, literally meaning “on surface arrangement”, was introduced by an early theory of epitaxial growth based on structural matching.<sup>2</sup> Discrepancy between atomic or molecular spacings is measured by the quantity  $(d - d_0)/d_0$ , expressed as a percent, where  $d$  and  $d_0$  are the lattice periodicities in the direction of interest of absorbed and substrate phase, respectively. In general 10 ~ 15 % discrepancies are considered as an upper limit for epitaxy to occur.<sup>2</sup>

Epitaxial crystallization has been observed to occur from the vapor phase, melt, and solution.<sup>3,4</sup> Numerous examples of this phenomenon range from the deposition of single atoms through more complex organic molecules to high molecular weight polymers. Several literature reviews have been devoted to the epitaxy of low molecular weight (mainly inorganic) materials on crystalline inorganic substrates for growth and structural studies of thin films.<sup>3,4</sup> Here I briefly review the epitaxial crystallization of polymers onto various kinds of substrates such as inorganic, organic and even other polymers.

#### 1.3.2.1 Epitaxy of polymers

Epitaxy of polymeric materials was first observed on alkali halide substrates by Willems<sup>5</sup> and by Fischer<sup>6</sup> in the 1950s. The use of inorganic substrates has revealed the major structural and morphological features of polymer epitaxy. There are several detailed reviews covering these aspects in the literature.<sup>2,7,8</sup> As a general rule, the deposited polymer chains lie with their chain axis parallel to the substrate surface; the

crystalline lamellae that are built up on further growth thus stand edge-on, i.e. are normal to the surface as shown in a schematic of Figure 1.6.



**Figure 1.6** Schematic of a polymer epitaxy on a crystalline substrate

An unambiguous and quantitative understanding of the mechanism of epitaxial crystallization of polymers require knowledge of the interfacial binding forces, or, equivalently, the polymer-substrate energetics. Purely geometric theories involving favorable lattice superpositions are obviously inadequate to explain all aspects of polymer epitaxy. Hardly applicable are previous theories of interfacial energy and elastic strain of epitaxial overgrowths of low molecular weight materials.<sup>9,10</sup>

The adsorption and configuration of flexible polymer chains from solution or melt onto surfaces have been theoretically investigated using statistical mechanics<sup>11,12</sup>, but these studies did not provide specific atom-atom interactions of polymer and substrate. A molecular theory of heterogeneous nucleation of polymer was incorporated to explain polymer epitaxy because the rate constants are a function of the activation energy.<sup>13</sup> However, this kinetic description is not based on a fundamental theory of explicit molecular interactions, but utilizes macroscopic factors such as surface energies and heats of fusion.

Other theoretical models<sup>15</sup> are based upon fundamental pairwise interactions between atoms in the polymer and substrate. Similar to conformational analysis, this approach minimizes the total energy of the polymer-substrate system on a two dimensional lattice with respect to the interfacial geometry to locate the most favorable molecular arrangements. The substrate effects a lowering of the activation free energy for nucleation with its anisotropic force field, leading to orientation of the depositing material. Both the chemical nature and the geometric locations of the constituent atoms in the substrate affect the form of this surface potential. At the first time, the cap-continuum method for calculation of van der Waals forces is used to examine the polymers on alkali halide substrates.<sup>15</sup> In this method, the substrate is broken into two regions: a hemispherical cap of discrete atoms and the remainder, which is modeled as a continuum where the atoms have a uniform density distribution in space. A more advanced model<sup>16</sup> overcame the limitations of the previous work to represent a closed-form of infinite summing of van der Waals interactions. In this study, the interactions between polymer and crystalline substrate were assumed to involve only van der Waals or dispersive-repulsive forces. The potential  $V_{ij}$  between the two atoms  $i$  and  $j$  is represented by a Lennard-Jones function;

$$V_{ij} = -\frac{A_{ij}}{r_{ij}^6} + \frac{B_{ij}}{r_{ij}^{12}} \dots\dots\dots(1.7)$$

where  $A_{ij}$  and  $B_{ij}$  are constants characteristic of the interacting atomic pair, and  $r_{ij}$  is the corresponding interatomic distance. The  $A_{ij}$  values are calculated from the like atom constants using the geometric mean approximation:

$$A_{ij} = (A_{ii}A_{jj})^{1/2} \dots\dots\dots(1.8)$$

The  $A_{ii}$  values for various organic species have been reported.<sup>17</sup> The repulsive constants are then calculated by constraining the potential gradient to be zero at the equilibrium position; thus

$$B_{ij} = \frac{1}{2} A_{ij} (r_{ij}^0)^6 \dots\dots\dots(1.9)$$

where  $r_{ij}^0$  is the equilibrium distance reported in the literature <sup>18</sup>

The interaction of the polymer segment with the substrate involves the summation of interactions of the individual constituent atoms of a representative polymer chain segment with the substrate. The simple summation turned out to be impossible due to slow convergence. Success was made with a special transformation method, which had been developed in several areas of crystal physics. In this method, the interatomic distance  $r_{ij}$  was decomposed into two vectors, one with its projection parallel to the substrate layer and the other normal to the substrate, i.e. the height above the substrate,  $\rho$ . Using the unit cell developed earlier, the interaction  $V_i^L$  of all the substrate atoms in a given layer with a polymer atom  $i$  is given by

$$V_i^L = -A_i \sum_{k=1}^2 \sum_{l_1=-\infty}^{+\infty} \sum_{l_2=-\infty}^{+\infty} [(r_k - r_l)^2 + \rho^2]^{-3} + B_i \sum_{k=1}^2 \sum_{l_1=-\infty}^{+\infty} \sum_{l_2=-\infty}^{+\infty} [(r_k - r_l)^2 + \rho^2]^{-6} \dots(1.10)$$

where  $r_l$  and  $r_k$  are the lattice vector ( $l_1, l_2$  integer) and the projection of the polymer atom minus the projection of the  $k$ th atom in the unit cell, respectively. Application of the transform to the equation yields a more mathematically complicated, but easily convergent form thanks to the presence of the Bessel function. The complete calculations for real polymer/inorganic substrate systems such as polyethylene/graphite provided good agreement with the experimental data.<sup>16</sup>

### 1.3.2.1.1 Epitaxy on inorganic substrates

Alkali halides such as NaCl, KCl and so on are the principal substrates for the investigation of polymer epitaxy. The first investigation employed optical microscopy of solution of polyethylene in decalin placed on the (001) surface of a NaCl single crystal.<sup>5</sup> Electron microscopy was used to characterize the detailed molecular chain arrangement with respect to the substrate surface shortly afterward.<sup>6,19</sup> The “edge-on” lamellar single crystal whose basal plane is perpendicular to the substrate surface was obtained. Near

perfect matching between the chain separation along the monoclinic PE axis and the distance between rows of like-charged ions in the [110] direction of NaCl developed the epitaxial orientation.<sup>6</sup> The polymer whose epitaxial behavior on alkali halides has been studied next most intensively to PE is polyoxymethylene (POM). The epitaxy of POM from dilute solution on cleaved (001) alkali halide was reported.<sup>20</sup> Isotactic polypropylene was also epitaxially oriented on alkali halides.<sup>21</sup>

Other inorganic substrates such as graphite and quartz have also been used to orient semicrystalline homopolymers in an epitaxial manner. PE was isothermally crystallized between 90 and 115 °C on graphite from dilute xylene solution.<sup>22</sup> The “edge on” lamellae structure was obtained with the molecular chains and (110)<sub>PE</sub> plane parallel to the basal plane (0001) of graphite substrate. Quartz was also utilized as substrate to study the epitaxial relations between the substrate and the polymers involving nylon-6, nylon-6,6, nylon-8, and polyacrylonitrile.<sup>23</sup>

#### **1.3.2.1.2 Epitaxy on organic substrates**

Epitaxy of polymers on organic surfaces has been primarily in an effort to investigate the molecular interactions prevailing at the interface between polymers and organic additives.<sup>8</sup> Willems was the first to demonstrate oriented growth of paraffins (nC<sub>18</sub>H<sub>38</sub>) on aromatic hydrocarbons such as chloranil and anthraquinone crystals.<sup>5</sup> More relevant to polymers, Walton et al.<sup>24</sup> reported the epitaxial crystallization of isotactic polypropylene on potassium hydrogen phthalate. Other examples can be found in the work done by Morawetz et al.<sup>25</sup> They described the epitaxial crystallization of nylon 6 on its own monomer crystal, ε-aminocaproic acid. A major advance has been accomplished by the pioneering studies of Smith and Pennings on polymer eutectics with organic diluents.<sup>26,27</sup> Thereafter Wittmann and St. John Manley reported that eutectic solidification can lead to the epitaxial crystallization of the polymer on the diluent crystal grown in-situ.<sup>28,29</sup> The PE component of the eutectic formed crystalline lamellae which are highly oriented with the chains in the (110) contact plane parallel to the tribromobenzene needle axes due to an epitaxy between the PE and the substrate.<sup>29</sup> This approach of using polymer/low molecular weight, crystallizable solvent mixtures in which a combination of eutectic solidification and oriented growth of the polymers on the



single solvent crystals are extended to semicrystalline block copolymer/crystallizable solvent mixtures to utilize multiple interactions during the phase separation, leading to ordered molecular chain as well as microdomains in this thesis.

PE has been epitaxially crystallized on various organic single crystal surfaces such as benzoic acid, anthracene, p-terphenyl, p-Br benzoic acid, K benzyl penicillin and p phenyl benzoic acid.<sup>8,30,31</sup> Most aromatic carboxylic acids, aromatic hydrocarbons and linear polyphenyls are good candidates for PE epitaxy.<sup>31</sup>

A straightforward extension of the results with PE, can be made for paraffins and a large number of shorter chains with polymethylene segments (including biological alkane chain lipids), owing to the similar crystal structure.<sup>32,33</sup> Dorset et al. have determined the crystal structure of not only paraffins but also cycloalkanes<sup>34</sup>, and phospholipids<sup>35</sup> using an epitaxial growth method on benzoic acid substrates.

In addition, aliphatic polyesters<sup>31</sup>, polyamides<sup>31</sup> and polycarbonate of bisphenol A<sup>8</sup> have been epitaxially crystallized with aromatic acid crystals after recrystallization of an aromatic acid from a homogeneous mixture with a polymer. The investigations have shown that polyethylene terephthalate, polybutylene terephthalate and polycarbonate do crystallize epitaxially on aromatic substrates such as anthracene or p-terphenyl. In both cases, these resulting orientations correspond to the layers containing the phenyl rings parallel to the substrate surface.

Although epitaxy of helical polymers are less favorable than for linear polymers due to the lower symmetry of the helix and its usually large diameter, several epitaxies of helical polymers on organic substrates have been reported.<sup>36-38</sup> Isotactic and syndiotactic polypropylenes were epitaxially crystallized on independently prepared benzoic acid and p-terphenyl, and  $\gamma$ -quinacridone crystal substrates respectively.<sup>36-38</sup> Each single crystal was produced by slow cooling of a xylene solution from its boiling temperature; a drop of suspension was deposited onto the solution cast polymer film at room temperature, leaving, after evaporation of xylene, large, flat crystals scattered on top of the polymer film.<sup>37</sup> An inorganic helical polymer, selenium, was also oriented on linear polyphenyl crystals (p-terphenyl, quaterphenyl), resulting in epitaxial crystallization similar to PE.<sup>39</sup>

### 1.3.2.1.3 Epitaxy on polymer substrates

Polymer-polymer epitaxy can be considered as a specific interfacial interaction between two distinct macromolecular species. The underlying assumption that crystallographic interactions, and more specifically epitaxy, may result in improved adhesion between the two (in general incompatible) phases and ultimately lead to a synergism of mechanical properties of the polymer composite systems. For example, in the iPP-PE system,<sup>40</sup> the laminates of highly oriented iPP coated with thin PE layer displayed the improvement of adhesion due to the epitaxy of PE.

Epitaxy has been observed on various types of polymer substrates. Transcrystallization and the resulting morphologies were investigated with sandwiched two melt polymers.<sup>41</sup> Melt crystallization of iPP and PEO in contact with poly(2,6-dimethyl phenylene oxide) (PPO) and Nylon 6 respectively revealed nucleating abilities of surfaces. On an active substrate (PPO), transcrystallization occurred while on an inactive substrate (Nylon 6) spherulitic structure was obtained.<sup>41</sup> An attempt was made to orient a number of polymers from the melt on the drawn and annealed polytetrafluoroethylene (PTFE).<sup>42</sup> High density PE, polycaprolactone, nylon-6 and PP were crystallized in epitaxial fashion. For example, PE crystals with their c axis were aligned parallel to the molecular axis of PTFE. Needle shaped crystals of poly(oxyethylene) (POM) were used to provide a unique substrate for the crystallization of the same polymer and an acetal copolymer from the molten state.<sup>43</sup> The crystallization on the crystalline surface formed a cylindrite, comprising a pile of chain folded lamellar crystallites.<sup>43</sup> A system similar to homoepitaxy of a polymer on its own crystal was reported by Buleon et al.<sup>44</sup> They observed that cellulose I extended chain microfibrils can be used as a substrate for the epitaxial growth of cellulose II folded chain lamellae.

A new process was developed by Wittmann and Smith to create flat and smooth PTFE substrates.<sup>45-50</sup> The method was based on the creation of thin polymer films on glass substrates by the friction force generated while a heated PTFE bar was slowly moved under pressure over a glass surface. Regularly arranged polymer chains well aligned along the moving direction acted as single crystal surface. The method enabled examination of numerous polymers such as PE, iPP, nylon 6, 11, poly(p-oxybenzoate)

etc. on the highly oriented PTFE surface. In some cases, more than two polymers were deposited on the PTFE substrate to study the relative interactions between epitaxy and transcrystallization among the polymers.<sup>50</sup>

### 1.3.2.2 References

1. Seifert, H. in Gomer R. and Smith, C. S. eds., *Structure and Properties of Solid Surfaces*, **1953** University of Chicago Press, Chicago, Ill., p318.
2. Swei, G. S.; Lando, J. B.; Rickert, S. E.; Mauritz, K. A. *Encyclopedia of Polymer Science and Engineering*, **1986**, 6, 209.
3. Chopra, K. L. *Thin Film Phenomena* **1969**, McGraw-Hill, Inc., New York.
4. Matthews, J. W. *Epitaxial growth*, **1975**, Academic Press, New York.
5. Willems, J. "Über orientierte aufwachsungen von paraffinen auf aromatischen kohlenwasserstoffen und alkalihalogeniden" *Naturwissenschaften* **1955**, 42, 176.
6. Fischer, E. W. "Orientierte kristallisation des polyathylens auf steinsalz" *Kolloid-Z.* **1958**, 159, 108.
7. Mauritz, K. A.; Baer, E.; Hopfinger, A. J. *J. Polym. Sci., Macromol. Rev.* **1978**, 13, 1.
8. Wittmann, J. C.; Lotz, B. "Epitaxial crystallization of polymers on organic and polymeric substrates" *Prog. Polym. Sci.* **1990**, 15, 909.
9. Van der Merwe, J. H. in Francombe, H. and Sato, S. eds., *Single Crystal Films*, **1964**, MacMillan, New York.
10. Brooks, H. *Metal Interfaces*, **1952**, American Society of Metals, Cleveland, Ohio.
11. Lax, M. J. *Chem. Phys.* **1974**, 61, 4133.
12. Mark, P.; Windwer, S. "Polymer adsorption on a surface by an exact enumeration" *Macromolecules* **1974**, 7, 690.
13. Hoffman, J. D. *SPE Trans.* **1964**, 4, 315.
14. Hoffman, J. D.; Lauritzen, J. I.; Passaglia, E.; Ross, G. S.; Frolen, L. J.; Weeks, J. J. "Kinetics of polymer crystallization from solution and the melt" *Kolloid Z* **1967**, 231, 564.
15. Mauritz, K. A.; Hopfinger, A. J. "Theory of the epitaxial crystallization of polymers on alkali halide substrates. III. Solvation effects" *J. Phys. Chem.* **1976**, 80, 706.
16. Baukema, P. R.; Hopfinger, A. J. "The energetics of the epitaxial deposition of polyethylene onto the basal plane (0001) of graphite" *J. Polym. Sci. Polym. Phys. Ed.* **1982**, 20, 399.
17. Hopfinger, A. J. *Conformation Properties of Macromolecules*, **1973**, Academic Press, Inc., New York. P 12.
18. Kiselev, A. V.; Poshkus, D. P. "Molecular-statistical calculation of the thermodynamic characteristics of adsorption of saturated and unsaturated hydrocarbons on graphitized thermal carbon black" *J. Chem. Soc. Faraday Trans. 2* **1976**, 72, 950.
19. Shen, M.; Hansen, W. N.; Romo, P. C. "Thermal expansion of the polyethylene unit cell" *J. Chem. Phys.* **1969**, 51, 425.
20. Koutsky, J. A.; Walton, A. G.; Baer, E. "Heterogeneous nucleation of polyethylene melts on cleaved surfaces of alkali halides" *J. Polym. Sci. Polym. Lett. Ed.* **1967**, 5, 185.
21. Koutsky, J. A.; Walton, A. G.; Baer, E. "Epitaxial crystallization of homopolymers on single crystals of alkali halides" *J. Polym. Sci. A-2*, **1966**, 4, 611.
22. Tuinstra, R.; Baer, E. "Epitaxial crystallization of polyethylene on graphite" *J. Polym. Sci. Polym. Lett. Ed.* **1970**, 8, 861.

23. Muller-Buschbaum, B.; Seifert, H. "Epitaxie von polyacrylnitril auf quarz" *Kolloid Z.* **1965**, 205, 46.
24. Walton, A. G.; Carr, S. H.; Baer, E. *Polym Prep. Am. Chem. Soc.* **1968**, 9, 603.
25. Morosoff, N.; Lim, D.; Morawetz, H. *J. Polym. Sci. A-1* **1968**, 6, 2033.
26. Smith, P.; Pennings, A. J. "Eutectic crystallization of pseudo binary systems of polyethylene and high melting diluents" *Polymer* **1974**, 15, 413.
27. Smith, P.; Pennings, A. J. "Eutectic solidification of the pseudo binary system of polyethylene and 1,2,4,5-tetrachlorobenzene" *J. Mater. Sci.* **1976**, 11, 1450.
28. Wittmann, J. C.; John Manley, R. ST. "Polymer-monomer binary mixtures. I. Eutectic and epitaxial crystallization in poly( $\epsilon$ -caprolactone)-trioxane mixtures" *J. Polym. Sci. Polym. Phys. Ed.* **1977**, 15, 1089.
29. Hodge, A. M.; Kiss, G.; Lotz, B.; Wittmann, J. C. "Eutectic solidification and oriented growth in mixtures of polyethylene and 1,3,5-tribromobenzene" *Polymer* **1982**, 23, 985.
30. Wittmann, J. C.; Lotz, B. "Epitaxial crystallization of polyethylene on organic substrates: a reappraisal of the mode of action of selected nucleating agents" *J. Polym. Sci. Polym. Phys. Ed.* **1981**, 19, 1837.
31. Wittmann, J. C.; Hodge, A. M.; Lotz, B. "Epitaxial crystallization of polymers onto benzoic acid: polyethylene and paraffins, aliphatic polyesters, and polyamides" *J. Polym. Sci. Polym. Phys. Ed.* **1983**, 21, 2495.
32. Dorset, D. L.; Hanlon, J.; Karet, G. "Epitaxy and structure of paraffin-diluent eutectics" *Macromolecules*, **1989**, 22, 2169.
33. Dorset, D. L. "Bridged lamellae: crystal structure(s) of low molecular weight linear polyethylene" *Macromolecules* **1999**, 32, 162.
34. Dorset, D. L.; Hsu, S. L. "Polymethylene chain packing in epitaxially crystallized cycloalkanes-an electron diffraction study" *Polymer* **1989**, 30, 1596.
35. Dorset, D. L.; Pangborn, W. A. "Epitaxial crystallization of alkane chain lipids for electron diffraction analysis" *J. Biochem. Bioph. Meth* **1983**, 8, 29.
36. Lotz, B.; Wittmann, J. C. "The molecular origin of lamellar branching in the alpha-(monoclinic) form of isotactic polypropylene" *J. Polym. Sci. Polym. Phys. Ed.* **1986**, 24, 1541.
37. Stocker, W.; Schumacher, M.; Graff, S.; Lang, J.; Wittmann, J. C.; Lovinger, A. J.; Lotz, B. "Direct observation of right and left helical hands of syndiotactic polypropylene by atomic force microscopy" *Macromolecules* **1994**, 27, 6948.
38. Stocker, W.; Schumacher, M.; Graff, S.; Thierry, A.; Wittmann, J. C.; Lotz, B. "Epitaxial crystallization and AFM investigation of a frustrated polymer structure: isotactic poly(propylene),  $\beta$  phase" *Macromolecules* **1998**, 31, 807.
39. Wittmann, J. C.; Lotz, B. "Epitaxial crystallization of selenium on linear polyphenyls" *J. Mater. Sci.* **1984**, 19, 1439.
40. Lee, I. H.; Schultz, J. M. "Bonding of highly oriented polypropylene sheets by epitaxial crystallization of polyethylene" *J. Mater. Sci.* **1988**, 23, 4237.
41. Chatterjee, A. M.; Price, F. P.; Newman S., "Heterogeneous nucleation of crystallization of high polymers from the melt. I. Substrate-induced morphologies" *J. Polym. Sci. Polym. Phys. Ed.* **1975**, 13, 2369.

42. Takahashi, T.; Teraoka, F.; Tsujimoto, I. "Epitaxial crystallization of crystalline polymers on the surface of drawn polytetrafluoroethylene" *J. Macromol. Sci. Phys.* **1976**, 10, 303.
43. Iguchi, M.; Watanabe, Y. "Oriented overgrowth crystallization on needle shaped polyoxymethylene single crystals from molten polymers" *Polymer* **1977**, 18, 265.
44. Buleon, A.; Chanzy, H.; Roche, E. "Epitaxial crystallization of cellulose II on valonia cellulose" *J. Polym. Sci. Polym. Phys. Ed.* **1976**, 14, 1913.
45. Wittmann, J. C.; Smith, P. "Highly oriented thin films of poly(tetrafluoroethylene) as a substrate for oriented growth of materials" *Nature* **1991**, 352, 414.
46. Frey, H.; Sheiko, S.; Moller, M.; Wittmann, J. C.; Lotz, B. "Highly oriented poly(di-N-alkylsilylene) films on oriented PTFE substrates" *Adv. Mater.* **1993**, 5, 917.
47. Fenwick, D.; Smith, P.; Wittmann, J. C. "Epitaxial and graphoepitaxial growth of materials on highly oriented PTFE substrates" *J. Mater. Sci.* **1996**, 31, 128.
48. Damman, P.; Dosiere, M.; Wittmann, J. C. "Epitaxial polymerization of poly(p-oxybenzoate) on friction-transfer poly(tetrafluoroethylene) substrates" *Macromolecules* **1997**, 30, 8386.
49. Yan, S.; Katzenberg, F.; Petermann, J.; Yang, D.; Shen, Y.; Straupe, C.; Wittmann, J. C.; Lotz, B. "A novel epitaxy of isotactic polypropylene (alpha phase) on PTFE and organic substrates" *Polymer* **2000**, 41, 2613.
50. Yan, S.; Petermann, J. "A method for comparing the nucleation ability of PTFE, iPP and sPP on PE" *Polym. Bull.* **1999**, 43, 75.

### **1.3.3 Summary**

Two types of interactions: directional solidification and epitaxy which can potentially couple to molecular chains and/or microdomain structures of block copolymers were reviewed. Eutectic directional solidification, originally observed in many metal alloys, was dealt with in the first section. A brief review of thermodynamics of lamellar-forming eutectics was given and more importantly polymer-diluent mixture eutectics were considered. Theoretical as well as experimental evidences were presented. Finally the extension to block copolymer-diluent mixtures were tried. Non-equilibrium experimental phase behaviors of block copolymer/crystallizable organic solvent mixtures implied a possible eutectic formation.

Various polymer epitaxies were presented in the next section. Several theoretical methods for prediction of crystalline polymer/crystalline substrate epitaxy were demonstrated first. Categorized polymer epitaxies were described, depending on the types of substrates. Many experimental works with various inorganic, organic and polymer substrates were reviewed. In particular the idea of using crystallizable organic solvents as a substrate for epitaxy was extended to semicrystalline block copolymers.

## **1.4 Summary**

Chapter 1 described the motivation and background of the thesis. Many nanotechnological applications using block copolymers were reviewed. Focus was on control of block copolymer microdomains which is a key for realization of the potential technologies. Various techniques to achieve orientation of block copolymer microdomains were discussed. Next new types of interactions: directional solidification and epitaxy which can couple to block copolymer microdomains were proposed. General background of these two interactions was given such as thermodynamics of eutectic directional solidification, energetic interaction of epitaxy and various experimental evidences.

Next chapter 2 describes materials and experimental methods used in Part I and II. Detailed synthesis and characterization of block copolymers are presented. In addition, various film preparation and structural characterization methods are illustrated.

Part I deals with orientation of a semicrystalline block copolymer in bulk. Flow induced mechanical field creates orientation of amorphous microdomains and following crystallization in between amorphous microdomains is influenced by the pre-existing orientation of amorphous microdomains. Not only microdomains orientation, but also molecular chain orientation of crystalline block is discussed.

In Part II, new types of interaction discussed in this chapter are extended to block copolymer systems. Various controlled microdomain orientations are shown, depending on block copolymers and interactions: directional solidification, epitaxy and combination of both.



## CHAPTER 2: Materials and Experimental Methods

Chapter 2 describes materials and experimental methods used in this work. Three different types of semicrystalline block copolymers and two amorphous block copolymers are presented. Synthesis, molecular characterization of the block copolymers and melting/crystallization properties of the semicrystalline block copolymers are dealt with in the first section. The second section demonstrates various experimental methods such as solution and roll cast film preparation, transmission electron microscope (TEM), atomic force microscope (AFM), simultaneous small (SAXS) and wide angle X-ray scattering (WAXS) and more importantly thin film preparation using crystallizable organic solvent for directional solidification and/or epitaxy.

### 2.1 Materials

#### 2.1.1 Semicrystalline block copolymers

Three different types of semicrystalline block copolymers were used in this work. The PS/PEP/PE terpolymer and the PS/PE diblock copolymers, used in Chapter 3, 4, 7 and 8 have been prepared by catalytic hydrogenation of poly(styrene-*b*-1,4-isoprene-*b*-1,4-butadiene) (PS/PI/PB), and poly(styrene-*b*-1,4-butadiene) (PS/PB) block copolymers at Exxon Research Co. by Dr. L. J. Fetters, respectively. The polymer precursors PS/PI/PB and PS/PB were prepared by anionic polymerization in benzene at 20 °C with *sec*-Butyllithium as initiator according to the standard high vacuum techniques.<sup>1</sup> The polymerizations were performed in a sequential fashion commencing with styrene. The 1,4 additions of butadiene units in the PS/PI/PB and PS/PB block copolymers give rise, after hydrogenation, to the polyethylene blocks, whereas the hydrogenation of the 1,4 isoprene units in the PS/PI/PB block copolymer gives rise to the alternating copolymer of ethylene and propylene (PEP) in the PS/PEP/PE copolymer. Small percent of 3,4 additions of isoprene units produces, after hydrogenation, isopropyl branches in the PEP block, while small percent of 1,2 additions of butadiene units produces ethyl branches in the PE blocks. The presence of two ethyl branches per 100 backbone carbon atoms in the PE blocks of both block copolymers was estimated. The hydrogenation reaction was carried out using the standard procedure described elsewhere.<sup>2</sup> The method used leads to

complete saturation of the polydiene segments while leaving the polystyrene segment unchanged.

The poly(ethylene-*b*-(ethylene-*alt*-propylene)-*b*-ethylene) triblock copolymer (PE/PEP/PE), used in Chapter 5, was prepared by catalytic hydrogenation of poly(1,4-butadiene-*b*-1,4-isoprene-*b*-1,4-butadiene) (PB/PI/PB) by Dr. L. J. Fetters. The latter was synthesized again by anionic polymerization in benzene at 20 °C with *sec*-butyllithium as initiator according to the standard high vacuum techniques.<sup>1</sup> The 1,4 additions of butadiene and isoprene units in the PB/PI/PB block copolymer give rise, after hydrogenation, to the PE end-blocks and the alternating copolymer of ethylene and propylene (PEP) in the PE/PEP/PE copolymer. The small percentage of 3,4 additions of isoprene units again produces, after hydrogenation, isopropyl branches in the PEP block, while the small percentage of 1,2 additions of butadiene units produces ethyl branches in the PE blocks. The estimated number of ethyl branches per 100 backbone carbon atoms in the PE block is two. The hydrogenation reaction was carried out using the same procedure described above.<sup>2</sup> The solvent was heptane and the catalyst was palladium on calcium carbonate. <sup>1</sup>H NMR showed that no double bonds remained.

Molecular weight characterizations were done using a combination of size exclusion chromatography (SEC) and low angle laser light scattering. Tetrahydrofuran was used as solvent in all cases. For the PS/PI/PB sample the average molecular weight via light scattering was  $M_w = 103,000$  g/mol, while SEC gave  $M_z/M_w$  and  $M_w/M_n$  ratios of 1.02 and 1.04, respectively. The molecular weights of the polystyrene, polyisoprene and poly(1,4-butadiene) blocks were 15000, 75000, and 15000 g/mol, respectively. The same molecular weights results for the corresponding hydrogenated blocks in the PS/PEP/PE sample. The volume fractions of the PS, PEP and PE blocks are 0.13, 0.71 and 0.16 at the above the melting point of PE block (98 °C), respectively.

For the PS/PB sample the average molecular weight via light scattering was  $M_w = 50,000$  g/mol. The molecular weights of the polystyrene and poly(1,4-butadiene) blocks were 40000 and 10000 g/mol, respectively. The same molecular weights results for the corresponding hydrogenated blocks in the PS/PE sample, and the volume fraction of the PE block is 0.24.

For the PB/PI/PB sample the average molecular weight via light scattering was  $M_w = 55,000$  g/mol, while SEC gave  $M_z/M_w$  and  $M_w/M_n$  ratios of 1.02 and 1.03, respectively. The molecular weight of each poly(1,4-butadiene) end-block was approximately 10,000 g/mol, while that of the polyisoprene mid-block was approximately 35,000 g/mol. Essentially the same molecular weights result for the corresponding hydrogenated blocks in the PE/PEP/PE sample. From the weight fractions of the blocks and assuming for the PE and PEP blocks densities at 140 °C of 0.78 and 0.79 g/cc,<sup>3</sup> respectively, a volume fraction of the PE blocks in the block copolymer melt of 0.37 was estimated. Molecular characteristics of the semicrystalline block copolymers are summarized in Table 2.1. Flory-Huggin's interaction parameter,  $\chi_{PE-PEP}$  and  $\chi_{PS-PEP}$  were obtained from the literatures.<sup>4,5</sup>

	$M_o$ (g/ repeat unit) <sup>a</sup>	$M_w$ (g/ mol)	Vol. frac. (%)	N ( $M_w/M_o$ )	$N_{total}$	$\chi_N$ (413K)
PE	56	20000	37	357	857	4
PEP	70	35000	63	500		
PE	56	15000	16	268	1411	78
PEP	70	70000	71	1000		
PS	105	15000	13	143		
PE	56	10000	24	179	560	40
PS	105	40000	76	381		

**Table 2.1.** Molecular characteristics of three semicrystalline block copolymers.

The melting temperatures and the crystallinity indices were obtained with calorimetric measurements using a differential scanning calorimeter Perkin-Elmer DSC-7, performing scans in a flowing  $N_2$  atmosphere at a heating rate of 2 °C/min. The crystallinity indices was calculated from the values of the experimental melting enthalpy and the value of the equilibrium melting enthalpy of a perfect crystal of PE (289 J/g).<sup>6</sup> The melting temperatures of the as-prepared PS/PEP/PE, PS/PE and PE/PEP/PE samples were 98, 96 and 102 °C, respectively, significantly lower than that of a high density

polyethylene, indicative of the presence of the ethyl branches. The glass transition of the PS block in the PS/PEP/PE was of nearly 80 °C, but that of the PS block in PS/PE was not detected due to overlap with the melting peak of PE block. The glass transition temperature of the PS block in PS/PE was chosen to be approximately 100 °C, based on the literature.<sup>7</sup>

The crystallinity index of PS/PEP/PE sample crystallized from the melt by cooling at 2 °C/min, was nearly 40% with respect to the crystallizable PE block, corresponding to nearly 6 % with respect to the total weight of the block copolymer. For the melt-crystallized PS/PE samples the crystallinity index of nearly 25% with respect to the crystallizable PE block, corresponding to nearly 5 % with respect to the total weight of the block copolymer, was evaluated. The crystallinity index of a PE/PEP/PE sample crystallized from the melt was nearly 30%, with respect to the crystallizable PE blocks, corresponding to only about 10 % with respect to the total weight of the block copolymer sample. The melting and crystallization properties of the semicrystalline block copolymers are summarized in Table 2.2.

	HDPE	PE/PEP/PE	PS/PEP/PE	PE/PS
T <sub>m</sub> (°C)	140	102	98	96
T <sub>c</sub> (°C)	140	92	66	61
Heat (J/g)	289	30	16	14
Crystallinity(%)	60 ~ 80	Total: 10 PE part: 30	Total: 6 PE part: 37	Total: 5 PE part: 25

**Table 2.2** Melting and crystallization properties of high density polyethylene and three semicrystalline block copolymers

### 2.1.2 Amorphous block copolymers

Two different types of amorphous block copolymers were used in Chapter 6 and 9: a polystyrene-*block*-poly(methylmetacrylate), PS/PMMA (26/32) diblock copolymer and a polystyrene-*block*-polyisoprene diblock copolymer, PS/PI(45/12). The sample

PS/PMMA(26/32) has a total molecular weight of 58,500 g/mol, a polydispersity of 1.06, with PS and PMMA blocks of 26,000 and 32,000 g/mol, respectively. This sample presents a bulk lamellar microstructure (evidenced by small angle X-ray scattering (SAXS):  $d_{100}^{lam} \approx 39 \text{ nm}$ ), consistent with the 49% volume fraction of the PS block. The sample PS/PI(45/12) has a total molecular weight of 57,000 g/mol with polystyrene (PS) and polyisoprene (PI) blocks 45,000 and 12,000 g/mol, respectively. Since the volume fraction of the PI block is 24%, the bulk sample displays a hexagonally packed cylindrical microstructure of the minority PI component (evidenced by SAXS:  $d_{10\bar{1}0}^{cyl} \approx 42 \text{ nm}$ ). The PS/PMMA(26/32) was purchased from Polymer Laboratories, while the PS/PI(45/12) block copolymer was supplied by Dr. L. J. Fetters of Exxon Research .

## 2.2 Experimental Methods

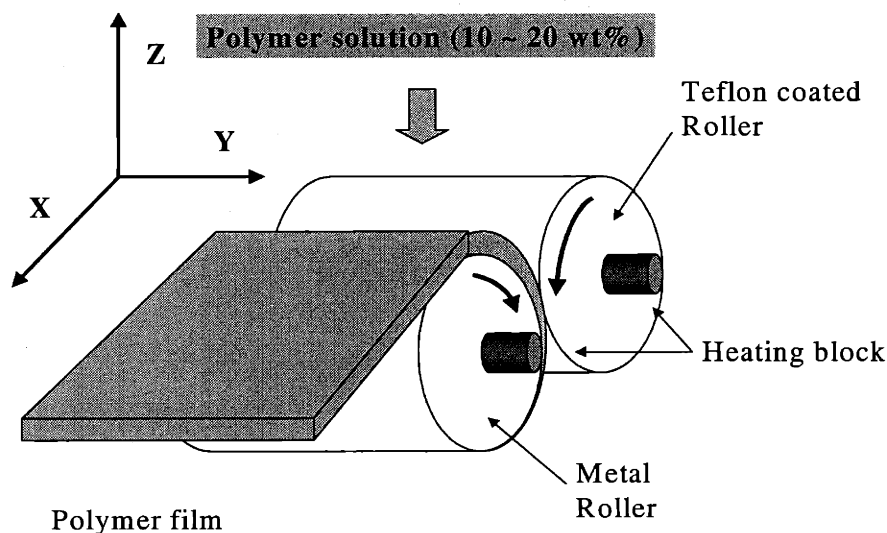
### 2.2.1 Solution cast films

The bulk samples of the PS/PEP/PE and PS/PE block copolymer were prepared by evaporation of the solvent from 5 wt% decalin solution of the block copolymer. The obtained samples were annealed at 150 °C for 10 days and quenched in liquid N<sub>2</sub> to eliminate the effect of the PE crystallization on the microstructure. The bulk samples of the PE/PEP/PE block copolymer were prepared by melting and recrystallization in order to eliminate any previous thermal history.

### 2.2.2 Roll cast films

Anisotropic thick films (1mm thickness) of PS/PEP/PE terpolymer were made by pouring the polymer solution (15 wt% in decalin) between two temperature controlled counter-rotating adjacent cylinders while at the same time the solvent was allowed to evaporate. The angular velocity of each cylinder was about 30 rpm. The flow direction corresponds to X, the neutral direction to Y and the through thickness direction to Z. The roll casting process was performed at the elevated temperature (90 °C) to avoid any effects of the crystallization of the PE block, (which occurs at 70 °C) on the structure. Roll cast films were subsequently quenched in liquid N<sub>2</sub> to preserve the oriented PS microstructure formed above the crystallization temperature of PE and dried in a vacuum

oven at 40 °C for 24 h in order to remove all traces of the solvent. They were then annealed for an additional 10 days under vacuum at 140 °C, significantly above both the glass transition temperature of polystyrene segments ( $T_g \sim 80$  °C) and the melting temperature of polyethylene segments. The films were then subsequently slowly cooled down to room temperature with a cooling rate of 2 °C/min. A schematic diagram of roll casting apparatus is shown in Figure 2.1.



**Figure 2.1** Schematic diagram of roll casting apparatus. A typical radius of roll is 20 mm and a film with the thickness of 2 mm is obtained after process.

### 2.2.3 Transmission electron microscope (TEM) and atomic force microscope (AFM)

Thin sections of the bulk films were prepared for TEM using a Reichert-Jung FC4E Ultracut microtome at -110 °C. For thin film samples obtained via directional solidification and/or epitaxy (see 2.2.4), The interior surface of the coverslip was then scored with a knife and small sections of the carbon film were floated off onto distilled water and picked up by TEM grids (200 mesh).

The PS/PEP/PE, PS/PE and PS/PMMA(26/32) samples were subsequently stained for 20 min with  $\text{RuO}_4$ , a preferential stain for the PS block. PS/PI(45/12) films were then exposed to  $\text{OsO}_4$  for 2 hours to stain the PI microdomains.

Amorphous block copolymer films were analyzed in the TEM in bright field and semicrystalline block copolymer films analyzed in bright and dark field mode as well as in selected area diffraction. A JOEL 200CX and Philips CM12 TEM, operating a 200 kV and 120 kV, were used.

The computer simulated Fast Fourier Transforms (FFTs) were made from the TEM image, using a software program, image SXM. This program performs the FFT and outputs the data on a log scale as a 2 D image.

The surface topology of thin films was examined with 226  $\mu\text{m}$  long etched silicon tip which had a radius of curvature of about 10 nm and spring constants ranging from 1.7 to 3  $\text{Nm}^{-1}$ , using “tapping mode” method of the Nanoscope III instrument (Digital Instrument). Height and amplitude contrasts were used.

#### **2.2.4 X-ray scattering**

Simultaneous SAXS and WAXS measurements were carried out at the Advanced Polymer beamline, X27C, National Synchrotron Light Source (NSLS), Brookhaven National Laboratory (BNL). The wavelength used was  $\lambda = 0.1307$  nm, and the beam size at the sample position was about 0.4 mm in diameter. A three  $2^\circ$  tapered tantalum pinhole collimation system was used with a sample to detector distances of 1560 mm and 108 mm, for the SAXS and WAXS patterns, respectively. Scattering angles  $2\theta$  down to 1.5 mrad, corresponding to a spacing ( $d = 2\pi/q$ , where  $q = 4\pi\sin\theta/\lambda$ ) of about 100 nm, were achieved in the SAXS pattern. The SAXS and WAXS patterns were recorded at various temperatures using a single-cell heating stage (maximum temperature: 350  $^\circ\text{C}$ ). The sample was melted and the patterns recorded at different temperatures starting from the melt and cooling to room temperature at a cooling rate of 2  $^\circ\text{C}/\text{min}$ . Fuji imaging plates were used to collect the scattering data with exposure times of 1 min per frame. The isotropic diffraction data were circularly averaged over the azimuthal coordinate of the two-dimensional patterns and plotted as a function of the scattering vector  $q$ , and the Bragg angle  $2\theta$ , for the SAXS and WAXS pattern, respectively.

### 2.2.5 Directional Solidification and/or Epitaxy

The processing method is based on the use of the low molecular weight organic crystallizable solvents such as benzoic acid (BA) and anthracene (AN). The process employs three main steps:

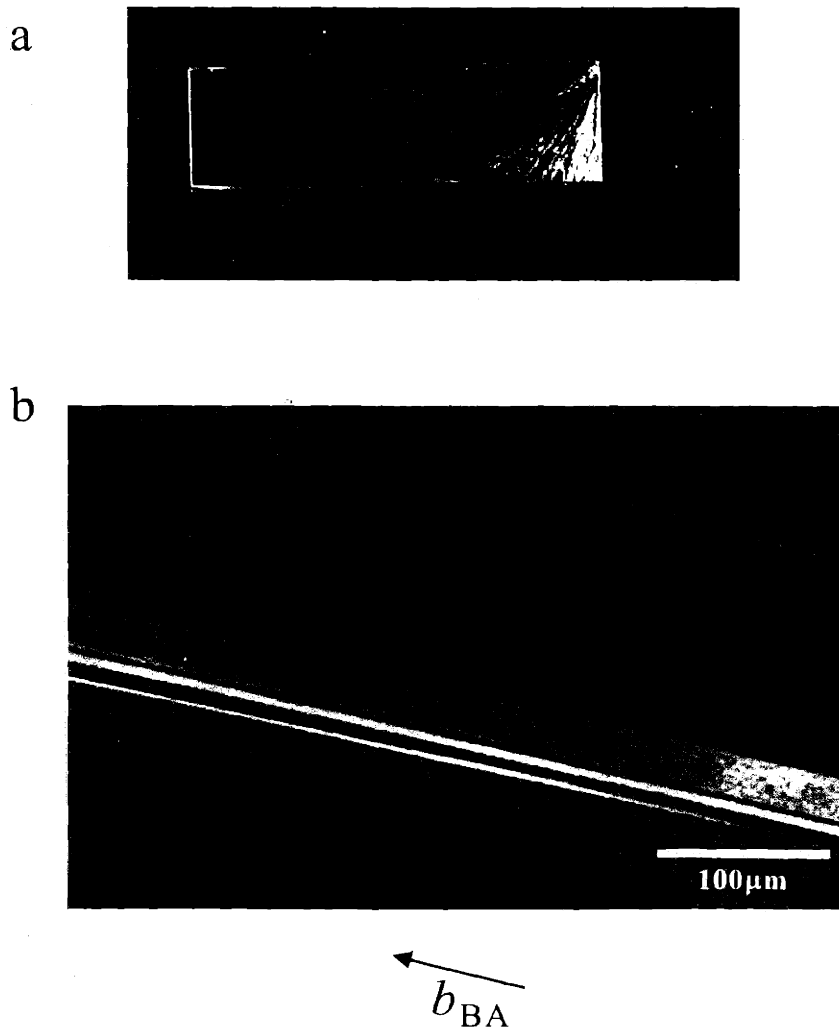
1) Thin films of the block copolymer (~100 nm thickness) were first formed on carbon coated coverslip glass, by evaporation of the solvent from a xylene solution (0.1- 0.3 wt%).

2) Crystalline BA or AN powders are then spread over a glass slide, the coverslip is placed polymer side down on the BA or AN and melted at 150 °C and 240 °C, respectively, whereupon the molten BA or AN dissolves the block copolymer. The solution is then supercooled by placing the glass slide on a hot bar at 110 °C for BA and at 190 °C for AN and contacting the edge of the coverslip with tweezers to induce directional crystallization of the BA (melting temperature  $T_m \cong 123$  °C) or the AN ( $T_m \cong 220$ °C). Rapid crystallization of BA or AN occurs (growth front velocity  $\cong 2$  mm/sec) resulting in large, elongated crystals with the *b* axis parallel to growth front direction. Figure 2.2a and b shows a photograph and a polarized optical microscope image of directionally crystallized BA. Large flat and elongated crystals of BA are seen. Finally the slide is moved to a position on the hot bar with a temperature of 60°C (or 140°C) and held for a minute to complete the crystallization of the BA (or the AN), then cooled to room temperature.

3) A razor blade is used to fracture-open the solidified material (cleavage occurs easily on the (001) BA and AN planes). Ethanol at 50°C is then used to wash away either the BA or the AN from the coverslip.

Polarized light microscopy of the films after BA or AN removal demonstrates that there is a strong texture, most apparent from some elongated regions of thicker polymeric material which formed between the BA or AN crystals. This direction corresponds to the fast growth direction of the BA or AN (the *b*-axis).





**Figure 2.2** (a) photograph and (b) polarized optical microscope image of directionally crystallized BA crystals. The large, flat and elongated BA crystals are aligned with the  $b$  axis parallel to growth front direction. BA single crystals with various thicknesses lead to different colors under polarized light.

## 2.3 References

1. Morton, M.; Fetters, L. J. "Anionic polymerization of vinyl monomers" *Rubber Chem. Tech.* **1975**, *48*, 359.
2. Rachapudy, H.; Smith, G. G., Rayn, V. R.; Graessley, W. W. "Properties of amorphous and crystallizable hydrocarbon polymers. III studies of the hydrogenation of polybutadiene" *J. Polym. Sci. Polym. Phys. Ed.* **1979**, *17*, 1211.
3. Xu, Z.; Hadjichristidis, N.; Fetters, L. J.; Mays, J. W. "Structure chain flexibility relationships of polymers" *Adv. Polym. Sci.* **1995**, *120*, 1.
4. Rangarajan, P.; Haisch, C. F.; Register, R. A.; Adamson, D. H.; Fetters, L. J. "Influence of semicrystalline homopolymer addition on the morphology of semicrystalline diblock copolymer" *Macromolecules* **1997**, *30*, 494.
5. Sakurai, S.; Hashimoto, T.; Fetters, L. J. "Morphology of polystyrene block poly(ethylene alt propylene) diblock copolymers in the strong segregation limit" *Macromolecules* **1995**; *28*: 7947.
6. Wunderlich, B. *Macromolecular Physics* Vol.1 Academic Press, N.Y. **1973**, Ch.4
7. Brandrup, J.; Immergut, E. H. *Polymer Handbook*, IV/411 **1989**.

# PART I

## **Orientation of Block Copolymer Microdomains in Bulk**

**CHAPTER 3** (modified from *Polymer* **2000**, 41, 2971)

**CHAPTER 4** (modified from *Macromolecules* **2000**, 33, 7931)

## CHAPTER 3: Spherical to Cylindrical Microdomain Transformation by Application of a Flow Field

A structural transformation from a spherical microdomain structure to a cylindrical one in a semicrystalline polystyrene-*b*-polyethylenepropylene-*b*-polyethylene (PS/PEP/PE) terpolymer having a total molecular weight of 103 Kg/mole under a strong external flow field was observed. Quiescently formed samples made by evaporation of the polymer in decalin show the disordered spherical microdomain structure of polystyrene (PS). The roll cast process generated a cylindrical PS microdomain structure well oriented along the flow direction as determined by TEM and SAXS. The observed structural transformation is explained by an analogy to the behavior of surfactant systems under external forces and furthermore this chapter demonstrates that the cylindrical structure is an example of a facilitated equilibrium morphology development by an external force.

### 3.1 Introduction

The mechanical, transport and other properties of multicomponent and multiphase polymer systems largely rely upon their phase morphology and the nature of the interface between these phases. Control of morphology is the key to manipulating the properties of such systems. In addition, controlling phase transitions is essential to advance our knowledge of material properties in multi-component and multi-phase systems.

A number of methods have been found which can induce a shape transformation in a self- assembled system. The transition from vesicle to cylindrical micelle has been observed in the surfactant/solvent systems in three different ways, namely, by an increase in temperature<sup>1</sup>, an addition of a surfactant<sup>2</sup>, or upon mechanical shearing.<sup>3,4</sup> Similar shape transitions from a randomly dispersed spherical structure to an elongated cylindrical structure have been observed in polymer systems including homopolymer/solvent systems<sup>5</sup>, homopolymer /homopolymer /solvent ternary systems<sup>6,7</sup> and homopolymer/block copolymer surfactant systems<sup>8</sup> due to application of mechanical or electrical fields.

Phase transitions in block copolymers have been induced in many ways. Most of the phase transitions in block copolymers have been achieved by evaporating solvent, altering temperature<sup>9</sup> or pressure.<sup>10</sup> Block copolymer microdomain structure can also be altered by simply adding homopolymer of one of the block components.<sup>11-14</sup> Here, solubilization of homopolymer into the same polymer component phase results in the change of the volume fraction of that component which induces a phase transition. A related approach to control the shape of the microdomain is to blend a low molecular weight additive which can preferentially swell one of the block components.<sup>15</sup>

External forces such as shear flow<sup>16-19</sup>, surface orientation<sup>20</sup>, and electric fields<sup>21-23</sup> have generally been applied to obtain a well oriented microphase separated structure rather than to induce phase transitions in block copolymer systems. Attaining a well-oriented structure is useful for both material characterization and detailed investigation of the full tensor properties. The methods using surfaces with specific interactions and electrical fields, however, are limited to relatively thin films, and block copolymers composed of blocks with significantly different dielectric constants, respectively. The application of a flow field to a molten but already microphase separated sample, creates a highly aligned structure due to the forced rotation of the many originally misaligned grains (due to their individual mechanical anisotropy) but leads to numerous morphological defects in the final material.

An orientation method called 'roll casting' developed in our lab can be a good method to obtain a thick and relatively defect-free globally aligned film. This method subjects the material to a hydrodynamic flow as the solvent evaporates and the initially homogeneous solution undergoes microphase separation. Previous studies show that the resultant global orientation of block copolymer films with cylindrical or lamellar morphology is almost single-crystal like using this method.<sup>24-26</sup> Recently a highly oriented spherical microdomain structure arranged on a body-centered cubic lattice as well as an oriented double gyroid bicontinuous cubic microdomain structure have also been produced using the roll cast method.<sup>18,27</sup>

Only a few reports have appeared on the effect of the external forces on phase transformation of block copolymer melts. Hamley et al.<sup>28</sup> detected various intermediate metastable phases between the lamellae and cylindrical phases of a diblock copolymer upon shearing through the transition region. The nature of these intermediate structural states is related to the transformation pathway of the lamellar to the cylindrical microdomain structure. The intermediate structures are termed hexagonally modulated lamellae and layered hexagonal-packed channels. The coexistence of two cylindrical microdomain structures of different lattice symmetries has been observed in a sheared triblock copolymer as reported by Jackson et al.<sup>29</sup> Shearing of a spherical domain structure near the order-disorder transition temperature was shown to transform the material into cylinders. Upon cessation of shearing, the material converts back to the spherical domain structure via epitaxial growth from the oriented cylinder structure resulting in a texture with the [111] direction in the cubic phase parallel to the [001] direction of the hexagonal phase.<sup>30</sup> Recently, Vigild et al.<sup>31</sup> showed a similar epitaxial growth of the double gyroid phase either from a hexagonal perforated layer phase or from a hexagonal cylinder phase obtained by shear aligning. Dair et al.<sup>27</sup> also reported an epitaxial growth of the gyroid phase from a roll cast oriented hexagonal phase of a PS/PI/PS triblock by annealing.

In block copolymer systems, it is well known that the microdomain geometry depends on the relative volume fraction of each segment and their respective degree of polymerization. Flow field energy can, however, shift the zero field phase diagram, as observed in both experimental<sup>32,33</sup> and theoretical<sup>34,35</sup> studies. The suppression of the composition fluctuations by external fields such as shearing drives the system towards the mean-field limit, resulting in an apparent increase of order-disorder transition temperature. For example, Amundson et al.<sup>23</sup> demonstrated that an ordered structure persisted even after heating the materials 14K above the critical temperature of the zero electric field (electric-field-induced shift of the microphase separation).

Most of the phase transitions promoted by applied fields observed in block copolymer melts took place when the phase present under zero field conditions was not

far from a phase boundary, in which case, the external forces need only to provide a small bias to affect the transition. In addition, the field induced structures revert to the previous zero field (equilibrium) structures after cessation of the forces and annealing.

In this chapter, TEM and SAXS are employed to study structure formation in a crystallizable block terpolymer consisting of polystyrene (PS), polyethylene propylene (PEP), and polyethylene (PE) microphase separated with and without the presence of an applied flow field. The chapter shows that the development of the thermodynamically stable morphology can be facilitated by application of an external force during microphase separation. Such an ABC linear terpolymer with one glassy end block (PS) and a crystallizable end block (PE) which are connected via a rubbery midblock (PEP) presents a novel situation in which the crystallization of the end block within the microphase separated structure is partially screened by the rubbery midblock. Since PEP and PE are completely miscible above the  $T_m$  of PE, the microdomain morphology consists of PS domains segregated within a mixed matrix of PE and PEP.<sup>36</sup> The sample is allowed to microphase separate above the  $T_c$  of PE using both the roll casting and simple casting methods, and the films obtained are subsequently quenched in liquid  $N_2$  to limit crystallization. When the temperature drops below the crystallization temperature of PE, phase separation between the PE and PEP blocks will take place within the matrix, leading to some type of crystalline PE morphology. The influence of the crystallization of the PE block on the microdomain structure will be described in the next chapter.

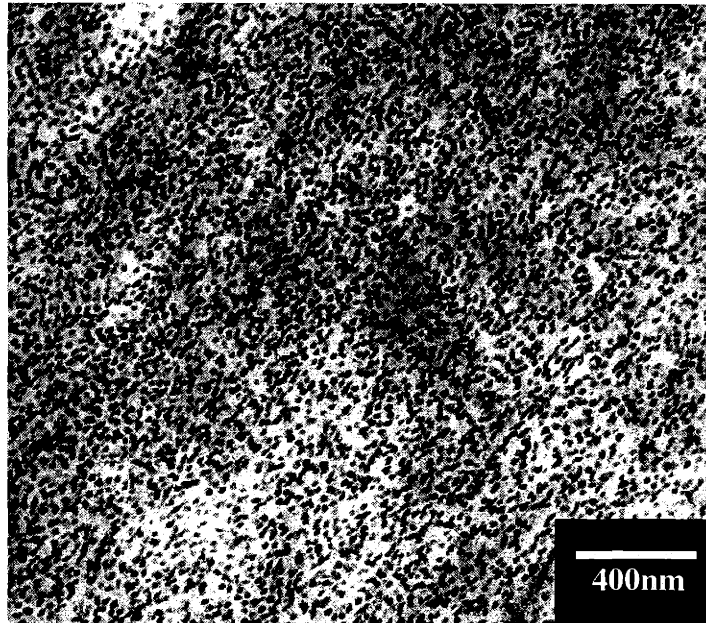
### 3.2 Results and Discussion

The morphology of the simple cast film is shown in the bright field TEM images of Figure 3.1a. A spherical microdomain structure of PS is clearly evident as the dark circular regions selectively stained with  $RuO_4$ . The PS spheres are arranged in the PEP/PE matrix without significant long range order. This is likely due to the weak correlation between PS spheres at the low volume fraction of PS and/or possibly due to the crystallization of PE in the matrix which could disrupt the sphere packing at room temperature.

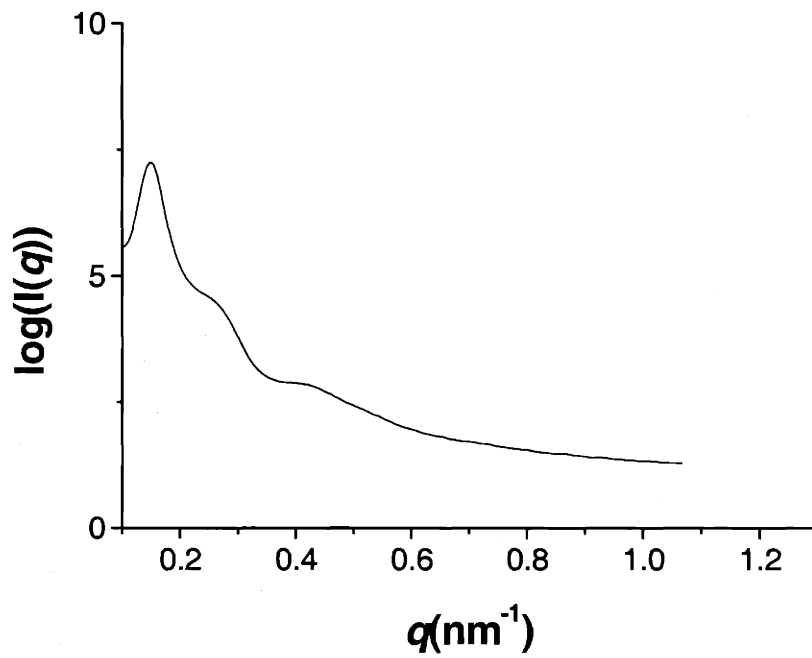
The possibility that crystallization of the PE lamellae disrupts the ordering of the PS spheres was investigated using temperature-controlled SAXS. Figure 3.1b shows the SAXS scattered intensity vs. scattering angle at 140 °C for the simple cast film. There is a distinct low angle reflection and with a shoulder at a  $q$  of approximately  $0.27 \text{ nm}^{-1}$  followed by a broad maximum centered at  $q \sim 0.43 \text{ nm}^{-1}$ . This pattern is similar to those previously observed by Kinning and Thomas<sup>37-39</sup> and Bates et al.<sup>40</sup> for PB micelles packed on a bcc lattice in polystyrene homopolymer/PS-*b*-PB diblock blends. The average inter-sphere distance can be estimated as 42 nm from the first peak( $d_{110}$ ) position. Assuming the broad high  $q$  peak at  $q \sim 0.43 \text{ nm}^{-1}$  arises from the sphere form factor, allows the sphere radius to be estimated as 10 nm. This compares reasonably well to the sphere diameter of 20 nm determined from the TEM image. The small crystals of PE formed during the quenching process apparently do not alter the spherical microdomain structure developed during simple casting and annealing. Bates et al.<sup>41</sup> also showed that quenching a diblock copolymer could result in very fine scale crystallization of the PE block which does not disrupt the microdomain structure established by a high temperature annealing treatment.

Figures 3.2 and 3.3 show 2-dimensional SAXS patterns of a roll cast film. The coordinate system is chosen so the flow direction corresponds to x, the neutral direction to y and the through thickness direction to z. When the incident beam is parallel to the flow direction, an approximate 6-fold symmetric set of intense reflections appear (see Figure 3.2a and b). This indicates that the roll casting process has induced a well oriented, highly ordered structure. The azimuthal averaged intensity scan is shown in Figure 3.2c. The set of Bragg peaks have approximate  $q_n/q_1$  values of 1.0,  $3^{1/2}$ ,  $4^{1/2}$ ,  $7^{1/2}$ ,  $9^{1/2}$  etc. which corresponds well with hexagonal packing. Figure 3.3a and b show 2-dimensional SAXS patterns with the incident beam perpendicular to the flow direction (parallel to y direction). The scattering is concentrated along the normal to the flow direction with peaks again in the ratio of 1.0,  $3^{1/2}$ ,  $4^{1/2}$ ,  $7^{1/2}$  etc. indicating the structure is only two dimensionally ordered as for example, hexagonal packing of cylinders.



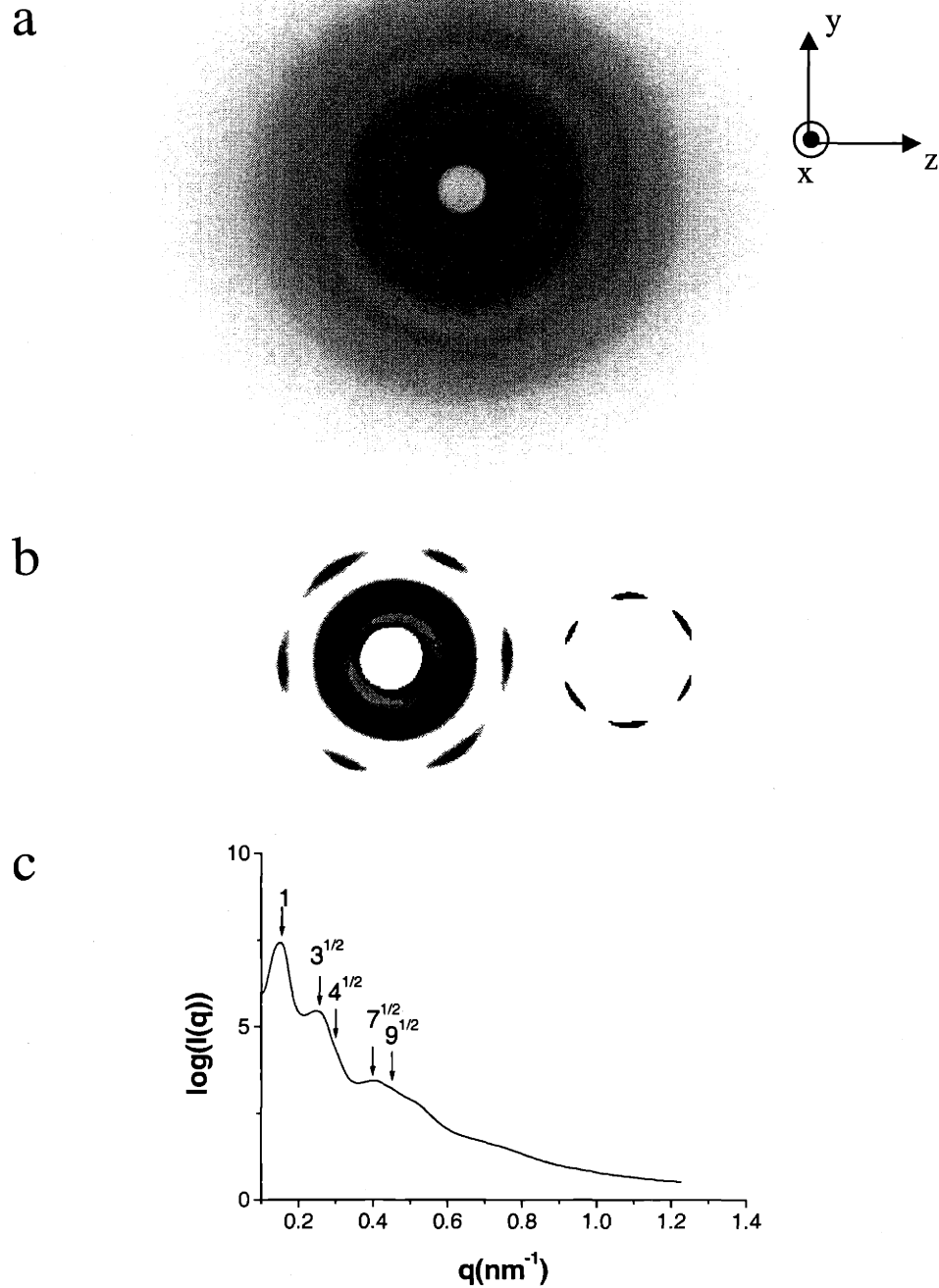


a

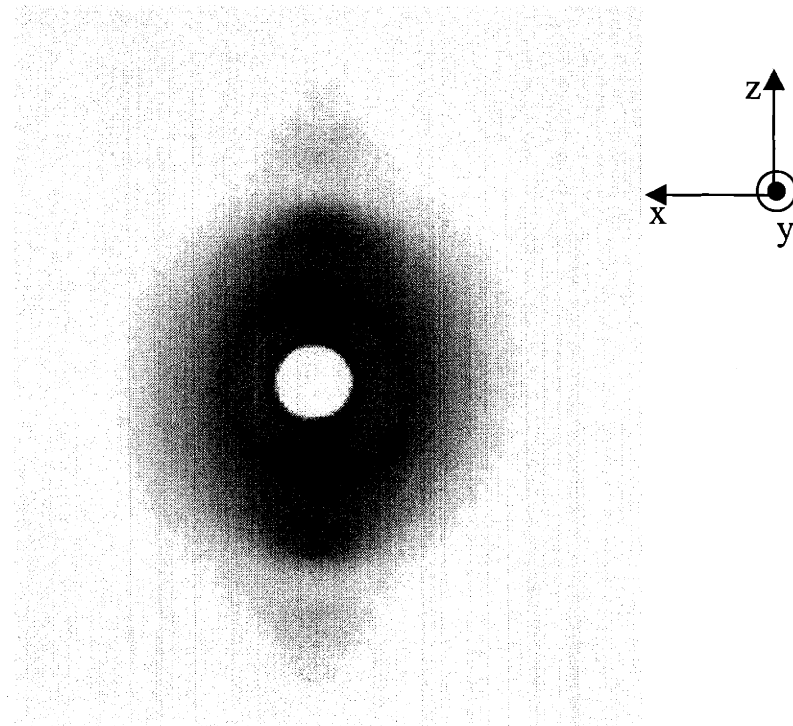


b

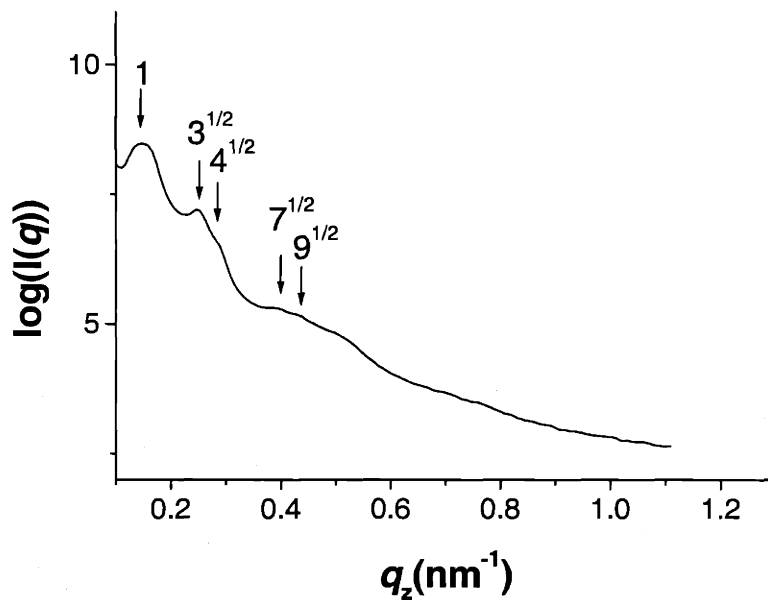
**Figure 3.1** (a) Bright field TEM micrograph for the simple cast PS/PEP/PE (15/70/15) film. The film was stained with  $\text{RuO}_4$  for 20 min so that the PS domains appear dark. Poorly ordered PS spheres are shown. (b) SAXS profiles at 140 °C for the simple cast PS/PEP/PE film.



**Figure 3.2** (a) 2-dimensional SAXS pattern with the incident beam along the flow direction, normal to the YZ plane. (b) SAXS patterns with different threshold cut off to emphasize 6-fold symmetry. (c) Azimuthal averaged SAXS profile shows peaks in the ratio of 1.0,  $3^{1/2}$ ,  $4^{1/2}$ ,  $7^{1/2}$ ,  $9^{1/2}$ .



a



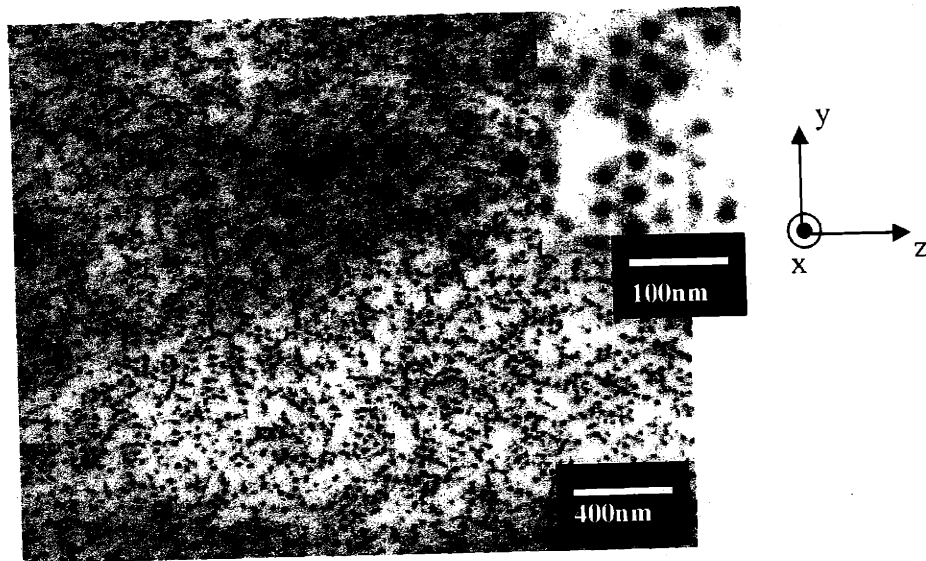
b

**Figure 3.3** (a) 2-dimensional SAXS pattern with the incident beam along the normal to the XZ plane. Several strong reflections are shown perpendicular to the flow direction. (b) SAXS profile along the vertical direction of (a) also shows peaks in the ratio of 1.0, 3<sup>1/2</sup>, 4<sup>1/2</sup>, 7<sup>1/2</sup> etc. confirming the structure is hexagonal packing.

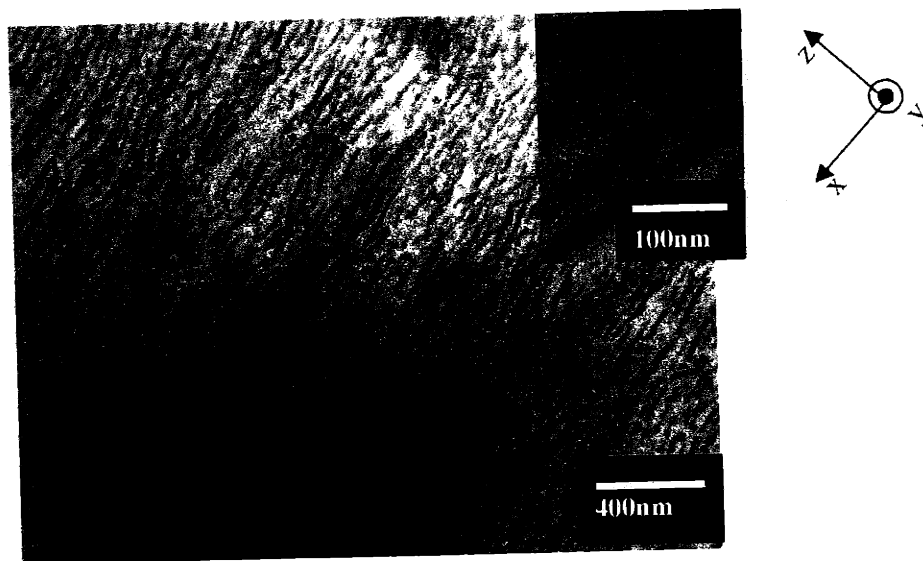
TEM micrographs of the RuO<sub>4</sub> stained sections for views along the flow direction and normal to the flow direction (parallel to y direction) are shown in Figures 3.4a and b. The magnified inset selected area in Figure 3.4a shows that the PS domains clearly self assemble onto a hexagonal lattice during microphase separation under the applied flow field. Interestingly there are many lattice points in the image without any apparent PS domains. These “PS vacancy” defects shown in the micrograph seem not to result from misalignment of many small grains because relatively few grain boundaries are apparent, but from a local deficiency of PS implying gaps of the PS cylinders along the flow direction. The three dimensional structure of the roll cast film becomes plainly evident when examining the view perpendicular to the flow direction. Short cylindrical PS domains and strings of PS spheres are seen everywhere to be oriented along the flow direction. Some spheres are elongated to a prolate ellipsoid shape as apparent in the magnified inset of figure 3.4b. The diameters of the spherical and cylindrical shaped PS domains correspond approximately to 22 and 20 nm respectively.

The morphological examination made for the different directions of the roll cast film demonstrates that the flow field created by the co-rotating cylinders induced a shape transformation from the spherical domain structure of the quiescent film to a cylindrical domain structure during self assembly of the roll cast film. Since after the roll casting, the films were first annealed for 10 days at 140 °C (well above T<sub>g</sub> of PS as well as T<sub>m</sub> of PE), the roll cast-induced phase transformation is a stable state. To determine whether the transformed cylindrical structure is thermodynamically stable or metastable, an even higher temperature annealing was employed. 2D SAXS patterns for the sample annealed at 190 °C for 48 hours are almost the same as those after annealing at 140 °C for 10 days (data not shown), implying that the cylindrical structure is an equilibrium state in spite of a low PS volume fraction (13 vol%). Annealing at a higher temperature than 190 °C was tried but the sample began to degrade at around 200 °C.

The work done by Sakurai et al.<sup>42</sup> confirms the claim of an equilibrium cylindrical microdomain structure at only 13 vol.% minority component. Sakurai et al.<sup>42</sup> obtained the cylindrical morphology of a PS/ PEP block copolymer with a 12.8 vol% polystyrene content by annealing at 300 °C. The material they used is quite similar to the one in the



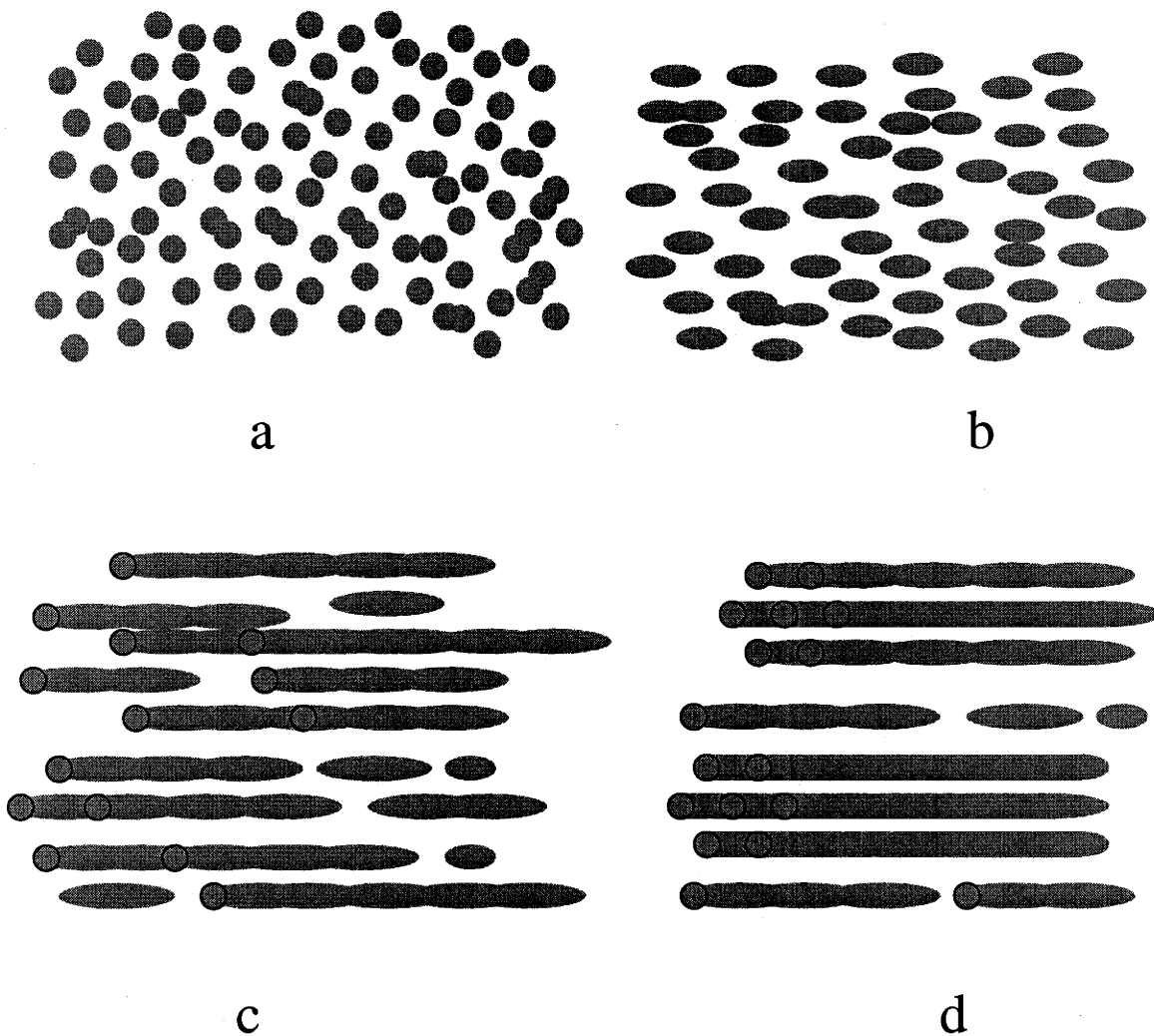
a



b

**Figure 3.4** (a) Bright field TEM micrograph for the roll cast PS/PEP/PE (15/70/15) film: view normal to YZ. The film was stained with  $\text{RuO}_4$ . Circular regions of PS are evident. Inset of the selected area magnified from (a) shows a hexagonally ordered structure but with many regions without PS domains.  
 (b) Bright field TEM micrograph for the roll cast PS/PEP/PE (15/70/15) film: view normal to XZ. Needle shape and prolate spherical PS domains are shown parallel to the roll casting direction. Inset of the selected area magnified from (b) shows an elongated PS domains.

current study in composition as well as in molecular weight. The only difference is that the current material has a small amount of PE component which is completely miscible with PEP above the  $T_m$  of PE. They explained their results by suggesting that conformational asymmetry between the PS segment and PEP segment leads to the shift of the phase boundary toward the PS axis. Thus, it is concluded that the spherical PS morphology obtained by simple casting is a metastable structure and that the cylindrical PS structure developed in the presence of a bias flow field is thermodynamically stable in the current material whose degradation temperature does not allow sufficiently high temperature processing to achieve structural equilibrium. In the simple casting process, the microphase separation during evaporation of the solvent first forms spherical PS microdomains. The subsequent annealing at the experimentally accessible temperature does not provide sufficient energy to overcome the activation energy barrier and transform the metastable sphere structure to the equilibrium cylindrical morphology. However, when energy generated by a strong bias flow field is provided such as in the roll casting process, the sphere morphology becomes unstable under external forces, as predicted by Huang and Muthukumar<sup>35</sup>, and at the same time the structure can overcome the activation energy barrier, leading to the equilibrium morphology with cylindrical microdomains. The factors which coalesce the PS spheres along the flow direction are interfacial energy and viscosity differences. This clustering ultimately leads to the formation of cylinders. The cylinders are aligned in the flow direction as expected, since this orientation represents a minimum in the potential energy when compared with other possible orientations. A similar phase transformation from spherical micelles to cylinder was observed when a block copolymer/homopolymer/solvent blend was subjected to a strong electrical field<sup>7,8</sup> as well as when surfactant solutions were subjected to an applied flow field.<sup>3,4</sup> The transformed structures formed in the other systems are, however, all metastable. A schematic diagram of domain formation and transformation by the flow field is shown in Figure 3.5a – 3.5d.



**Figure 3.5** Schematic diagram of the proposed mechanism of cylinder formation under the flow field with solvent evaporation. (a) Microphase separation is initiated at a certain concentration of polymer solution during the evaporation of solvent in roll casting process. Solvent swollen PS spheres are formed. (b) The PS spheres become prolate and align along the flow direction. (c) The development of needle shape PS cylinders. (d) PS cylinders arrange to form a hexagonally packed structure

The imperfect cylinder structure may be due to the lack of time to form long continuous cylindrical domains even with a strong coupled field due to the dramatic drop in molecular diffusivity resulting from the evaporation of the solvent during roll casting.

The resultant domain structure contains, in addition to cylinders, prolate spheres and pearl shaped strings of PS shown in Figure 3.4b.

Since most block copolymers have relatively low degradation temperatures, a metastable spherical microdomain morphology is likely a common occurrence. This may be a reason that the boundary volume fractions between spherical and cylindrical structure predicted by theories are usually lower than those obtained by experiments.<sup>43</sup>

### 3.3 Conclusions

The metastable spherical structure observed in the quiescently formed solvent cast film of PS/PEP/PE terpolymer can be essentially transformed into a thermodynamically equilibrium cylindrical structure under application of a strong external flow field during microphase separation by the roll cast process. Highly ordered 6-fold SAXS pattern with the incident beam along the flow direction and TEM micrograph of the same plane show a well defined hexagonal arrangement of the PS microdomains. Highly ordered SAXS scattering peaks perpendicular to the flow direction when the incident beam is perpendicular to the flow direction and TEM micrographs also confirm that the spherical microdomain structure was converted into cylindrical structure. The high temperature and long time annealing process verified that the flow field induced cylindrical structure is an equilibrium state which is consistent with the work done by Sakurai et al.<sup>42</sup> The similar observations in some surfactant systems under external forces suggest the mechanism shown in Figure 3.5 to explain the phase transformation.

This chapter illustrates clear experimental evidence of how an equilibrium morphology can be facilitated by an applied field. In addition, it is the first real space study by TEM to investigate the shape transformation from the spherical to cylindrical microdomain structure.



### 3.4 References

1. Salkar, R.A.; Hassan, P. A.; Samant, S. D.; Valaulikar, B. S.; Kumer, V. V.; Kern, F.; Candau, S. J.; Manohar, C. "A thermally reversible vesicle to micelle transition driven by a surface solid-fluid transition" *J Chem Soc Chem Commun* **1996**; 1223.
2. Hassan, P. A.; Valaulikar, B. S.; Manohar, C.; Kern, F.; Bourdieu, L.; Candau, S. J. "Vesicle to micelle transition: Rheological investigations" *Langmuir* **1996**; 12:4350.
3. Oda, R.; Panizza, P.; Schmutz, M.; Lequeux, F. "Direct evidence of the shear-induced structure of wormlike micelles: Gemini surfactant 12-2-12" *Langmuir* **1997**; 13: 6407.
4. Mendes, E.; Narayanan, J.; Oda, R.; Kern, F.; Candau, S. J. "Shear-induced vesicle to wormlike micelle transition" *J Phys Chem B* **1997**; 101: 2256.
5. Wirtz, D.; Berend, K.; Fuller, G. G. "Electric-field induced structure in polymer solutions near the critical point" *Macromolecules* **1992**; 25: 7234.
6. Winoto, D.; Carr, H. "Grating diffraction of blends involving NLO random copolymers" *Macromolecules* **1996**; 29: 5149.
7. Xi, K.; Krause, S. "Droplet deformation and structure formation in two-phase polymer/polymer/toluene mixtures in an electric field" *Macromolecules* **1998**; 31: 3974.
8. Serpico, J. M.; Wnek, G. E.; Krause, S.; Smith, T. W.; Luca, D. J.; Van Laeken, A. "Electric field induced morphologies in polystyrene/poly(styrene-b-ethylene oxide) blends" *Macromolecules* **1992**; 25: 6373.
9. Khandpur, A. K.; Forster, S.; Bates, F. S.; Hamley, I. W.; Ryan, A. J.; Bras, W.; Almdal, K.; Mortensen, K. "Polyisoprene-polystyrene diblock copolymer phase diagram near the order-disorder transition" *Macromolecules* **1995**; 28: 8796.
10. Pollard, M.; Russell, T. P.; Ruzette, A. V.; Mayes, A. M.; Gallot, Y. "The effect of hydrostatic pressure on the lower critical ordering transition in diblock copolymers" *Macromolecules* **1998**; 31: 6493.
11. Tanaka, H.; Hasegawa, H.; Hashimoto, T. "Ordered structure in mixtures of a block copolymer and homopolymers. 1. Solubilization of low molecular weight homopolymers" *Macromolecules* **1991**; 24: 240.
12. Winey, K. I.; Thomas, E. L.; Fetters, L. J. "Ordered morphologies in binary blends of diblock copolymer and homopolymer and characterization of their intermaterial dividing surfaces" *J Chem Phys* **1991**; 95: 9367.
13. Winey, K. I.; Thomas, E. L.; Fetters, L. J. "Isothermal morphology diagrams for binary blends of diblock copolymer and homopolymer" *Macromolecules* **1992**; 25: 2645.
14. Sakurai, S.; Irie, H.; Umeda, H.; Nomura, S.; Lee, H. H.; Kim, J. K. "Gyroid structures and morphological control in binary blends of polystyrene-block-polyisoprene diblock copolymers" *Macromolecules* **1998**; 31: 336.
15. Prasman, E.; Thomas, E. L. "High-strain tensile deformation of a sphere-forming triblock copolymer mineral oil blend" *J Polym Sci Part B Polym Phys* **1998**; 36: 1625.
16. Folkes, M. J; Keller, A.; Scalisi, F. P. "An extrusion technique for the preparation of "single crystals" of block copolymers" *Colloid Polym. Sci.* **1973**, 251, 1.

17. Hadziioannou, G.; Mathis, A.; Skoulios, A. "Obtention de monocristaux de copolymères trisequences styrene/isoprene/styrene par cisaillement plan" *Colloid Polym. Sci.* **1979**, 257, 136.
18. Morrison, F. A.; Winter, H. H. "Effect of unidirectional shear on the structure of triblock copolymers.1. polystyrene polybutadiene polystyrene" *Macromolecules* **1989**; 22: 3533.
19. Morrison, F. A.; Winter, H. H.; Gronski, W. Barnes, J. D. "Effect of unidirectional shear on the structure of triblock copolymers. 2. Polystyrene polyisoprene polystyrene" *Macromolecules* **1990**; 23: 4200.
20. Anastasiadis, S. H.; Russell, T. P.; Satija, S. K.; Majkrzak, F. "The morphology of symmetric diblock copolymers as revealed by neutron reflectivity" *J Chem Phys*, **1990**; 92: 5677.
21. Amundson, K.; Helfand, E.; Davis, D. D.; Quan, X.; Patel, S.; Smith, S. D. "Effect of an electric field on block copolymer microstructure" *Macromolecules* **1991**; 24:6546.
22. Amundson, K.; Helfand, E.; Davis, D. D.; Quan, X.; Smith, S. D. "Alignment of lamellar block copolymer microstructure in an electric field. 1.alignment kinetics" *Macromolecules* **1993**; 26: 2698.
23. Amundson, K.; Helfand, E.; Davis, D. D.; Quan, X.; Hudson, S. D.; Smith, S. D. "Alignment of lamellar block copolymer microstructure in an electric field. 2.mechanisms of alignment" *Macromolecules* **1994**; 27: 6559.
24. Albalak, R. J.; Thomas, E. L. "Microphase separation of block copolymer solutions in a flow field" *J Polym Sci Part B Polym Phys* **1993**; 32: 37.
25. Albalak, R. J.; Thomas, E. L. "Roll casting of block copolymers and of block copolymer homopolymer blends" *J Polym Sci Part B Polym Phys* **1994**; 32: 341
26. Albalak, R. J.; Thomas, E. L.; Capel, M. S. "Thermal annealing of roll cast triblock copolymer films" *Polymer* **1997**; 38: 3819.
27. Dair, B. J.; Avgeropoulos, A.; Hadjichristidis, N.; Honeker, C. C.; Capel, M.; Thomas, E. L. "Oriented double gyroid films via roll casting" *Polymer* **2000** 41 6231.
28. Hamley, I. W.; Koppi, K. A.; Rosedale, J. H.; Bates, F. S.; Almdal, K.; Mortensen, K. "Hexagonal mesophases between lamellae and cylinders in a diblock copolymer melt" *Macromolecules* **1993**; 26: 5959.
29. Jackson, C. L.; Barnes, K. A.; Morrison, F. A.; Mays, J. W.; Nakatani, A. I.; Han, C. C. "A shear induced martensitic like transformation in a block copolymer melt" *Macromolecules* **1995**; 28: 713.
30. Koppi, K. A.; Tirrell, M.; Bates, F. S.; Almdal, K.; Mortensen, K. "Epitaxial growth and shearing of the body centered cubic phase in diblock copolymer melts" *J Rheo* **1994**; 38: 999.
31. Vigild, M. E.; Almdal, K.; Mortensen, K.; Hamley, I. W.; Fairclough, J. P. A.; Ryan, A. J. "Transformations to and from the Gyroid Phase in a Diblock Copolymer" *Macromolecules* **1998**; 31: 5702.
32. Koppi, K. A.; Tirrell, M.; Bates, F. S. "Shear induced isotropic to lamellar transition" *Phys Rev Lett* **1993**; 70; 1449.
33. Alan, I.; Nakatani, A. I.; Sung, L.; Hobbie, E. K.; Han, C. C. "Shear-Induced Order in a Homopolymer Blend with Block Copolymer Surfactant" *Phys Rev Lett* **1997**; 79: 4693.

34. Cates, M. E.; Milner, S. T. "Role of shear in the isotropic to lamellar transition" *Phys Rev Lett* **1989**; 62: 1856.
35. Huang, C. Y.; Muthukumar, M. "Effect of shear on order-disorder and order-order transitions in block copolymers" *J Chem Phys* **1997**; 107: 5561.
36. Rangarajan, P.; Haisch, C. F.; Register, R. A.; Adamson, D. H.; Fetters, L. J. "Influence of semicrystalline homopolymer addition on the morphology of semicrystalline diblock copolymers" *Macromolecules* **1997**; 30: 494.
37. Kinning, D. J.; Thomas, E. L.; Fetters, L. J. "Morphological studies of micelle formation in block copolymer homopolymer blends" *J Chem Phys* **1989**; 90: 5806.
38. Kinning, D. J.; Winey, K. I.; Thomas, E. L. "Structural transitions from spherical to nonspherical micelles in blends of poly(styrene butadiene) diblock copolymer and polystyrene homopolymers" *Macromolecules* **1988**; 21: 3502.
39. Kinning, D. J.; Thomas, E. L. "Hard sphere interactions between spherical domains in diblock copolymers" *Macromolecules* **1984**; 17: 1712.
40. Bates, F. S.; Berney, C. V.; Cohen, R. E. "Microphase structure of solvent cast diblock copolymers and copolymer homopolymer blends containing spherical microdomains" *Macromolecules* **1983**; 16: 1101.
41. Khandpur, A.; Macosko, C. W.; Bates, F. S. "Transmission electron microscopy of saturated hydrocarbon block copolymers" *J Polym Sci Part B Polym Phys* **1995**; 33: 247.
42. Sakurai, S.; Hashimoto, T.; Fetters, L. J. "Morphology of polystyrene block poly(ethylene alt propylene) diblock copolymers in the strong segregation limit" *Macromolecules* **1995**; 28: 7947.
43. Vavasour, J. D.; Whitmore, M. D. "Self consistent field theory of block copolymers with conformational asymmetry" *Macromolecules* **1993**; 26: 7070.

## **CHAPTER 4: Influence of an Oriented Glassy Cylindrical Microdomain Structure on the Morphology of Crystallizing Lamellae in a Semicrystalline Block Terpolymer**

The effect of an oriented microphase separated structure, induced by an applied flow bias field (roll casting), on the crystallization of the polyethylene (PE) block in a semicrystalline polystyrene-*block*-(polyethylene-*alt*-propylene)-*block*-polyethylene terpolymer has been analyzed. The orientation and morphology of the emerging crystals with respect to the pre-existing glassy cylindrical microdomain structure has been investigated by simultaneous wide angle and small angle X-ray scattering and transmission electron microscopy.

The oriented hexagonally packed cylinders induce oriented crystallization of the PE block in the matrix upon slow cooling below the crystallization temperature. The texture which develops has the *b* and *c* axes of the PE crystals predominantly parallel and perpendicular to the PS cylinder axes, respectively. The lateral packing of the PS cylinders is disrupted by the crystallization, but the longitudinal orientation of the cylinders is maintained.

### **4.1 Introduction**

Semicrystalline block copolymers have been studied for their possible application as replacements for glassy/rubbery block thermoplastic elastomers due to their improved mechanical properties as well as better thermal stability.<sup>1-23</sup> In addition, semicrystalline block copolymers have been recently shown to provide new means to nanoscale patterned thin films.<sup>24</sup> There exists strong scientific interest in these materials because they can undergo at least two thermodynamic transitions during their process history. Understanding how the competition of the crystallization, the microphase separation, and the glass transition leads to the final morphology is the key in furthering our knowledge of the properties of semicrystalline block copolymers.

In general, one can expect that the microstructure and physical properties of the material will be significantly influenced by the nature of the chain and domain

organization in both the non-crystalline and crystalline blocks. The process pathway of structure formation is of prime importance in that the first forming structures present to those emerging a prescribed geometry into which the new structure must evolve. Studies have been done on anionically synthesized model block copolymers having a crystallizable block to reveal how the final sample morphology depends not only on the sequence of transitions the material experiences, but also on the relative thermodynamic strengths of the transitions. Various groups<sup>1-24</sup> have shown that the morphology of semicrystalline block copolymers is path dependent; different microdomain structures are obtained if the crystallization occurs from a homogeneous melt (in this case the crystallization drives the microphase separation) or it occurs from an already microphase separated heterogeneous melt (in this case microphase separation precedes crystallization and provides a microstructure within which crystallization takes place).

When the block incompatibility is small, as for instance for the block copolymers composed of crystallizable polyethylene (PE) blocks and poly(ethylene-*alt*-propylene) (PEP) or poly(ethylene) amorphous blocks, such as those analyzed by Rangarajan et al.,<sup>6,9</sup> crystallization occurs from a homogeneous melt resulting in the formation of alternating lamellar microdomains in a spherulitic superstructure regardless of the copolymer composition,<sup>5</sup> as has been assumed in theoretical treatments.<sup>25,26</sup>

When the block segments have a larger interaction parameter and also have high molecular weights, microphase separation in the melt occurs prior to crystallization. The presence of microdomains in the ordered melt may affect the crystallization process and the final morphology.<sup>1,2,4,7,8,14,17-19,21,23</sup> However, when the order-disorder transition is close to the melting temperature of the crystallizable block, the energy barrier for destruction of the ordered melt is small and the crystallization may alter the order achieved during the microphase separation. For example, a weakly segregated lamellar structure of the melt of ethylene/head-to-head propylene block copolymer was transformed into a strongly segregated spherulitic microstructure containing crystalline lamellae after crystallization of PE block. A caprolactone-butadiene diblock copolymer<sup>5</sup> also clearly showed the replacement of the melt microstructure by a crystallization-driven morphology. Ryan et al.<sup>11</sup> showed that a cylindrical microstructure of the melt of

poly(ethylene-*b*-ethylethylene) diblock copolymer is reorganized upon crystallization into a final spherulitic lamellar morphology.

In an AB diblock copolymer where the B block is crystallizable, the microdomain melt morphology can be preserved, when the  $T_g^A$  (the glass transition temperature of A block)  $> T_c^B$  (the crystallization temperature of B block). Such a situation confines the crystals to grow within or between the pre-existing microseparated domains. Crystallization confined in pre-existing lamellar<sup>4,7,8,14,21,23</sup> spherical<sup>2</sup> or cylindrical<sup>1,17-20</sup> microdomains has been observed.

Globally aligned semicrystalline block copolymers permit determination of the orientation of the crystals and the unit cell with respect to the microdomain interfaces. Cohen et al.<sup>7,8</sup> first used a channel die to orient PE containing semicrystalline block copolymers and showed that the chain axis of PE crystals is perpendicular to the normal direction of microphase separated lamellar surfaces. Other workers also studied lamellar systems using the shear forces for alignment of the microphase separated block copolymer structures and found that the orientation of the chain axis of crystals depends on several factors such as molecular weight of the block copolymer and the crystallization conditions.<sup>14,15,23</sup> Quiram et al.<sup>20</sup> recently used a channel die to study the crystal orientation in a sample wherein the crystallizable block constituted the cylindrical microdomains and demonstrated that the crystalline PE lamellae grow along the PE cylinder axis.

Studies of the oriented microstructure in the case that the crystallizable component forms and aligns within the majority matrix phase due to the pre-existing minority glassy microstructure are not yet reported in single block copolymer system. Liu et al. showed that the crystalline poly(tetrahydrofuran) (PTHF) block is oriented due to the confinement in between the cylindrical poly(methylmethacrylate) (PMMA) microdomains in the blend of the diblock copolymer and homo PTHF.<sup>27</sup> However, they did not provide direct evidence of the molecular chain orientation.

In this chapter I use simultaneous wide angle X-ray scattering (WAXS) and small angle X-ray scattering (SAXS), transmission electron microscopy (TEM) to study the morphology of a polystyrene-*block*-(polyethylene-*alt*-propylene)-*block*-polyethylene terpolymer (PS/PEP/PE). Since the PEP and PE blocks are completely miscible above the

melting temperature ( $T_m$ ) of PE (Chapter 3), a microstructure of PS microdomains in a matrix of mixed PE and PEP blocks is expected above the  $T_m$  of the PE component. When the temperature drops below the crystallization temperature of PE, another phase separation takes place within the matrix, due to the crystallization of PE. The PS and PE end-blocks are connected via the rubbery PEP mid-block, presenting a novel situation in which the crystallization of the PE end-block between the microphase separated glassy PS structure is partially screened by the rubbery mid-block. In order to study the influence of the presence of well aligned minority PS microdomains on the growth and organization of the PE molecular chains and PE crystalline lamellae, I employ the roll cast method at temperature above the crystallizing point of the PE and well below the microphase separation temperature to obtain an aligned hexagonally packed PS cylindrical microdomain structure.<sup>28-30</sup> The development of oriented crystalline PE microdomains was observed upon slow cooling in the well defined microseparated PS structure by scattering and microscopy.

## 4.2 Results and Discussion

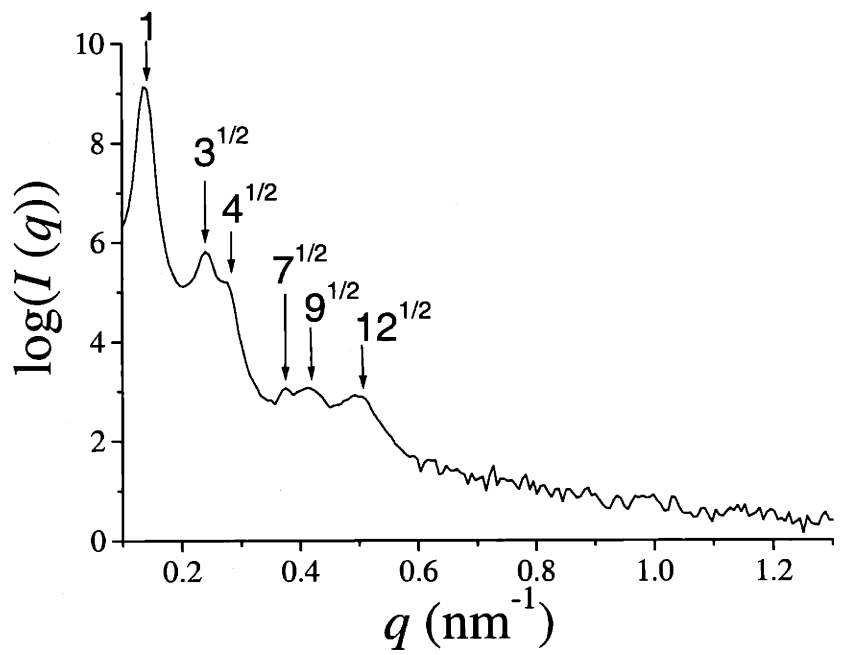
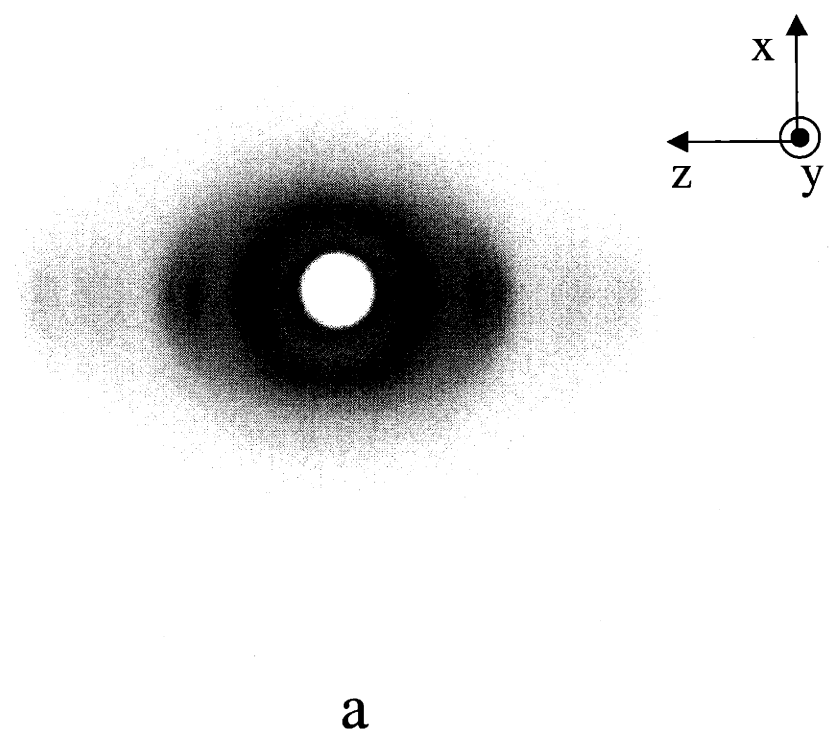
Figure 4.1a shows the SAXS pattern of a roll cast sample after long term annealing, heated to 150 °C with the incident beam normal to the XZ plane, perpendicular to the flow direction. The scattering is concentrated along the normal to the flow direction. The intensity scan across the equator as a function of the scattering vector is shown in Figure 4.1b. The set of Bragg peaks present in Figure 4.1a have  $q_n/q_1$  approximate values of 1.0,  $\sqrt{3}$ ,  $\sqrt{4}$ ,  $\sqrt{7}$ ,  $\sqrt{9}$  etc. (where  $q_1$  is the scattering vector of the first peak  $q_1 = 0.14 \text{ nm}^{-1}$ ), which corresponds well with a hexagonal packing. Figure 4.1c shows the SAXS pattern of the roll cast film recorded with the incident X-ray beam along the normal to the YZ plane, parallel to the flow direction. Adjusting the threshold cut off intensity allows emphasis of the 6-fold symmetry of both the first and the second order reflection in Figure 4.1d. As expected, the pattern presents an approximate 6-fold symmetric set of intense reflections, which indicates that the roll casting process has induced a well oriented, highly ordered structure. SAXS therefore indicates that the structure is a two dimensionally ordered hexagonal packing of PS cylinders whose axes are parallel to the flow direction. The value of the scattering vector of the first peak ( $q_1 = 0.14 \text{ nm}^{-1}$ ),

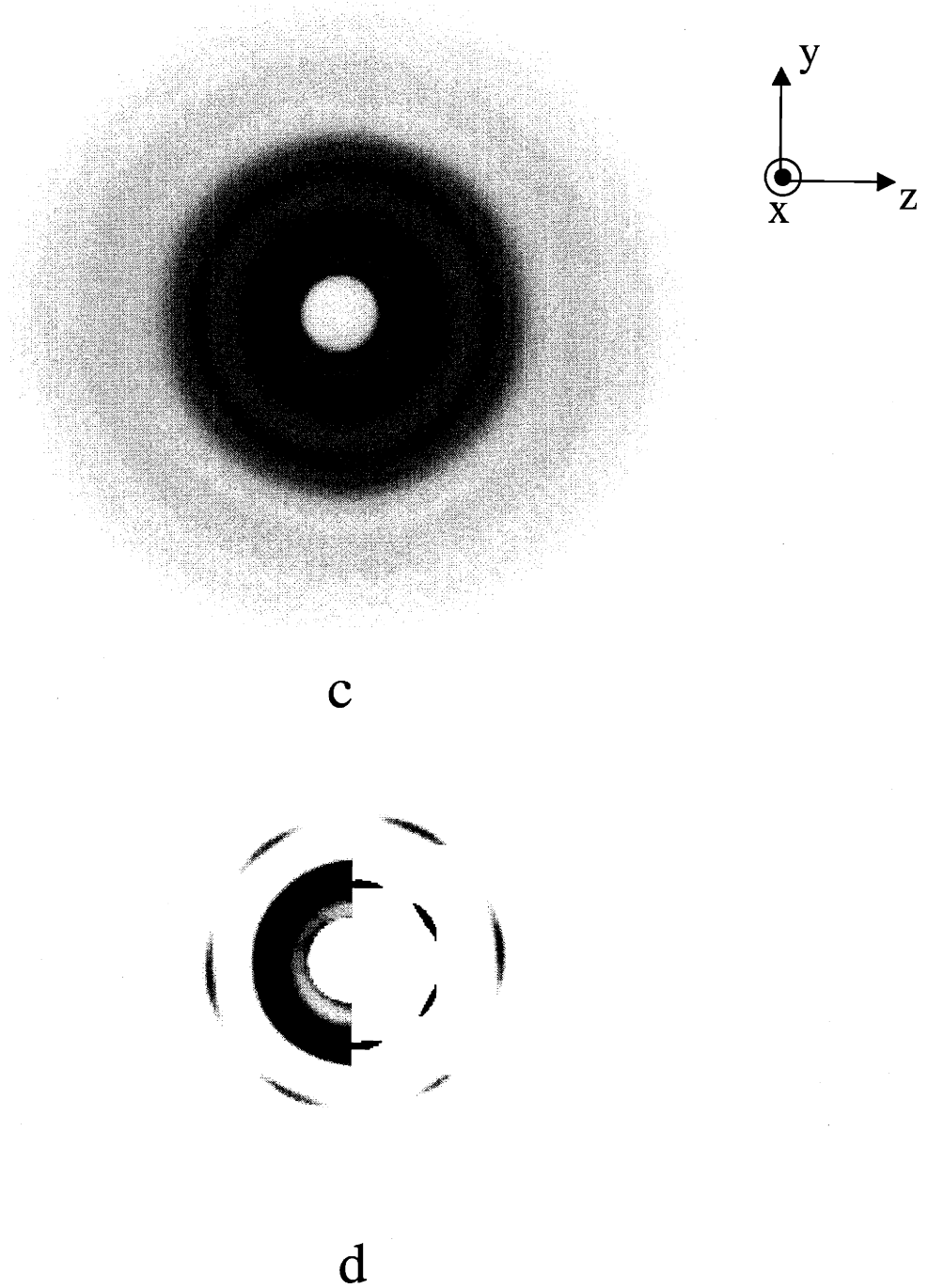
corresponding to the  $(10\bar{1}0)$  reflection, indicates that the hexagonal lattice has a periodicity of 45 nm. The 150 °C SAXS patterns for the two different incident beam directions are very similar to those of the quenched roll cast sample in the chapter 3 (Figure 3.2). Since the small PE crystals developed during the quenching step do not disturb the cylindrical PS microdomain structure, the microstructure at room temperature after quenching can be assumed the same as that at 150 °C as mentioned in the chapter 3. The TEM micrographs of the quenched samples in our previous work suggest that the microstructure at 150 °C is a hexagonally packed cylinder structure as expected from the SAXS results. However, the PS cylinders are not the customary infinitely long straight units. Rather they display a range of prolate structures aligned along the flow direction. Many defect points along the cylinder axis occur due to low volume fraction of the PS block (0.13) as well as due to high activation energy to reach the equilibrium cylindrical microstructure.

The SAXS patterns, recorded during the cooling with the rate of 2 °C/min do not change much with decreasing temperature until around 70 °C. At this temperature the first and higher order peaks broaden and a shoulder appears at high  $q$  region. The patterns become diffuse above  $q = 0.2 \text{ nm}^{-1}$ , indicating disturbance of the microdomain pattern by the PE crystals and the superposition of peaks arising from the inter-lamellae scattering of the crystalline PE regions in the matrix. A similar thermal treatment of the hydrogenated 1,4 PB homopolymer with a molecular weight of 65,000 g/mol and the same butyl content ratio, give a first order reflection peak around  $q \sim 0.2 \text{ nm}^{-1}$  and a broad intermediate peak ( $q \sim 0.4 \text{ nm}^{-1}$ ).

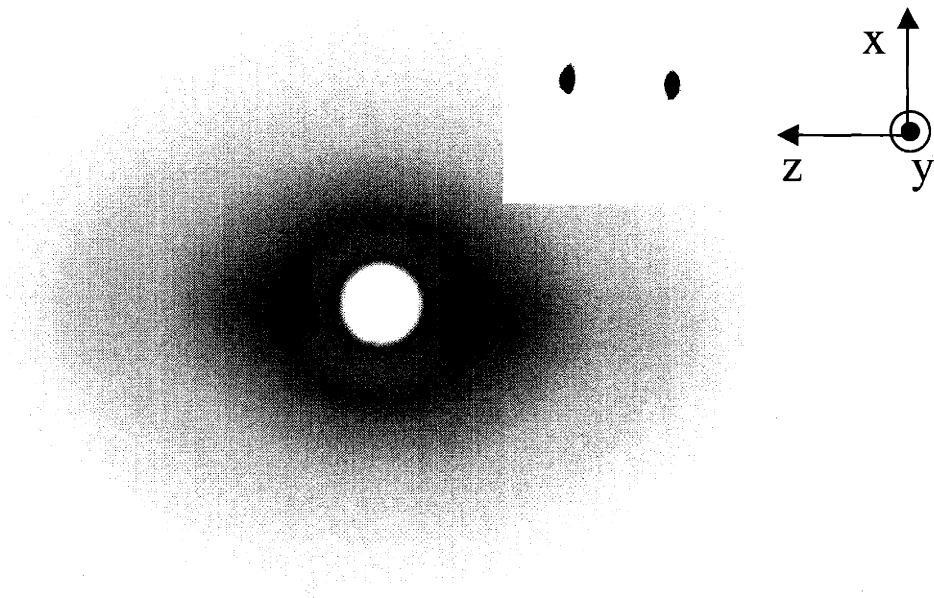
Figure 4.2 shows the SAXS patterns of the slowly cooled sample at 50 °C, when the incident beam is perpendicular to the XZ (3.2a) and YZ planes (3.2c), respectively. The intensity scan across the equator of the block copolymer melt, recorded at 50 °C is compared to that for 150 °C in Figure 4.2b. The increased intensity around  $q \sim 0.2 \text{ nm}^{-1}$  and broad scattering intensity at  $q \sim 0.4 - 0.5 \text{ nm}^{-1}$ , in the pattern at 50 °C, are due to scattering from the crystalline PE lamellae and/or due to the partial distortion of the pre-existing microstructure (Figure 4.2b). The invariant location of the first peak at  $q = 0.14 \text{ nm}^{-1}$  (compare with the pattern at 150 °C), and the retention of the 2 fold and the 6 fold



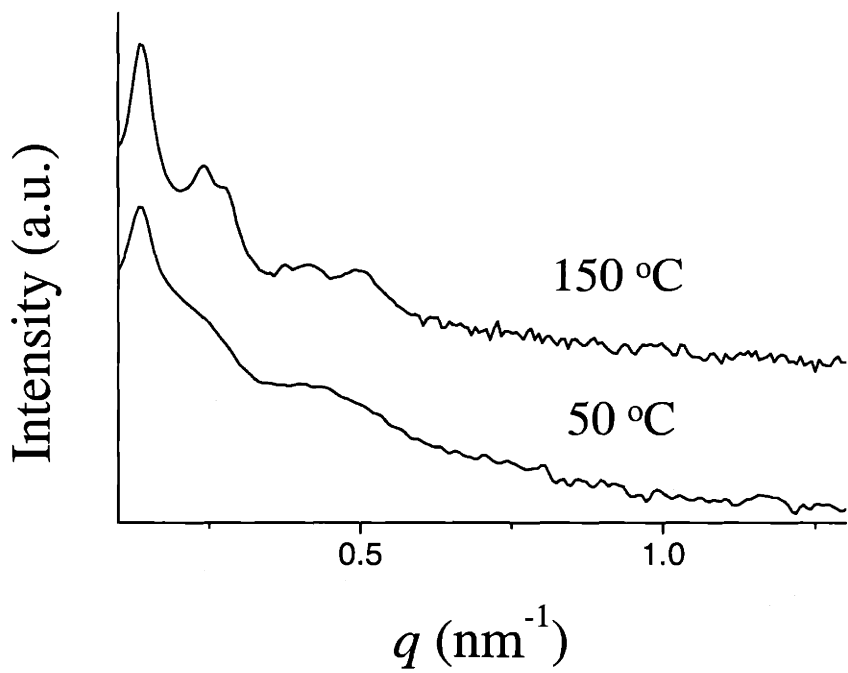




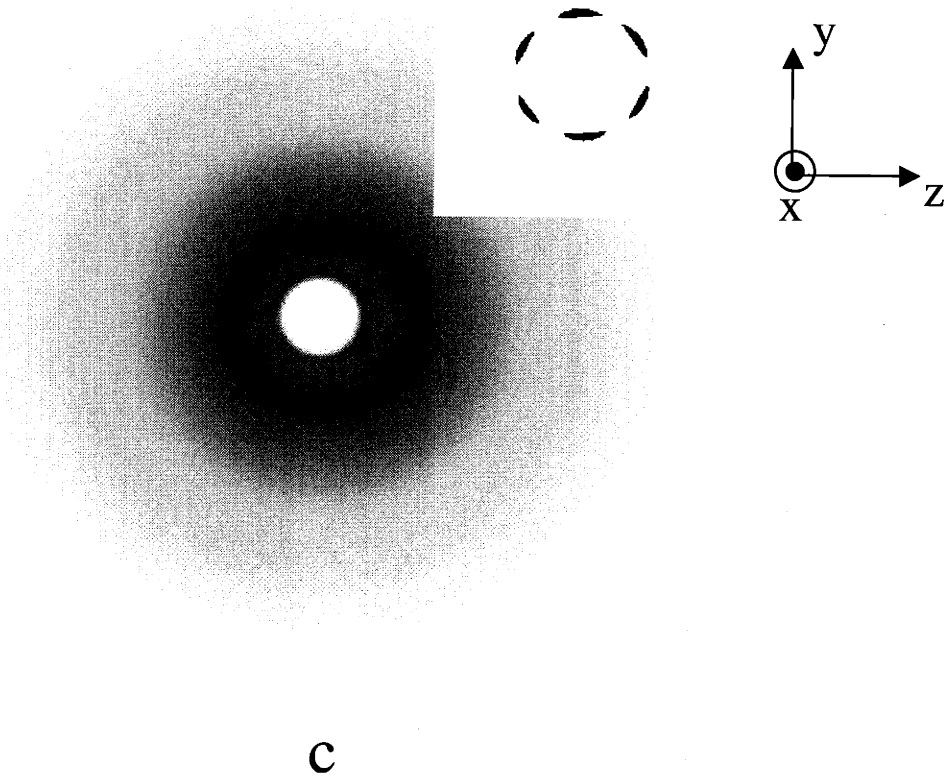
**Figure 4.1** (a) 2-dimensional SAXS pattern of the roll cast sample taken at 150 °C with the incident beam perpendicular to the flow direction, normal to the XZ plane. Several strong reflections are shown perpendicular to the flow direction. (b) SAXS profile along the horizontal (equatorial) direction of (a) shows peaks in the ratio of  $1:\sqrt{3}:\sqrt{4}:\sqrt{7}:\sqrt{9}:\sqrt{12}$  etc., implying the structure is characterized by a hexagonal packing of cylinders. (c) 2-dimensional SAXS pattern of the roll cast sample at 150 °C with the incident beam along the flow direction, normal to the YZ plane. (d) SAXS pattern with different threshold cut off to emphasize the 6-fold symmetry of the first and second order reflection.



a



b



**Figure 4.2** (a) 2D SAXS pattern of the slowly cooled sample taken at 50 °C when the incident beam perpendicular to the XZ plane. The pattern with a different threshold cut off to emphasize the first order reflection is shown in the inset. It confirms that the oriented structure of the PS microdomains formed by the applied flow field is preserved after the crystallization of PE.

(b) Comparison between the SAXS profiles along the horizontal (equatorial) direction ( $\pm 10^\circ$  sector slice) at 150 °C and at 50 °C. The increase of the scattering intensity at the high  $q$  region ( $q = 0.4 \sim 0.5 \text{ nm}^{-1}$ ), due to the presence of the crystalline PE lamellae is apparent in the 50 °C pattern.

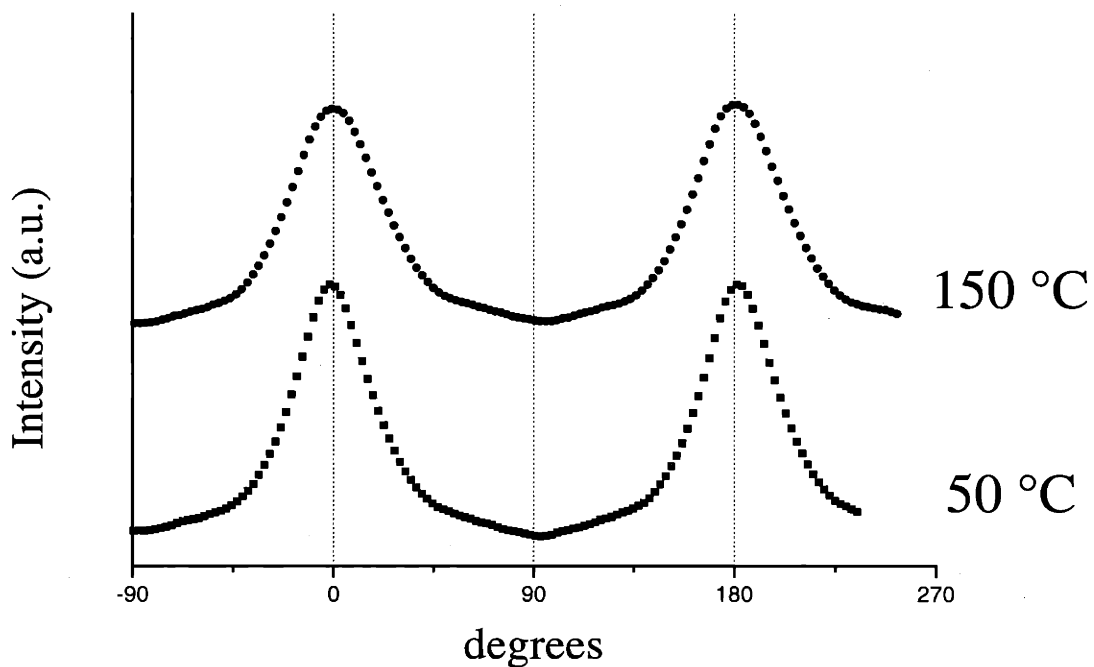
(c) 2D SAXS pattern of the slowly cooled sample at 50 °C when the incident beam along the flow direction normal to YZ plane. The same pattern with a different threshold cut off to emphasize the 6 fold symmetry of the first  $\sqrt{1}$  reflection, is shown in the inset. The  $\sqrt{3}$  reflection is only observed as a weak, broad continuous ring. It indicates that the lateral packing of the PS microdomain structure developed during the roll cast was perturbed by the crystallization of PE.

symmetry axes, clearly shown in the insets of Figures 4.2a and 4.2c respectively, indicate that the texture developed during the roll cast process remains after crystallization. The SAXS patterns indicate that the axes of PS cylinders are still parallel to the flow direction and the average distance between the hexagonally packed cylinders is still 48 nm. The distortion of the microstructure due to the crystallization of the PE primarily affects the inter-cylinder lateral packing, resulting in the loss of the higher order reflections.

The effect of the PE crystallization on the orientation of the cylindrical PS microdomains along the flow direction can be made by comparing the Full Width Half Maximum (FWHM) values at 50 °C to those at 150 °C. The azimuthal scattered intensity distributions of the  $(10\bar{1}0)$  reflection at 50 °C and at 150 °C of Figure 4.2a and 4.1a respectively are shown in Figure 4.3. Both azimuthal FWHM are approximately 45°, indicating that the orientation of the cylindrical PS microdomains does not change along the flow direction due to crystallization of the PE component.

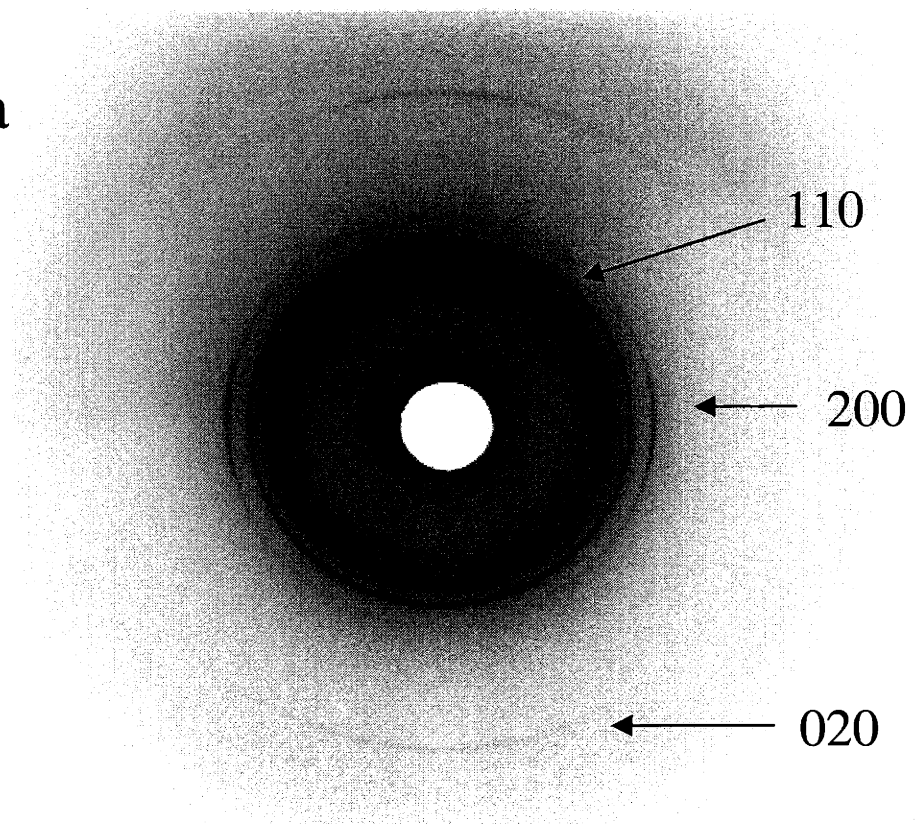
The WAXS pattern of the slowly cooled sample recorded at 50 °C with the incident beam normal to the XZ plane is shown in Figure 4.4a. The pattern presents four evident rings: an unoriented, broad innermost ring due to scattering from amorphous PS, PEP and PE regions and three oriented, narrow, outer rings corresponding to the (110), (200) and (020) reflections arising from the PE crystals in the usual orthorhombic form. It is apparent that the (110) reflection is textured into four off-axis regions of high intensity, while the less intense (200) and (020) reflections show two arcs concentrated on the equator and on the meridian respectively. A schematic of the WAXS pattern is given in Figure 4.4b. The presence of four arcs for the 110 reflection, two equatorial arcs for the (200) reflections and two meridian arcs for (020) indicates that the PE lamellae are oriented with the *b* axis parallel to the flow direction. The SAXS (Figure 4.2a) and WAXS (Figure 4.4a) patterns, therefore, suggest that the crystalline PE lamellae are primarily oriented with their *b* axis parallel, and the chain axis normal, to the axes of the PS cylinders. The measure of azimuthal separation of the (110) reflection peaks is approximately 114° which indicates within experimental uncertainty that the PE crystal stems are preferentially oriented perpendicular to the PS cylinder axis.<sup>20</sup> The WAXS pattern with the incident X-ray beam directed along the X axis, parallel to the flow

direction, and therefore parallel to the  $b$  axis, reported in Figure 4.4c, displays isotropic rings for the (110) and (200) reflection. Although the six-fold symmetry of the oriented  $\sqrt{1}$  reflection of the cylindrical PS microdomain structure is still evident after the PE crystallization (Figure 4.2c), the PE crystals formed in-between the PS cylinders show  $\infty$  fold rotational symmetry of their  $b$  axes around the PS cylinder axis. Strong crystallization forces disturb the long range lateral packing of the PS cylinders as described earlier.

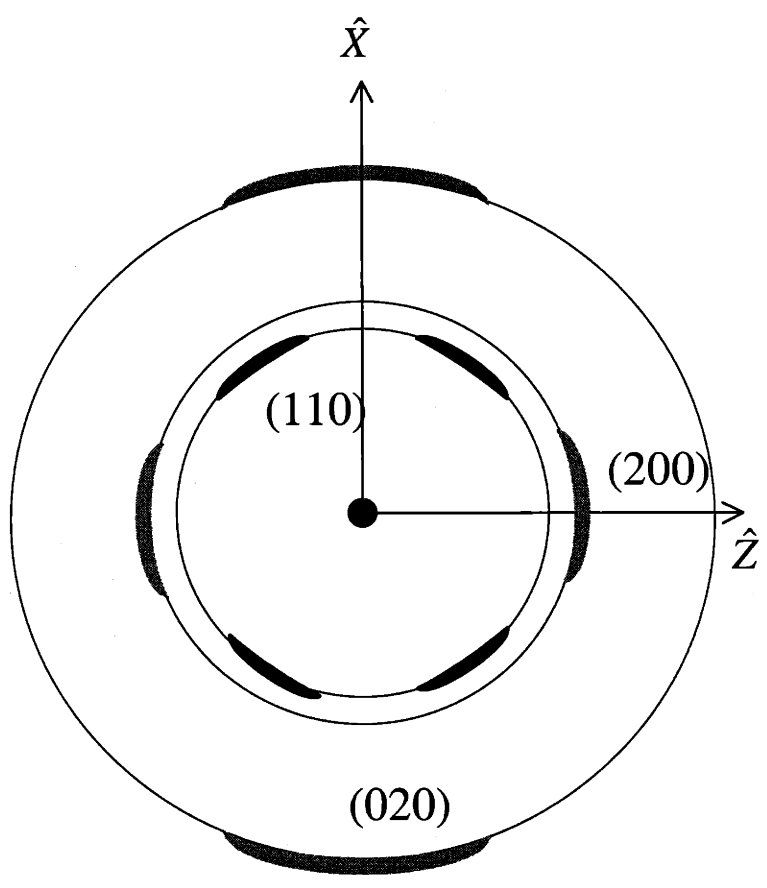


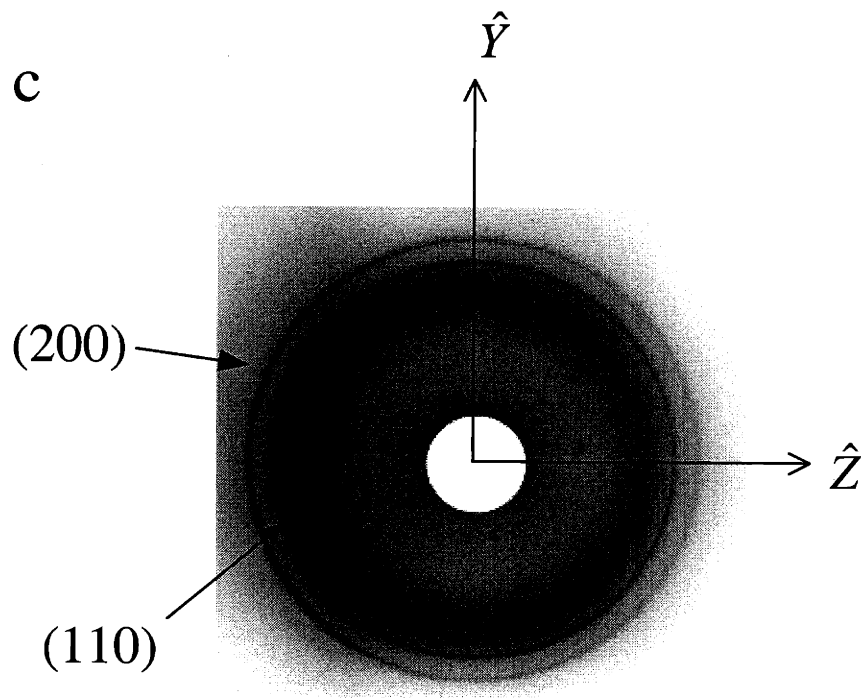
**Figure 4.3** The equatorial azimuthal intensity distribution profiles of the  $(10\bar{1}0)$  reflection at 150 °C in figure 4.1a and at 50 °C in figure 4.2a. Two highly oriented peaks appear at 0 ° and 180 ° at both temperatures. The FWHM value of the peak is approximately 45 ° in both cases, indicating that the crystallization of the PE block does not disturb the orientation of the cylindrical PS microdomains along the flow direction.

a



b





**Figure 4.4** (a) 2-dimensional WAXS patterns, obtained simultaneously with the SAXS pattern of figure 2a, of the slowly cooled sample with the incident beam normal to the XZ plane. The diffuse inner ring is the unoriented amorphous halo. The first crystalline reflection corresponds to (110) reflection of orthorhombic PE crystals and displays four off-axis regions of high intensity. The (200) and (020) reflections are preferentially located on the equator and on the meridian respectively. These features indicate that the PE lamellae are oriented with the *b* axis normal to the X-ray beam, therefore parallel to the flow direction.

(b) Schematic diagram of the WAXS pattern with indexed reflections.

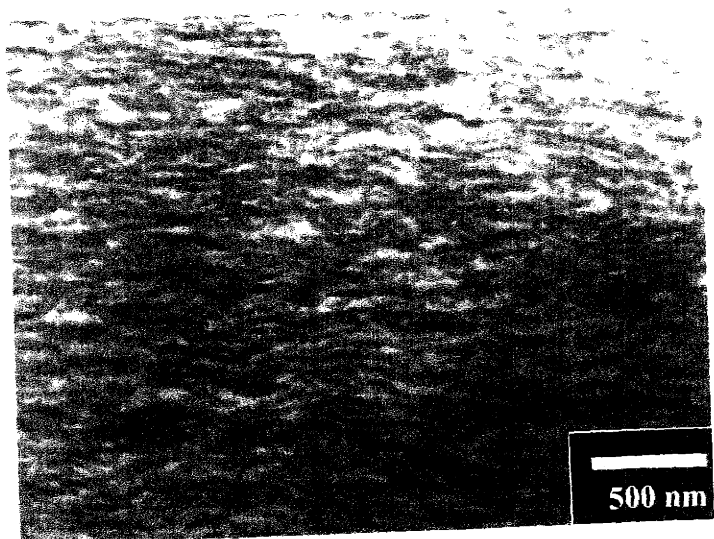
(c) 2-dimensional WAXS pattern, obtained simultaneously with SAXS pattern of figure 4.2c, of the slowly cooled sample with the incident beam normal to the YZ plane. The isotropic (110) and (200) diffraction rings indicate uniaxial symmetry around the *b* axis of the PE crystals.



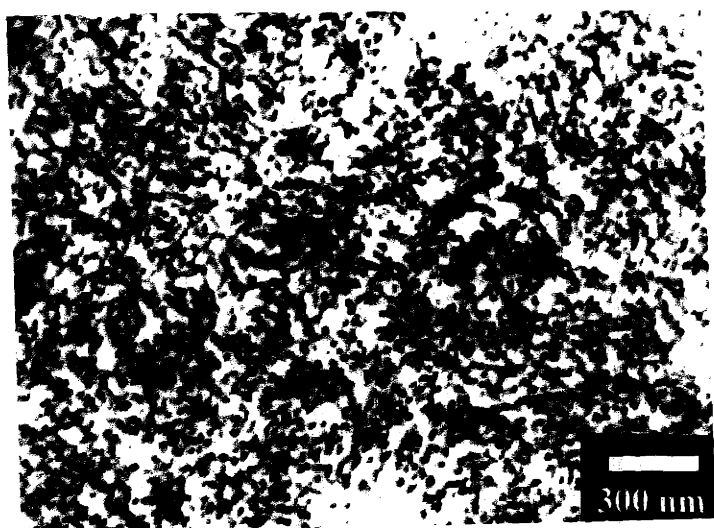
The axial orientation of the PE crystals can be also assessed by the FWHM of the (020) reflection of Figure 4.4a. The FWHM value corresponds to the degree of the orientation of the  $b$  axis of the PE crystals along the flow direction. The value is about  $45^\circ$  which is consistent with the degree of the orientation of the PS cylinders along the flow direction measured by the azimuthal FWHM of the  $(10\bar{1}0)$  reflection at  $50^\circ\text{C}$  in Figure 4.3 ( $\sim 45^\circ$ ). An approximately axi-symmetric orientation of the PE lamellae around the  $b$  axis, which is parallel to the PS cylinder axis, accounts for WAXS patterns of Figure 4.4c.

When cooled below  $T_c^{\text{PE}}$ , crystalline PE lamellae nucleate and grow in various directions. The fast growth direction of the PE crystals is the  $b$  axis direction.<sup>31</sup> In the present work, when the fast growth direction of the crystalline PE lamellae is parallel to the cylinder axis of the PS microdomains, large crystals can grow, whereas in other directions, the crystals encounter the PS microdomains. This bias results in the preferred alignment of the  $b$  axis of the PE parallel to the PS cylinder axis.

TEM of the  $\text{RuO}_4$  stained sections permits direct visualization of the PS cylinders in the slowly cooled sample. A transverse view of the PS cylinders parallel to the flow field is observed in Figure 4.5a. The PS cylinders display waviness and a distribution of lengths. The average diameter of the PS cylindrical microdomains is nearly 20 nm, and the average distance between the cylinders is 40 ~ 50 nm, in agreement with the SAXS data. The oriented structure along the flow direction in Figure 4.5a is very similar to that of the quenched sample in the chapter 3 (Figure 3.4b). The crystallization of the PE block does not much affect the pre-oriented PS microstructure along the flow direction consistent with the FWHM data (Figure 4.3). However, the hexagonally packed structure is disturbed by the crystallization of PE in the matrix as evident from Figure 4.5b. The axial view of the structure shows circular cross sections of the  $\text{RuO}_4$  stained PS cylinders with poor lateral registry. In comparison with Figure 3.4a in the chapter 3, the crystallization of the PE lamellae via the slow cooling significantly disrupts the hexagonal packing of the PS cylinders.

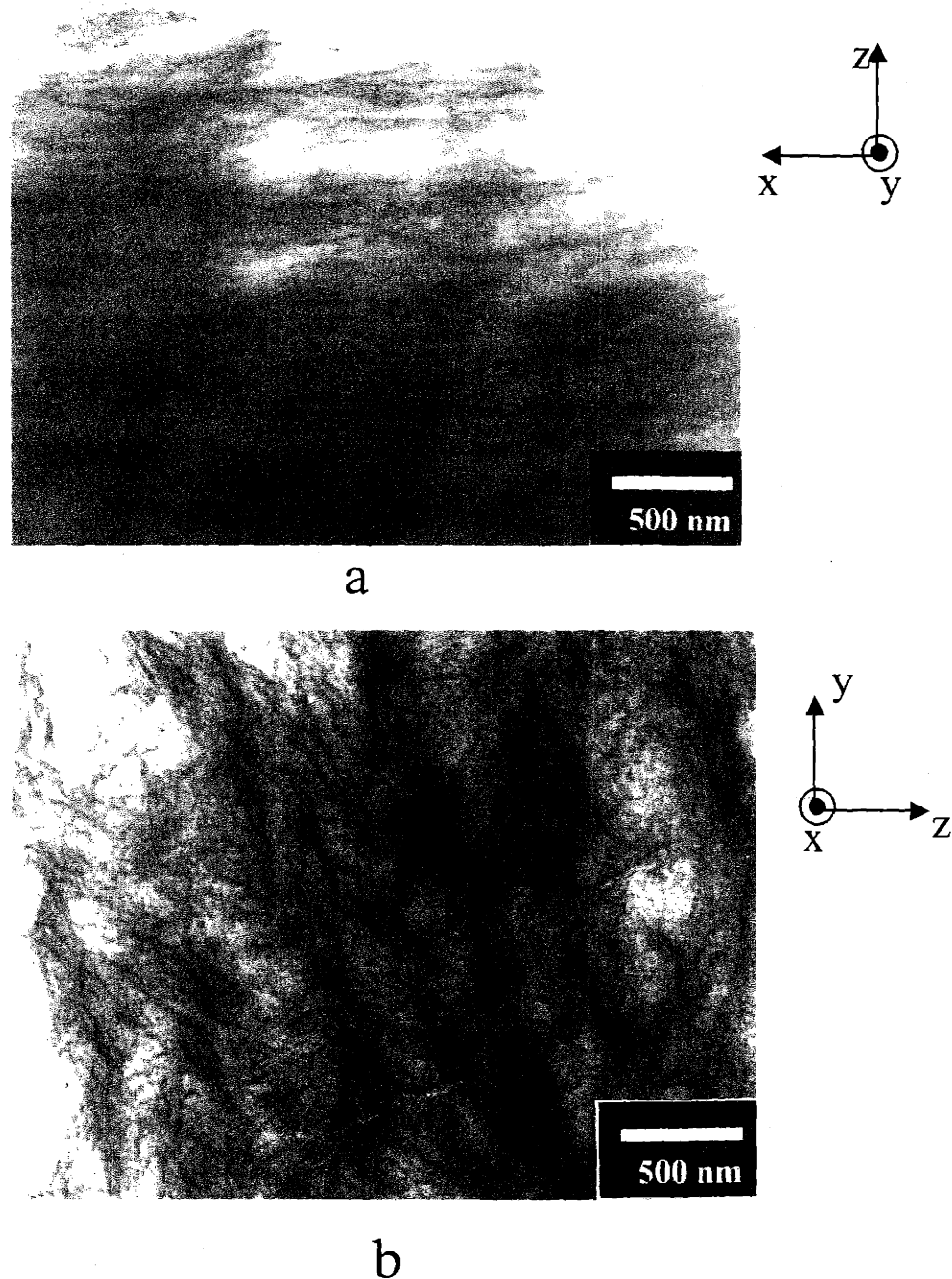


a



b

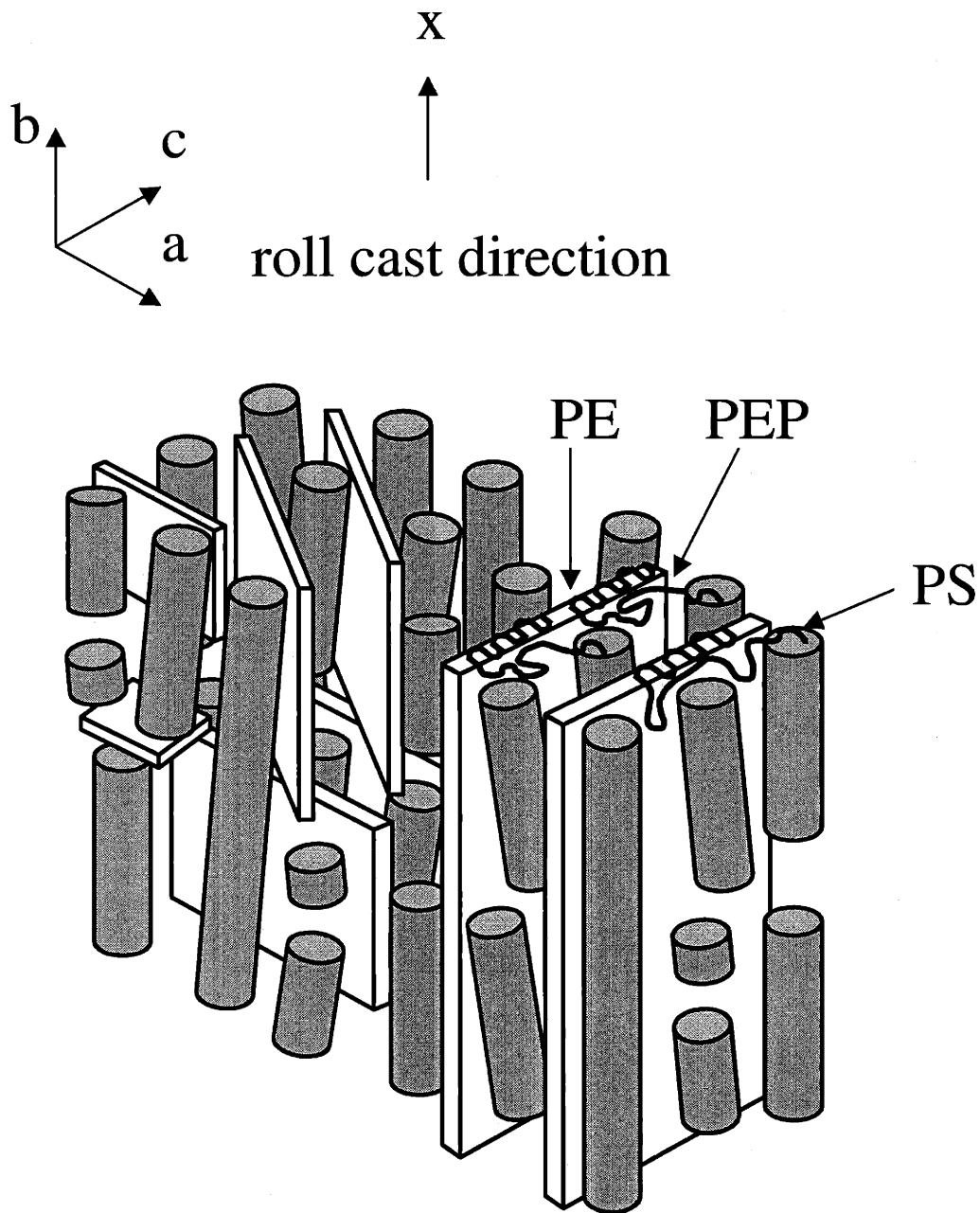
**Figure 4.5** Bright field TEM images of the microtomed sections of the slowly cooled roll cast films stained with  $\text{RuO}_4$ .  
 (a) Transverse view showing PS cylinders aligned parallel to the flow direction. The orientation of PS cylinders is still preserved after the crystallization of PE.  
 (b) Axial view showing circular cross sections of PS cylinders. The hexagonally packed structure, observed in the SAXS pattern taken at  $150^\circ\text{C}$ , is disrupted by the crystallization of PE in the matrix.



**Figure 4.6** Underfocus phase contrast bright field TEM images of the microtomed sections of the unstained roll cast films slowly cooled to room temperature.  
 (a) Transverse view showing crystalline PE lamellae (seen edge-on) (dark region), oriented along the roll casting direction. The thickness of lamellae ranges from 10 nm to 20 nm.  
 (b) Axial view showing crystalline PE lamellae (seen edge-on) oriented in various directions.

The crystalline PE lamellae can be seen in the TEM micrographs of the unstained sample as reported in Figure 4.6a,b. Phase contrast obtained by underfocus of the objective lens makes the noncrystalline regions appear bright.<sup>32</sup> The phase contrast is proportional to the mean inner potential difference between microdomains projected through the specimen. The mean inner potentials of the blocks in the terpolymer are 7.35, 7.08 and approximately 6.3 for the PE crystal, the PS and amorphous PE and PEP respectively.<sup>32</sup> Thus, those lamellae which are oriented edge-on to the electron beam direction and completely traverse the sample provide the highest contrast. For the regions where the projection across the sample includes the PS, PEP and PE domains, the contrast is much lower and does not uniquely correspond to domain size. When viewed along the normal to the XZ plane (Figure 4.6a), those crystalline PE lamellae, for which the *b* axis is parallel to the PS cylinders are evident. The thickness of lamellae is estimated as 10 to 20 nm. In the TEM image viewed along the flow direction, i.e. along the axes of the PS cylinders and the *b* axis of the PE lamellae, the crystalline PE lamellae are seen edge-on oriented in various directions (Figure 4.6b). The TEM images confirm that the PE lamellae are oriented with their *b* axes parallel to the axes of the PS cylinders but have many orientations around the *b* axis.

A model of the PS-PEP-PE terpolymer microstructure after the crystallization of the PE block is shown in Figure 4.7. The crystallization of PE is confined between the pre-existing pseudo hexagonally packed PS cylinders. The PE chain axis is preferentially oriented orthogonal to the PS cylinder axis with the fast growth *b* axis direction of PE parallel to the axis of the cylinders. This type of unit cell orientation occurs because it allows the PE lamellae to grow long in the direction parallel to the PS cylinders. This orientation was also observed by Quiram et al.<sup>20</sup> in the case of a poly(ethylene-*b*-vinylcyclohexane) where the crystallization occurred within the cylindrical PE microdomains. Rotation of crystalline lamellae around the average cylinder axis direction may occur when the growing lamellae encounter some defects such as, for instance, misaligned PS cylinders and prolate PS spheres as shown in TEM micrographs of Figure 4.5a. The development of lamellae with different orientations results in the partial disturbance of the long range hexagonal packing of the PS cylinders. In an ideal hexagonal packing microstructure, three different orientations of the planar crystalline



**Figure 4.7** Schematic diagram of the microdomain structure of the slowly cooled roll cast sample. The crystallization of PE is confined between the preformed hexagonally packed PS cylinders, and  $b$  and  $c$  axes of the PE crystals are preferentially parallel and perpendicular to the axes of the PS cylinders respectively. Various orientations of the crystalline PE lamellae develop on the view of the YZ plane not only due to the hexagonal symmetry of the cylindrical PS microdomains but also due to many defects and misaligned PS cylinders in the roll cast microstructure. In addition, random nucleation of the PE crystals in the matrix generates various other orientations.

lamellae on the view of the YZ plane could be expected. However, in our sample, the initial roll cast structure is not perfect in terms of cylinder packing, orientation and defects. Also the random nucleation of the PE crystals results in a variety of lamellar orientation with the strong forces of crystallization tending to disrupt the lateral packing of the PS microdomains. Those crystallizing lamellae, which have their *b* axes parallel to the PS cylinder axis, develop preferentially leading to an overall orientation of the PE *b* axis.

### 4.3 Conclusions

The crystallization of PE component in the matrix of the semicrystalline PS/PEP/PE block terpolymer does not significantly disturb the orientation of the pre-existing cylindrical PS microdomain structure, but does disrupt the lateral packing of the PS cylinders. The oriented microstructure of the minority PS phase induces orientation of the crystallizing PE microdomains. Crystalline PE lamellae organize themselves with the fast growth direction of the PE following the orientation of the PS cylinders. The strong forces of crystallization disrupt the lateral packing of the PS cylinders. The *b* and *c* axes of the PE crystals are predominantly parallel and perpendicular to the axes of the PS cylinders, respectively.

A preformed oriented microstructure is shown to be able to induce orientation of the subsequent lamellae crystallizing in the matrix. Furthermore, this study, using the model semicrystalline block terpolymer, provides a way to control the morphology of the nanocomposite of semicrystalline polymer and fillers (organic and inorganic types). Pre-aligned nanoscale anisotropic fillers such as nanotube and clays could induce the orientation of the crystalline phase of the semicrystalline polymer matrix.

## 4.4 References

1. Seguela, R.; Prud'homme, J.: "Structural and mechanical properties of a polyethylene-based thermoplastic elastomer" *Polymer*, **1989**, 30, 1446.
2. Cohen, R.E.; Cheng, P.L.; Douzinas, K.C.; Kofinas, P.; Berney, C.V.: "Path-dependent morphologies of a diblock copolymer of polystyrene/hydrogenated polybutadiene." *Macromolecules* **1990**, 23, 324.
3. Douzinas, K.C.; Cohen, R.E.; Halasa, A.F.: "Evaluation of domain spacing scaling laws for semicrystalline diblock copolymers." *Macromolecules* **1991**, 24, 4457.
4. Douzinas, K.C.; Cohen, R.E.: "Chain folding in EBEE semicrystalline diblock copolymers": *Macromolecules* **1992**, 25, 5030.
5. Nojima, S.; Kato, K.; Yamamoto, S.; Ashida, T. "Crystallization of block copolymers. 1. small angle X ray scattering study of an epsilon caprolactone butadiene diblock copolymer" *Macromolecules* **1992**, 25, 2237.
6. Rangarajan, P.; Register, R.A.; Fetters, L.J.: "Morphology of semicrystalline block copolymers of ethylene-(ethylene-*alt*-propylene)." *Macromolecules* **1993**, 26, 4640.
7. Cohen, R.E.; Bellare, A.; Drzewinski, M.A.: "Spatial organization of polymer chains in a crystallizable diblock copolymer of polyethylene and polystyrene." *Macromolecules* **1994**, 27, 2321.
8. Kofinas, P.; Cohen, R.E.: "Morphology of highly textured poly(ethylene)/poly(ethylene-propylene) (E/EP) semicrystalline diblock copolymers." *Macromolecules* **1994**, 27, 3002.
9. Rangarajan, P.; Register, R.A.; Adamson, D.H.; Fetters, L.J.; Bras, W.; Naylor, S.; Ryan, A.J.: "Dynamics of structure formation in crystallizable block copolymers" *Macromolecules* **1995** 28, 1422.
10. Rangarajan, P.; Register, R.A.; Fetters, L.J.; Bras, W.; Naylor, S.; Ryan, A.J.: "Crystallization of a weakly segregated polyolefin diblock copolymer." *Macromolecules* **1995**, 28, 4932.
11. Ryan, A. J.; Hamley, I. W.; Bras, W.; Bates, F. S. "Structure development in semicrystalline diblock copolymers crystallizing from the ordered melt" *Macromolecules* **1995**, 28, 3860.
12. Yang, Y.-W.; Tanodekaew, S.; Mai, S.-M.; Booth, C.; Ryan, A. J.; Bras, W.; Viras, K. "Structures of oxyethylene oxybutylene diblock copolymers in their solid and liquid states" *Macromolecules* **1995**, 28, 6029.
13. Khandpur, A. K.; Macosko, C. W.; Bates, F. S. "Transmission electron microscopy of saturated hydrocarbon block copolymers" *J. Polym. Sci. Polym. Phys. Ed.* **1995**, 33, 247.
14. Hamley, I.W.; Fairclough, J.P.A.; Terrill, N.J.; Ryan, A.J.; Lipic, P.M.; Bates, F.S.; Andrews, E.: "Crystallization in oriented semicrystalline diblock copolymers." *Macromolecules* **1996**, 29, 8835.
15. Hamley, I. W.; Fairclough, J. P. A.; Ryan, A. J.; Bates, F. S.; Town-Andrews, E. "Crystallization of nanoscale-confined diblock copolymer chains" *Polymer* **1996**, 37, 4425.
16. Ryan, A. J.; Fairclough, J. P. A.; Hamley, I. W.; Mai, S.-M.; Booth, C. "Chain folding in crystallizable block copolymers" *Macromolecules* **1997**, 30, 1723.

17. Rangarajan, P.; Haisch, C. F.; Register, R. A.; Adamson, D. H.; Fetters, L. J. "Influence of semicrystalline homopolymer addition on the morphology of semicrystalline diblock copolymer" *Macromolecules* **1997**, *30*, 494.
18. Quiram, D. J.; Register, R. A.; Marchand, G. R. "Crystallization of asymmetric diblock copolymers from microphase-separated melts" *Macromolecules* **1997**, *30*, 4551.
19. Quiram, D. J.; Register, R. A.; Marchand, G. R.; Ryan, A. J. "Dynamics of structure formation and crystallization in asymmetric diblock copolymers" *Macromolecules* **1997**, *30*, 8338.
20. Quiram, D. J.; Register, R. A.; Marchand, G. R.; Adamson, D. H. "Chain orientation in block copolymers exhibiting cylindrically confined crystallization" *Macromolecules* **1998**, *31*, 4891.
21. Hillmyer, M.A.; Bates, F.S.: "Influence of crystallinity on the morphology of poly(ethylene oxide) containing diblock copolymers." *Macromol. Symp.* **1997**, *117*, 121.
22. Balsamo, V.; von Gyldenfeldt, F.; Stadler, R. "Thermal behavior and spherulitic superstructures of SBC triblock copolymers based on polystyrene (S), polybutadiene (B) and a crystallizable poly(epsilon-caprolactone) (C) block" *Macromol. Chem. Phys.* **1996**, *197*, 3317.
23. Zhu, L.; Cheng, S. Z. D.; Calhoun, B. H.; Ge, Q.; Quirk, R. P.; Thomas, E. L.; Hsiao, B. S.; Yeh, F.; Lotz, B. "Crystallization temperature-dependent crystal orientations within nanoscale confined lamellae of a self-assembled crystalline-amorphous diblock copolymer" *J. Am. Chem. Soc.* **2000** *122*, 5957.
24. Reiter, G.; Castelein, G.; Hoerner, P.; Riess, G.; Blumen, A.; Sommer, J.U. "Nanometer-scale surface patterns with long-range order created by crystallization of diblock copolymers" *Phys. Rev. Letters* **1999**, *83*, 3844.
25. Di Marzo, E. A.; Guttman, C. M.; Hoffman, J. D. "Calculation of lamellar thickness in a diblock copolymer, one of whose components is crystalline." *Macromolecules* **1980**, *13*, 1194.
26. Whitmore, M. D.; Noolandi, J. "Theory of crystallizable block copolymer blends" *Macromolecules* **1988**, *21*, 1482.
27. Liu, L. Z.; Chu, B. "Crystalline structure and morphology of microphases in compatible mixtures of poly(tetrahydrofuran-methyl methacrylate) diblock copolymer and polytetrahydrofuran" *J. Polym. Sci., Part B: Polym. Phys.* **1999**, *37*, 779.
28. Albalak, R. J.; Thomas, E. L. "Microphase separation of block copolymer solutions in a flow field" *J Polym Sci Part B Polym Phys* **1993**; *32*: 37.
29. Albalak, R. J.; Thomas, E. L. "Roll casting of block copolymers and of block copolymer homopolymer blends" *J Polym Sci Part B Polym Phys* **1994**; *32*: 341
30. Albalak, R. J.; Thomas, E. L.; Capel, M. S. "Thermal annealing of roll cast triblock copolymer films" *Polymer* **1997**; *38*: 3819.
31. Keith, H.D.; Padden, F.J.; Vadimsky, R.G. "Intercrystalline links in polyethylene crystallized from the melt" *J. Polym. Sci. Part A-2*, **1966**, *4*, 267.
32. Handlin, D. L.; Thomas, E. L. "Phase contrast imaging of styrene isoprene and styrene butadiene block copolymers" *Macromolecules* **1983**, *16*, 1514.



# PART II

## **Orientation of Block Copolymer Microdomains in Thin Films**

**CHAPTER 5** (modified from *Macromolecules* **2000**, 33, 4791)

**CHAPTER 6** (modified from *Macromolecules* **2001**, 34, 2602)

**CHAPTER 7** (modified from *Nature* **2000**, 405, 433)

**CHAPTER 8** (modified from *Advanced Materials* in press)

**CHAPTER 9**

## CHAPTER 5: Epitaxy

### Control of Molecular and Microdomain Orientation in a Semicrystalline Block Copolymer Thin Film by Epitaxy

Epitaxial crystallization is utilized to control both molecular chain orientation and microdomain structure in a thin film of a semicrystalline triblock copolymer, composed of crystallizable polyethylene (PE) end blocks and an amorphous ethylene-*alt*-propylene (PEP) mid-block where the microphase separation is driven by crystallization from a homogeneous melt, characterized by small angle and wide angle X-ray diffraction. Surface interaction due to a crystallographic matching of unit cells between the crystalline PE block and benzoic acid (BA) substrate induces high orientation of the crystalline PE block, resulting in a well ordered parallel lamellar microphase separated structure. The excellent orientation induced by the surface interaction is evidenced by the selected area electron diffraction (SAD) pattern and bright-field (phase contrast) and dark-field (diffraction contrast) transmission electron microscope (TEM) images of the block copolymer thin film. The data clearly show that the chain axis ( $\hat{c}$ ) of PE is parallel to the normal ( $\hat{n}$ ) of the microphase separated lamellar surfaces.

#### 5.1 Introduction

The driving force for microphase separation in amorphous block copolymers is the incompatibility between the blocks that are chemically linked.<sup>1</sup> The resulting ordered microstructures have periods on the order of the polymer chain dimensions; different microphase-separated morphologies can form depending on the inherent block incompatibility (characterized by  $\chi$ , the Flory-Huggins segmental interaction parameter, which is generally found to be inversely proportional to the temperature), the total degree of polymerization ( $Nt$ ) and the volume fraction of the components.<sup>2</sup> For high values of the product  $\chi Nt$ <sup>2-4</sup> the block copolymer is strongly segregated and well organized microdomain structures result. For low values of the product  $\chi Nt$  (low block incompatibility and/or low molecular weight and/or at high temperature) the block copolymer presents a homogeneous disordered phase.

In block copolymers which contain one or more crystallizable blocks, microphase separation can result either from incompatibility of the blocks or by crystallization of some block. The final morphology will be the result of the interplay between microphase separation of the component blocks and the crystallization of the crystallizable blocks.

Early work by Skoulios et al.<sup>5</sup> and Lotz et al.<sup>6</sup> on semicrystalline block copolymers was concerned with the influence of an attached amorphous block on the nature of the chain folding of the crystalline block in poly(styrene-*b*-ethyleneoxide). More recently, various groups<sup>7-30</sup> have shown that the morphology of semicrystalline block copolymers is path dependent; different microdomain structures are obtained if the crystallization occurs from a homogeneous melt (in this case the crystallization drives the microphase separation) or it occurs from an already microphase separated heterogeneous melt (in this case microphase separation precedes crystallization and provides a microstructure within which crystallization takes place).

When the block incompatibility is small, as for instance for the block copolymers composed of crystallizable polyethylene (PE) blocks and poly(ethylene-*alt*-propylene) (PEP) or poly(ethylene) amorphous blocks, such as those analyzed by Rangarajan et al.,<sup>12,15</sup> crystallization occurs from a homogeneous melt resulting in the formation of alternating lamellar microdomains in a spherulitic superstructure regardless of the copolymer composition,<sup>12</sup> as has been assumed in theoretical treatments.<sup>31,32</sup>

When the segments are highly incompatible and also have large molecular weights, microphase separation in the melt occurs prior to crystallization. The presence of microdomains in the ordered melt may affect the crystallization process and the final morphology.<sup>7,8,11,19,25-27,30</sup>

The orientation of the chain axis ( $\hat{c}$ ) within crystalline lamellae in the confined superstructure has also been widely studied.<sup>10,12-15,20,25,27,28,30</sup> The relationship between  $\hat{c}$  and the normal direction ( $\hat{n}$ ) of microphase separated lamellar surfaces turned out to be very complex, influenced by many factors such as molecular weight of the block copolymer and crystallization temperature of the crystalline block and so on. A model in which  $\hat{c}$  is oriented *parallel* to  $\hat{n}$  of microphase separated lamellar surfaces has been proposed on the basis of experimental observations on PE containing block copolymers,<sup>12,15</sup> for which the polymer is crystallizing from a homogeneous melt or

within a weakly microphase segregated state. On the other hand, other experimental observations have indicated that crystallization from an ordered microphase-separated melt results in  $\hat{c}$  aligned *perpendicular* to  $\hat{n}$  of the lamellar microdomain surfaces.<sup>10,13,14,20,30</sup>

An important parameter which influences the orientation of the chains with respect to the domain interface in lamellar systems seems to be the molecular weight.<sup>20,28</sup> Ryan et al.<sup>18,22</sup> have shown that the number of folds in the low molecular weight regime is coupled to the conformational state of the amorphous block. The metastable structures developed during various heat treatments show different folding behavior of the semicrystalline block. In addition, the equilibrium conformation of the semicrystalline block depends on the molecular weights of both the semicrystalline and amorphous blocks.<sup>23</sup> As the total molecular weight increases, the interfacial area per junction is increased and the crystalline stems tilt and eventually become parallel to the lamellar interface to match the preferred interfacial area of the amorphous chain.<sup>20,28</sup> Recently Zhu et al. showed that the variation of the crystallization temperature of the crystalline block develops different orientations ( $\hat{c} \perp \hat{n}$  at low  $T_c$ , inclined at intermediate  $T_c$  and  $\hat{c} // \hat{n}$  at the highest  $T_c$ ) of the crystals with respect to the microphase separated structure at fixed molecular weight.<sup>30</sup>

It is worth noting that in many of the cited papers, the determination of the orientation of the chains in the crystalline domains has been achieved by employing methods which are normally used to induce alignment of the microdomains, that is by application of an external bias field, such as thermo-mechanical plane strain compression (channel die),<sup>13,14,25,27</sup> or oscillatory shear.<sup>10,20</sup> These methods achieve good alignment of the microdomains, however the resulting orientation of the molecular chains in the crystalline phase, usually detected by wide angle X-ray diffraction, is often very low, making detailed modeling of the crystalline structure and microdomain structure problematic and raising the issue of the role of the applied field on the boundary conditions so formed. In addition, these processing methods are hardly applicable for patterning thin films.

The epitaxial crystallization of PE homopolymer on various substrates has been extensively studied; inorganic substrates (e.g. alkali halides),<sup>33</sup> polymer substrates (e.g.

oriented films of polytetrafluoroethylene),<sup>34</sup> and organic substrates (e.g. benzoic acid, condensed aromatic hydrocarbons and linear polyphenyls)<sup>35,36</sup> have been successfully used to grow well oriented crystals of PE. Although the versatility of these substrates has been clearly shown, attempts of using them to control the crystallization and its orientation as well as to investigate the resulting morphology of the thin film of semicrystalline block copolymers is new.

In this chapter the PE blocks in a semicrystalline triblock copolymer are epitaxially crystallized onto the surface of crystals of benzoic acid (BA). A goal is to obtain a high orientation of the crystals in a semicrystalline triblock copolymer thin film. The triblock has PE as crystallizable end blocks and a non crystalline rubbery mid-block composed of alternating ethylene and propylene units. The external field generated by the crystallographic matching of PE crystal and BA crystal provides a way to control not only the molecular chain orientation of PE block but also the resulting microphase separated structure. In addition, the high orientation of the suprastructure allows precise determination of the angle between  $\hat{c}$  and  $\hat{n}$  by employing SAD, bright field (BF) and dark field (DF) TEM.

## 5.2 Results and discussion

Bulk samples of the PE/PEP/PE block copolymer were analyzed by simultaneous WAXS and SAXS in order to check if the crystallization of the PE blocks occurs from a homogeneous melt or from an already microphase separated heterogeneous state. Thin films were analyzed by electron diffraction and electron microscopy under both bright and dark field mode in order to observe the orientation of the PE crystals and the microdomain morphology which develop in the epitaxial crystallization process.

### 5.2.1. Bulk samples

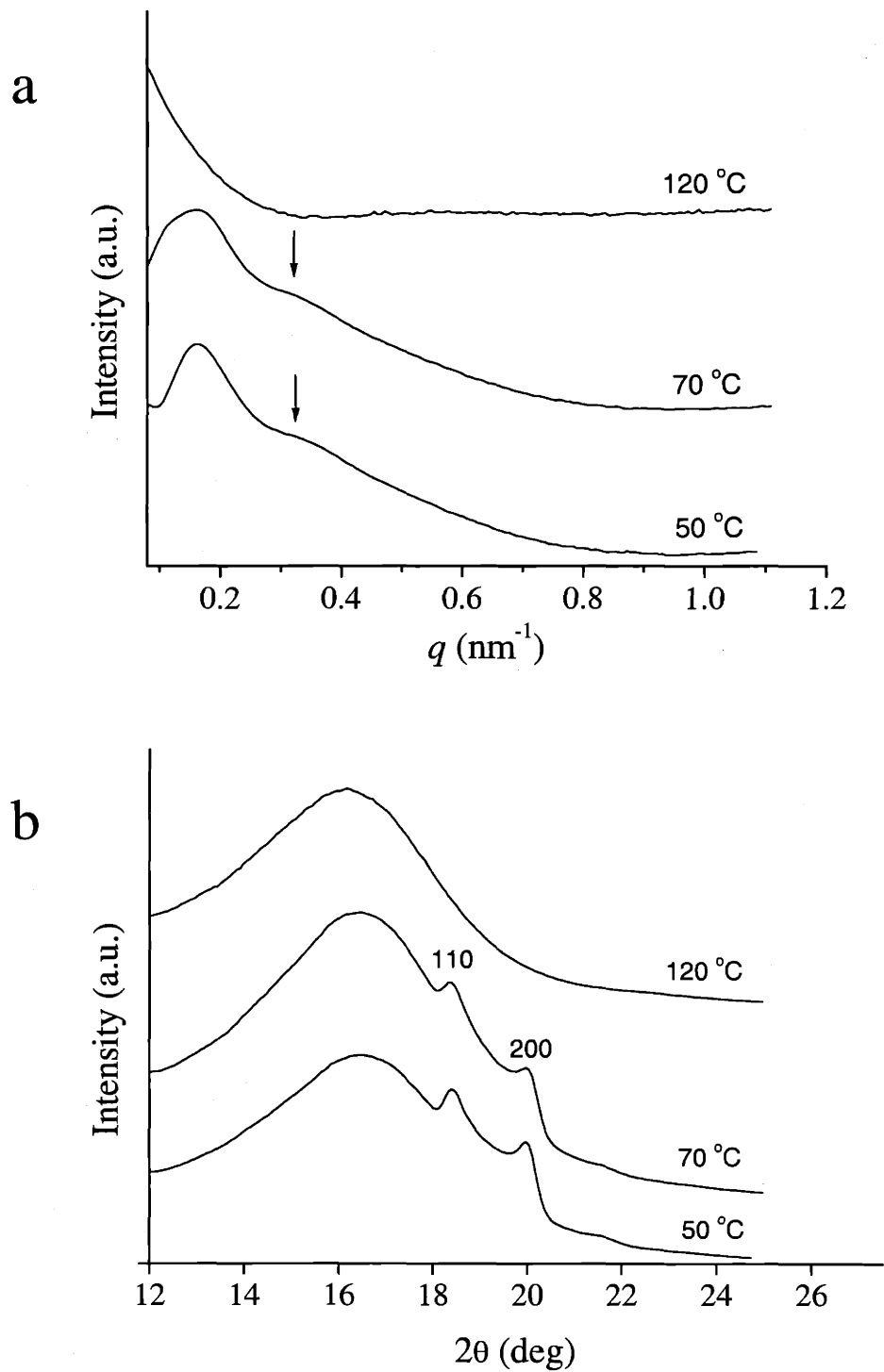
SAXS and WAXS patterns of the PE/PEP/PE bulk sample, recorded simultaneously at a series of temperatures, starting from the melt and cooling to room temperature, are shown in Figure 5.1 (a) and (b), respectively. It is apparent that the SAXS pattern at 120°C is essentially featureless indicating that no microdomain structure is present in the melt. The correlation hole peak normally found in the disordered state of block

copolymers is absent because of the very low electron density contrast between the PE and PEP blocks.<sup>15</sup> This is contrary to the higher molecular weight sample analyzed by Seguela and Prud'homme<sup>7</sup>, which yielded a microphase separated melt. In our sample, the PE and PEP blocks are miscible in the melt (120 °C), which appears therefore as a homogeneous phase. The WAXS pattern of the melt (Figure 5.1(b)) at 120°C presents a typical amorphous halo. The intensity of the amorphous halo decreases due to the crystallization of PE block (at 70 °C and 50°C). The two crystalline peaks correspond to the {110} and {200} reflections of the usual orthorhombic form of PE.<sup>37</sup> In good correspondence to the temperature at which the crystalline peaks develop in the WAXS pattern, a peak at  $q=0.16 \text{ nm}^{-1}$ , corresponding to a Bragg distance of 40 nm, develops in the SAXS patterns, indicating the formation of a microphase-separated microstructure. The weak broad reflection around  $0.32 \text{ nm}^{-1}$ , indicated by arrows in Figure 5.1a, gives a ratio  $q_2/q_1$  of about 2, characteristic of a lamellar structure, as was previously found in the weak segregated semicrystalline block copolymers.<sup>12,15</sup> The parallel growth of the WAXS and SAXS peaks in the cooling step indicates that in this sample of PE/PEP/PE block copolymer, the microphase separation is driven by crystallization from a single phase melt.

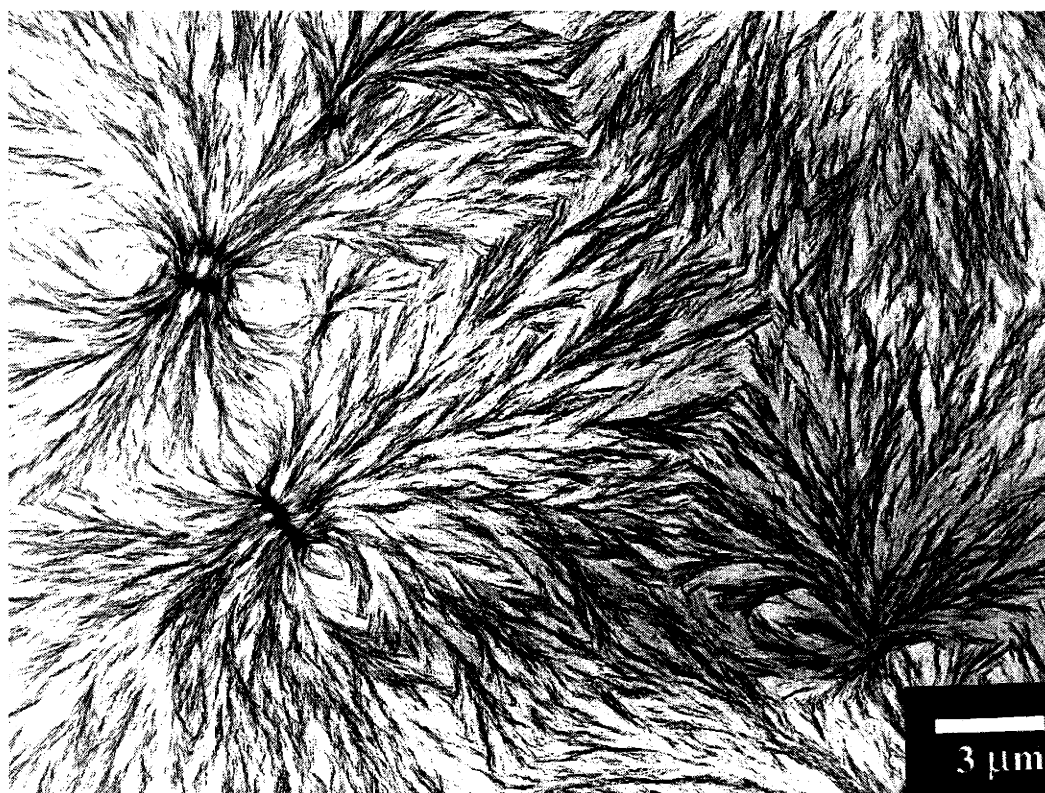
### 5.2.2. Thin films

A bright-field TEM image of a thin film of the PE/PEP/PE sample, prepared by casting at room temperature on a microscope glass slide from dilute xylene solution, is shown in Figure 5.2. The PE blocks crystallize by evaporation of the solvent, and in Figure 5.2 radially oriented lamellar PE microdomains comprise volume filling crystalline spherulites having an average diameter of 5-10  $\mu\text{m}$ .

In order to avoid the typical spherulite structure and control the morphology, thin films of the block copolymer were epitaxially crystallized onto the (001) surface of crystals of BA following the method outlined in the experimental section. The selected area electron diffraction pattern of the PE/PEP/PE block copolymer using a 6 $\mu\text{m}$  diameter SAD aperture is shown in Figure 5.3. The pattern essentially presents only the  $0kl$  reflections of PE; therefore it corresponds to the  $b^*c^*$  section of the reciprocal lattice

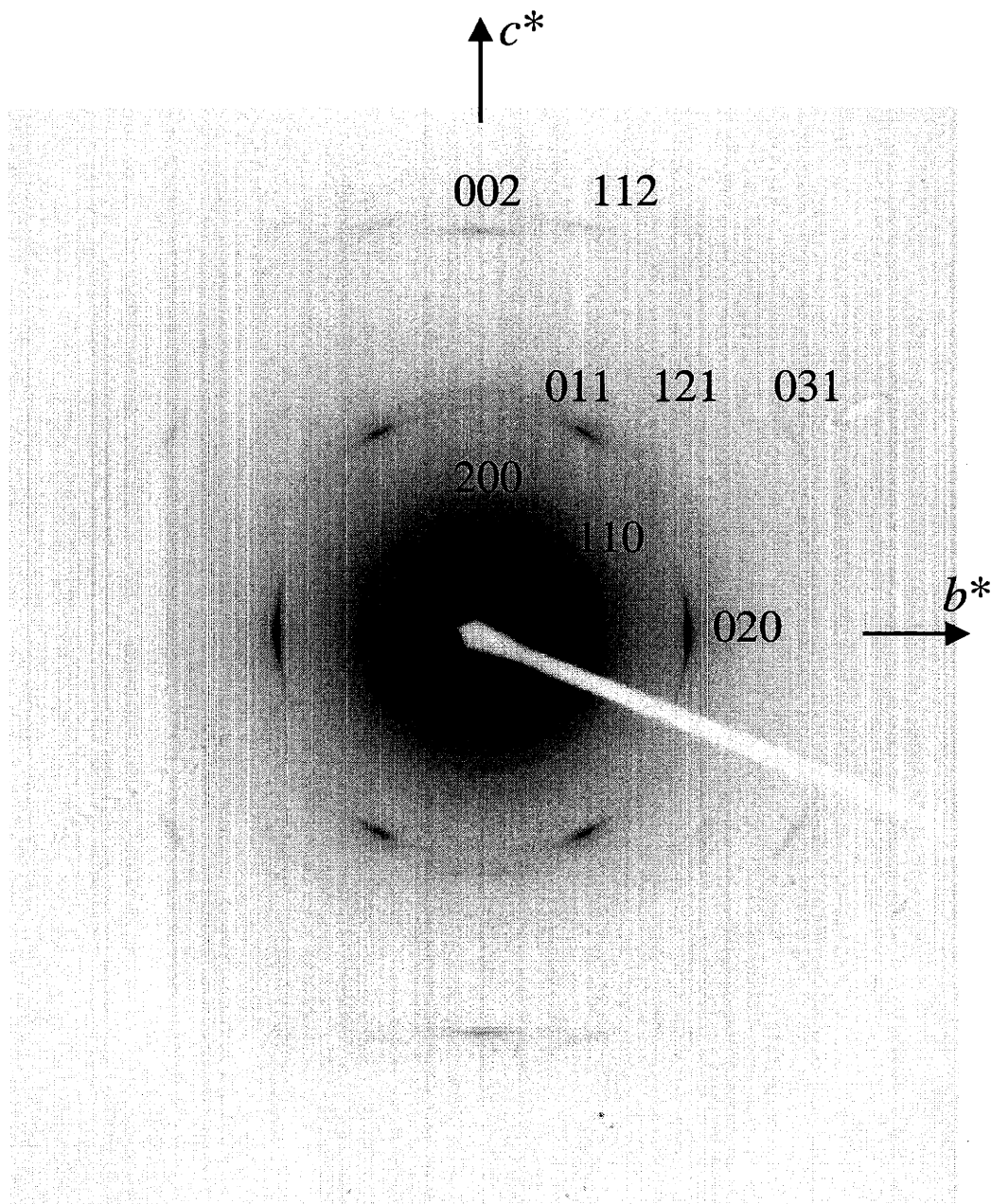


**Figure 5.1.** (a) Small angle X-ray diffraction patterns and (b) wide angle X-ray diffraction patterns of a bulk sample of the PE/PEP/PE block copolymer recorded at the indicated temperatures during cooling from a homogeneous melt.

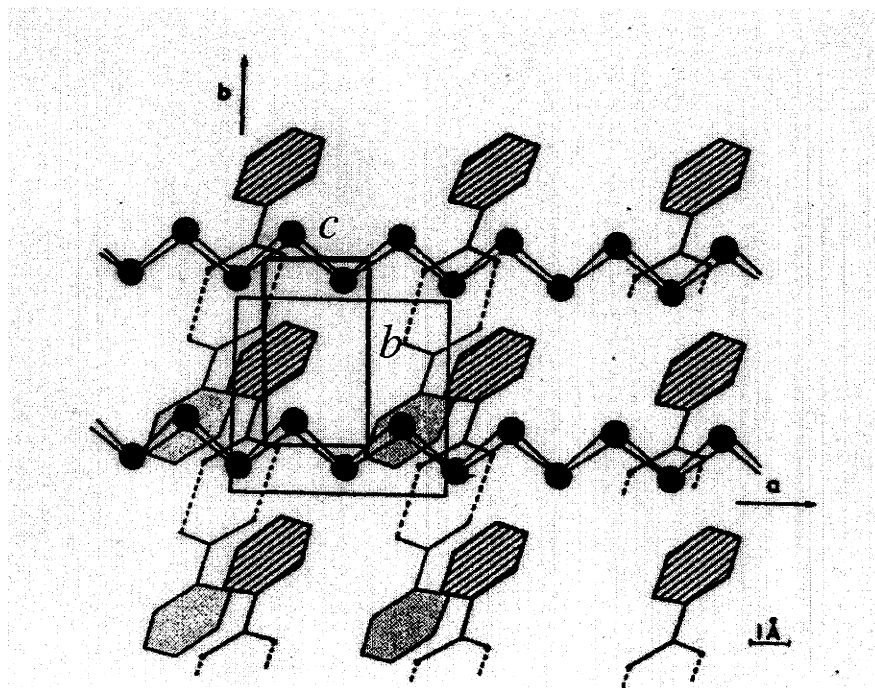


**Figure 5.2** TEM bright-field image of a thin film of PE/PEP/PE block copolymer obtained by casting from a xylene solution. Radially oriented lamellar PE microdomains, characterized by crystalline spherulites having size of 5-10  $\mu\text{m}$ , are imaged through the diffraction contrast.





**Figure 5.3** Selected area electron diffraction pattern of a thin film of PE/PEP/PE block copolymer epitaxially crystallized onto BA. The pattern presents mainly the  $0kl$  reflections of PE, hence it indicates that the (100) plane of PE is normal to the electron beam and parallel to the (001) exposed face of the BA crystals. A small tilting of the lamellae around the  $b$  axis, or progressive tilting of successive stacks of lamellae, accounts for the presence of arced reflections as well as the  $1kl$  and  $2kl$  type reflections (in particular, 121 and 112 reflections) and the weak 110 and 200 reflections.



$$2c_{\text{PE}} \sim a_{\text{BA}} \text{ and } b_{\text{PE}} \sim b_{\text{BA}}$$

BA  
 $a = 5.52 \text{ \AA}$   
 $b = 5.14 \text{ \AA}$   
 $c = 21.9 \text{ \AA}$

PE  
 $a = 7.40 \text{ \AA}$   
 $b = 4.93 \text{ \AA}$   
 $c = 2.53 \text{ \AA}$

**Figure 5.4** Schematic diagram of the epitaxial relationship between PE and BA crystals.

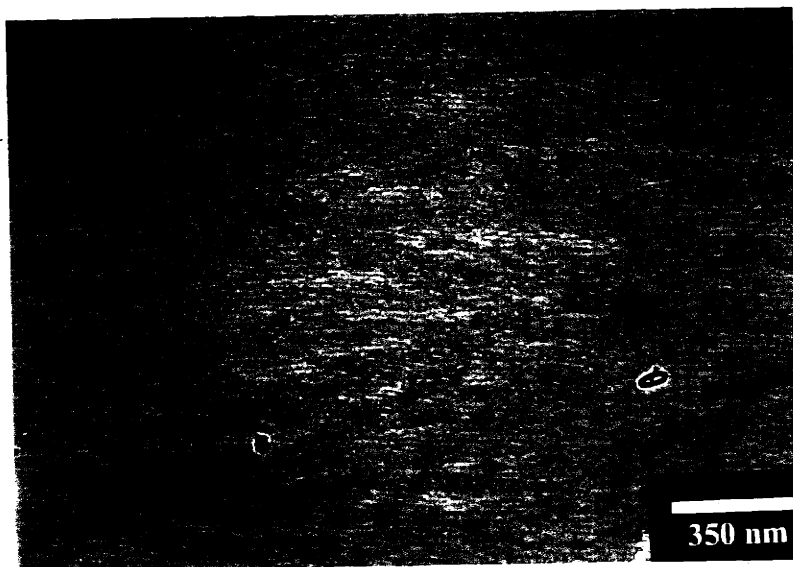
of PE. This indicates that a high orientation (single crystal-like) of the chain molecules in the crystalline phase has been achieved. Since the  $b^*c^*$  section of the reciprocal lattice is in the diffraction condition, the chain axis of the crystalline PE lies flat on the substrate surface and oriented parallel to the  $a$  axis of BA crystals, as in the case of the PE homopolymer.<sup>35</sup> The (100) plane of PE is in contact with the (001) plane of BA,<sup>35</sup> therefore the crystalline PE lamellae stand edge-on on the substrate surface, with PE  $b$  axis oriented parallel to the  $b$  axis of BA.<sup>35</sup> The relative orientation of PE and substrate lattices is therefore identical to that obtained for the polyethylene homopolymer.<sup>35</sup>

Schematic diagram of epitaxial relationship between PE and BA is shown in Figure 5.4. The  $b$  and  $c$  axes of PE are parallel to the  $b$  and  $a$  axes of BA, respectively; this epitaxy is well explained in terms of matching the PE inter-chain distance of the  $b$  PE axis periodicity (4.95 Å) with the  $b$  periodicity of the BA unit cell (5.25 Å).<sup>34</sup>

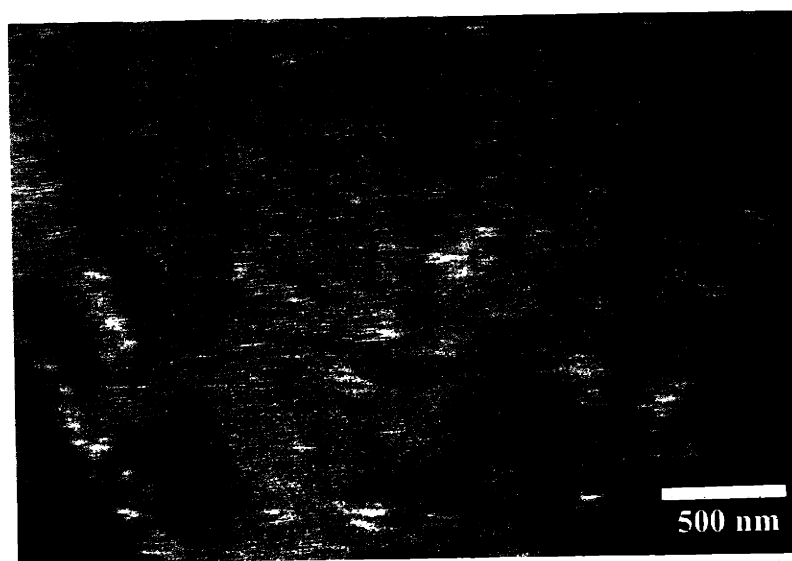
A bright field TEM image of the film epitaxially crystallized onto BA is shown in Figure 5.5a. Instead of a spherulitic structure, the epitaxy has produced a highly aligned lamellar structure with long, thin crystalline PE lamellae, with a thickness of 10-15 nm, oriented along the  $[010]_{PE} // [010]_{BA}$  direction. The average distance between the lamellae is 30 - 40 nm, in agreement with the bulk SAXS data, and the order extends over larger than 100  $\mu\text{m}^2$  region.

Further details of the structure and orientation of the film can be made by dark field (DF) imaging of the PE crystalline lamellae. Since the film has a single-crystal-like orientation, dark field imaging using a single diffraction spot should reveal the entire set of crystalline regions. In view of the limited lifetime of PE crystals under the electron beam, it is preferable to use the strongest 110 reflection to record DF images.<sup>38</sup> For this purpose, the epitaxially crystallized film was tilted by 34° about the  $c$  axis of PE in order to bring the 110 reflection in diffracting position. The corresponding DF image shown in Figure 5.5b reveals the same parallel array of crystalline PE lamellae, oriented along the  $b$  axis of BA crystals, with 40 ~ 50 nm inter-lamella spacing. The dark areas in the image correspond to regions slightly out of the Bragg condition due to a small amount of tilting. The thickness of the crystalline PE domains is approximately 10-15 nm, almost comparable to that of amorphous PE and PEP layer. Based on the PE volume fraction, bulk crystallinity (30 %), and microdomain lamellar repeat, a crystal thickness of around

a



b



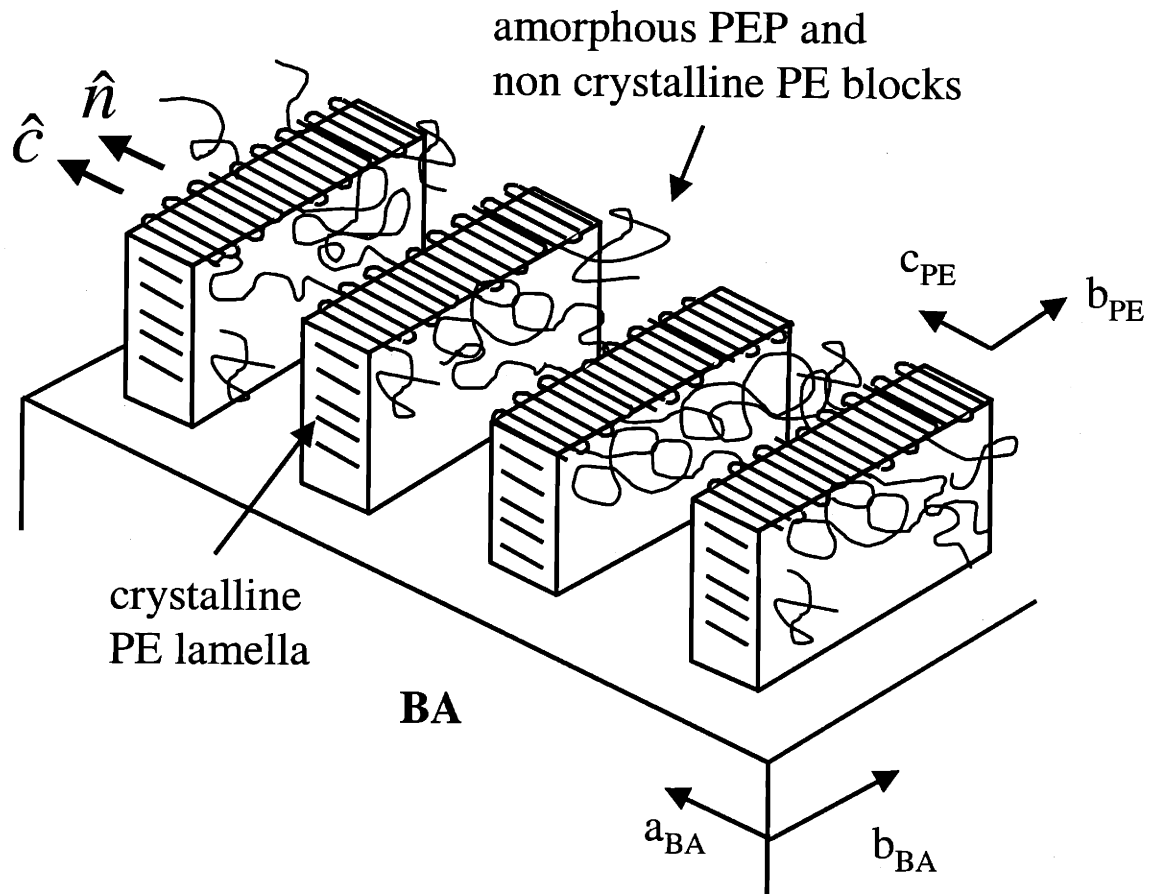
**Figure 5.5** (a) Under-focused TEM bright-field image of a thin film of PE/PEP/PE block copolymer epitaxially crystallized onto BA corresponding to an area similar to that of Figure 5.3. The light noncrystalline regions appear bright due to phase contrast. The dark regions correspond to the denser crystalline PE phase, which form long lamellae standing edge-on on the substrate surface. The lamellae are preferentially oriented with the  $b$  axis of PE parallel to the  $b$  axis of the BA. (b) TEM (110) dark-field image of a thin film of PE/PEP/PE block copolymer epitaxially crystallized onto BA corresponding to an area similar to that of Figure 5.3. Long thin, highly parallel alternating regions of bright/dark contrast are evident over the field of view. The bright regions correspond to the crystalline PE lamellae in the Bragg condition. Dark regions crossing the lamellar structure, correspond to crystalline areas where the crystals are tilted or twisted out of the Bragg condition.

4-5 nm would be expected for bulk crystallized material. The larger crystal thickness observed may be due to an enhancement of crystallinity by the substrate.<sup>39</sup>

The following chapter 7 and 8 will show that in strongly segregated semicrystalline block copolymers, epitaxially crystallized onto an organic substrate, the resulting structure can be understood in terms of a combination of directional solidification of the eutectic solution of the block copolymer in the crystallizable organic solvent and the following epitaxial crystallization of the crystalline block onto the organic crystalline substrate. The eutectic behavior of binary solutions of a semicrystalline homopolymer and a crystallizable organic solvent has been described in the literature.<sup>40-42</sup> In the present case, where the two blocks are miscible above the crystallization temperature of the PE block (melt compatible semicrystalline block copolymer), the orientation of the microdomains occurs only due to epitaxial relationship of the PE block with the BA.

### 5.3 Conclusions

The chapter demonstrates how to control the microstructure of a semicrystalline block copolymer by a highly specific molecular interaction with the substrate. High orientation of the crystals and microdomains of a PE/PEP/PE triblock copolymer has been achieved through epitaxial crystallization of the copolymer, from the homogeneous melt, onto benzoic acid substrate crystals. The epitaxial crystallization is used to control the crystallization and the morphology of a thin film of block copolymer. Since the microphase separation is driven by crystallization from a homogeneous melt, the long range orientation of the crystalline unit cell induces excellent alignment of the microdomains, as shown in the schematic model of Figure 5.6. The PE microdomains consist of long crystalline lamellae aligned parallel to a preferential crystallographic direction of the substrate (the  $b$  axis of the benzoic acid crystals, parallel to the  $b$  axis of PE). The combination of electron diffraction and bright and dark field images allows clear determination of the molecular chain orientation of PE with respect to the suprastructure of crystalline PE lamellae and PEP layers. The orientation of the PE unit cell, induced by the epitaxial relationship with the crystalline lattice of the substrate, is such that the PE molecular chain axis ( $\hat{c}$ ) is *parallel* to the normal direction ( $\hat{n}$ ) of lamellar plane, as shown in Figure 5.6. This result is in agreement with the model



**Figure 5.6** Schematic model showing the crystalline and amorphous microdomains in the PE/PEP/PE block copolymer epitaxially crystallized onto BA. Epitaxial relationship shows the relative orientation of the polyethylene lamellae on the benzoic acid.  $(100)_{PE} // (001)_{BA}$ , and  $c_{PE} // a_{BA}$ ,  $b_{PE} // b_{BA}$ . The orientation of the PE molecular chains perpendicular to the lamellar plane  $\hat{c} // \hat{n}$  is also shown.

proposed by Rangarajan et al.<sup>12,15</sup> for semicrystalline block copolymer crystallized from the homogeneous melt. The result is a consequence of the interaction with the substrate surface in the thin film and yields a globally oriented single crystal like texture of vertically oriented PE/PEP lamellae.

## 5.4. References

1. Bates, F.S.; Fredrickson, G.H.: "Block copolymer thermodynamics: theory and experiment." *Ann. Rev. Phys. Chem.* **1990**, *41*, 525.
2. Leibler, L. "Theory of microphase separation in block copolymers" *Macromolecules* **1980**, *13*, 1602.
3. Fredrickson, G. H.; Helfand, E. "Fluctuation effects in the theory of microphase separation in block copolymers" *J. Chem. Phys.* **1987**, *87*, 697.
4. Bates, F. S.; Bair, H. E.; Hartney, M. A. "Block copolymers near microphase separation transition. 1. preparation and physical characterization of a model system" *Macromolecules* **1984**, *17*, 1987.
5. Skoulios, A.E.; Tsouladze, G.; Franta, E. "Macromolecular chain configuration of block copolymer in concentrated solution. An example with polystyrene/polyethylene oxide block copolymer and polyethylene oxide/polypropylene oxide block copolymer in solution with preferential solvent of one of the two species in each copolymer." *J. Polym. Sci.: Polym. Symp.* **1963**, *C4*, 507.
6. Lotz, B.; Kovacs, A. J.; Bassett, G. A.; Keller, A. "Properties of copolymers composed of one polyethylene oxide and one polystyrene block" *Kolloid Z.* **1966**, *209* (2), 115.
7. Seguela, R.; Prud'homme, J. "Structural and mechanical properties of a polyethylene-based thermoplastic elastomer" *Polymer*, **1989**, *30*, 1446.
8. Cohen, R.E.; Cheng, P.L.; Douzinas, K.C.; Kofinas, P.; Berney, C.V. "Path-dependent morphologies of a diblock copolymer of polystyrene/hydrogenated polybutadiene." *Macromolecules* **1990**, *23*, 324.
9. Douzinas, K.C.; Cohen, R.E.; Halasa, A.F. "Evaluation of domain spacing scaling laws for semicrystalline diblock copolymers." *Macromolecules* **1991**, *24*, 4457.
10. Douzinas, K.C.; Cohen, R.E. "Chain folding in EBEE semicrystalline diblock copolymers": *Macromolecules* **1992**, *25*, 5030.
11. Nojima, S.; Kato, K.; Yamamoto, S.; Ashida, T. "Crystallization of block copolymers. 1. small angle X ray scattering study of an epsilon caprolactone butadiene diblock copolymer" *Macromolecules* **1992**, *25*, 2237.
12. Rangarajan, P.; Register, R.A.; Fetters, L.J. "Morphology of semicrystalline block copolymers of ethylene-(ethylene-*alt*-propylene)." *Macromolecules* **1993**, *26*, 4640.
13. Cohen, R.E.; Bellare, A.; Drzewinski, M.A. "Spatial organization of polymer chains in a crystallizable diblock copolymer of polyethylene and polystyrene." *Macromolecules* **1994**, *27*, 2321.
14. Kofinas, P.; Cohen, R.E. "Morphology of highly textured poly(ethylene)/poly(ethylene-propylene) (E/EP) semicrystalline diblock copolymers." *Macromolecules* **1994**, *27*, 3002.
15. Rangarajan, P.; Register, R.A.; Adamson, D.H.; Fetters, L.J.; Bras, W.; Naylor, S.; Ryan, A.J. "Dynamics of structure formation in crystallizable block copolymers" *Macromolecules* **1995** *28*, 1422.
16. Rangarajan, P.; Register, R.A.; Fetters, L.J.; Bras, W.; Naylor, S.; Ryan, A.J. "Crystallization of a weakly segregated polyolefin diblock copolymer." *Macromolecules* **1995**, *28*, 4932.

17. Ryan, A. J.; Hamley, I. W.; Bras, W.; Bates, F. S. "Structure development in semicrystalline diblock copolymers crystallizing from the ordered melt" *Macromolecules* **1995**, *28*, 3860.
18. Yang, Y.-W.; Tanodekaew, S.; Mai, S.-M.; Booth, C.; Ryan, A. J.; Bras, W.; Viras, K. "Structures of oxyethylene oxybutylene diblock copolymers in their solid and liquid states" *Macromolecules* **1995**, *28*, 6029.
19. Khandpur, A. K.; Macosko, C. W.; Bates, F. S. "Transmission electron microscopy of saturated hydrocarbon block copolymers" *J. Polym. Sci. Polym. Phys. Ed.* **1995**, *33*, 247.
20. Hamley, I.W.; Fairclough, J.P.A.; Terrill, N.J.; Ryan, A.J.; Lipic, P.M.; Bates, F.S.; Andrews, E. "Crystallization in oriented semicrystalline diblock copolymers." *Macromolecules* **1996**, *29*, 8835.
21. Hamley, I. W.; Fairclough, J. P. A.; Ryan, A. J.; Bates, F. S.; Town-Andrews, E. "Crystallization of nanoscale-confined diblock copolymer chains" *Polymer* **1996**, *37*, 4425.
22. Ryan, A. J.; Fairclough, J. P. A.; Hamley, I. W.; Mai, S.-M.; Booth, C. "Chain folding in crystallizable block copolymers" *Macromolecules* **1997**, *30*, 1723.
23. Mai, S.-M.; Fairclough, J.P.A.; Viras, K.; Gorry, P.A.; Hamley, I.W.; Ryan, A.J.; Booth, C. "Chain folding in semicrystalline oxyethylene/oxybutylene diblock copolymers" *Macromolecules* **1997**, *30*, 8392.
24. Rangarajan, P.; Haisch, C. F.; Register, R. A.; Adamson, D. H.; Fetters, L. J. "Influence of semicrystalline homopolymer addition on the morphology of semicrystalline diblock copolymer" *Macromolecules* **1997**, *30*, 494.
25. Quiram, D. J.; Register, R. A.; Marchand, G. R. "Crystallization of asymmetric diblock copolymers from microphase-separated melts" *Macromolecules* **1997**, *30*, 4551.
26. Quiram, D. J.; Register, R. A.; Marchand, G. R.; Ryan, A. J. "Dynamics of structure formation and crystallization in asymmetric diblock copolymers" *Macromolecules* **1997**, *30*, 8338.
27. Quiram, D. J.; Register, R. A.; Marchand, G. R.; Adamson, D. H. "Chain orientation in block copolymers exhibiting cylindrically confined crystallization" *Macromolecules* **1998**, *31*, 4891.
28. Hillmyer, M.A.; Bates, F.S. "Influence of crystallinity on the morphology of poly(ethylene oxide) containing diblock copolymers." *Macromol. Symp.* **1997**, *117*, 121.
29. Balsamo, V.; von Gyldenfeldt, F.; Stadler, R. "Thermal behavior and spherulitic superstructures of SBC triblock copolymers based on polystyrene (S), polybutadiene (B) and a crystallizable poly(epsilon-caprolactone) (C) block" *Macromol. Chem. Phys.* **1996**, *197*, 3317.
30. Zhu, L.; Cheng, S. Z. D.; Calhoun, B. H.; Ge, Q.; Quirk, R. P.; Thomas, E. L.; Hsiao, B. S.; Yeh, F.; Lotz, B. "Crystallization temperature-dependent crystal orientations within nanoscale confined lamellae of a self-assembled crystalline-amorphous diblock copolymer" *J. Am. Chem. Soc.* **2000** *122*, 5957.
31. Di Marzo, E. A.; Guttman, C. M.; Hoffman, J. D. "Calculation of lamellar thickness in a diblock copolymer, one of whose components is crystalline." *Macromolecules* **1980**, *13*, 1194.



32. Whitmore, M. D.; Noolandi, J. "Theory of crystallizable block copolymer blends" *Macromolecules* **1988**, *21*, 1482.
33. Wellinghoff, S. H.; Rybnikar, F.; Baer, E. "Epitaxial crystallization of polyethylene" *J. Macromol. Sci. (Phys.)* **1974**, *B10*, 1.
34. Wittmann, J. C.; Smith, P. "Highly oriented thin films of poly(tetrafluoroethylene) as a substrate for oriented growth of materials" *Nature* **1991**, 352, 414.
35. Wittmann, J. C.; Hodge, A. M.; Lotz, B. "Epitaxial crystallization of polymers onto benzoic acid – polyethylene and paraffins aliphatic polyesters and polyamides" *J. Polym. Sci. Polym. Phys. Ed.*, **1983**, *21*, 2495.
36. Wittmann, J. C.; Lotz, B. "Epitaxial crystallization of polyethylene on organic substrate: a reappraisal of mode of action of selected nucleating agents" *J. Polym. Sci. Polym. Phys. Ed.* **1981**, *19*, 1837.
37. Bunn, C. W. *Trans. Faraday Soc.* **1939**, *35*, 482.
38. Hall I. H. *Structure of crystalline polymers* Elsevier applied science, NY **1984**, Ch.3.
39. Wu, S. *Polymer Interface and Adhesion*, Marcel Dekker, NY 1982, Ch. 5.
40. Smith, P.; Pennings, A. J. "Eutectic crystallization of pseudo binary systems of polyethylene and high melting diluents" *Polymer* **1974**, *15*, 413
41. Wittmann, J. C.; John Manley, R. ST. "Polymer-monomer binary mixtures. 1.eutectic and epitaxial crystallization in poly( $\epsilon$ -caprolactone)-trioxane mixtures" *J. Polym. Sci. Polym. Phys. Ed.* **1977**, *15*, 1089.
42. Hodge, A. M.; Kiss, G.; Lotz, B.; Wittmann, J. C. " Eutectic solidification and oriented growth in mixtures of polyethylene and 1,3,5-tribromobenzene" *Polymer* **1982**, *23*, 985.

## CHAPTER 6: Directional Solidification

### Orientation of Block Copolymer Microdomains via Directional Solidification

A fast method for inducing alignment of microdomains in noncrystalline block copolymers is presented. The method is based on the use of crystalline organic materials, which are solvents for the block copolymers above their melting temperatures, and, when cooled and directionally crystallized, act as a substrate on which thin films of the block copolymers are formed. Both lamellar and cylindrical type microdomains in a symmetric polystyrene-*block*-poly(methylmethacrylate) diblock copolymer and in an asymmetric polystyrene-*block*-polyisoprene, respectively, are globally aligned using either benzoic acid (BA) or anthracene (AN) as the crystallizable solvent. The fast directional solidification during the phase separation leads to alignment of the inter material dividing surface (IMDS) of both types of microdomains parallel to the fast growth direction of BA and AN crystals (*b* axis direction in both cases). With respect to the processing methods currently used to induce orientation in block copolymers, our method allows attainment of ordered patterns over large distances within a few seconds without annealing.

#### 6.1 Introduction

The self-assembly of block copolymers produces microstructures on the nanoscopic length scale.<sup>1</sup> Such periodic nanostructures are very useful, for instance, in thin films as templates for lithography.<sup>2-5</sup> By removing one polymer chemically, the patterns may be transferred to a substrate through either reactive etching or by thermal evaporation of a component into the previously removed regions.<sup>2-5</sup> Additionally the domains can be used as template for decoration with nanoparticles.<sup>6-8</sup>

Optimal utilization of nanoscopic patterns, however, requires spatial and orientational control of the microdomains. Indeed, the microdomains composed of the different blocks, having sizes of several tens of nanometers, typically nucleate randomly and grow into a polygranular texture, with periodic ordering maintained only over distances of only 50 lattice constants (i.e., a grain size of only 1 ~ 2 microns). A greater

range of engineering applications demands control over the orientation and position of the microdomains. Thus, the development of processing techniques which create global orientation of the microdomains in block copolymer thin films is an important goal.

Several techniques are currently used for inducing alignment of the microdomains in block copolymers.<sup>9-25</sup> They rely on the ability to couple an externally applied field to some molecular and/or supermolecular feature in the polymer, and thus achieve directional properties, such as transport, optical and mechanical properties. Therefore, if an applied bias field (mechanical, electric etc.) is present during the self-assembly process, then instead of random nucleation of microdomains, preferential orientation can develop.

Flow provides an efficient and versatile means of achieving global alignment. In typical processing methods involving flow fields, the material with an initial polygranular texture is subjected, for instance, to capillary extrusion<sup>9</sup>, oscillatory and steady shear,<sup>10-14</sup>, extensional flow<sup>15</sup> or compression.<sup>16</sup> The flows cause certain domain orientations to be favored and eventually a near-single crystal structure can be developed in bulk materials. Alternatively, instead of re-alignment of an existing polydomain structure, use of low molecular weight samples for which the material is initially above its order-disorder transition temperature and subsequently cooled during processing can result in well aligned samples within a few hours.<sup>14</sup> The roll-casting method utilizes a volatile solvent to permit processing of higher molecular weight polymers from an initially homogeneous solution through the order-disorder concentration into a well aligned state in approximately one hour.<sup>17</sup> Flow field techniques, however, cannot be easily applied to thin films due to flow instabilities.

Recently, Hashimoto et al.<sup>18</sup> have shown that a single grain lamellar microdomain orientation can be achieved using an applied temperature gradient. Also in this case, the process is very slow (~2 mm/day). The spatial variation of the dielectric constant of block copolymers is another means for alignment under electric fields of the nanoscale patterns in bulk<sup>19</sup> as well as in thin film.<sup>20</sup> In particular Morkved et al. demonstrated that in-plane cylindrical polymethylmethacrylate (PMMA) microdomains were aligned along the electric field in a thin polystyrene (PS)/ polymethylmethacrylate (PMMA) block copolymer film.<sup>20</sup>

The simplest technique to make a uniform *thin film* is spin casting. However, after long time annealing, the thin film typically displays a polygranular texture.<sup>2-4</sup>

Variation of thin film thickness is another way to control the orientations of block copolymers. Fasolka et al.<sup>21</sup> recently studied the extensive morphological phase behavior of the lamellar forming block copolymer thin film whose thicknesses are less than the period of block copolymer on native SiO<sub>2</sub> surface. They showed that either parallel or perpendicular ordering can be obtained simply depending on film thickness.

A bias field induced by surface interactions such as preferential wetting of the contact surface can also control the thin film microstructure.<sup>22</sup> Surface modification with a random copolymer provided a neutral surface upon which a perpendicular lamellae structure formed in approximately 100 nm thickness film.<sup>22</sup> However, due to degenerate azimuthal orientations, a film containing many defects and grain boundaries is produced.

Multiple interactions can be used for control, for example, the physical structure of the substrate surface and the chemical nature of both the polymer and pre-patterned substrate. The surface topography of substrate is another means to influence the orientation of the microdomains.<sup>23</sup> A one dimensional groove pattern was prepared from Si(113) single crystal wafer miscut by a certain angles towards the (001) crystal plane. The period and amplitude of the grooves on the surface were controlled by the miscut angle of the surface, the annealing temperature and time. The lamellar forming block copolymer thin film with two different film thicknesses overlaid on the patterned substrate exhibits a laterally patterned ordering.<sup>23</sup> In addition one dimensional groove pattern previously mentioned was treated with the subsequent evaporation of metal atoms with a certain incidence angle and successfully generated a chemically and topographically modified nanoscale pattern substrate.<sup>24</sup> A lamellae forming block copolymer on the substrate showed a controlled pattern structure when the periodicity of block copolymer was comparable with that of groove.<sup>24</sup>

The chemically modified pre-patterned substrates were obtained by micro-contact printing of self assembled monolayer, based on soft lithography. A parallel and perpendicular lamellae microstructures formed on the patterned substrate with two different surface properties (preferential and neutral surfaces).<sup>25</sup>

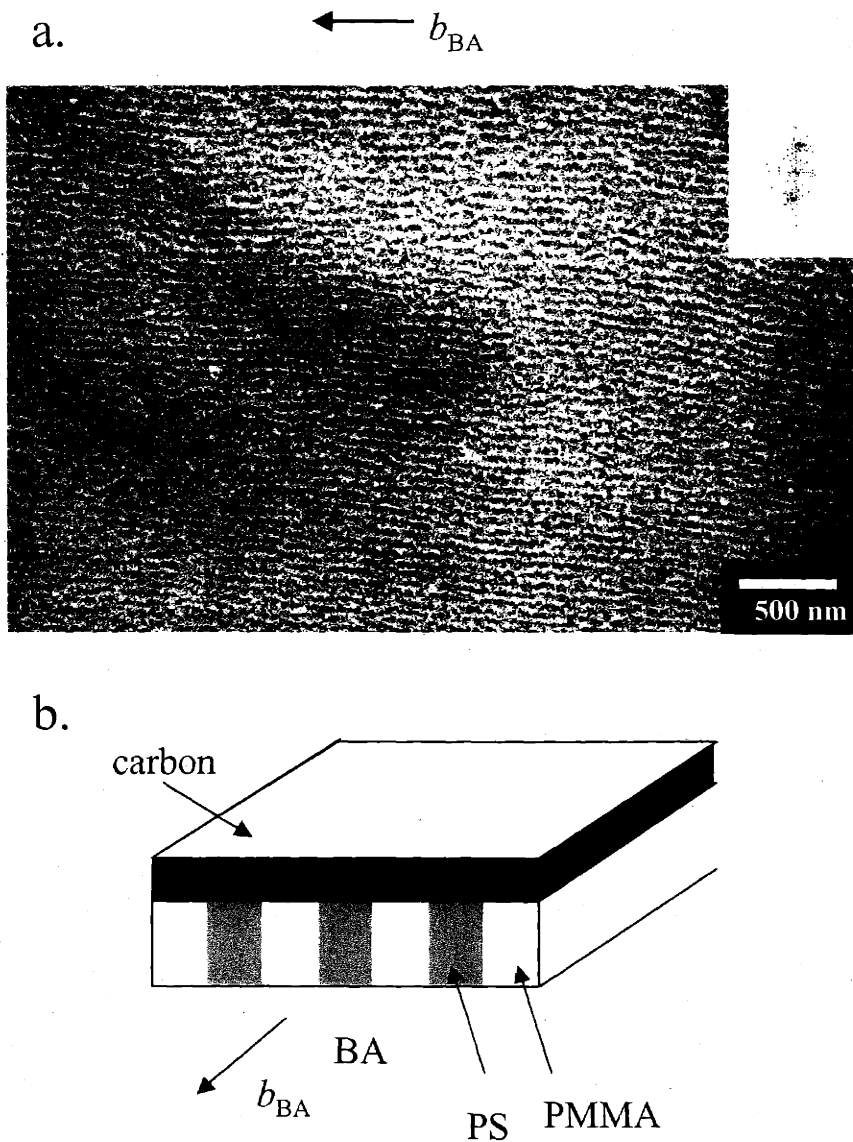
The previous chapter 5 introduced a new process involving two driving forces, i.e. directional solidification and epitaxy, and demonstrated that epitaxy is a way to control both the molecular and the microdomain orientation in a semicrystalline block copolymer thin film.

This chapter describes that the simple and fast process developed for the semicrystalline block copolymers can be employed to induce the alignment of lamellar and cylindrical microdomains of amorphous diblock copolymers. In this case, directional solidification is involved. Understanding of this effect will give new insight into the physics of the ordering process in block copolymers.

## 6.2 Results and Discussion

A bright field TEM image of a thin film of PS/PMMA (26/32) block copolymer prepared using BA is shown in Figure 6.1a. The darker regions correspond to the RuO<sub>4</sub> stained PS microdomains. Edge-on parallel lamellae of PS and PMMA are well aligned along the fast growth direction of the BA crystals. The PS lamellae appear thicker than the PMMA lamellae because the PMMA microdomains beam damage and shrink under electron irradiation. The well aligned parallel lamellae extend over regions larger than 50  $\mu\text{m}^2$ . The FFT power spectrum in the inset of Figure 6.1a shows spot-like first reflection located on the meridian, indicating the nearly single crystal-like microstructure.

The schematic model of the microstructure of the PS/PMMA block copolymer after directional solidification with BA is shown in Figure 6.1b. Vertically alternating PS and PMMA lamellae are very well oriented along the *b* axis of BA crystal. The fast directional microstructure formation during the phase separation and thin film thickness approximately less than a half lamellar period avoid preferential wetting of one of the blocks on the substrate, leading to the oriented lamellae microdomain structure where the interface of the microdomains is parallel to the normal of the substrate surface. The structure is kinetically driven and subsequently vitrified at room temperature. Importantly in thicker regions approximately thicker than a half lamellar period the perpendicular lamellae orientation switches to in-plane parallel one and large planer regions (no TEM contrast) are produced.



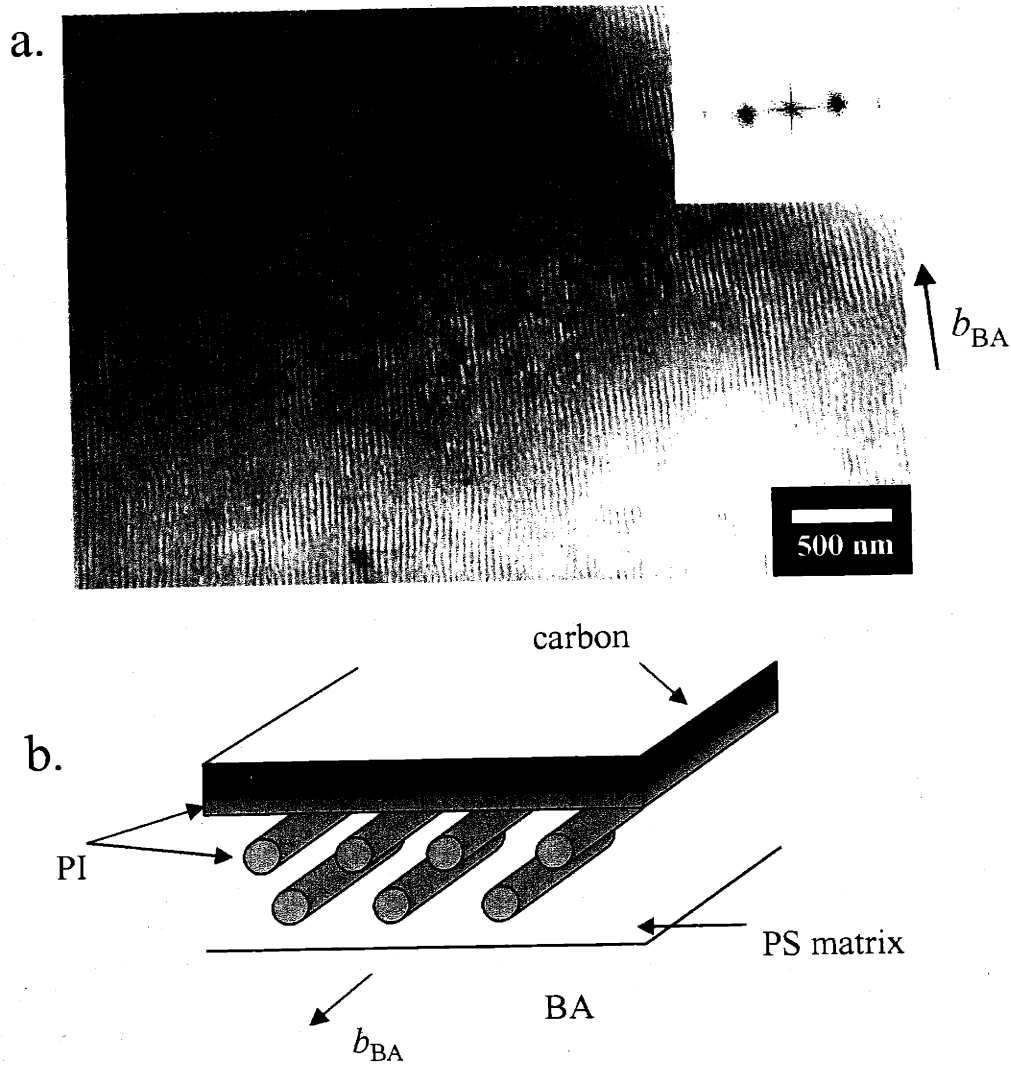
**Figure 6.1** (a) TEM bright-field image of a thin film of PS/PMMA(26/32) block copolymer, directionally solidified with BA, and stained with RuO<sub>4</sub>. The dark regions correspond to the stained PS microdomains. The lamellae are well aligned along the fast growth direction of the BA crystals (crystallographic  $b$  axis). Inset shows the FFT power spectrum of the TEM micrograph. Spot-like first reflection located on the meridian shows the nearly single crystal-like microstructure.

(b) Schematic model of the microstructure of PS/PMMA processed with BA. Alternating lamellae of PS and PMMA microdomains are aligned along the  $b$  axis of BA crystal.

A bright-field TEM image of a thin film of the PS/PI(45/12) block copolymer, prepared with the BA, is shown in Figure 6.2a. The darker regions in Figure 6.2a correspond to the OsO<sub>4</sub> stained PI microdomains. It is apparent that the PI cylinders, lying in-plane, are well oriented along the crystallographic *b* axis of the BA. The ordered of parallel cylinder structure also extends over regions larger than 50 μm<sup>2</sup>. The average diameter of the PI cylindrical microdomains is approximately 20 nm, while the average distance between the cylinders is 40-50 nm consistent with the bulk SAXS data. A schematic model of microstructure of PS/PI block copolymer after the directional solidification with the BA is shown in Figure 6.2b. In-plane PI cylinders are aligned along the *b* axis of BA crystal. It is assumed that the lower surface tension PI block is preferentially at the carbon interface while the PS block forms the interface with the BA surface due to its more favorable interaction.

In order to confirm that this simple process can be applied with other organic crystallizable solvents, AN was employed which has a melting temperature 100 °C higher than that of BA. A TEM bright-field image of a thin film of the PS/PI(45/12) block copolymer, directionally solidified with the AN, is shown in Figure 6.3. A microstructure similar to that obtained with BA is observed. The cylindrical PI microdomains are again aligned along the fast growth direction of AN crystals. However, in terms of the perfection of ordering, the microstructure produced with AN is much more defective with many more dislocations than when BA is used. The FFT power spectrum of Figure 6.3 (inset) shows only one arced reflection. Whereas the FFT power spectrum of Figure 6.2a (inset) clearly shows spot-like multi order reflections perpendicular to the cylinder axis of PI microdomains. This decrease in microdomain ordering is due in part because the shape anisotropy of the AN crystals is lower than that of BA crystals as observed with optical microscopy.

In the case with AN, PS/PI (45/12) block copolymer was observed to de-wet on the AN crystal in some area. Low magnification TEM bright field image, shown in Figure 6.4a, displays a highly aligned dewetted block copolymer films along the fast growth direction of AN crystals, confirming the directional solidification due to anisotropic crystal growth of the AN crystals. The zoom-in TEM bright field image of certain area in



**Figure 6.2** (a) TEM bright-field image of a thin film of PS/PI(45/12) block copolymer, directionally solidified with BA, and subsequently stained with OsO<sub>4</sub>. The dark regions correspond to the stained PI cylinders, while the white regions correspond to the PS matrix. The cylindrical PI microdomains are well aligned along the fast growth direction of the BA crystals. No grain boundaries are evident. A few dislocation defects are seen. Inset shows the Fast Fourier Transform (FFT) power spectrum of the TEM micrograph. Spot-like reflections located on the equator at  $q_0$  and  $2q_0$  indicate a nearly single crystal-like microstructure. In particular absence of the  $\sqrt{3}q_0$  reflection in this FFT power spectrum demonstrates that there is no rotation and tilting of microdomain lattice along the cylinder axis.

(b) Schematic model of the microstructure of PS/PI processed with BA. Cylindrical PI microdomains are edge-on to the crystalline substrate and aligned along the  $b$  axis of BA crystal.

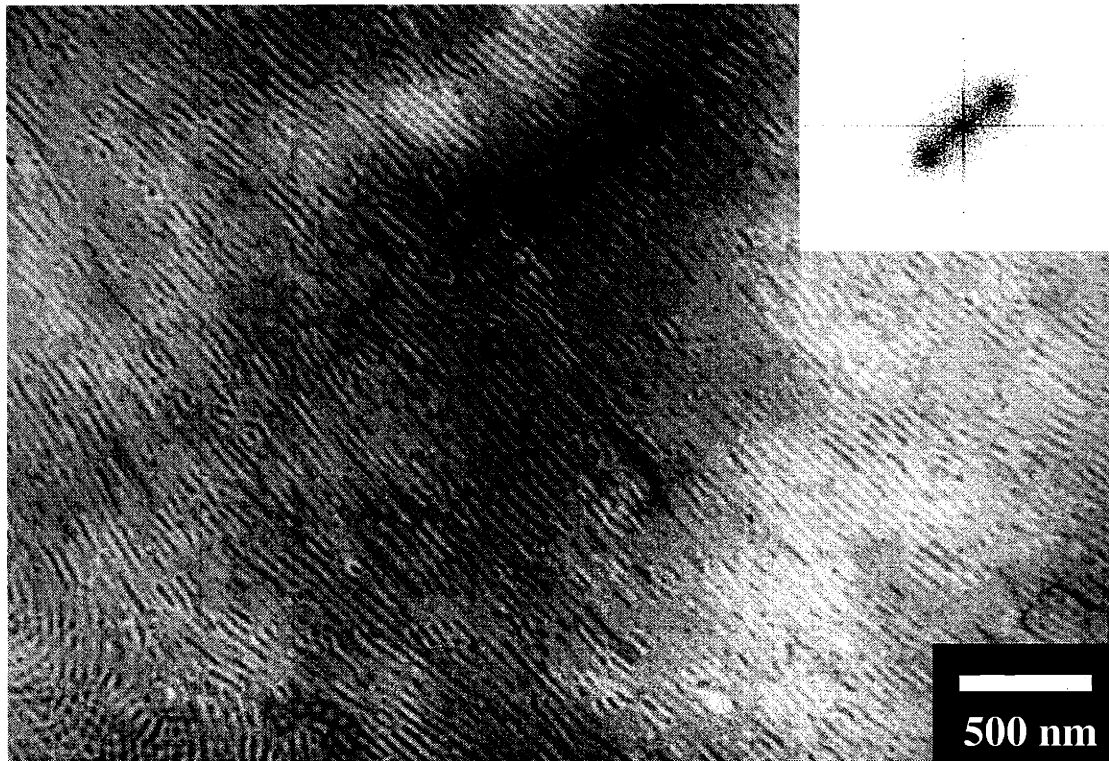


Figure 6.4a clearly shows that the cylindrical PI microdomains are parallel to the macroscopic growth direction (Figure 6.4b).

The essential aspects of overall phase transformation can be understood assuming the possible formation of a eutectic mixture of the block copolymer and the crystallizable solvent (See Chapter 1). In a hypothetical solvent-polymer phase diagram an eutectic may be present due to the intersection of the melting point depression liquidus curve of the crystallizable solvent and the microphase separation transition depression liquidus curve of the block copolymer. The initial homogeneous solution confined between the glass substrates transforms due to the imposed directional solidification into large crystals of BA (or AN) having (001) surfaces coexisting with a thin liquid layer near the eutectic composition. Dropping the temperature further then causes this layer to also directionally solidify by thickening the preexisting (BA or AN) crystal with simultaneous formation of a thin, metastable vertically oriented *lamellar* microdomain film (see Chapter 7). In the case of the PS/PMMA block copolymer, the vertical lamellar structure is vitrified due to the high glass transition temperatures of both blocks. In the case of PS/PI block copolymer with a low volume fraction of PI block, however, the vertical lamellar microstructure is transformed into in-plane cylindrical microstructure due to the interfacial instability of thin lamellae, film thickness and preferential wetting of PI block.

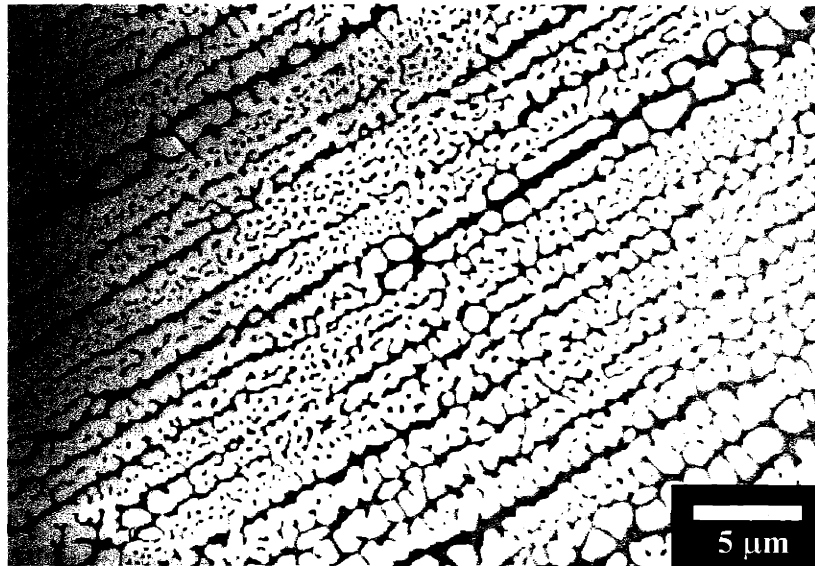
A thinner PS/PI film (approximately 20 nm thickness) prepared with more dilute solution undergoes vertical undulation instability, resulting in vertically aligned cylindrical structure. The experimental evidence of a vertically undulated and a resulting vertically aligned cylindrical structures of PS/PI films, using BA are shown in Figure 6.5a and b respectively. The dark OsO<sub>4</sub> stained vertically aligned cylindrical PI microdomains are oriented into rows along the *b* axis of BA crystal (Figure 6.5b). The FFT power spectrum in the inset of Figure 6.5b displays spot-like first reflections with 6-fold symmetry, indicating approximate hexagonal packing of the PI microdomains.

Several noncrystalline block copolymers with different molecular weights, compositions and architectures were also processed, using BA. In general, the kinetically controlled process gives poorer orientation with higher molecular weight block copolymers. Better orientation is achieved with higher PS-containing block copolymers probably because of better solubility of the PS block in BA. At high PI block content, the

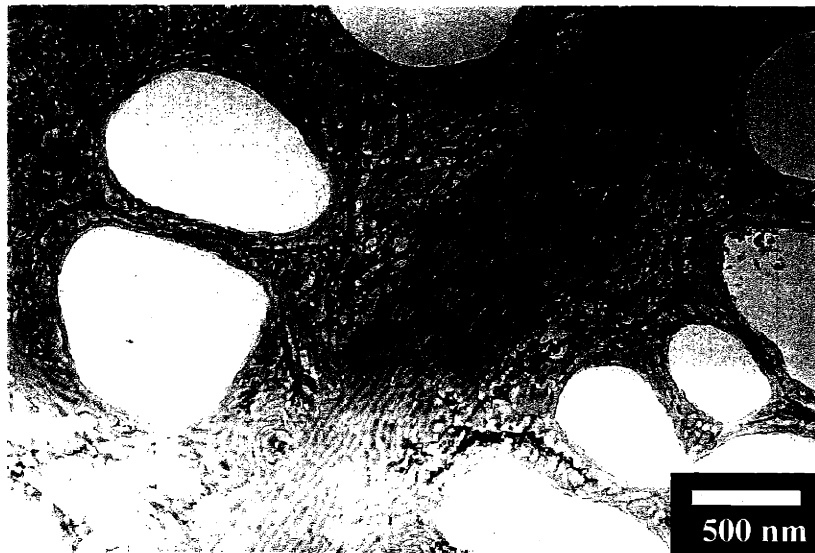


**Figure 6.3** TEM bright-field image of a thin film of PS/PI(45/12) block copolymer, directionally solidified with AN, and stained with OsO<sub>4</sub>. The dark regions correspond to the stained PI cylinders, while the white regions corresponds to the PS domains. The cylindrical PI microdomains are not so well aligned along the same direction, which corresponds to the fast growth direction of the AN crystals. Many dislocation defects are observed. Inset is the FFT power spectrum of the TEM micrograph. The arced first order reflection perpendicular to  $b$  axis of AN crystals demonstrates the orientation of the PI microdomains observed in TEM, which is not as good as when the PS/PI copolymer is processed with BA.

a.

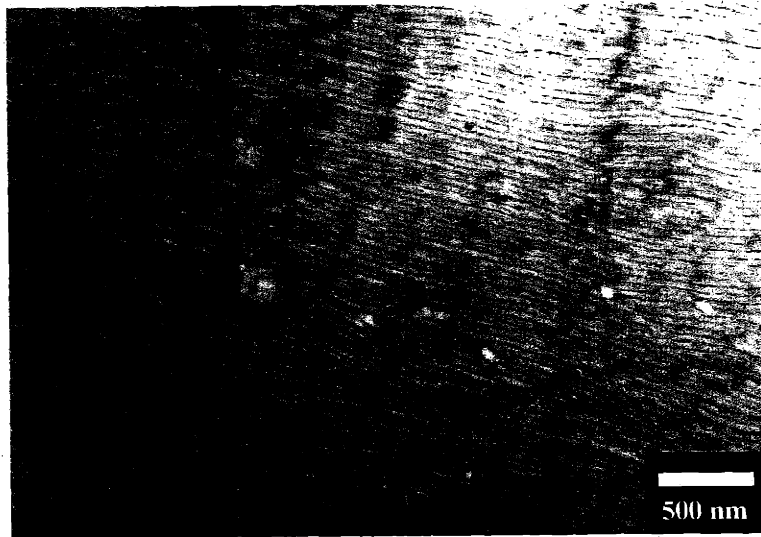


b.

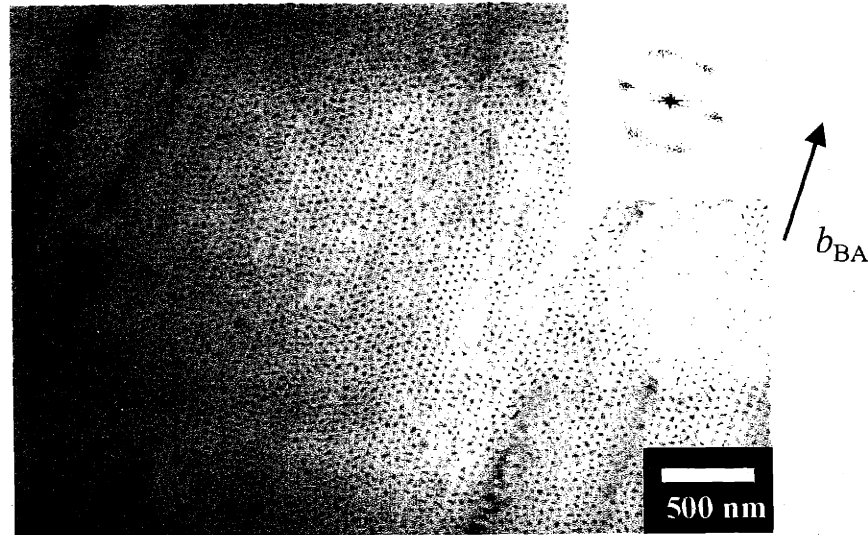


**Figure 6.4** TEM bright-field images of a thin film of PS/PI(45/12) block copolymer, directionally solidified with AN, and stained with OsO<sub>4</sub>. (a) Block copolymer has dewetted on the AN crystals. Low magnification image shows that directional solidification occurred macroscopically. (b) The magnified image of certain area of (a) shows that cylindrical PI microdomains are aligned parallel to the macroscopic solidification direction. The dark regions correspond to the stained PI cylinders, while the white regions corresponds to the PS domains.

a.



b.



**Figure 6.5** TEM bright-field images of a thin film of PS/PI(45/12) block copolymer, directionally solidified with BA, and stained with OsO<sub>4</sub>. The dark regions correspond to the stained PI cylinders, while the white regions corresponds to the PS domains. (a) Cylindrical PI microdomains are aligned along the fast growth direction of BA crystal. Vertically undulated PI microdomains are observed (b) Due to very thin film thickness, vertically undulated PI cylinders transform into hexagonally packed cylinders oriented perpendicular to the BA substrate. Inset shows the FFT power spectrum of the TEM micrograph. Spot-like first reflections with 6-fold symmetry shows the nearly hexagonally packed microstructure.

block copolymer film dewets on the glass substrate after removal of BA at room temperature.

### **6.3 Conclusions**

The process is an effective way to develop unidirectional long range ordering of conventional amorphous block copolymers. The orientation of microdomains occurs within a few seconds without any long time annealing procedures. Several types of microdomain alignment were possible: (1) vertical lamellae, (2) in-plane cylinders and (3) vertical cylinders, depending on film thickness. The method could be applied to different block copolymers with various compositions, and generalized by using other crystallizable provided the solvents dissolve block copolymers above their melting temperature and directionally crystallize. In addition, this process can be combined with topologically and/or chemically modified patterned substrates for better control of microdomain structures.

## 6.4 References

1. Bates, F.S.; Fredrickson, G.H.: "Block copolymer thermodynamics: theory and experiment." *Ann. Rev. Phys. Chem.* **1990**, 41, 525.
2. Mansky, P.; Chaikin, P.; Thomas, E. L. "Monolayer films of diblock copolymer microdomains for nanolithographic applications" *J. Mat. Sci.* **1995**, 30, 1987.
3. Thomas, E. L.; Kinning, D. J.; Alward, D. B.; Henkee, C. S. "Ordered packing arrangements of spherical micelles of diblock copolymers in 2 and 3 dimensions" *Macromolecules* **1987**, 20, 2934.
4. Lammertink, R. G. H.; Hempenius, M. G.; Van den Enk, J. E.; Chan, V. Z-H.; Thomas, E. L.; Vancso, G. J. "Nanostructured thin films of organic-organometallic block copolymers: One-step lithography with poly(ferrocenylsilanes) by reactive ion etching" *Adv. Mater.* **2000**, 12, 98.
5. Park, M.; Harrison, C.; Chaikin, P. M.; Register, R. A.; Adamson, D. H. "Block copolymer lithography: Periodic arrays of similar to 10(11) holes in 1 square centimeter" *Science* **1997**, 276, 1401.
6. Boontongkong, Y.; Cohen, R. E.; Rubner, M. F. "Selective electroless copper deposition within block copolymer microdomains" *Chem. Mater.* **2000**, 12, 1628.
7. Fogg, D. E.; Radzilowski, L. H.; Dabbousi, B. O.; Schrock, R. E.; Thomas, E. L. Bowendi, M. G. "Fabrication of quantum dot-polymer composites: Semiconductor nanoclusters in dual-function polymer matrices with electron-transporting and cluster-passivating properties" *Macromolecules* **1997**, 30, 8433.
8. Fink, Y.; Urbas, A. M.; Bawendi, B. G.; Joannopoulos, J. D.; Thomas, E. L. "Block copolymers as photonic bandgap materials" *J. Light Tech.* **1999**, 17, 1963.
9. Keller, A.; Pedemonte, E.; Willmouth, F. M. "Macro-lattice from segregated amorphous phases of a three block copolymer" *Nature* **1970**, 225, 538.
10. Hadziioannou, G.; Mathis, A.; Skoulios, A. "Obtention de monocristaux de copolymères trisequences styrene/isoprene/styrene par cisaillement plan" *Colloid Polym. Sci.* **1979**, 257, 136.
11. Morrison, F. A.; Winter, H. H.; Gronski W.; Barnes, J. D. "Effect of unidirectional shear on the structure of triblock copolymers. 2. Polystyrene polyisoprene polystyrene" *Macromolecules* **1990**; 23: 4200.
12. Vigild, M. E.; Almdal, K.; Mortensen, K.; Hamley, I. W.; Fairclough, J. P. A.; Ryan, A. J. "Transformations to and from the Gyroid Phase in a Diblock Copolymer" *Macromolecules* **1998**; 31: 5702.
13. Koppi, K. A.; Tirrell, M.; Bates, F. S.; Almdal, K.; Mortensen, K. "Epitaxial growth and shearing of the body centered cubic phase in diblock copolymer melts" *J Rheo* **1994**; 38: 999.
14. Pinheiro, B. S.; Winey, K. I. "Mixed parallel-perpendicular morphologies in diblock copolymer systems correlated to the linear viscoelastic properties of the parallel and perpendicular morphologies" *Macromolecules* **1998**, 31, 4447.
15. Lee, H. H.; Register, R. A.; Hajduk, D. A.; Gruner, S. M. "Orientation of triblock copolymers in planar extension" *Polym. Eng. and Sci.* **1997**, 36 (10), 1414.
16. Quiram, D. J.; Register, R. A.; Marchand, G. R.; Adamson, D. H. "Chain orientation in block copolymers exhibiting cylindrically confined crystallization" *Macromolecules* **1998**, 31, 4891.

17. Albalak, R. J.; Thomas, E. L. "Microphase separation of block copolymer solutions in a flow field" *J Polym Sci Part B Polym Phys* **1993**; 32: 37.
18. Hashimoto, T.; Bodycomb, J.; Funaki, Y.; Kimishima K. "Single grain lamellar microdomain from a diblock copolymer" *Macromolecules* **1999**, 32, 2075.
19. Amundson, K.; Helfand, E.; Davis, D. D.; Quan, X.; Hudson, S. D.; Smith, S. D. "Alignment of lamellar block copolymer microstructure in an electric field. 2.mechanisms of alignment" *Macromolecules* **1994**; 27: 6559.
20. Morkved, T. L.; Lu, M.; Urbas, A. M.; Ehrichs, E. E.; Jaeger, H. M.; Mansky, P.; Russel, T. P. "Local control of microdomain orientation in diblock copolymer thin films with electric fields" *Science* **1996**, 273, 931.
21. Fasolka, M. J.; Banerjee, P.; Mayes, A. M.; Pickett, G.; Balazs, A. C. "Morphology of ultrathin supported diblock copolymer films: Theory and experiment" *Macromolecules* **2000**, 33, 5702.
22. Huang, E.; Russell, T. P.; Harrison, C.; Chaikin, P. M.; Register, R. A.; Hawker, C. J.; Mays, J. "Using surface active random copolymers to control the domain orientation in diblock copolymer thin films" *Macromolecules* **1998**, 31, 7641.
23. Fasolka, M. J.; Harris, D. J.; Mayes, A. M.; Yoon, M.; Mochrie, S. G. J. "Observed substrate topography mediated lateral patterning of diblock copolymer films" *Phys. Rev. Lett.* **1997**, 79, 3018.
24. Rockford, L.; Liu, Y.; Mansky, P.; Russell, T. P. "Polymers on nanoperiodic, heterogeneous surfaces" *Phys. Rev. Lett.* **1999**, 82, 2602.
25. Heier, J.; Genzer, J.; Kramer, E. J.; Bates, F. S.; Krausch, G. "Transfer of a chemical substrate pattern into an island forming diblock copolymer film" *J. Chem. Phys.* **1999**, 111, 11101.

## CHAPTER 7: Directional Solidification and Epitaxy

### 7.1 Microdomain Patterns via Directional Eutectic Solidification and Epitaxy

The creation of a regular surface pattern on the nanometer scale is important for many applications. For instance, periodic arrays constructed by optical microlithography are used as separation media in electrophoresis,<sup>1</sup> island structures are used for high density magnetic recording devices,<sup>2</sup> and block copolymer patterns can be used for sub-30 nm lithography.<sup>3-5</sup> However, in order for block copolymers to be useful for many thin film technologies, researchers must learn how to make chemically patterned surfaces substantially defect-free over large areas with tailored domain orientation and periodicity. Control over domain orientation has been achieved in several ways.<sup>6-9</sup> By rapidly solidifying a semi-crystalline block copolymer from a crystallizable solvent between glass substrates using directional solidification and epitaxy, A new, extremely fast process is introduced to form large area, uniform thickness, thin films with 2D periodic, vertically aligned cylindrical domains each containing precisely one crystalline lamella. The film is both chemically and structurally periodic, therefore providing new opportunities for more selective and versatile nanopatterned surfaces.

#### 7.1.1 Introduction

Block copolymers consist of chemically distinct macromolecules covalently linked to form a single chain and due to their mutual repulsion, the dissimilar blocks tend to segregate into different domains whose shape, size and spacing are determined by the relative amount of the block components and their respective molecular weights.<sup>10,11</sup> Control over the microdomain patterns has been achieved by employing electric fields, temperature gradients, patterned substrates and neutral confining surfaces. For example, Bodycomb et al.<sup>12</sup> has used a temperature gradient to produce a vertically aligned lamellar structure with excellent long range order. To obtain a well ordered structure slow growth (mm/day) in a large gradient (700 °C/cm) is required.



In crystalline materials, control of the solidification process is key to many technologies which rely on the features of the resultant microstructure for achieving optimum properties. For example, the directional solidification of a eutectic metal alloy can lead to rod or lamellar structures well aligned along to the growth direction<sup>13</sup>. In crystalline polymeric materials, orientation of crystallizable macromolecules has been achieved by mechanical forces as in fiber spinning and also by epitaxial crystallization onto substrates.<sup>14,15</sup> Reiter et al.<sup>16</sup> have utilized crystallization from the microphase separated state of a low molecular weight diblock copolymer adjacent to boundaries formed by dewetting from the substrate to achieve a vertically oriented lamellar structure. Smith and Pennings first demonstrated that mixtures of polyethylene and a crystallizable solvent (tetra-chlorobenzene) form a binary eutectic<sup>17</sup>. Wittmann et al.<sup>18</sup> showed that polyethylene homopolymer epitaxially crystallizes on benzoic acid. Dorset et al.<sup>19</sup> showed that benzoic acid and paraffin form a eutectic and that the paraffin grows epitaxially onto the crystallized benzoic acid. This section thus presents a semicrystalline block copolymer dissolved in a crystallizable and epitaxy-forming solvent yields interesting directionally solidified structures.

A polystyrene-*block*-polyethylene (PS/PE) diblock copolymer is employed which was prepared by hydrogenation of polystyrene-*block*-1,4-butadiene, previously synthesized via sequential anionic polymerization. The amorphous PS block and the crystallizable PE block have molecular weights of 40,000 and 10,000 g/mol respectively, the volume fraction of the PE block is 0.24 with a melting point of 98 °C. SAXS of bulk films of PS/PE shows multiple low angle reflections characteristic of hexagonally packed PE cylinders with the first Bragg peak at  $q=0.15 \text{ nm}^{-1}$  corresponding to a cylinder-cylinder spacing of 42 nm.

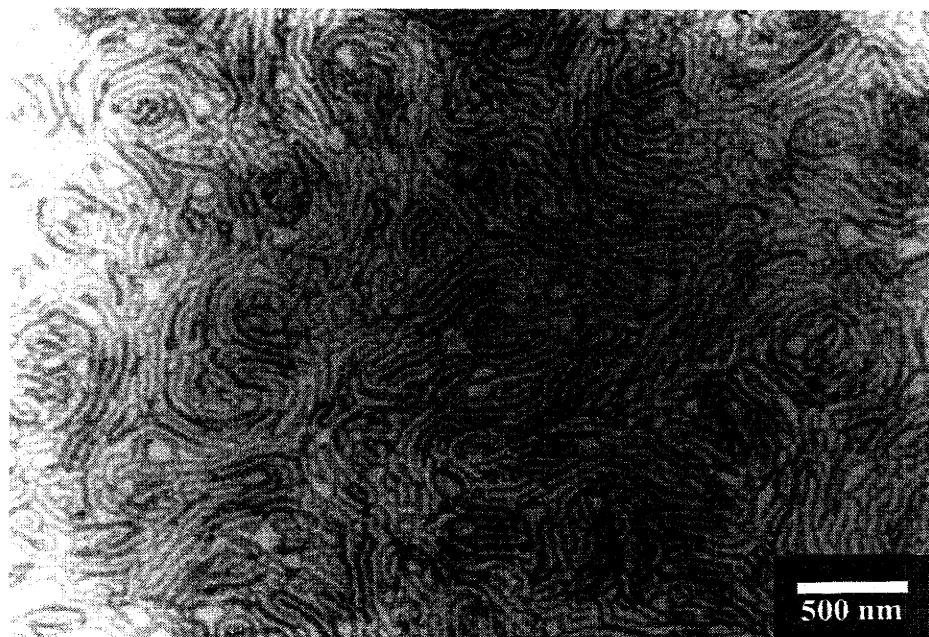
### 7.1.2 Results and Discussion

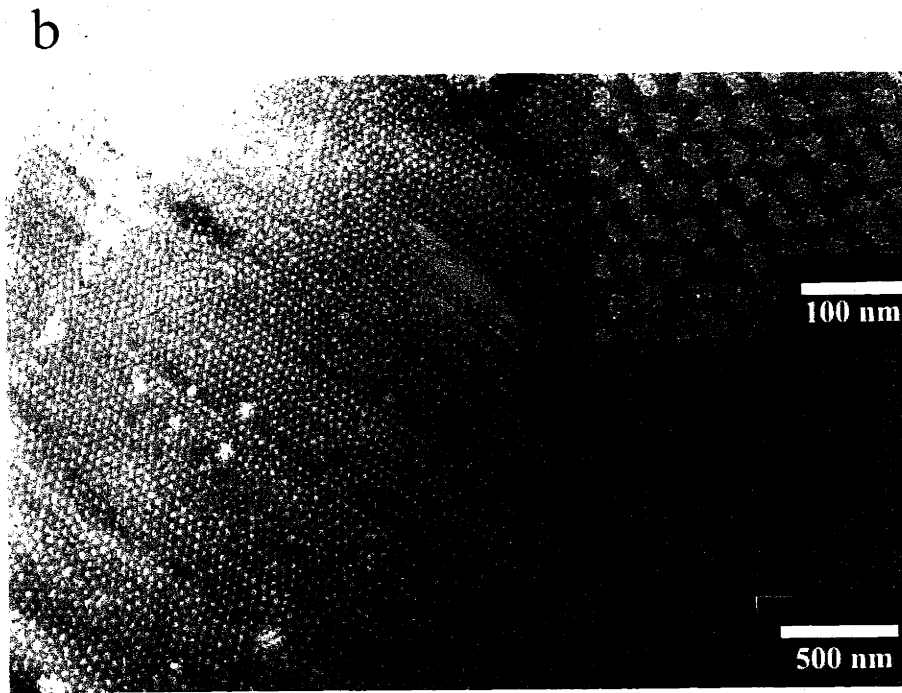
When cast from dilute xylene solution onto a carbon support film, the structure consists of in-plane meandering cylinders of PE in the PS matrix (Figure 7.1.1a). In order to control the PS/PE microdomain and crystalline PE structures, The diblock in benzoic acid (BA) is first dissolved the, and then the solution is crystallized between glass slides in two stages using a modest temperature gradient (10 °C/cm). In the first directional

solidification done at 110 °C, the BA forms large 200 x 500 micron shaped crystals with the (001) planar surfaces parallel to the substrate and the *b* axis (the fast growth direction) well aligned along the temperature gradient. The remaining solution is then directionally solidified at 60 °C. A thin polymer layer forms adjacent to the glass surfaces and can be examined by microscopy. A bright field image of the RuO<sub>4</sub> stained film shows well ordered arrays of light unstained PE domains in a dark stained PS matrix (Figure 7.1.1b). The light domains are packed on a hexagonal lattice with good long range order extending over 20 micron diameter areas.

Tilting the film in the TEM demonstrates the light domains are cylindrical shaped rather than spherical. A magnified image shows the shape of the interface between the PS and PE is non-circular (see image inset). The diameter of the PE domains along the *b*<sub>BA</sub> direction is about 50% larger on average than in the perpendicular direction (30 nm vs 20 nm). This point will be addressed later in the discussion of the dark field (DF) images and the mechanism of structure formation.

a





**Figure 7.1.1** TEM micrographs of simple cast and directionally solidified and epitaxially crystallized block copolymers.

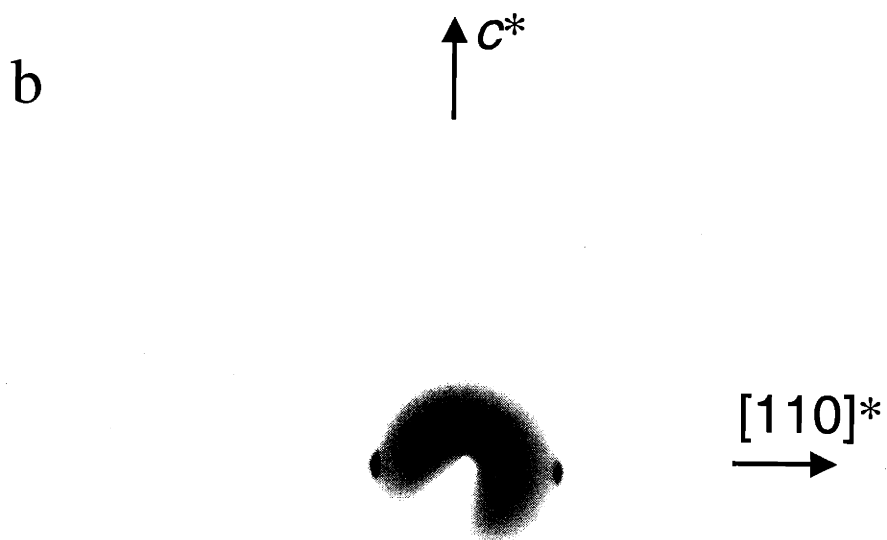
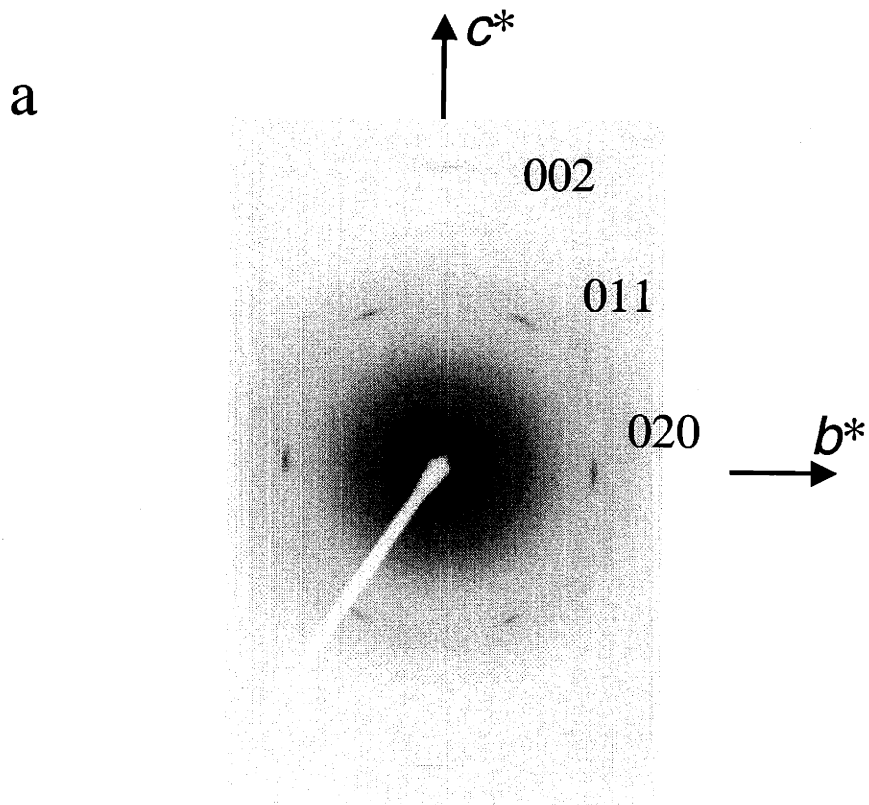
(a) Solvent cast thin film of PS/PE block copolymer stained with  $\text{RuO}_4$ . The bright field TEM image shows a poorly ordered microphase separated structure. The lighter regions correspond to the PE cylindrical domains, the gray regions to the PS matrix. Darker regions appear due to island areas of greater film thickness.

(b) Uniform thickness well ordered thin film of PS/PE block copolymer formed by directional solidification of a solution of the block copolymer in BA. The PE component forms cylinders oriented perpendicular to the film surface and packed in a pseudo-hexagonal lattice. The interdomain spacing is 40 nm along the b-axis direction of BA, and about 10-15% smaller along the other 2 directions. Inset: Magnified region showing the noncircular shape of the PS-PE interface.

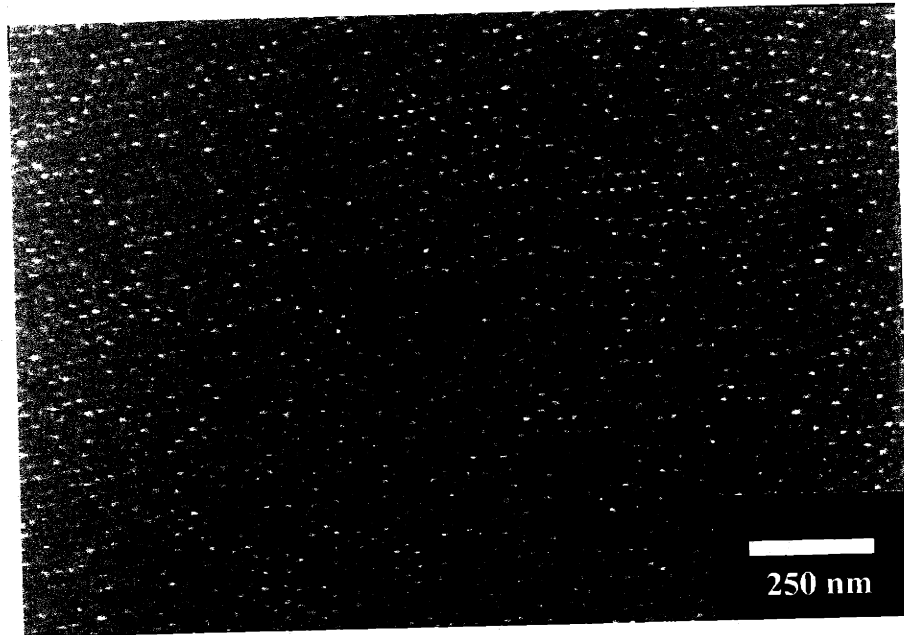
An electron diffraction pattern from an unstained film in Figure 7.1.2a shows very well oriented near-single crystal like reflections which index to the (0kl) reciprocal lattice section of orthorhombic polyethylene (space group  $Pna2_1$ ). The (020) reflection of the PE lies along the BA b-axis direction with the (002) PE chain axis reflection along the perpendicular direction. This situation corresponds perfectly to the known epitaxy between homopolyethylene and BA: namely the (100) plane of PE is in contact with the (001) plane of BA, with the  $b$  and  $c$  axes of PE parallel to the  $b$  and  $a$  axes of BA respectively<sup>18</sup>. Considering the sample has a total bulk crystallinity of less than 10%, such an impressive diffraction pattern may be due to the extraordinary alignment into the diffraction condition of nearly all of the crystals within the selected area as well as the enhancement of crystallinity by the substrate<sup>20</sup>.

The PE crystals can be visualized with DF imaging employing a rotation-tilt stage to bring the strongest diffracting (110) planes into the Bragg condition (Figure 7.1.2b). Low dose imaging<sup>21</sup> shows a periodic array of small rectangular shaped crystals (Figure 7.1.2c). The crystals are arranged in a pseudo-hexagonal lattice whose orientation and average center to center spacing are in very good correspondence with the orientation and spacings of the cylindrical PE domains seen in the BF image. Their size and spacing shows there is precisely one crystalline PE lamella centered in each cylinder and with the  $b$  axis of the lamella oriented parallel to the  $b$  axis of the BA, confirming the epitaxy of PE on BA demonstrated by the electron diffraction pattern. This information also *proves* that the minority PE component was in direct contact with the BA crystals and hence is present at least at the BA-facing surface of the thin film. The longest dimension of the PE crystals is along the  $b$  axis and parallel to the longest diameter of the noncircular interface of the PE domain. This suggests that during crystallization, the anisotropic growth of the crystallizing PE lamellae deforms the microdomain interface.

The essential aspects of the overall phase transformation can be understood by dividing the process into 3 stages using a hypothetical solvent-polymer phase diagram (depicted schematically in Figure 7.1.3). A key feature of the phase diagram is the presence of a eutectic due to the intersection of the melting point depression liquidus curve of the BA with the microphase separation transition depression liquidus curve of the block copolymer. The hypoeutectic system begins as a homogeneous liquid (point 1),



C



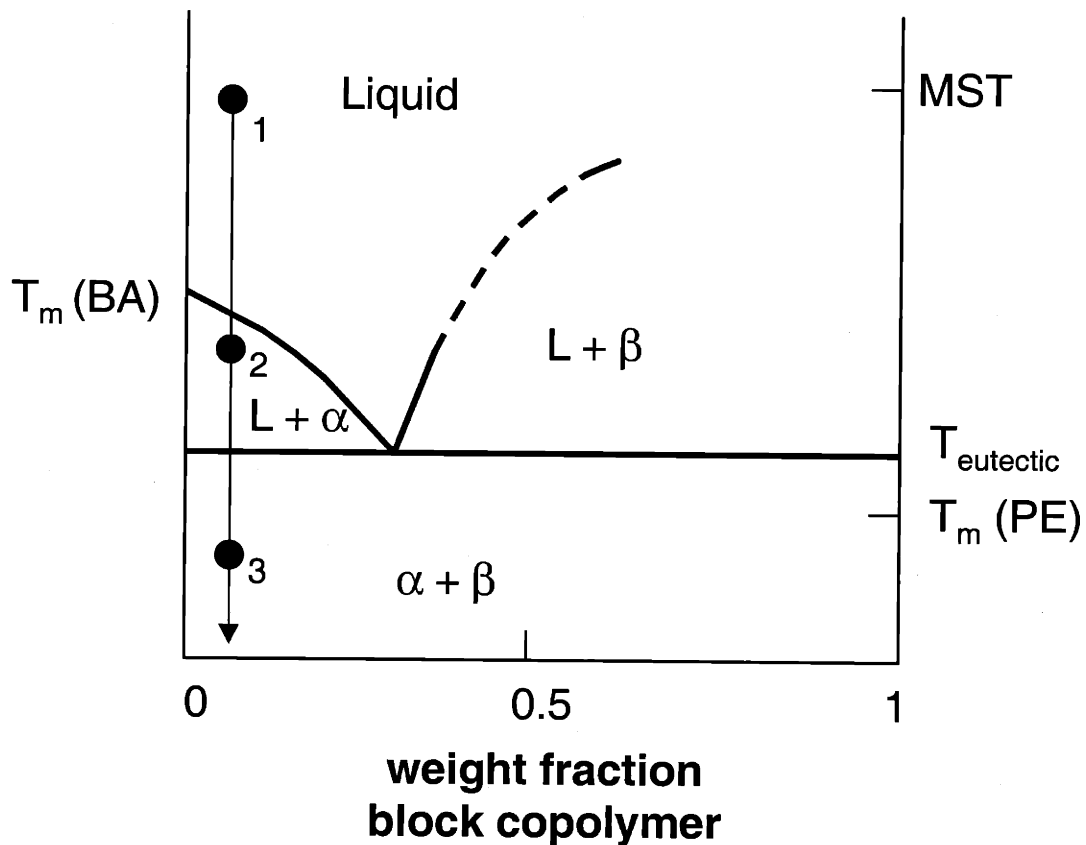
**Figure 7.1.2** Diffraction patterns and dark field image of directionally solidified and epitaxially crystallized block copolymer.

(a) Selected area electron diffraction pattern of an unstained film of PS/PE block copolymer crystallized from BA demonstrating epitaxy. The pattern exhibits only  $0kl$  reflections of PE, which indicates that the (100) plane of PE is normal to the electron beam and parallel to the (001) face of the BA crystals. The  $c$  and  $b$  axes of the PE crystals are parallel to the  $a$  and  $b$  axes of the BA crystal.

(b) Diffraction pattern from a similar sample after tilting  $34^\circ$  about the chain axis direction of PE. The strong (110) diffraction peaks of PE are prominent.

(c) Dark field image of the PS/PE film using the (110) diffraction spot. Small rectangular PE crystals are observed well aligned along the  $b$  axis direction of the BA crystals and packed on a pseudo-hexagonal lattice whose size and orientation is the same as seen in Figure 7.1.1b. The PE crystals are 7nm thick by 20nm long with their longest dimension parallel to  $[110]^*$ .

the temperature is then dropped below the liquidus and growth of BA crystals is initiated by directional solidification (point 2) which increases the copolymer content of the remaining liquid toward the eutectic composition. Further cooling below both the eutectic temperature and the crystallization temperature of the PE results in the transformation of the eutectic liquid into crystalline BA and an ordered, microphase separated block copolymer within which the PE block crystallizes (point 3). A similar phase behavior was achieved in the current material system (PS/PE and BA mixtures) as illustrated in Figure 1.3a.



**Figure 7.1.3** Hypothetical phase diagram of the BA-PS/PE block copolymer system showing the melting points of benzoic acid ( $T_m(\text{BA})$ ) and polyethylene ( $T_m(\text{PE})$ ) as well as the microphase separation transition temperature of the PS/PE block copolymer (MST) and the eutectic point and eutectic temperature ( $T_e$ ). The dilute polymer solution is cooled from location 1 to 3 during the film formation process.

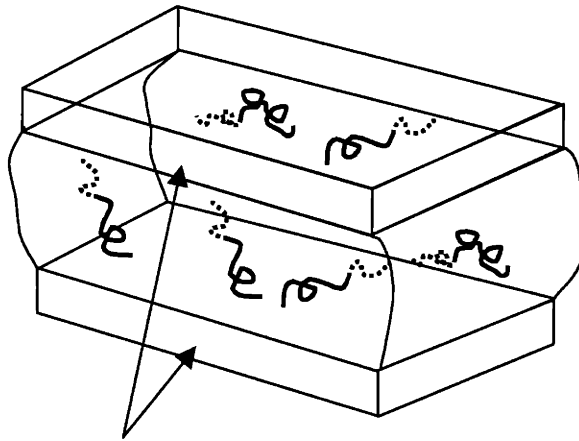
The morphological evolution of the system is schematically depicted in Figure 7.1.4a-e. The initial homogeneous solution confined between the glass substrates (a) transforms due to the imposed directional solidification into large  $\alpha$  crystals of BA having (001) surfaces coexisting with a thin liquid layer near the eutectic composition (b). Dropping the temperature then causes this layer to also directionally solidify by thickening the preexisting BA crystal and the formation of a thin, metastable vertically oriented *lamellar* microdomain film (c). This can be understood by noting that in the thin liquid layer, the spatial distribution of the junction points of the block copolymer molecules is nearly random and upon rapid extraction of the solvent during the second directional solidification process, the junctions must quickly localize onto periodic interfaces defining the domains. For microdomain interfaces parallel to the fast growth direction, this is readily accomplished, whereas for interfaces which are normal to the fast growth direction, repeated nucleation of these junction surfaces is required. For this 24 vol % PE diblock, there is more interface/unit volume in a lamellar structure than in a cylindrical one, so the first structure to form is that which forms the fastest, namely domain layers oriented with their surface normal orthogonal to the fast growth direction of the BA. Of the degenerate set of such orientations, parallel and vertical layers are the most suitable because inclined orientations necessitate junction area density variations near the surface regions. Depending on the affinity of the respective blocks for the substrate surfaces, the polymer film thickness, microdomain period, and the type of epitaxy and crystallizable block chain orientation with respect to the crystalline substrate, many scenarios are possible. In the present PS/PE - BA system, for an assumed parallel lamellar orientation, the subsequent transformation into cylinders embedded in a PS matrix would be highly degenerate, so the final morphology would consist of small grains of in-plane cylinders, whereas, the actual structure is well aligned, vertically oriented, pseudo-hexagonally packed PE microdomains with a 10% larger intercylinder spacing along the fast growth direction. For an assumed vertical lamellar domain orientation, the structure would transform again due to the instability of the flat interface at this composition as well as from the in-plane PE c axis orientation induced by the epitaxy. Cylinder growth from a vertical layer orientation is more consistent with the observed film morphology since the domains evolve from an aligned precursor state (d), into the



final structure (e). To check for the stability of the vertically oriented cylindrical structure, the sample was heated to 115 °C (above the  $T_g$  of the PS (80 °C) and the  $T_m$  of the PE but below the  $T_m$  of the BA), for 1 day and then quenched to vitrify the PS domains and to crystallize the PE block. Note after about 30 minutes the BA completely sublimed. TEM showed that the cylinders were still standing up in the thin film indicating that the vertically oriented structure is the equilibrium state or at least a strongly metastable state. The resultant electron diffraction pattern of the quenched film showed {110} powder diffraction rings, indicating small, randomly oriented PE crystals.

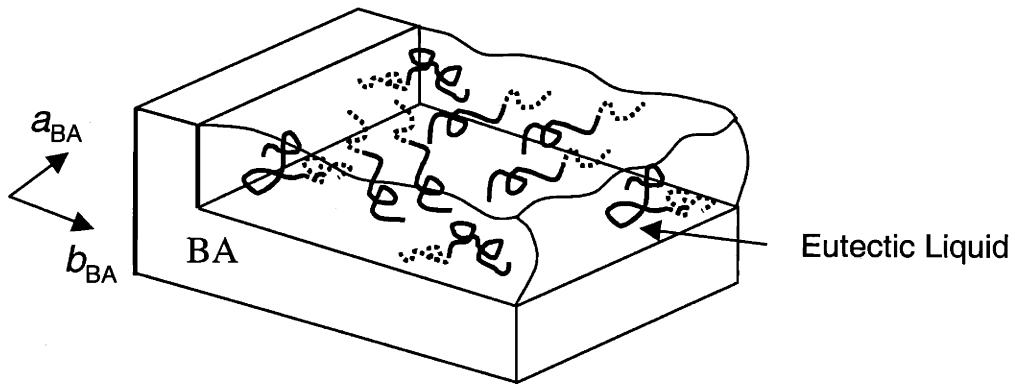
This suggests that kinetic control of pattern formation via a combination of microphase separation and crystallization along a temperature gradient can organize the block copolymer molecules into ordered microphase separated structures. This fast process via the rapid directional extraction of the solvent from the polymer solution by crystallization may have wide applicability to nanopatterning of thin films.

**a** Homogeneous Mixture of BA and Block Copolymer

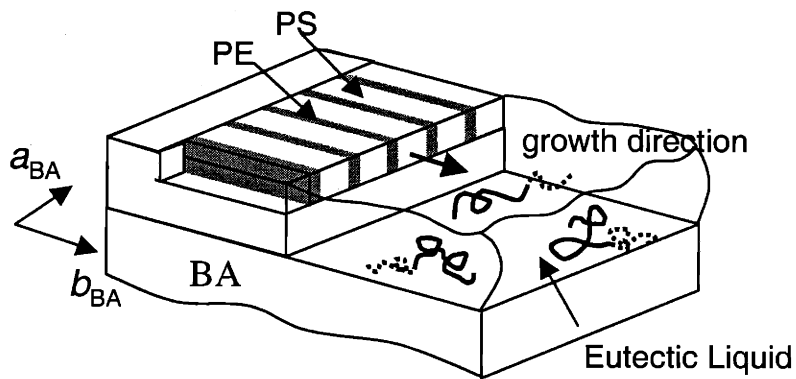


glass substrates

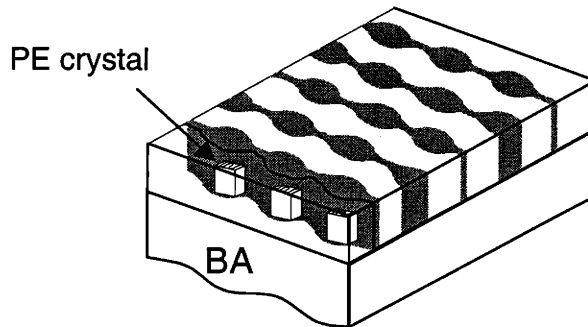
**b** Directional Crystallization of BA



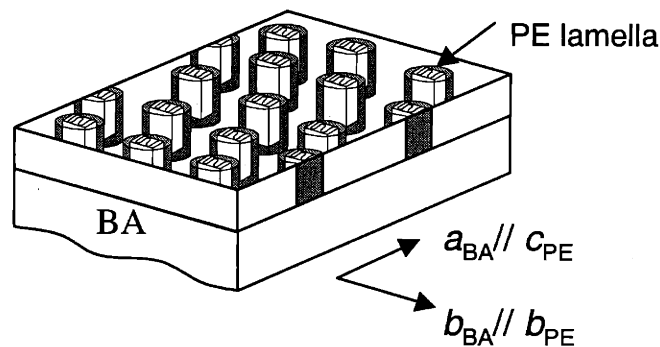
**c** Directional Eutectic Solidification



**d** Crystallization Induced Undulation  
Instability of Thin Lamellae ( $T < T_c$  (PE))



**e** Oriented Cylinder Formation  
and Epitaxial Crystallization



**Figure 7.1.4** Schematics depicting the evolution of the structure during the directional eutectic solidification and epitaxial crystallization of the block copolymer from the crystallizable solvent.

- (a) Homogeneous solution of PS/PE in BA between two glass substrates.
- (b) Directional solidification forms  $\alpha$  crystals of BA coexisting with a liquid layer of more concentrated polymer.
- (c) Second directional solidification showing the eutectic liquid layer transforming into BA crystal (which grows on the pre-eutectic BA- $\alpha$  crystal) and an ordered lamellar block copolymer ( $\beta$ ).
- (d) Due to the highly asymmetric composition of the block copolymer and the epitaxial crystallization of the PE in contact with the BA substrate, the flat interfaces of vertically oriented lamellae are unstable and spontaneously deform in order to achieve a more preferred interfacial curvature and allow epitaxial growth of PE.
- (e) The layers transform into an array of vertically oriented, pseudo-hexagonally packed semicrystalline PE cylinders. A single chain folded PE lamella is formed in each cylinder. The PE crystals have their (100) planes contacting the (001) plane of the BA crystal with  $a_{BA} // c_{PE}$  and  $b_{BA} // b_{PE}$ .

## 7.2 Control of Molecular and Micropattern Orientation in Semicrystalline Block Copolymer Thin Films by Directional Solidification and Epitaxy

The directional solidification of semicrystalline block copolymers with crystallizable organic solvents and the subsequent epitaxial crystallization of the crystalline blocks onto the surface of the crystalline substrate, control both molecular chain orientations of the crystalline blocks and the microdomain structures of block copolymers. Semicrystalline polystyrene-*block*-poly(ethylene-*alt*-propylene)-*block*-polyethylene) (PS/PEP/PE) terpolymer and polystyrene-*block*-polyethylene) (PS/PE) diblock copolymer, containing the crystallizable polyethylene (PE) blocks, have been analyzed using benzoic acid (BA) and anthracene (AN) as crystallizable solvents. The directional solidification induces orientation of the microdomains and the surface interaction (epitaxy), due to the crystallographic matching of unit cells between the crystalline PE blocks and the crystalline substrates, develops high orientation of the crystalline PE blocks. The orientation of the PE crystals onto the substrate is evidenced by selected electron diffraction and bright field transmission electron microscope. In the case of the PS/PEP/PE terpolymer, the process induces the PS cylinders aligned parallel to the *b* axis of BA crystals. Long crystalline PE lamellae are oriented edge-on on the BA surface, with the *b* axis of PE parallel to the *b* axis of BA and parallel to the PS cylinders. In the case of PS/PE diblock copolymer, the PE cylinders are oriented perpendicular to substrate, packed on a hexagonal lattice. Each cylinder contains precisely one crystalline PE lamella oriented edge-on on the substrate. When BA is used the PE lamellae inside cylinders are oriented with the *b* axis parallel to the *b* axis of BA crystals. When AN is used as crystallizable solvent, due to the different epitaxial relationship between PE block and AN crystals, the PE lamellae are oriented along two equivalent directions, with the *c* axis parallel to the [110] and  $[\bar{1}10]$  direction of AN crystals.

### 7.2.1 Introduction

Semicrystalline block copolymers are characterized by a hierarchical structure ranging from the Angstrom to the micron scale and present at least two thermodynamic

transitions: crystal-melt and order-disorder transitions. In these materials the microstructure and the physical properties are significantly influenced by the nature of the organization of chains and microdomains in both the noncrystalline and crystalline blocks. Microphase separation can result either from incompatibility of the blocks or from crystallization of one or more blocks.

The process pathway of structure formation is of prime importance in that the first forming structures present to those emerging a prescribed geometry into which the new structure must evolve. Various types of path-dependent microstructures were discussed in the introduction sections of Chapter 4 and 5. In addition those introductions deliberately dealt with the previous studies of molecular chain orientation of crystalline block with respect to pre-existing microdomain structures.

Chapter 5 described that a high orientation of the crystals of a triblock copolymer containing PE as crystallizable end-blocks, has been achieved through epitaxial crystallization of the copolymer onto benzoic acid (BA) crystals. The epitaxial crystallization controlled the molecular chain orientation of the PE block, resulting in a well ordered parallel lamellar microstructure in the melt-compatible semicrystalline block copolymer. The method is based on the use of organic crystalline substances, which are solvents for the block copolymers above their melting temperatures, and, when crystallized, act as a substrate on which thin films of the block copolymers are formed.

The Chapter 6 also showed that a long range orientation of the microdomains in conventional amorphous block copolymers is obtained by the directional solidification, during the phase separation, of the block copolymer with organic crystallizable solvents.

Moreover, the previous section 7.1 presented the directional solidification of semicrystalline block copolymers from organic crystallizable solvents, combined with the epitaxial crystallization, to obtain high orientation of the molecular crystalline PE chains and vertically ordered cylindrical microstructure in thin films of the strongly segregated semicrystalline block copolymer.

In this section, the directional solidification and epitaxy of semicrystalline block copolymer with crystallizable organic solvent is more extensively studied. Two different semicrystalline block copolymers with crystallizable PE blocks, have been processed using the directional solidification and the epitaxial crystallization, employing two

different organic crystallizable solvents. A terpolymer, polystyrene-*block*-poly(ethylene-*alt*-propene)-*block*-polyethylene (PS/PEP/PE), and a diblock copolymer, polystyrene-*block*-polyethylene (PS/PE), presenting different microphase-separated microstructures in the melt, are analyzed. Benzoic acid (BA) and anthracene (AN), having the different crystal structures and epitaxial relationships with PE crystals, are used as crystallizable solvents. This section aims at clarifying the roles that the two driving forces: directional solidification and epitaxial crystallization play in the formation of the ordered microstructures in thin films of block copolymers.

## 7.2.2 Results and Discussion

### 7.2.2.1 PS/PEP/PE block terpolymer

The PS/PEP/PE terpolymer presents a novel situation in which the crystallization event of the PE end-block within the microphase separated structure is partially screened by the intervening rubbery PEP mid-block. The terpolymer is in the intermediate segregation regime at room temperature, due to the large incompatibility between PS and PE/PEP blocks leading to an order-disorder transition higher than 250 °C (Chapter 3). Thus PS microdomains form below the microphase separation temperature and above the melting point of the PE block. Once the sample is cooled below the crystallization temperature of PE blocks (70 °C), crystallization occurs in the matrix from the ordered microphase separated melt, and a further separation between the PEP and PE blocks results (Chapter 4). In spite of the low volume fraction the equilibrium microdomain structure is cylindrical PS (Chapter 3).

Thin films of the PS/PEP/PE block copolymer have been directionally solidified and epitaxially crystallized with BA following the method outlined in the experimental section.

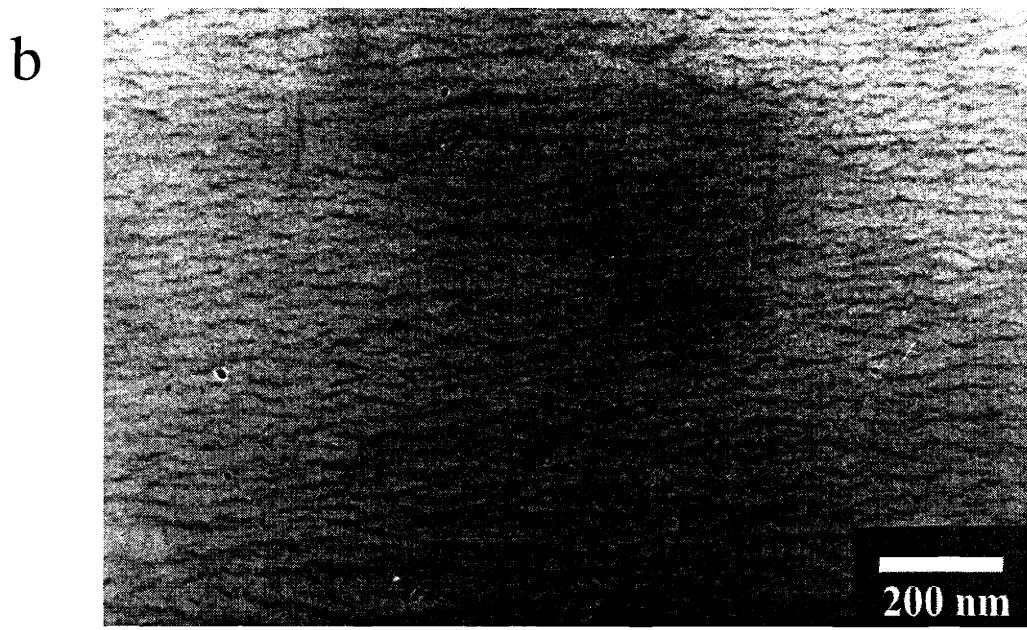
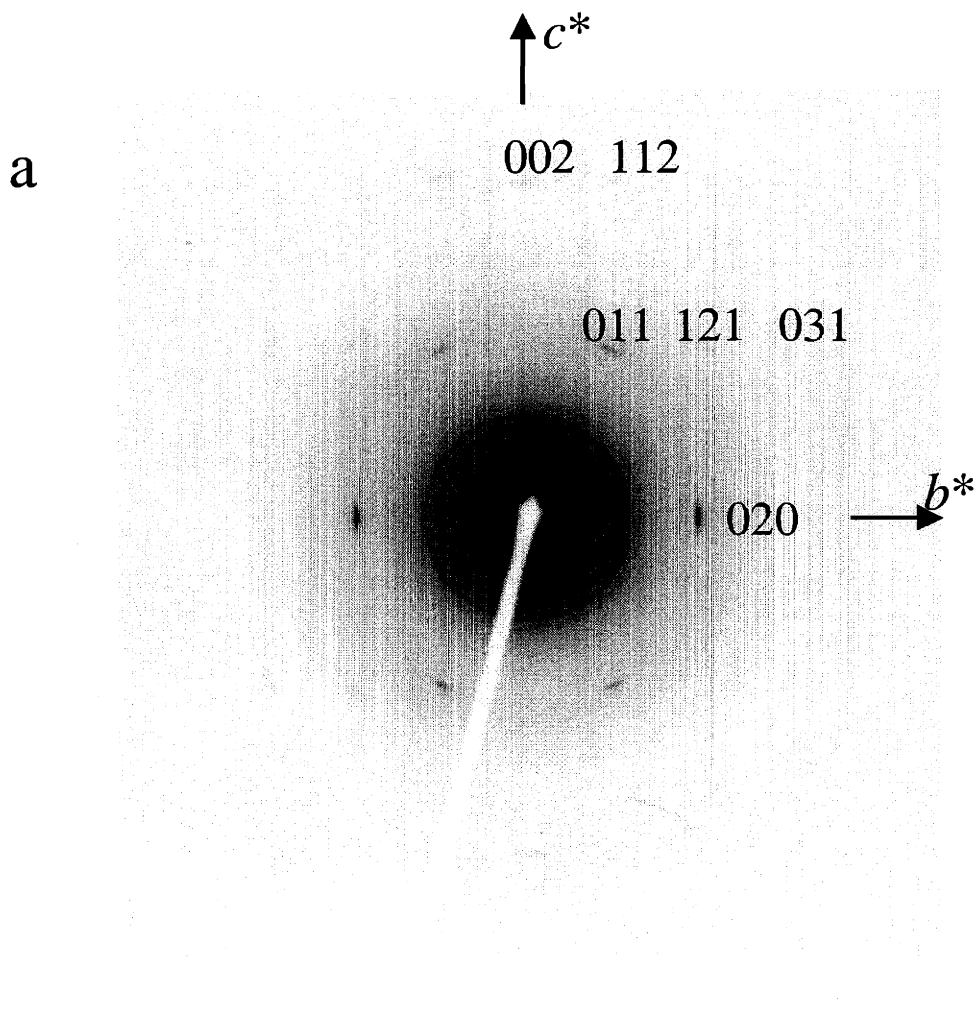
The SAD pattern of PS/PEP/PE block copolymer film, using a 6 $\mu$ m diameter SAD aperture, is shown in Figure 7.2.1a. The pattern of Figure 7.2.1a essentially presents only the  $0kl$  reflections of PE; therefore it corresponds to the  $b^*c^*$  section of the reciprocal lattice of PE. This pattern is very similar to that obtained for the melt-compatible PE/PEP/PE triblock copolymer, reported in Chapter 5. The orientation of the PE crystals in the PS/PEP/PE terpolymer is the same as that found for the PE/PEP/PE triblock

copolymer. Since the  $b^*c^*$  section of the reciprocal lattice is in diffraction, the chain axis of the crystalline PE molecules lies flat on the BA surface and oriented parallel to the  $a$  axis of BA crystals, as for the PE homopolymer.<sup>18</sup> The (100) plane of PE is in contact with the (001) plane of BA, therefore the crystalline PE lamellae are oriented edge-on on the substrate surface, and parallel to the  $b$  axis of BA.<sup>18</sup> The  $b$  and  $c$  axes of PE are parallel to the  $b$  and  $a$  axes of benzoic acid, respectively; this epitaxy is well explained in terms of matching the PE inter-chain distance of the  $b$  PE axis periodicity (4.95 Å) with the  $b$  periodicity of the BA unit cell (5.25 Å).<sup>18</sup> The low bulk crystallinity of nearly 6% implies that such diffraction pattern in thin film may be due to the high alignment into the diffraction condition as well as the enhancement of crystallinity by the substrate (Chapter 5).

A bright-field TEM image of the unstained film directionally solidified and epitaxially crystallized onto BA, is shown in Figure 7.2.1b. Phase contrast obtained by underfocus of the objective lens makes the noncrystalline regions appears bright.<sup>22</sup> It is apparent that the epitaxy has produced a highly oriented lamellar structure with long thin crystalline lamellae, having a thickness of 10-20 nm, oriented along the  $[010]_{PE} // [010]_{BA}$  direction, according to the electron diffraction pattern.

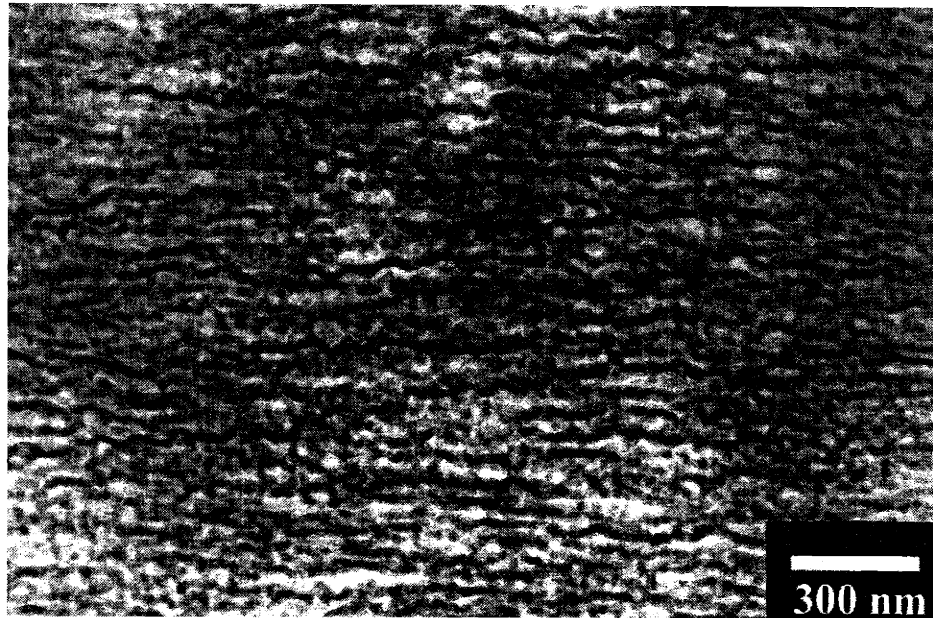
A bright-field image of the same sample after staining with  $\text{RuO}_4$  is shown in Figure 7.2.1c. In this amplitude contrast micrograph the darker regions correspond to the stained PS microdomains; it is apparent that the PS blocks are organized in parallel cylinders whose axes are generally oriented along the elongation direction of the crystalline lamellae (Figure 7.2.1b),  $[010]_{PE} // [010]_{BA}$ . The average diameter of the PS cylindrical microdomains is nearly 20 nm, while the average distance between the cylinders is 40-50 nm, according with the results in the bulk (Chapter 3).

The section 7.1 described that in the strongly segregated semicrystalline block copolymer, epitaxially crystallized onto an organic substrate, the resulting structure can be understood in terms of a combination of directional solidification of the eutectic solution of the block copolymer in the crystallizable organic solvent and the following epitaxial crystallization of the crystalline block onto the organic crystalline substrate.





C



**Figure 7.2.1** SAD pattern and TEM images of a thin film of PS/PEP/PE terpolymer directionally solidified and epitaxially crystallized onto BA.

(a) SAD pattern of a thin film of PS/PEP/PE terpolymer. The pattern presents the  $0kl$  reflections of PE, hence it indicates that the (100) plane of PE is normal to the electron beam and parallel to the (001) exposed face of the benzoic acid crystals. The  $c$  and  $b$  axes of the PE crystals are parallel to the  $a$  and  $b$  axes of the benzoic acid, respectively.

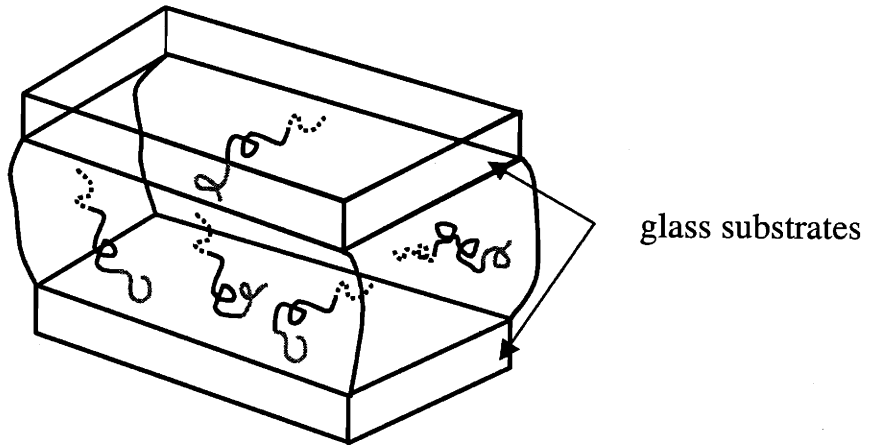
(b) TEM Bright-field image of the unstained thin film of PS/PEP/PE terpolymer corresponding to an area similar to that of (a). The image contrast is enhanced by underfocus of the objective lens. The dark regions correspond to the crystalline PE phase, which form long lamellae oriented edge-on, and aligned along the  $b$  axis of PE, parallel to the  $b$  axis of BA.

(c) TEM bright-field image of the stained thin film of PS/PEP/PE terpolymer with  $\text{RuO}_4$ . The dark regions correspond to the PS phase, which form cylinders aligned parallel to the crystalline lamellae.

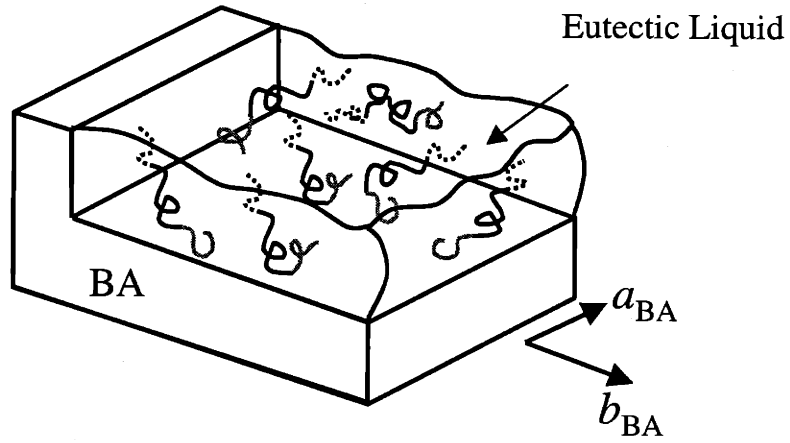
Binary solutions of block copolymers and crystallizable solvents may also present a eutectic composition due to the intersection of the melting point depression liquidus curve of the BA with the order-disorder transition depression liquidus curve of the block copolymer (Chapter 7.1). DSC experiment to determine a phase behavior of PS/PEP/PE and BA mixtures displayed a phase diagram analogous to a hypothetical eutectic phase behavior (Figure 1.3b).

A schematic model of the development of the microstructure is shown in Figure 7.2.2. From the initial homogeneous solution between two glass substrates (Figure 7.2.2a), large crystals of BA form due to the imposed directional solidification. The BA crystals have the (001) surfaces coexisting with a thin liquid layer near the eutectic composition (Figure 7.2.2b). Decreasing the temperature, this thin eutectic liquid layer also directionally solidify resulting in the thickening the preexisting BA crystal and the formation of a thin film of the microphase separated block copolymer presenting a metastable vertically oriented lamellar microdomains (Figure 7.2.2c). This metastable structure is the fastest one which may develop during the fast directional solidification. It then transforms again due to the instability of the highly unfavorable flat interface at this composition and the stable PS cylinders form (Figure 7.2.2d). A further decrease of the temperature at  $-60\text{ }^{\circ}\text{C}$  induces the epitaxial crystallization of the PE blocks, in the PE/PEP matrix, onto the BA crystals. Long, thin crystalline PE lamellae, oriented edge-on on the substrate form in between the PS cylinders (Figure 7.2.2e). The crystalline lamellae are oriented along the  $[010]_{\text{PE}}//[010]_{\text{BA}}$  direction, therefore parallel to the axes of the PS cylinders. Using BA, the directional solidification and epitaxial crystallization induce alignment of the PS cylinders and PE lamellae along the same direction.

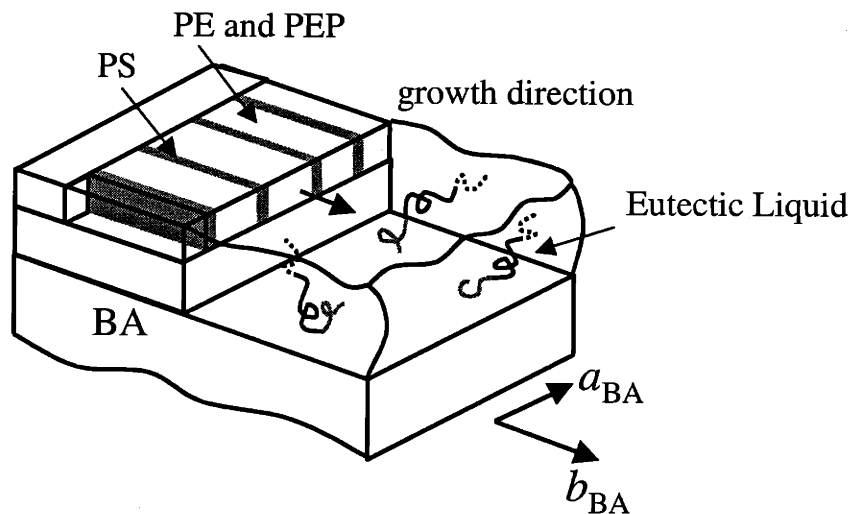
a. Homogeneous Mixture of BA and PS/PEP/PE



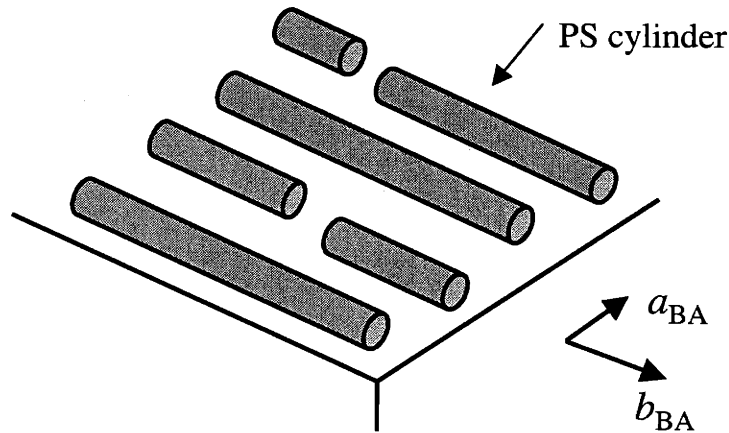
b. Directional Crystallization of BA



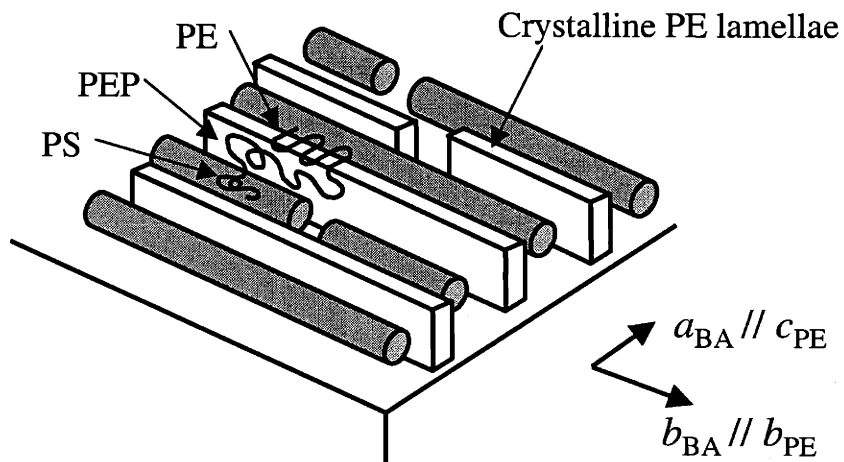
c. Directional Eutectic Solidification



d. Structural Transformation into In-plane PS cylinders



e. Epitaxy of PE blocks between PS cylinders onto BA



**Figure 7.2.2** Schematic model showing the development of the microstructure in thin films of the PS/PEP/PE terpolymer epitaxially crystallized onto BA.

- (a) Homogeneous solution of PS/PEP/PE in BA between two glass substrates.
- (b) Directional solidification forms crystals of BA coexisting with a liquid layer of more concentrated polymer.
- (c) Second directional solidification showing the eutectic liquid layer transforming into BA crystal (which grows on the pre-eutectic BA crystal) and an ordered lamellar block copolymer.
- (d) Due to the highly asymmetric composition of the block copolymer, the flat interfaces of vertically oriented lamellae are unstable and spontaneously deform in order to achieve a more preferred interfacial curvature.
- (e) Epitaxial crystallization of PE blocks onto the BA crystals occurs resulting in the formation of long, thin crystalline PE lamellae in between the PS cylinders. The PE crystals have their (100) planes contacting the (001) plane of the BA crystal with  $a_{BA} // c_{PE}$  and  $b_{BA} // b_{PE}$ .

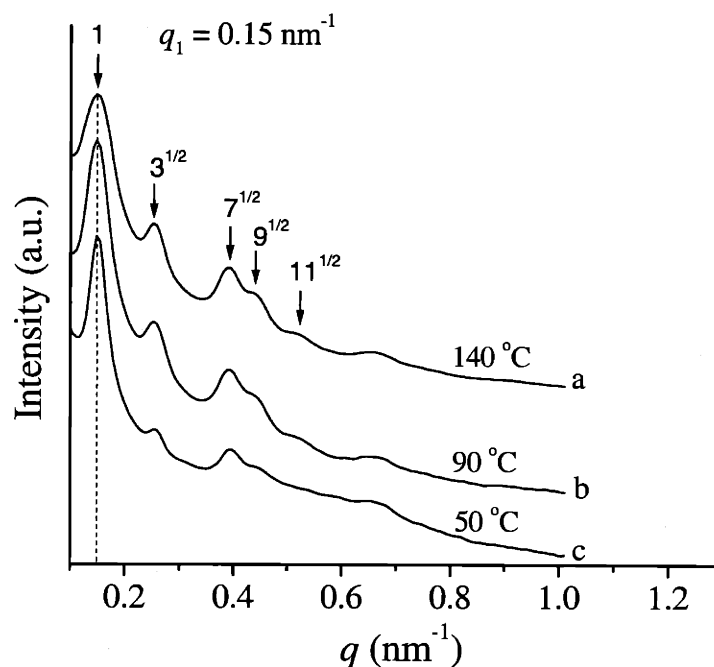
### 7.2.2.2 PS/PE diblock copolymer

SAXS patterns of the PS/PE bulk sample recorded at different temperatures, starting from the melt of the PE block and cooling to room temperature, are shown in Figure 7.2.3. The presence in the pattern at 140 °C (Figure 7.2.3a) of the diffraction peaks having diffraction vectors  $q_n$  in the ratios  $q_n/q_1$  equal to 1,  $\sqrt{3}$ ,  $\sqrt{7}$ ,  $\sqrt{9}$ ,  $\sqrt{11}$  indicates a microphase separated ordered microstructure of the melt, characterized by cylinders of PE packed in a hexagonal lattice. The first peak at  $q_1 = 0.15 \text{ nm}^{-1}$ , corresponding to the  $10\bar{1}0$  reflection, indicates a distance between the cylinders of 42 nm. The same hexagonal microstructure is preserved at lower temperatures (Figure 7.2.3b), and after the crystallization of PE (evidenced by WAXS pattern simultaneously obtained), which occurs at nearly 65 °C. In fact, the SAXS pattern recorded at 50 °C (Figure 7.2.3c) is very similar to that of the melt (Figure 7.2.3a). The peak positions are unaltered, indicating that the crystallization of PE occurs inside the cylinders present in the melt and does not disturb the cylindrical microstructure. Only a small variation of the intensities of the diffraction peaks is observed due to additional scattering of the PE crystals.

In order to control the PS-PE microdomain and the PE crystalline structure, thin films of PS/PE block copolymer have been directionally solidified and epitaxially crystallized employing BA and AN as crystallizable solvents.

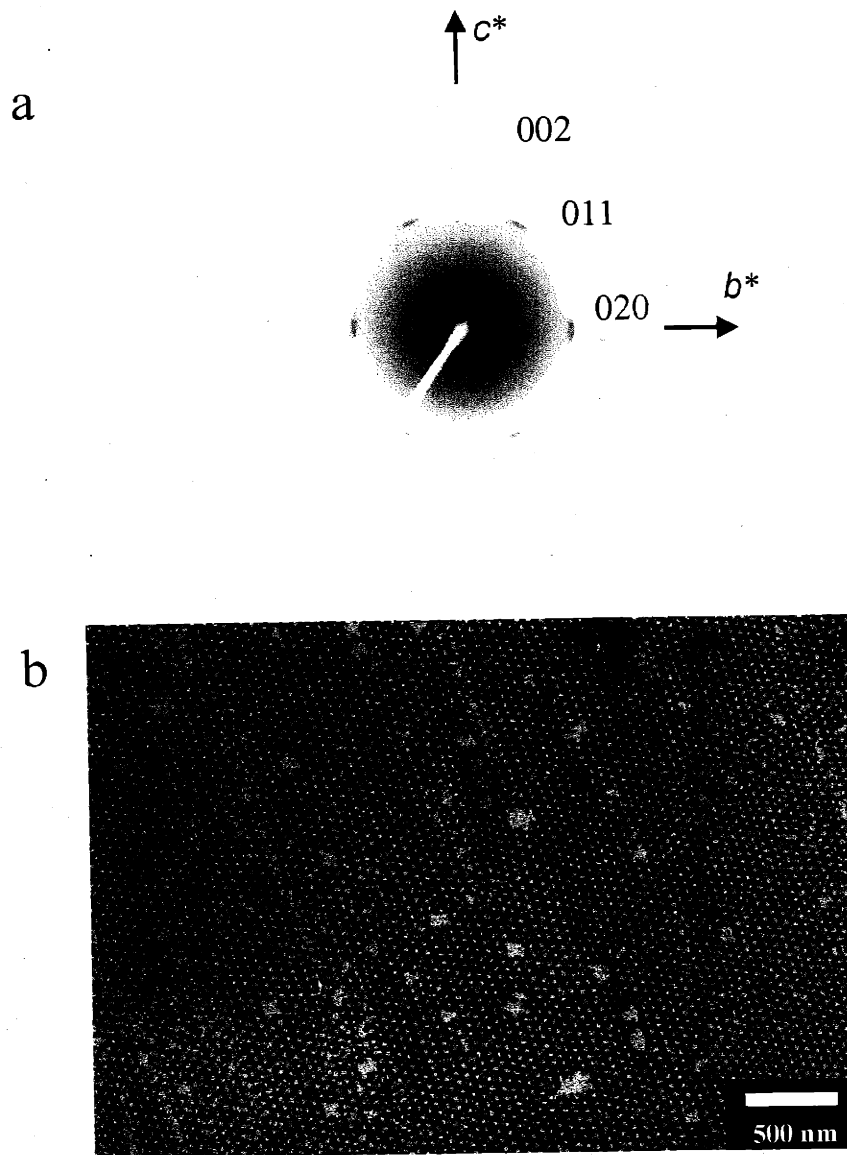
#### 7.2.2.2.1. Benzoic acid

The SAD pattern of an unstained film, using a SAD aperture of 6  $\mu\text{m}$ , is shown in Figure 7.2.4a. A high degree of orientation of the PE crystals has been obtained. The pattern presents only the  $0kl$  reflections of PE and is very similar to that obtained for the PS/PEP/PE (Figure 7.2.1a). The orientation of the PE crystals onto the (001) surface of BA crystals is therefore the same as that described for the PS/PEP/PE in the previous section. Due to the epitaxial relationship between PE and BA, crystalline PE lamellae are oriented edge-on on the substrate surface with the (001) plane of BA in contact with the (100) plane of PE, and the  $b$  and  $c$  axes of PE parallel to the  $b$  and  $a$  axes of BA, respectively.



**Figure 7.2.3** Small angle X-ray diffraction patterns of a bulk sample of the PS/PE block copolymer recorded at the indicated temperatures during the cooling from the melt. The ratios ( $q_n/q_1$ ) of the diffraction vectors  $q_n$ , with respect to that of the first peak at  $q = q_1 = 0.15 \text{ nm}^{-1}$ , are also shown. The ratios  $1, \sqrt{3}, \sqrt{7}, \sqrt{9}, \sqrt{11}$  indicates the presence of a microstructure characterized by a hexagonal packing of PE cylinders. The expected peak at  $q/q_1 = \sqrt{4}$  is probably concealed by the broad peak at  $q/q_1 = \sqrt{3}$ .

A bright field TEM image of a thin film of PS/PE block copolymer directionally solidified and epitaxially crystallized onto BA, and stained with RuO<sub>4</sub>, is shown in Figure 7.2.4b. The presence of a well ordered array of light unstained PE cylinders in the dark stained PS matrix, is apparent. Since the epitaxy requires the contact of the PE on BA crystal surface, chemically different pattern structure is obtained. Tilting the film in the TEM shows that the light domains are cylindrical rather than spherical. The cylinder are vertically aligned and are packed on a hexagonal lattice, having an average lattice constant of nearly 40 nm, in agreement with the SAXS data of the bulk sample, and the order extends to large distances ( $> 20 \mu\text{m}$ ), much larger than the picture shown in Figure 7.2.4b. The dark field image in the previous section (7.1) shows that only one crystalline PE lamella is occupied in each cylindrical PE microdomain.



**Figure 7.2.4** SAD pattern and TEM image of a thin film of PS/PE block copolymer directionally solidified and epitaxially crystallized onto BA.

(a) SAD pattern of a thin film of PS/PE block copolymer. The pattern presents only the  $0kl$  reflections of PE. This indicates that the (100) plane of PE is normal to the electron beam and parallel to the (001) exposed face of the BA crystals. The  $c$  and  $b$  axes of the PE crystals are parallel to the  $a$  and  $b$  axes of the BA, respectively.

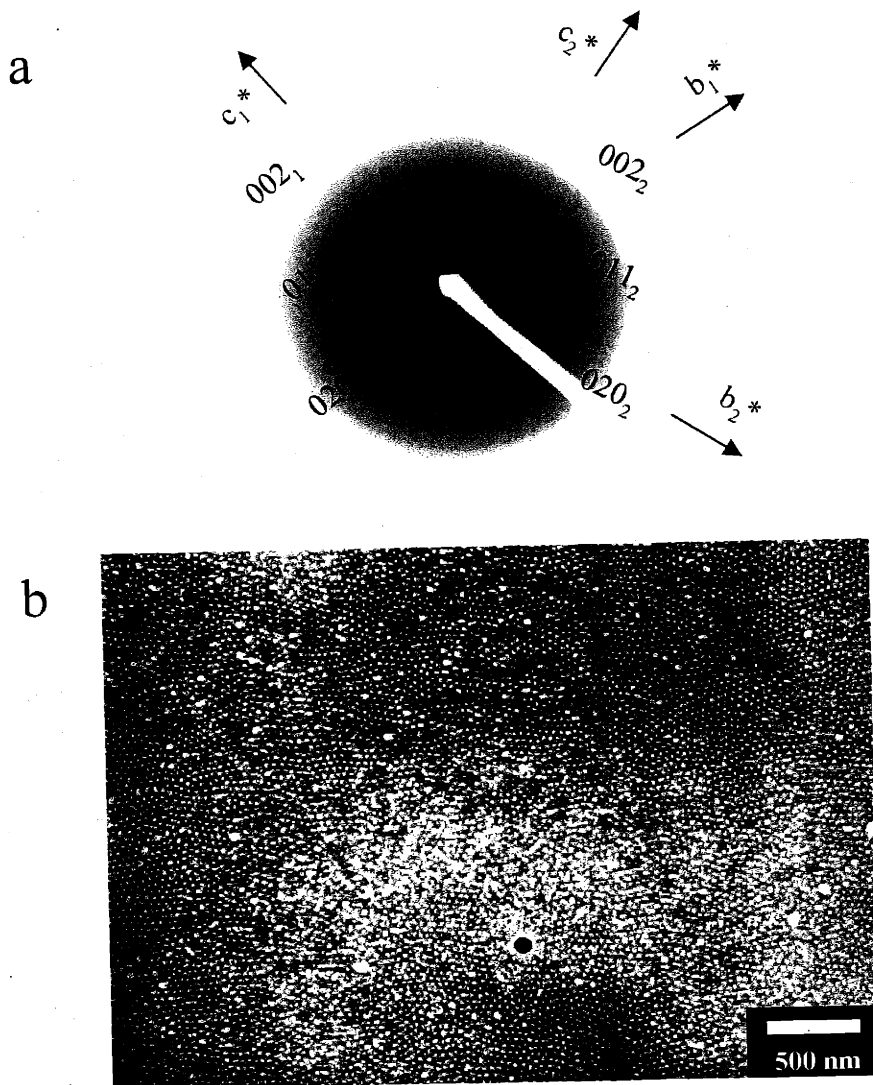
(b) TEM Bright-field image of a thin film of PS/PE block copolymer stained with  $\text{RuO}_4$ . The darker regions correspond to the stained PS matrix, while the light regions correspond to the crystalline PE microdomains, which form hexagonally packed cylinders oriented perpendicular to the substrate surface.

#### 7.2.2.2. Anthracene

The SAD pattern of an unstained film is shown in Figure 7.2.5a. The pattern exhibits the  $0kl$  reflections of PE of two different orientations similar to that found for PE homopolymer and semicrystalline block copolymer crystallized on AN.<sup>23</sup> The pattern indexes to the  $b^*c^*$  section of the PE reciprocal lattice symmetrically rotated by an angle of  $\pm 70^\circ$  to the  $a^*$  axis of the AN. Since the area selected for diffraction is approximately  $6 \mu\text{m}$  in diameter, it indicates that a high global double-orientation of the PE chain molecules in the crystalline phase is achieved. This angle of  $70^\circ$  corresponds to the angle made by  $[110]$  and  $[\bar{1}\bar{1}0]$  directions in the  $a^*b^*$  plane of AN, i.e., in the contact plane with PE. The  $c$ -axis of PE is therefore oriented parallel to the  $[110]$  and  $[\bar{1}\bar{1}0]$  directions of AN. Since only the  $0kl$  reflections are present, the  $bc$  plane ( $(100)$  plane) of PE crystals is normal to the electron beam and therefore parallel to the exposed  $(001)$  face of AN crystals. The crystalline PE lamellae stand edge-on on the substrate surface. The epitaxial relationship is similar to that obtained for the polyethylene homopolymer,<sup>23</sup> which can be well explained in terms of matching between  $b_{\text{PE}}$  and the AN  $d_{110}$  inter-row spacing and a second matching of the  $2c_{\text{PE}}$  with  $(1/2)d_{110}$  of AN. This epitaxial relationship gives two equivalent orientations (See Figure 8.1b in Chapter 8 for schematic of epitaxial relationship between PE and AN).

A bright field TEM image of the PS/PE block copolymer directionally solidified from AN and epitaxially crystallized onto AN crystals, and stained with  $\text{RuO}_4$ , is shown in Figure 7.2.5b. Also in this case the light unstained PE cylinders are vertically aligned and packed on a hexagonal lattice. A degree of order in the alignment of the PE cylinders along the fast growth direction of AN crystals ( $b$  axis), lower than in the case of BA crystals (Figure 7.2.4a), is obtained. This is probably because the shape anisotropy of AN crystals in growth process is lower than that of BA crystals, as observed with optical microscope (Chapter 6).





**Figure 7.2.5** SAD pattern and TEM image of a thin film of PS/PE block copolymer directionally solidified and epitaxially crystallized onto AN.

(a) SAD pattern of a thin film of PS/PE block copolymer. The pattern presents the  $0kl$  reflections of PE, hence indicates that the (100) plane of PE is parallel to the (001) exposed face of the AN crystals. The  $c$  axis of the PE crystals is parallel to the  $[110]$  and  $[\bar{1}\bar{1}0]$  directions of AN crystal. Therefore, two diffraction patterns rotated by an angle of  $70^\circ$  and oriented symmetrically relative to the  $a^*$  axis of the AN crystals is shown along the  $[110]$  and  $[\bar{1}\bar{1}0]$  directions of AN crystals.

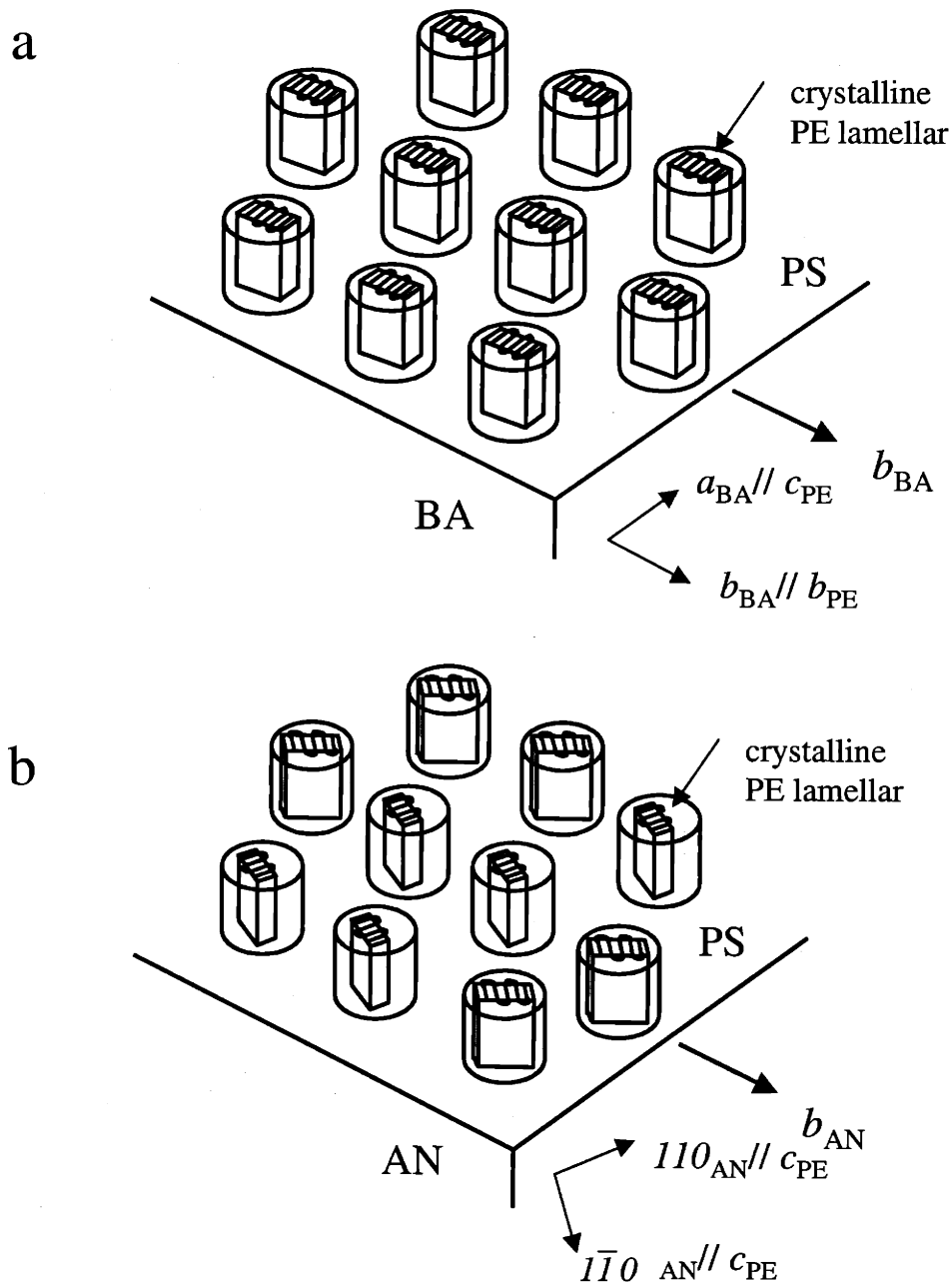
(b) TEM Bright-field image of a thin film of PS/PE block copolymer stained with  $\text{RuO}_4$ . The darker regions correspond to the stained PS matrix, while the light regions correspond to the crystalline PE microdomains, which form hexagonally packed cylinders oriented perpendicular to the substrate surface.

The mechanism of the pattern formation of PS/PE on BA or AN is basically the same as that shown in Figure 7.2.2 for the PS/PEP/PE block copolymer. The directional solidification of the organic crystal (BA or AN) and the successive solidification of the eutectic liquid mixture of organic crystal and block copolymer, produce the formation of thin metastable vertically oriented lamellar microdomain film. Instead of forming in-plane PS cylinders for PS/PEP/PE, the instability of the flat interface at this composition as well as the in-plane PE *c*-axis orientation induced by the epitaxy in the thin vertical lamellae transforms into vertically oriented PE cylinders eventually containing one crystalline lamella after complete epitaxy. The plasticization of PS matrix from BA or AN (the decrease of the glass transition temperature of PS was evidenced by DSC) enables the epitaxial crystallization to transform the microstructure. The structural difference between using BA and AN results from the different epitaxial relationships. When BA is used the PE block epitaxially crystallizes with one orientation in which the *b* and *c* axes of PE are parallel to the *b* and *a* axes of BA (Figure 7.2.6a). Whereas when AN is used the degenerate epitaxy of PE block on the AN surface induces two different orientations of PE crystals inside cylinders. The *c*-axis of PE is oriented parallel to the  $[110]$  and  $[\bar{1}10]$  directions of AN (Figure 7.2.6b).

### 7.2.3 Conclusions

The section 7.2 has shown that the microstructure of semicrystalline block copolymers can be controlled by a combination of the directional solidification of a eutectic solution of the block copolymer in crystallizable organic solvents, and the following epitaxial crystallization of the crystalline block onto the organic crystalline substrate. Depending on the nature of the block copolymer and on the crystallizable solvent, various microstructures were achieved in thin films.

In the case of PS/PEP/PE terpolymer the directional solidification induces the parallel PS cylinders oriented along the *b* axis of BA. The subsequent epitaxial crystallization of the PE blocks onto BA crystals creates the long, thin crystalline PE lamellae between the PS cylinders, oriented edge-on on the substrate and with the *b* axis parallel to the *b* axis of BA and therefore parallel to the axes of the PS cylinders.



**Figure 7.2.6** Schematic models of the microstructures in thin films of the PS/PE block copolymer directionally solidified and epitaxially crystallized onto BA (a) or AN (b). (a) Vertically oriented PE cylinders are packed on a hexagonal lattice and contain one crystalline PE lamella oriented edge-on on the substrate with the  $b$  axis parallel to the  $b$  axis of BA crystal. (b) Vertically oriented PE cylinders are packed on a hexagonal lattice and contain one crystalline PE lamella oriented edge-on on the substrate with two different orientations in which the  $c$  axis of PE lamella is parallel to either  $[110]$  or  $[\bar{1}\bar{1}0]$  directions of AN crystals.

In the case of PS/PE block copolymer the use of either BA or AN generates the vertically oriented PE cylinders in the PS matrix. The following epitaxial crystallization was confined into the PE cylinders. Each cylinder contains precisely one crystalline PE lamella. Due to the different epitaxial relationship of PE crystals with BA and AN, the crystalline PE lamellae are oriented with the  $b$  axis parallel to the  $b$  axis of BA, while the two different orientations onto AN with the  $c$  axis of PE parallel to the  $[110]$  and  $[\bar{1}\bar{1}0]$  directions of AN crystals are obtained.

These results indicate that the method could be successfully used to form, in thin films of semicrystalline block copolymers, periodically ordered microdomain patterns, which can be used in various applications for nanostructure fabrication.

## 7.3 References

1. Volkmuth, W. D. & Austin, R. H. "DNA electrophoresis in microlithographic arrays." *Nature* **1992**, 358, 600.
2. Chou, S. Y.; Wei, M. S.; Krauss, P. R. & Fischer, P. B. "Single-domain magnetic pillar array of 35-nm diameter and 65-Gbits/in<sup>2</sup> density for ultra high density quantum magnetic storage." *J. Appl. Phys.* **1994**, 76, 6673.
3. Mansky, P.; Chaikin, P. M. & Thomas, E. L. "Monolayer films of diblock copolymer microdomains for nanolithographic applications." *J. Mater. Sci.* **1995**, 30, 1987.
4. Park, M.; Harrison, C.; Chaikin, P. M.; Register, R. A.; Adamson, D. H. "Block copolymer lithography: Periodic arrays of similar to 10(11) holes in 1 square centimeter" *Science* **1997**, 276, 1401.
5. Lammertink, R. G. H.; Hempenius, M. G.; Van den Enk, J. E.; Chan, V. Z-H.; Thomas, E. L.; Vancso, G. J. "Nanostructured thin films of organic-organometallic block copolymers: One-step lithography with poly(ferrocenylsilanes) by reactive ion etching" *Adv. Mater.* **2000**, 12, 98.
6. Morkved, T. L.; Lu, M.; Urbas, A. M.; Ehrichs, E. E.; Jaeger, H. M.; Mansky, P.; Russell, T. P. "Local control of microdomain orientation in diblock copolymer thin films with electric fields" *Science* **1996**, 273, 931.
7. Mansky, P.; DeRouchey, J.; Russell, T. P.; Mays, J.; Pitsilalis, M.; Morkved, T.; Jaeger, H. "Large area domain alignment in block copolymer thin films using electric fields" *Macromolecules* **1998**, 31, 4399.
8. Fasolka, M. J.; Harris, D. J.; Mayes, A. M.; Yoon, M.; Mochrie, S. G. J. "Observed substrate topography mediated lateral patterning of diblock copolymer films" *Phys. Rev. Lett.* **1997**, 79, 3018.
9. Huang, E.; Rockford, L.; Russell, T. P.; Hawker, C. J. "Nanodomain control in copolymer thin films" *Nature* **1998**, 395(6704), 757.
10. Muthukumar, M.; Ober, C. K.; Thomas, E. L. "Competing interactions and levels of ordering in self-organizing polymeric materials" *Science* **1997**, 277, 1225.
11. Hashimoto, T., Shibayama, M., Fujimura, M. & Kawai, H. *In Block Copolymers, Science and Technology*, D. J. Meier ed. (Harwood Academic Publ. London, p 63-108, (1983).
12. Hashimoto, T.; Bodycomb, J.; Funaki, Y.; Kimishima K. "Single grain lamellar microdomain from a diblock copolymer" *Macromolecules* **1999**, 32, 2075.
13. Flemings, M. C. *Solidification Processing* (McGraw Hill, NY, 1974).
14. Swei, G. S.; Lando, J. B.; Reichert, S. E. & Mauritz, K. A. *Encyclopedia of Polymer Science and Engineering* (Wiley, New York, 6, 209, 1986).
15. Wittmann, J. C. & Lotz, B. "Epitaxial crystallization of polymers on organic and polymeric substrates." *Prog. Polym. Sci.* **1990**, 15, 909.
16. Reiter, G.; Castelein, G.; Hoerner, P.; Riess, G.; Blumen, A.; Sommer, J. "Nanometer scale surface patterns with long range order created by crystallization of diblock copolymers" *Phys. Rev. Lett.* **1999**, 83, 3844.
17. Smith, P. & Pennings, A. J. "Eutectic crystallization of pseudo binary systems of polyethylene and high melting diluents." *Polymer* **1974**, 15, 413.

18. Wittmann, J. C.; Hodge, A. M. & Lotz, B. "Epitaxial crystallization of polymers onto benzoic-acid-polyethylene and paraffins, aliphatic polyesters, and polyamides." *J. Polym. Sci. Polym. Phys. Ed.* **1983**, 21, 2495.
19. Dorset, D. L.; Hanlon, J. & Karet, G. "Epitaxy and Structure of Paraffin-Diluent Eutectics" *Macromolecules* **1989**, 22, 2169.
20. Wu, S. *Polymer Interface and Adhesion*, **1982**, Marcel Dekker, NY.
21. Thomas, E. L. & Ast, D. "Image intensification and the electron microscopy of radiation sensitive polymers." *Polymer* **1974**, 15, 37.
22. Handlin, D. L.; Thomas, E. L. "Phase contrast imaging of styrene-isoprene and styrene-butadiene block copolymers" *Macromolecules* **1983**, 16, 1514.
23. Wittmann, J. C.; Lotz, B. "Epitaxial crystallization of monoclinic and orthorhombic polyethylene phase" *J. Polym. Sci. Polymer* **1989**, 30, 27.

## CHAPTER 8: New Micropattern Structure

### Alteration of Classical Microdomain Patterns by Degenerate Epitaxy

Degenerate epitaxial crystallization of a semicrystalline block terpolymer alters the normal microdomain structure. The strong interaction created by crystallographic matching of unit cells between the crystalline polyethylene block and the anthracene substrate forces the amorphous PS cylindrical microdomains into a new nanoscale pattern.

#### 8.1 Introduction

Pattern formation for nanostructure fabrication requires the achievement of periodic long range order. For instance periodically ordered microdomain patterns in block copolymer thin films are useful for lithographic templates.<sup>1,2</sup> By removing one polymer chemically or by etching, the patterns may be transferred to a substrate through further etching or by depositions (chemical vapor deposition, thermal evaporation etc.).<sup>1,2</sup> Another possibility is to use metal containing block copolymer microstructures as nanoreactor for decoration with nanoparticles.<sup>3,4</sup>

Block copolymers consist of chemically distinct macromolecules covalently linked to form a single chain. Owing to their mutual repulsion, dissimilar blocks tend to segregate into different domains, the spatial extent of the domains being limited by the constraint imposed by the chemical connectivity of the blocks and the molecular weight. Area minimization at the interface of two blocks takes place due to interfacial energy difference of two blocks. As a result self-organization of periodic microstructures occurs on the nanoscopic length scale. Advanced lithographic techniques can currently achieve feature sizes below 30 nm.<sup>5</sup> Various techniques for nanometer-scale surface patterning, based on the self-assembly in synthetic materials such as block copolymers, are being developed.<sup>6,7</sup>

Several approaches have been developed to manipulate the morphology and microdomain orientation in block copolymers.<sup>8-10</sup> If an applied bias field (mechanical, electric and magnetic etc.) is present during the self-assembly process, well oriented

microstructures can develop.<sup>8-10</sup> The microstructure can also be controlled by surface topography of a substrate.<sup>11</sup>

Crystallization in semicrystalline block copolymers has recently been shown as another way to control the orientations of the microdomains in thin films.<sup>12-14</sup> Reiter et al. demonstrated a vertically oriented lamellar structure by the combination of the crystallization and wetting-dewetting properties of the block copolymer on a native Si substrate.<sup>12</sup> Chapter 5 showed that well aligned, vertically oriented lamellae can be grown over large areas by epitaxy of semicrystalline block copolymer onto an organic crystal substrate. Chapter 7 also demonstrated a well ordered cylindrical microdomain structure oriented perpendicular to the substrate surface via directional solidification and epitaxy. However, most of previous works have been limited to improvement of orientation of the classical domain types (lamellar, cylindrical) in block copolymers. The broader engineering applications of the block copolymers demand more versatile 2 dimensional thin film regular patterns.

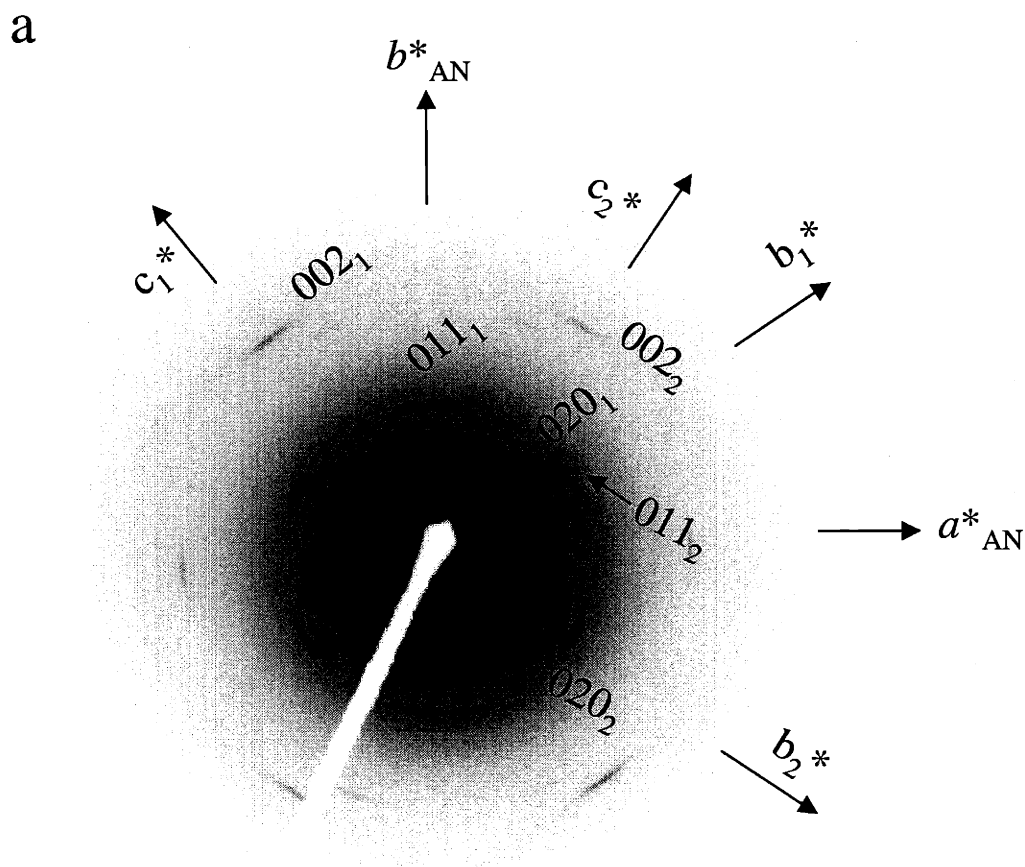
In this chapter the idea of using degenerate crystallization onto a crystalline substrate to induce a new microphase separated pattern is presented. The structure is initiated by the 2 equivalent epitaxial orientations with respect to the crystalline organic substrate: Anthracene (AN) of the crystallizable block of a semicrystalline block terpolymer, PS/PEP/PE (15/70/15). The double epitaxy is clearly evidenced by selected area diffraction (SAD). Phase and mass thickness bright field transmission electron microscopy (TEM) along with atomic force microscopy (AFM) is used to identify the lamellae and the cylindrical domains.

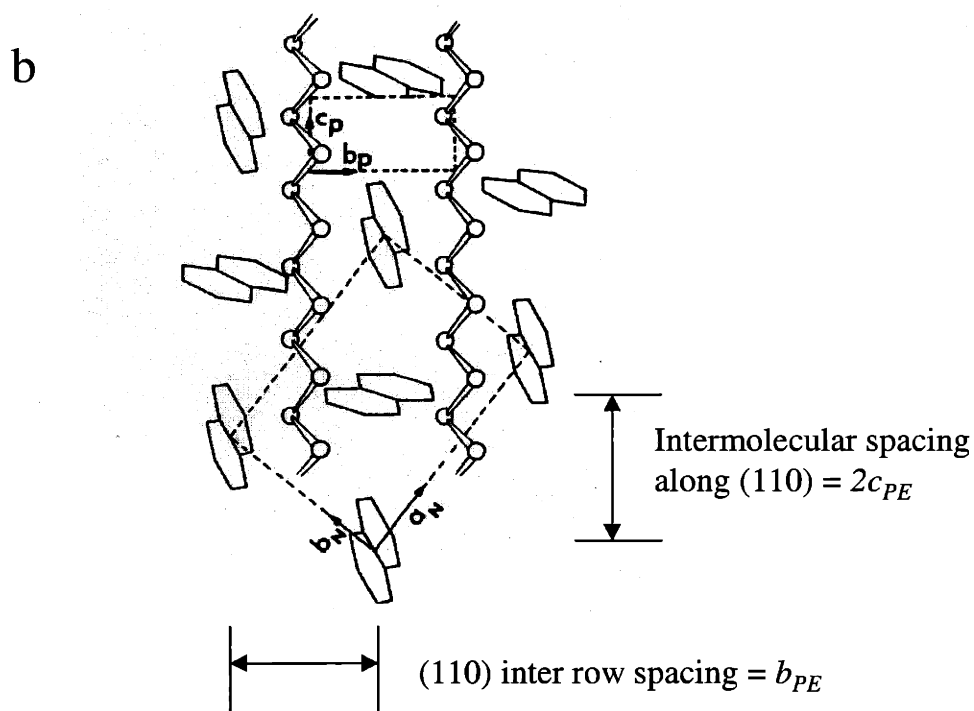
## 8.2. Results and Discussion

The SAD pattern (Figure 8.1a) exhibits PE  $0kl$  reflections of two different orientations similar to that found for PE homopolymer crystallized on AN.<sup>14</sup> The pattern indexes to the  $b^*c^*$  section of the PE reciprocal lattice symmetrically rotated by an angle of  $\pm 70^\circ$  with respect to the  $a^*$  axis of the AN. Since the area selected for diffraction is approximately  $6 \mu\text{m}$  in diameter, this indicates that a high global double-orientation of the PE chain molecules in the crystalline phase has been achieved. This result is relevant also considering the very low overall crystalline content of this material. This angle of



70° corresponds to the angle made by  $[110]$  and  $[\bar{1}\bar{1}0]$  directions in the  $a^*b^*$  plane of AN, i.e., in the contact plane with PE. The  $c$ -axis of PE is therefore oriented parallel to the  $[110]$  and  $[\bar{1}\bar{1}0]$  directions of AN. Since only the  $0kl$  reflections are present, the  $bc$  plane ((100) plane) of PE crystals is normal to the electron beam and therefore parallel to the exposed (001) face of AN crystals. The crystalline PE lamellae stand edge-on on the substrate surface. The epitaxial relationship is similar to that obtained for the polyethylene homopolymer.<sup>14</sup> Schematic diagram of the epitaxial relationship between PE and AN is shown in Figure 8.1b. The epitaxy was well explained in terms of matching between  $b_{PE}$  and the AN  $d_{110}$  inter-row spacing and a second matching of the  $2c_{PE}$  with  $(1/2)d_{110}$  of AN. This epitaxial relationship gives two equivalent orientations.





AN  
 $a = 8.235 \text{ \AA}$   
 $b = 6.038 \text{ \AA}$   
 $c = 11.184 \text{ \AA}$

PE  
 $a = 7.40 \text{ \AA}$   
 $b = 4.93 \text{ \AA}$   
 $c = 2.53 \text{ \AA}$

**Figure 8.1.** (a) Selected area electron diffraction pattern of a thin film of PS/PEP/PE block terpolymer epitaxially crystallized onto AN. The pattern presents the  $0kl$  reflections of PE, and hence indicates that the (100) plane of PE is normal to the electron beam and parallel to the (001) exposed face of the AN crystals. The  $c$  axis of the PE crystals is normal to the lamellar surface and parallel to the  $[110]$  and  $[\bar{1}\bar{1}0]$  directions of AN crystal due to the matching between  $b_{PE}$  and  $d_{110}$  inter-row spacing as well as due to the matching of the  $2c_{PE}$  with  $(1/2)d_{110}$  of AN. Therefore, two diffraction patterns rotated by an angle of  $70^\circ$  and oriented symmetrically relative to the  $a^*$  axis of the AN crystals is shown along the  $[110]$  and  $[\bar{1}\bar{1}0]$  directions of AN crystals. (b) Schematic of epitaxy between PE and AN.

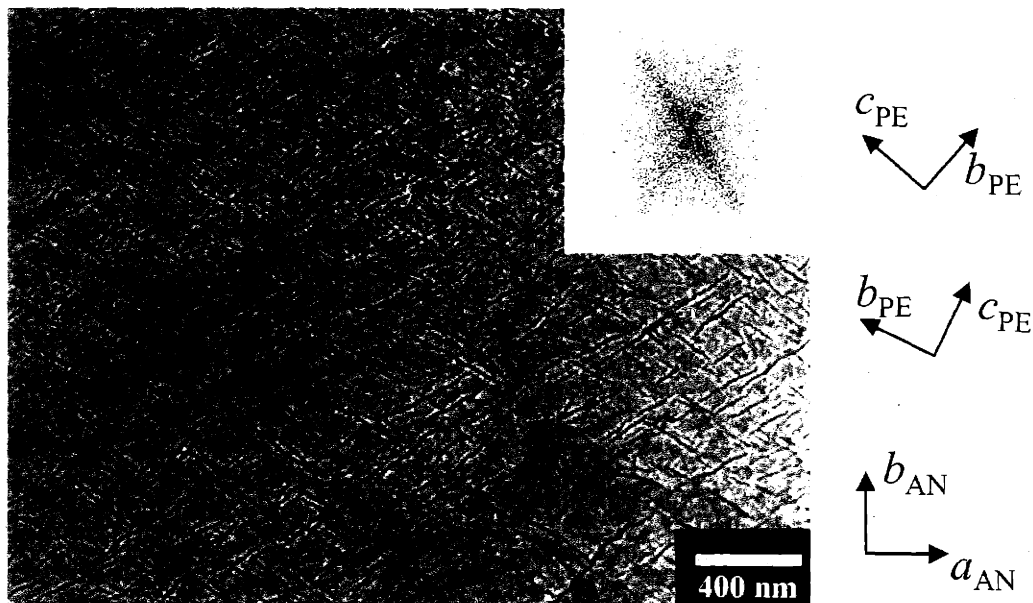
Defocused bright field (BF) phase contrast imaging of the unstained film permits direct visualization of the crystalline PE lamellae as shown in Figure 8.2a. In the under-focused BF image, the dark regions correspond to the crystalline PE phase. The phase

contrast is proportional to the mean inner potential difference between microdomains projected through the specimen. The mean inner potentials of the blocks in the terpolymer are 7.35, 7.08 and approximately 6.3 for the PE crystal, the PS and amorphous PE and PEP respectively.<sup>15</sup> Only those lamellae which are oriented edge-on to the electron beam direction provide good contrast. Regions containing PS and PEP blocks exhibit lower contrast of the PS microdomains. The nonuniform contrast visible in the matrix region results from the weak contribution to the phase contrast by the PS microdomains. The lamellae present a cross-oriented texture with an individual lamella having a thickness of 10-20 nm. Images show that the lamellae are predominantly oriented along two different directions whose acute angle is approximately 70° as expected from SAD. The FFT spectrum of Figure 8.2a in the inset confirms the double orientation of crystalline PE lamellae. Non-uniform distances between the long, thin PE lamellae in two orientations result in the streak-type pattern. The height contrast AFM image of the same sample shows that cross oriented crystalline PE lamellae protrude approximately 3-5 nm above the film surface (Figure 8.2b).

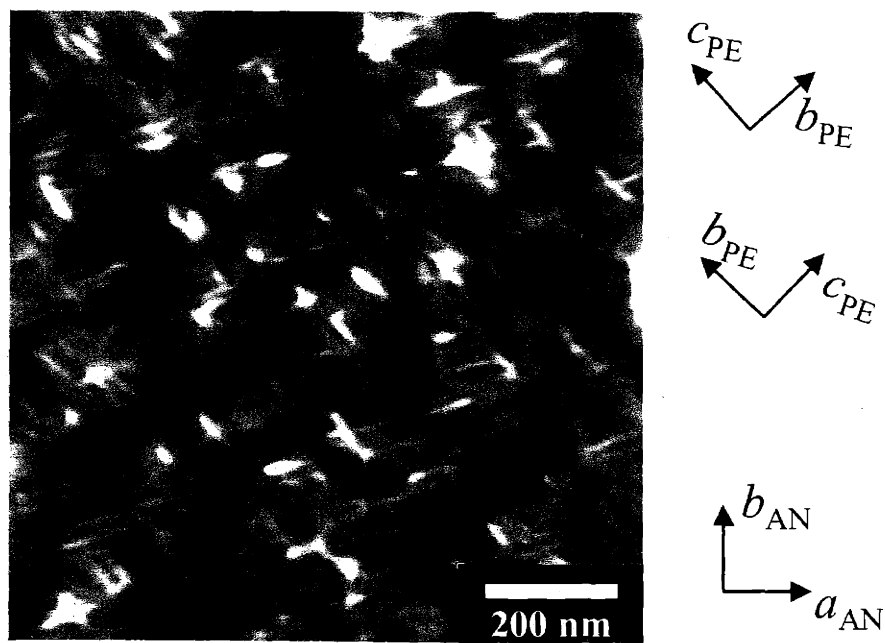
The orientation of PE chain axis (*c* axis) with respect to the crystalline PE lamellar normal was examined, comparing the Full Width Half Maximum (FWHM) value of the (002) reflection in Figure 8.1 with the FWHM of the oriented peak of FFT spectrum in the inset of Figure 8.2a. The measured FWHM value of the (002) reflection is approximately 9° which is consistent with the value from the inset of Figure 8.2a. It indicates that the chain axis of crystalline PE lamellae is parallel to the normal of the crystalline lamellae.

A BF image of a different region of the same sample after staining with RuO<sub>4</sub> is shown in Figure 8.2c. In this in-focus amplitude contrast micrograph, the darker regions correspond to the PS microdomains. It is apparent that the PS blocks are organized into a similar double oriented pattern. Some areas show loop-shape PS microdomains resulting from the confinement by the surrounding diamond-shape PE patterns (Figure 8.2a). The thickness of individual PS microdomain is about 20-25 nm consistent with the result in the bulk (Chapter 3). Some PS microdomains are thicker. This can be understood as due to the forced confinement of the PS microdomains by the PE lamellae which induces highly contorted structures in some regions.

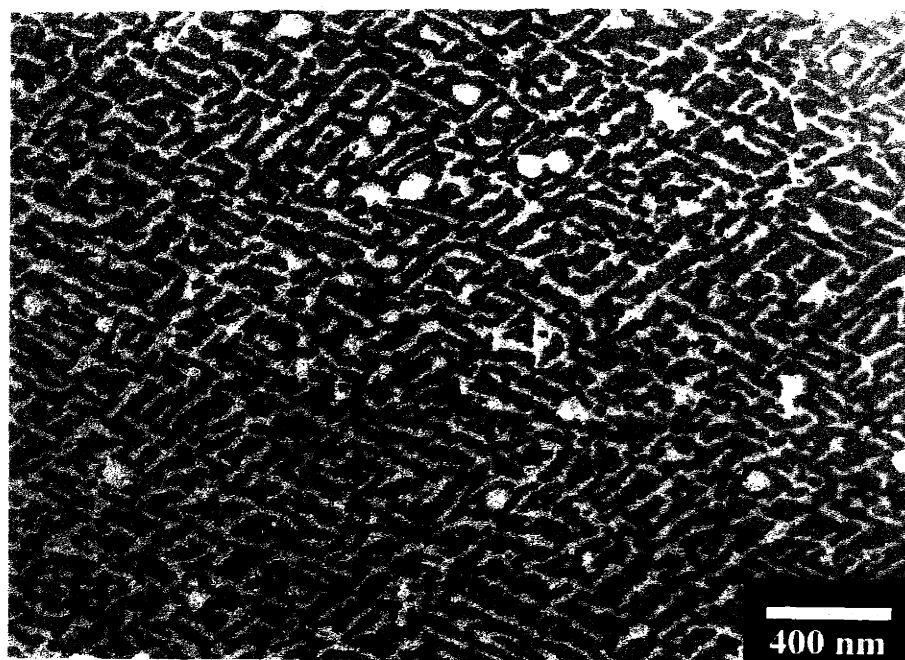
a



b



C



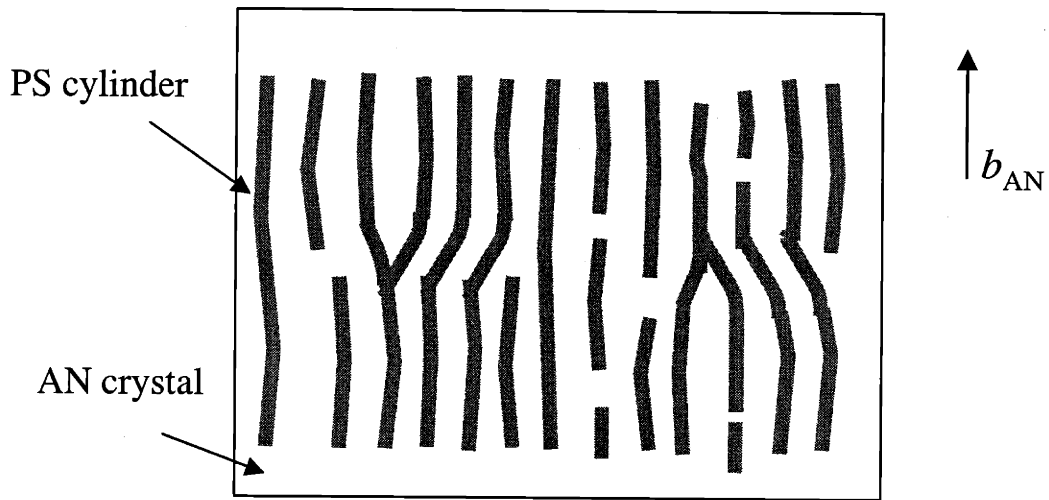
**Figure 7.2** TEM bright-field and AFM images of a thin film of PS/PEP/PE epitaxially crystallized on AN corresponding to an area similar to that of figure 1. a) TEM bright-field image of the unstained sample. The phase contrast is enhanced by underfocus of the objective lens. The dark regions correspond to the crystalline PE phase, which forms cross oriented PE lamellae standing edge-on. Inset shows FFT spectrum of the TEM image, confirming the two orientations of crystalline PE lamellae. b) Tapping mode AFM image of the unstained sample. The contrast results from the height difference. The cross oriented PE lamellae are shown to protrude on the surface. c) TEM bright-field image of the sample stained with RuO<sub>4</sub>. Image contrast is mass thickness amplitude contrast. The dark regions correspond to the PS phase, which forms a similar double oriented structure to that of the PE microdomains.

In the current process, the formation of the oriented semicrystalline block copolymer morphology and the oriented chain structure on the crystalline organic solvents can be understood in terms of a combination of the directional solidification of the eutectic solution and the subsequent epitaxial crystallization of PE block (Chapter 7). In the present case, the directional solidification induces oriented microphase separation of the PS cylinders from the PEP-PE matrix with the cylinder axis oriented along the fast growth direction of AN ( $b$  axis). The extremely rapid crystallization of the PE block in the thin film does not allow to freeze-in the straight PS cylindrical microdomain structure existing prior to the PE crystallization. Instead, the orientation of PS microdomain before epitaxy was indirectly obtained by employing a poly(styrene- $b$ -isoprene) (PS/PI) block copolymer with PE cylindrical microdomains (Chapter 6). The directional solidification of an amorphous PS/PI block copolymer on AN substrate shows that the cylindrical PI microdomains are aligned along the  $b$  axis of AN crystal (Figure 6.3). After further cooling, the crystallization of PE block occurs in the PEP-PE matrix (87 vol%), and long crystalline PE lamellae form with their long dimensions ( $b$  axis) along the  $[110]$  and  $[\bar{1}\bar{1}0]$  directions of the AN substrate. The crystallization of the PE presumably occurs near or slightly above the glass transition temperature ( $T_g$ ) of the PS block. The  $T_g$  of the PS block (nearly 80 °C without AN, as evaluated from DSC curves registered at cooling rate of 2 °C/min) is more depressed by plasticization from the AN (evidenced by DSC). In addition, the heterogeneous nucleation of the PE onto the AN crystals increases the crystallization temperature of the PE block.<sup>16</sup>

The strong crystallization forces guided by epitaxy of PE and AN are able to bend and/or buckle the pre-existing PS microstructure driven by the directional solidification into a new micropattern structure. In addition, since the PS microdomains obtained before the crystallization of the PE consist of short cylindrical sections with many defects (Chapter 3), the PS microdomains are more easily rearranged from the strong epitaxial crystallization forces.

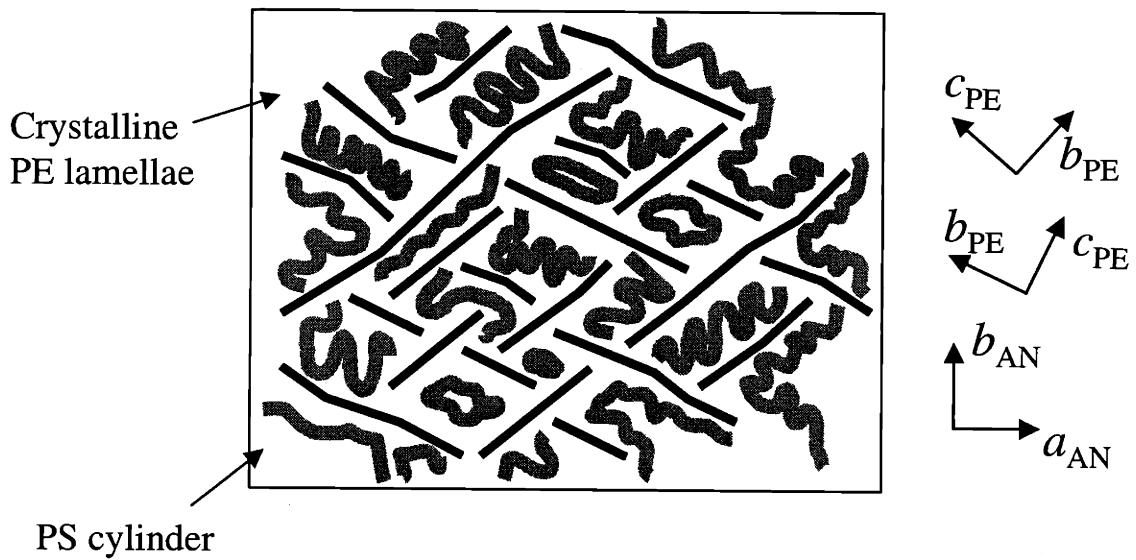
a

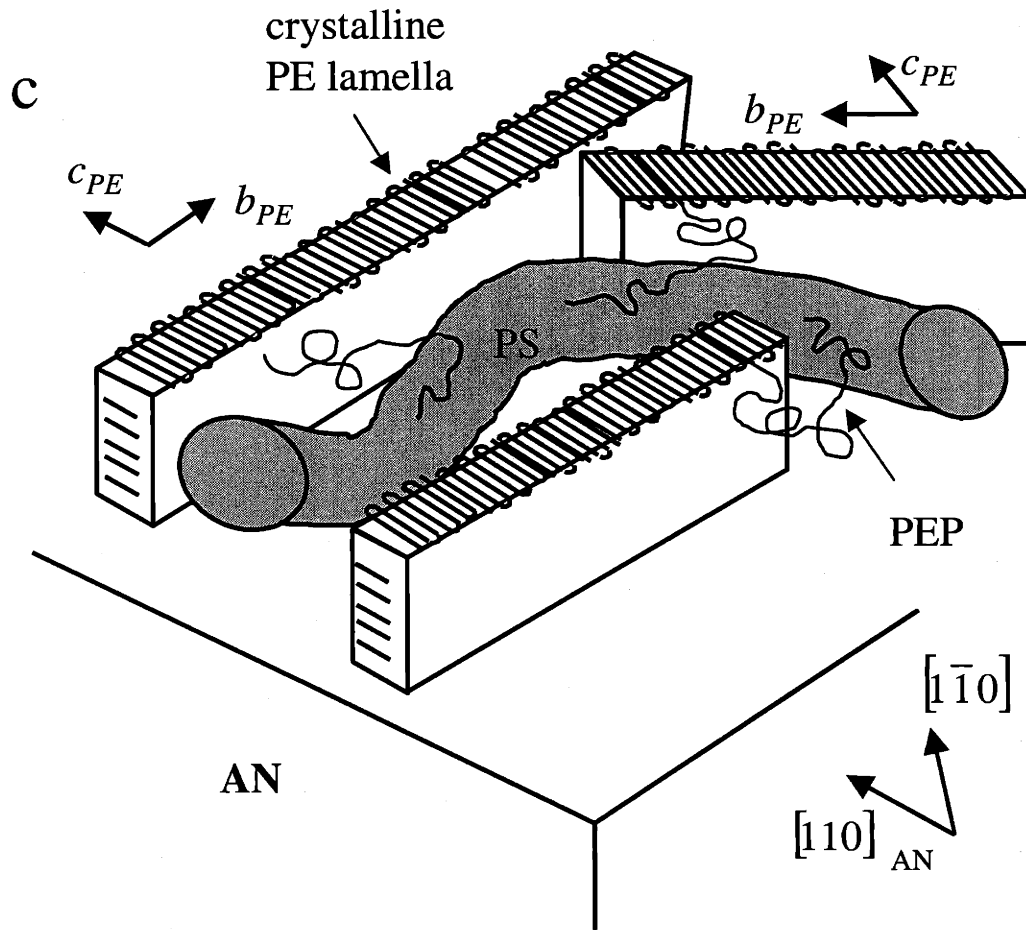
**Microphase Separation: Directional Solidification**



b

**Microstructure Reorganization of PS due to (110) Epitaxial Crystallization**





**Figure 8.3** Schematic model showing the relationship between the orientation of the crystalline phase and the alignment of the microdomains in a semicrystalline block copolymer. (a) The cylindrical PS microdomains are initially aligned along the fast growth direction of AN crystals ( $b$  axis) via the directional solidification prior to the crystallization of the PE. (b) The orientation of the molecular chains in the crystalline phase is induced by the epitaxial crystallization on the surface of AN crystal. The 2 dimensional orientation of the crystalline PE lamellae standing edge-on on the substrate surface, and oriented parallel to the  $[110]$  and  $[\bar{1}\bar{1}0]$  directions of AN crystal is obtained. The epitaxy of the PE on the AN crystal reorganizes the pre-oriented PS microdomains. (c) Schematic model showing the crystalline and amorphous microdomains in the PS/PEP/PE block terpolymer epitaxially crystallized onto AN. Epitaxial relationship shows the relative orientation of the polyethylene lamellae on AN.  $(100)_{PE} // (001)_{AN}$ , and  $c_{PE} // [110]_{AN}$ . The PS microdomain is shown in between the edge-on PE crystalline lamellae aligned into two different directions.



The schematic of the pattern formation is shown in Figure 8.3. The directional solidification of the mixture of the terpolymer and AN develops the orientation of the cylindrical PS microdomains along the fast growth direction of the AN crystals (*b* direction) before the crystallization of the PE (Figure 8.3a). The epitaxial crystallization induces a high orientation of the molecular chains of the crystalline phase, resulting in PE lamellae standing edge-on on the substrate surface, oriented into the two directions due to the crystallographic degeneracy (Figure 8.3b). This structure in turn induces reorganization and alignment of the pre-existing PS microdomains, and the similar structure of PS microdomains is formed by guidance of the patterned crystalline phase developed during the epitaxy (Figure 8.3b). The schematic model of molecular chain orientation of the terpolymer on AN substrate is shown in Figure 8.3c. The primary epitaxial relationship of matching between  $b_{PE}$  and the AN  $d_{110}$  inter-row spacing creates edge-on crystalline PE lamellae, leading to the re-organization of PS microdomains.

This thin film process suggests the possibility to design new 2D patterns via self assembled semicrystalline block copolymers using a combination of one or more crystallizable blocks and various crystalline organic substrates. Versatility of regular patterns of semicrystalline polymers on the organic crystalline substrates<sup>17</sup> guarantees the creation of various different patterns of the block copolymers when crystalline block is introduced in the block copolymer.

### 8.3 References

1. Park, M.; Harrison, C.; Chaikin, P. M.; Register, R. A.; Adamson, D. H. "Block copolymer lithography: Periodic arrays of similar to 10(11) holes in 1 square centimeter" *Science* **1997**, 276, 1401.
2. Lammertink, R. G. H.; Hempenius, M. G.; Van den Enk, J. E.; Chan, V. Z-H.; Thomas, E. L.; Vancso, G. J. "Nanostructured thin films of organic-organometallic block copolymers: One-step lithography with poly(ferrocenylsilanes) by reactive ion etching" *Adv. Mater.* **2000**, 12, 98.
3. Morkved, T. L.; Wiltzius, P.; Jaeger, H. M.; Grier, D. G.; Witten, T. A. "Mesoscopic self-assembly of gold islands on diblock copolymer films" *Applied. Phys. Lett.* **1994**, 64, 422.
4. Boontongkong, Y.; Cohen, R. E.; Rubner, M. F. "Selective electroless copper deposition within block copolymer microdomains" *Chem. Mater.* **2000**, 12, 1628.
5. Weiss, D.; Roukes, M. L.; Mensching, A.; Grambow, P.; von Klitzing, K.; Weiman, G. "Electron pinball and commensurate orbits in a periodic array of scatterers" *Phys. Rev. Lett.* **1991**, 66, 2790.
6. Muthukumar, M.; Ober, C. K.; Thomas, E. L. "Competing interactions and levels of ordering in self-organizing polymeric materials" *Science* **1997**, 277, 1225.
7. Bates, F.S.; Fredrickson, G.H.: "Block copolymer thermodynamics: theory and experiment." *Ann. Rev. Phys. Chem.* **1990**, 41, 525.
8. Vigild, M. E.; Almdal, K.; Mortensen, K.; Hamley, I. W.; Fairclough, J. P. A.; Ryan, A. J. "Transformations to and from the Gyroid Phase in a Diblock Copolymer" *Macromolecules* **1998**; 31: 5702.
9. Albalak, R. J.; Thomas, E. L. "Microphase separation of block copolymer solutions in a flow field" *J Polym Sci Part B Polym Phys* **1993**; 32: 37.
10. Morkved, T. L.; Lu, M.; Urbas, A. M.; Ehrichs, E. E.; Jaeger, H. M.; Mansky, P.; Russell, T. P. "Local control of microdomain orientation in diblock copolymer thin films with electric fields" *Science* **1996**, 273, 931.
11. Fasolka, M. J.; Harris, D. J.; Mayes, A. M.; Yoon, M.; Mochrie, S. G. J. "Observed substrate topography mediated lateral patterning of diblock copolymer films" *Phys. Rev. Lett.* **1997**, 79, 3018.
12. Reiter, G.; Castelein, G.; Hoerner, P.; Riess, G.; Blumen, A.; Sommer, J. "Nanometer scale surface patterns with long range order created by crystallization of diblock copolymers" *Phys. Rev. Lett.* **1999**, 83, 3844.
13. Wittmann, J. C.; Hodge, A. M.; Lotz, B. "Epitaxial crystallization of polymers onto benzoic acid – polyethylene and paraffins aliphatic polyesters and polyamides" *J. Polym. Sci. Polym. Phys. Ed.*, **1983**, 21, 2495.
14. Wittmann, J. C.; Lotz, B. "Epitaxial crystallization of monoclinic and orthorhombic polyethylene phase" *J. Polym. Sci. Polymer* **1989**, 30, 27.
15. Handlin, D. L.; Thomas, E. L. "Phase contrast imaging of styrene-isoprene and styrene-butadiene block copolymers" *Macromolecules* **1983**, 16, 1514.
16. J. Brandrup and E. H. Immergut, *Polymer Handbook*, IV/411 **1989**.
17. Wittmann, J. C. & Lotz, B. "Epitaxial crystallization of polymers on organic and polymeric substrates." *Prog. Polym. Sci.* **1990**, 15, 909.

## CHAPTER 9: Conclusions and Future Work

External fields which can interact with microstructure of materials can direct unorganized microdomain structures into a technologically desirable one. Manipulation of block copolymer microdomain structures by employing external fields thus promises realization of potential nanotechnological applications. In this chapter, the major two Parts of the thesis are summarized and various ideas concerning future studies are outlined for each Part. In particular two types of preliminary results extending the work presented in Part II are discussed.

### 9.1 Summary: PART I

In Part I of the thesis, a mechanically driven flow field generated by the 'roll casting' process was employed to the microstructure of a semicrystalline block terpolymer. In spite of the low volume fraction of PS block (13 %), results presented in Chapter 3 show that the flow field developed a cylindrical microdomain structure aligned along the flow direction. A metastable spherical microdomain structure, obtained in a simple cast film, was transformed to an equilibrium cylindrical structure under the flow field. Conformational asymmetry between PS and PEP/PE block was suggested to explain the observation. Large differences in Kuhn lengths with similar densities of PS and PE or PEP blocks resulted in an asymmetric phase behavior. The roll casting not only facilitated to achieve an equilibrium microstructure but also created an ordered structure.

The influence of the aligned PS cylindrical microdomain structure on the resultant crystallization of the PE block was also investigated in Chapter 4. The crystallization of the PE block when the sample was cooled below the crystallization temperature of PE block occurred in the matrix from the mixture of PEP and PE blocks. The crystallization of PE was significantly affected by the presence of ordered cylindrical PS microdomains. The pre-aligned PS microdomains along the flow direction of roll casting forced the primary growth direction of crystalline PE lamellae (*b* axis) to follow the PS cylinder axis. Preferred chain orientation of the PE block resulted in the ordering of the crystalline PE lamellae parallel to the PS cylinder axis, completely inhibiting the spherulites usually observed in semicrystalline block copolymers as well as semicrystalline polymers.

## 9.2 Future Work: PART I

Semicrystalline block copolymers provide great opportunity not only to improve existing material properties but also to develop new mechanical, optical properties. For example, uni-axially ordered microdomain structure without spherulite formation (presented in Chapter 4) leads to transparent block copolymer films with good anisotropic mechanical properties.

Although the control of microphase separated structure and crystalline microstructure was successfully achieved in Part I, this work can trigger many successive future works. First of all, different architectures of semicrystalline block copolymers might be interesting. In the present work, a noncrystalline rubbery PEP blocks separated the glassy PS and crystallizable PE end blocks of the terpolymer. In particular the case in which a crystalline PE block is directly connected to a glassy PS block deserves examination. Not only of interest is the effect of sequence on microstructure formation, but also a block copolymer provides a similar situation to transcrystallization of a PE polymer matrix with cylindrical fillers such as glass fibers. However in the case of the block copolymer the geometry is on the nanometer scale because the crystallization takes place directly next to cylindrical PS microdomain surfaces. A well-known phenomenon in the composites of semicrystalline polymers and fillers, transcrystallization could be systematically investigated. In addition, a scaling study of the transcrystallization would be possible with different length scales from millimeter, to micron to nanometer scales.

Another interesting work might be to study the effect of curvature of the IMDS on crystallization in semicrystalline block copolymers. The systematic change of molecular weights of block copolymers with constant relative volume fraction allows one to tune the size of cylindrical microdomains. In other words one of the principal curvatures of cylindrical microdomain could be controlled. Crystalline lamellae growth on these glassy cylinder surfaces could be influenced by the different surface curvatures. This work is relevant to the recent field of thermotropic nano-composites where fine size dispersed fillers with various shapes are incorporated in semicrystalline polymers.

Microstructure modification and control of semicrystalline block copolymers should as relate to their material properties. In particular, anisotropic mechanical properties of

both oriented glassy and crystalline microdomains are interesting. Using the roll cast PS/PEP/PE films examined in Part I, an *in-situ* deformation study is under way employing an uni-axial tensile stretcher mounted directly on a synchrotron X-ray scattering beamline. Simultaneous wide and small angle X-ray scattering will be used to monitor both molecular chain orientation of the crystalline phase and structural changes of microdomains. Stress-strain curves obtained simultaneously with in-situ scattering data enable us to relate the modified microstructures to their mechanical properties. In addition, high voltage cross linking technique allows us to fix microstructures after certain deformation. TEM experiments with these deformed and then “fixed” samples should reveal valuable real space microstructural information on the type and nature of deformation structures occurring as a function of strain and loading direction with respect to the textured microdomain sample.

Another possible idea with semicrystalline block copolymers would be to fabricate nanometer scale near-single-crystal wires of semicrystalline polymers by using a block copolymer template. In this case, a cylinder forming semicrystalline block copolymer is used in which cylinders are semicrystalline in a rubbery matrix. As shown in Part I, cylindrical microdomains can be aligned along the flow direction via the roll casting method. At this stage, crystallization of the crystalline blocks is confined into cylindrical microdomains, but it is far from a single crystal as the chain folded lamellae produce an orientation of the chain axis, essentially normal to the cylinder axis. Near single crystal cylindrical wires with the chain axis parallel to the cylinder axis could be made using slow uni-axial stretching of the film along the cylinder axis at just below the melting temperature of crystalline block. Very slow deformation near melting temperature could convert the folded chain crystal structure into an extended chain crystal structure with much higher crystallinity and modulus. Etching out matrix e.g. UV degradation of the PI block after completion of near single crystal cylinder might create separate individual wires with nano-meter length scales (“ultra fibers”). Alternatively the nano-composite could show extreme anisotropy due to high PE axial modulus (possibly 300 GPa) vs the low transverse modulus (approximately 1 GPa) dominated by the rubber.

### 9.3 Summary: PART II

In Part II of the thesis, new types of interactions are used to couple and control the microdomain structure of block copolymers. The two driving forces are epitaxy and directional solidification and are especially effective for thin block copolymer films. Depending on the block copolymers applied, one or both of interactions can be used. The basic idea in directional solidification is to utilize crystallizable organic solvents such as benzoic acid and anthracene. Block copolymers are dissolved in these solvents above their melting temperatures and when the solvent is crystallized in a temperature gradient the microdomains form with their IDMS aligned parallel to the growth front of single crystal of the solvent. The basic idea in epitaxy is to utilize a substrate with known preferred lattice matching to the crystallizable block to control the direction of growth of the chain-folded lamellae with form. Depending on the nature of the blocks in the polymer, crystallization may occur from a single phased homogeneous melt (low  $N\chi$ ) or a heterogeneous microphased separated melt (high  $N\chi$ ). We also developed a processing method in which *both* directional solidification and epitaxy serve to control the crystal orientation and microdomain orientation.

Chapter 5 examined the case of a melt compatible semicrystalline block copolymer which was epitaxially crystallized on the single crystal surface of benzoic acid. Since microphase separation was driven only by the crystallization of PE block, the directional crystallization of benzoic acid was coupled with the crystallization of the PE blocks. The strong epitaxial coupling between the BA (001) and PE (100) crystals determined the orientation of the microstructure as well as molecular chains with  $b_{PE} // b_{BA}$  and  $c_{PE} // a_{BA}$ .

When amorphous-amorphous block copolymers were employed (chapter 6), the directional crystallization of the crystallizable organic solvent was only coupled with the microphase separation transition of the block copolymer. Samples of PS/PMMA and PS/PI developed the lamellar and cylindrical microdomains ordered along the growth front direction respectively. In addition, the PS/PI block copolymer showed thickness dependent cylinder orientations. In thick film (approximately 50 nm thick), *in-plane* PI cylinders are aligned along the growth front. In thin film (approximately 20 nm thick) *vertically* ordered PI cylinders are oriented along the growth front.

Strongly segregated semicrystalline block copolymers in which the microphase separation temperatures of the block copolymers are much higher than the melting temperatures of the crystalline blocks were also investigated in Chapter 7. Starting from a homogeneous solution of the block copolymer and the crystallizable organic solvent, the directional crystallization of the solvents was first initiated which also caused microphase separation of the block copolymer. Subsequent epitaxy of the crystalline block onto the single crystal surface of the crystallizable solvent occurred in the presence of the microphase separated structure. We observed the epitaxial crystallization of the PE block in a PS/PE block copolymer onto BA. BA surface was delicately balanced to create the cylindrical microstructure vertically aligned to the BA surfaces in which each cylinder has one single lamellar PE crystal. When the AN was used as the crystallizable organic solvent, vertically ordered PE cylindrical microdomain structures form on the single crystal of AN. However, in this case, the crystalline PE lamellae inside the cylindrical microdomains have two degenerate orientations due to the known epitaxial relationship between PE and AN ( $c_{PE} // [110]_{AN}$ ). In another case where the epitaxial crystallization of PE block occurred in between the aligned cylindrical PS microdomains (PS/PEP/PE sample), the BA crystal allowed crystalline PE lamellae to orient and to alternately confine themselves in between the cylindrical PS microstructure formed previously via directional solidification.

We also explored the situation where the epitaxy with the substrate was degenerate. That is, where there are two equivalent orientations of the crystallizable block with respect to the substrate as explained above. The PS/PEP/PE terpolymer was chosen to probe how the subsequent PE crystallization could influence the PS cylinders since the 2 lamellar orientations were aligned at  $\pm 70^\circ$  to the  $b_{AN}$  axis. The subsequent strong crystallization forces of the growing PE lamellae caused a re-organization of uni-axially aligned cylindrical PS microdomain structure, obtained during directional solidification, into a double oriented microstructure. The confined PS cylinders in between crystalline PE lamellae were highly bent and/or buckled (Chapter 8).

## 9.4 Future Work: PART II

The utilization of crystallizable organic solvents has been found to be a very effective way to control the orientation of a variety of semicrystalline and noncrystalline block copolymer microdomain structures and even to force alteration of a classical microdomain structure into a new pattern. For better control of microdomains and further engineering applications, many future studies should be addressed.

First of all, many experimental parameters of the directional solidification and epitaxy technique introduced in Part II should be more carefully controlled. By using different supercoolings of the block copolymer/crystallizable organic solvent solution one can vary crystallization rates of the organic solvents which should influence the microstructures of block copolymers. Control of centimeter scale single crystals of organic solvents is also possible, for example, using extremely slow crystallization ('zone refining method'). These large substrates could then be used to fabricate a macroscopic device on which microdomains of a semicrystalline block copolymer are epitaxially ordered.

Control of environmental variables such as moisture, temperature and solvent purity is also important. Easy sublimation of most of crystallizable organic solvents makes it difficult to maintain constant thickness of the substrate crystal. In addition, impurities introduced during process can affect the quality of single crystals of organic solvents. Heterogeneous nucleation induced by impurities such as dust could restrict large area fabrication of highly ordered block copolymer thin films. Filters could be used to remove impurities in the block copolymer solution. A closed control box in which temperature and environmental variables are delicately controlled could prove useful.

Another important experimental parameter to be controlled is the gap between two glass substrates which resulted in different block copolymer film thicknesses. Pressure can be applied on the top substrate to keep the gap constant.

The means by which nucleation is initiated can be modified for control of very large areas. The tweezer method we employed created a single initiation point where crystallization started and then diverged out within an approximately 90 ° spread angle. This method created an ordered microdomain structure on the scale of the grain width. However, when one is interested in larger scale fabrication, the initiation method should



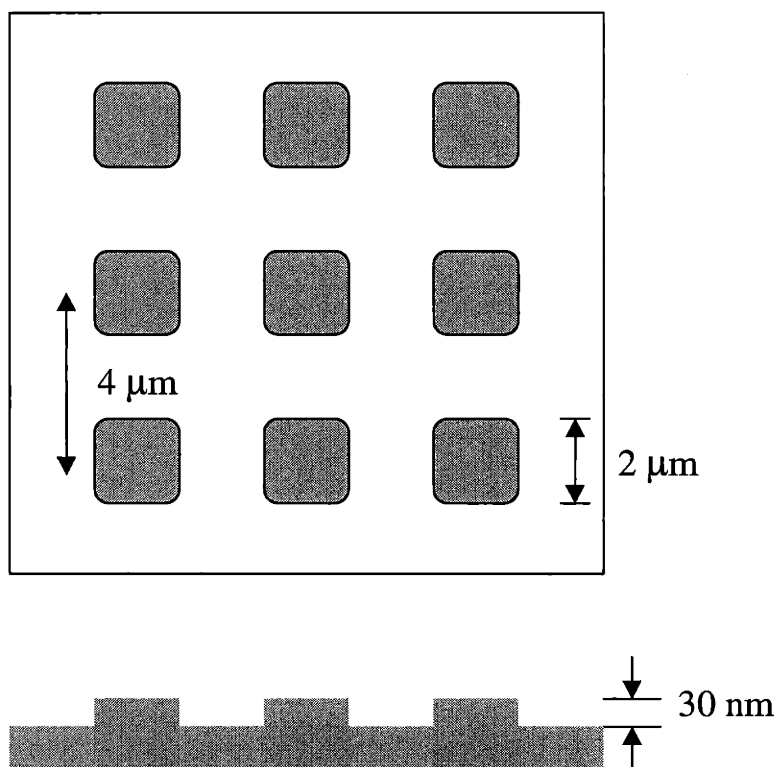
be changed. For example, line nucleation parallel to the growth direction of the single crystal instead of point nucleation can be useful for macroscopic fabrication. More specifically this can be accomplished using a needle shaped seed crystal of the organic. When previously prepared needle seed crystal lies on the edge of the supercooled solution, the solution undergoes multiple nucleation and directionally crystallizes from the surface of needle crystal, resulting in macroscopically parallel structure.

Topographically patterning of a substrate by conventional lithographic techniques can be combined with the main process described in Part II for better control of microdomain structures of block copolymers. The essential underlying idea is that the topographic pattern achieved with conventional lithographic techniques can assist the nanometer scale self assembly of block copolymers up to micron scale which is the typical scale of block copolymer grains. In addition, pattern regions of different height can induce a thickness dependent microdomain orientation. Furthermore, the ordered microdomain structures shown in Part II (in particular chapter 6) can be modified for engineering applications such as template for nanolithography and micropattern for magnetic media storage and so on (See the chapter 1.1). Control of microdomain structure of block copolymer using topographically patterned substrate and microstructure modification using either ozone or oxygen reactive ion etching method will be discussed in the next section.

#### **9.4.1 Orientation of block copolymer microdomains on topographically patterned substrate via directional solidification: Preliminary results<sup>1</sup>**

Directional solidification of the mixture of a polystyrene-*b*-isoprene (PS/PI) block copolymer and benzoic acid (BA) was done on a pre-patterned silicon substrate. The patterned substrate was produced via standard lithographic techniques by the MIT Microsystems Technology Laboratories. The substrate pattern consists of 30 nm high, 2 micron x 2 micron square mesas arranged in a square array with a 4 micron center to center spacing as shown schematically in Figure 9.1. The substrate has a silicon oxide surface. The square shape mesas are silicon oxide thermally grown for the lithographic process. Areas between the mesas have a native oxide layer. Prior to deposition of the

block copolymer/crystallizable organic solvent solution, the substrate was cleaned via one hour sonication in toluene followed by 2 hour immersion in chromic/sulfuric acid to



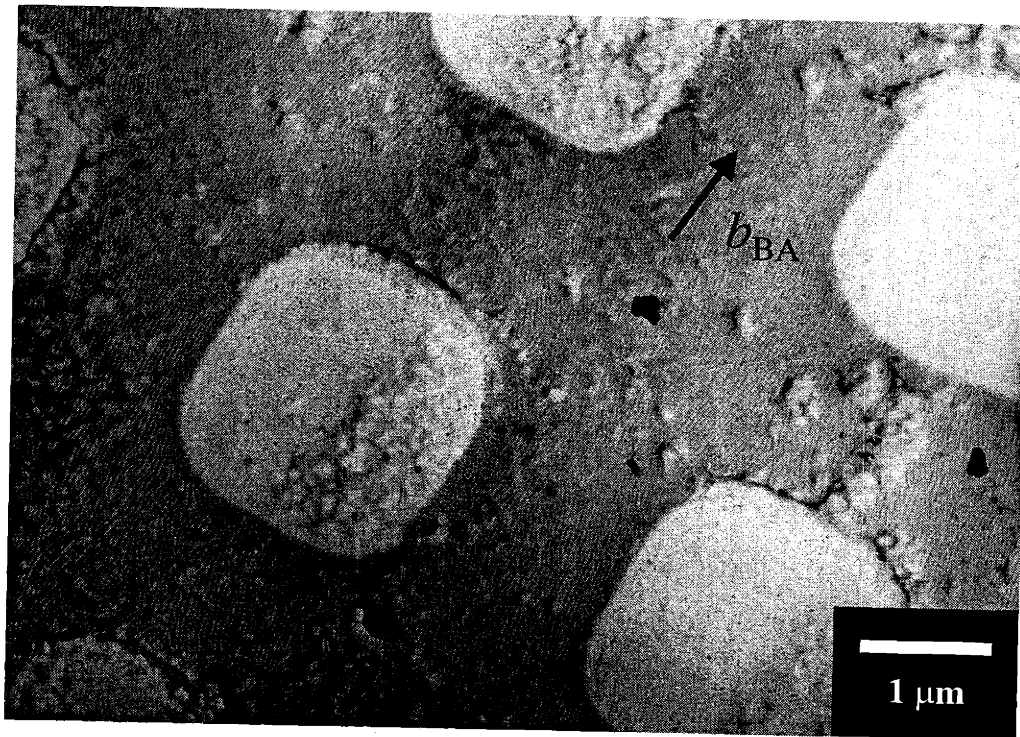
**Figure 9.1** Schematic of topographically pre-patterned silicon substrate

hydrolyze and remove any organic material adsorbed to the surface. Directional solidification was performed with the procedure described in Chapter 6.

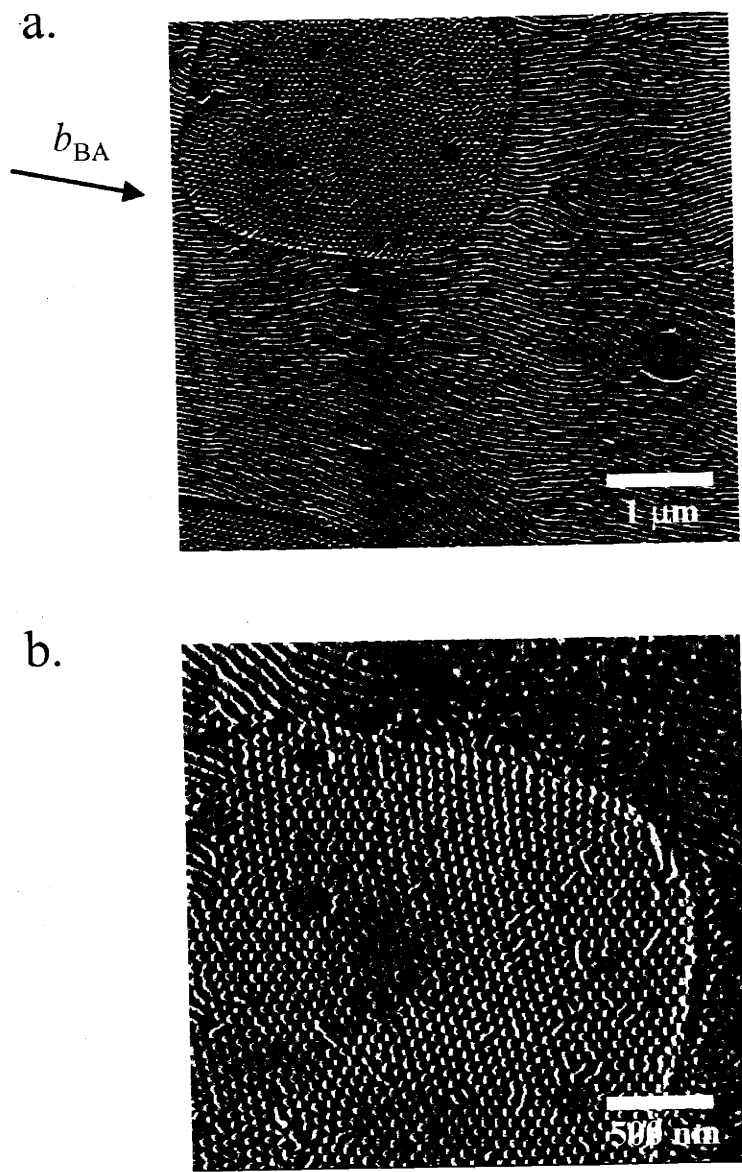
A bright field TEM micrograph of the PS/PI block copolymer, directionally solidified on the pre-patterned substrate, is shown in Figure 9.2a. Staining with OsO<sub>4</sub> provides good contrast, rendering the PI microdomains dark. Long range ordering of block copolymer structure is observed across the micron scale pre-patterned substrate. The directional solidification of the BA and the PS/PI mixture develops an in-plane orientation of cylindrical PI microdomains along the fast growth direction of BA crystal

(*b* axis) (see Chapter 6) within thicker regions while a vertical orientation of the cylindrical microdomains occurs in the thinner mesa regions.

Tapping mode AFM imaging at higher magnification (Figure 9.3a) also clearly shows the two different orientations of the PI microdomains. The cylindrical microdomains vertically oriented on the substrate are hexagonally packed in the thinner mesa regions. Figure 9.3b shows boundary between the two different orientation. The microdomains transform from vertical to parallel as they go from the mesa to matrix regions.

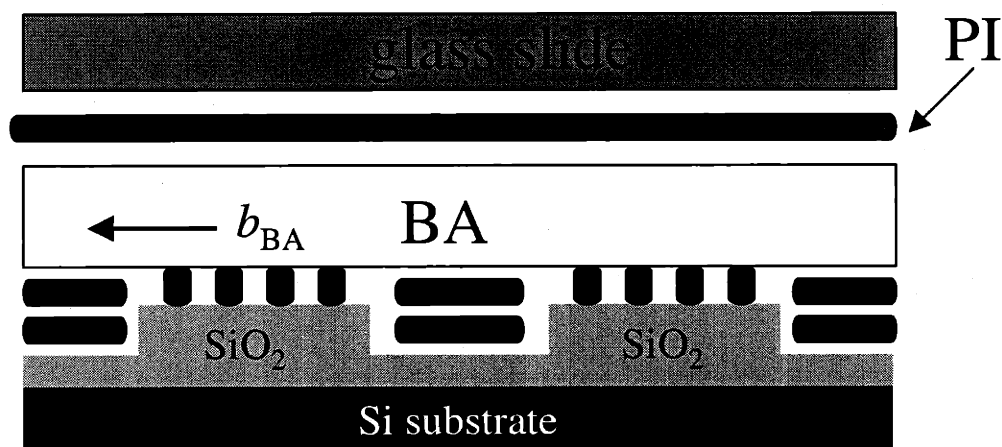


**Figure 9.2** TEM bright-field image of a thin film of PS/PI(45/12) block copolymer, directionally solidified with BA on the pre-patterned substrate, and stained with OsO<sub>4</sub>. The dark regions correspond to the stained PI microdomains. The cylindrical PI microdomains perpendicular and parallel to the substrate are shown in the square mesa (light) and matrix dark regions respectively.



**Figure 9.3** (a) Tapping mode AFM image of a thin film of PS/PI(45/12) block copolymer, directionally solidified with BA on the pre-patterned substrate. The amplitude contrast image is shown. The cylindrical PI microdomains with two different orientations with respect to the substrate are well aligned along the fast growth direction of the BA crystals. The square shape mesa regions show the PI cylinders perpendicular to the substrate. The thicker matrix regions show the in-plane PI cylinders. (b) Higher magnification AFM image of (a). Hexagonally packed PI cylinders vertically aligned to the substrate are observed. In addition, smooth transition is clearly seen from perpendicular to parallel orientation of PI cylinders.

The two different orientations observed on the substrate result from the thickness variation of block copolymer films. Both theoretical and experimental results support the notion that the equilibrium orientation of the block copolymer microdomains depends on film thickness.<sup>2-7</sup> Cylinder forming block copolymers show a transition from parallel to vertical when the film thickness is less than the diameter of cylinder.<sup>2-5</sup> In this case, the microphase separated block copolymer films form on BA single crystals between the top glass substrate and bottom pre-patterned substrate when they are directionally solidified as explained in Chapter 6. Block copolymer films contacting with the pre-patterned substrate undergo thickness variation as shown in the schematic of Figure 9.4. The film thickness of block copolymer in the mesa region (approximately 15 - 20 nm) is obtained from the mechanically torn film region with AFM. Since the diameter of PI cylinders is approximately 20 nm (Chapter 6), PI cylinders vertically aligned to the substrate are observed. Block copolymer films with the thickness of approximate 45 – 50 nm lead to the in-plane PI cylinders in the matrix region.

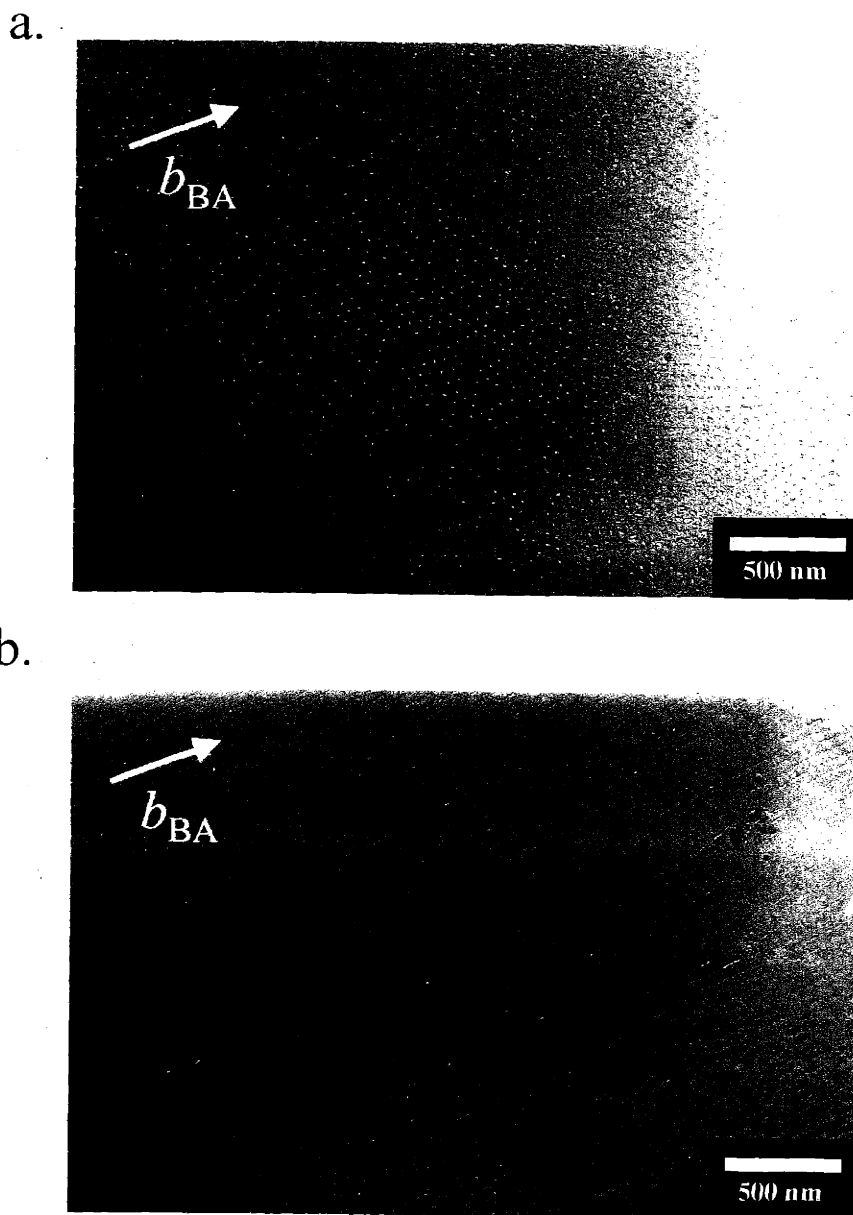


**Figure 9.4** Schematic of the PS/PI block copolymer orientations between top glass substrate and bottom pre-patterned substrate. The block copolymer films confined between BA crystal and the bottom pre-patterned substrate undergo thickness variation, leading to two different orientations.

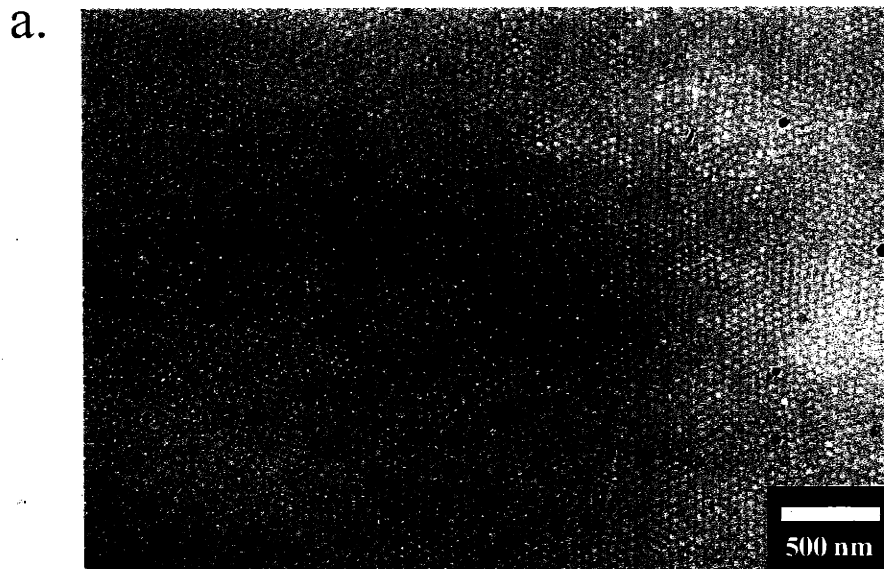
#### 9.4.2 Directionally solidified microdomain modifications via ozone and oxygen plasma reactive ion etching methods

The cylindrical PI microdomains aligned along the fast growth direction of BA crystal via directional solidification are modified for nanometer scale template. Either ozone or oxygen plasma reactive ion etching (O<sub>2</sub>-RIE) can be used to selectively remove the PI microdomains. Since polydiene chains are rapidly cleaved with ozone (O<sub>3</sub>) at a rate one million times faster than the scission of PS chains<sup>8</sup>, PI microdomains in the PS matrix can be selectively degraded and removed with ozone while not significantly affecting the PS matrix. The PS matrix becomes insoluble after ozone exposure due to cross linking. The directionally solidified PS/PI block copolymer films on a carbon film coated TEM grid were then exposed to a room temperature oxygen atmosphere containing about 2 % ozone, generated by a Pacific Ozone Technology Inc. Ozone Generator, Model L21, for 1 hour. After ozone exposure, the films were soaked in de-ionized water overnight to remove the isoprene fragments.<sup>9</sup>

Bright field TEM micrographs of the ozone treated PS/PI block copolymer film are clearly shown in Figure 9.5. Two different orientations of the block copolymer microstructures are observed in Figure 9.5a and b. As explained in Chapter 6, the cylindrical microdomains vertically aligned to the substrate form in the thinner regions, while ones parallel to the substrate in the thicker regions. Microdomains with both orientations are well oriented on the plane view along the fast growth direction of BA crystal. After ozonation, the mass difference between the PS matrix and the cylindrical voids provides a good TEM contrast without staining. Compared with the images stained with OsO<sub>4</sub> which makes the PI microdomains dark, the empty cylindrical microdomains appear brighter than the PS matrix due to less scattering of the electron beam, implying that the ozone treatment successfully removed the PI microdomains.



**Figure 9.5** TEM bright-field images of a thin film of PS/PI(45/12) block copolymer, directionally solidified with BA, and exposed to ozone. Void microdomain structure after removal of the PI cylinders by ozone appears brighter. (a) Thinner block copolymer film shows vertically ordered cylindrical microdomains to the substrate (b) Thicker block copolymer film shows directionally solidified PI microdomains oriented parallel to the substrate.



**Figure 9.6** TEM bright-field images of a thin film of PS/PI(45/12) block copolymer, directionally solidified with BA, and treated via O<sub>2</sub>-RIE. Void microdomain structure after removal of the PI cylinders by O<sub>2</sub>-RIE appears brighter. (a) Thinner block copolymer film shows vertically ordered cylindrical microdomains to the substrate (b) Thicker block copolymer film shows directionally solidified PI microdomains oriented parallel to the substrate.



O<sub>2</sub>-RIE can also be used to selectively remove the PI microdomains. However, etching rates of PS and PI under O<sub>2</sub>-RIE vary with the experimental parameters. Previously Harrison et al.<sup>10</sup> reported that the etching rates of homopolymer PS and PI under certain conditions of CH<sub>4</sub>-RIE are almost equal. In the current study, O<sub>2</sub>-RIE is directly applied to the directionally solidified PS/PI block copolymer films on carbon coated TEM grids. Reactive ion etching was performed on a Plasma Therm. Model 790 plasma etcher. O<sub>2</sub>-RIE using 5mtorr of O<sub>2</sub> and various bias conditions were used.

Bright field TEM images of the PS/PI block copolymer films after O<sub>2</sub>-RIE are shown in Figure 9.6. Similar to Figure 9.5, the cylindrical microdomains look brighter due to less mass of voids. Again vertically ordered cylinders to the substrate are seen in Figure 9.6a and in-plane cylinders aligned along the fast growth direction of the BA crystal is shown in Figure 9.6b. In the O<sub>2</sub>-RIE case, due to the small etching rate difference bright cylinder microdomains look thicker than in the ozone case (Figure 9.5) in both orientations, indicating that the PS matrix is also partially removed by O<sub>2</sub>-RIE.

Control of block copolymer microdomain patterns is very challenging but at the same time worth pursuing. Many nanotechnological applications await such materials. Part of this thesis suggests a simple new technique, involving two types of driving forces, to manipulate block copolymer microstructures. These new types of interactions: epitaxy and directional solidification not only draw much scientific interest but also provide diverse combinations with other interacting driving forces such as surface and confinement. Chemically and/or topographically patterned substrates, temperature gradients and epitaxy can work together to generate unprecedented microdomain control, leading us one step closer to technological realization.

## 9.5 References

1. This work is in collaboration with Dr. M. Fasolka.
2. Van Dijk, M. A.; van den Berg R. "Ordering phenomena in thin block copolymer films studied using atomic force microscopy" *Macromolecules* **1995**, *28*, 6773.
3. Suh, K. Y.; Kim, Y. S.; Lee, H. H. "Parallel and vertical morphologies in block copolymers of cylindrical domain" *J. Chem. Phys.* **1998**, *108*, 1253.
4. Huinink, H. P.; Brokken-Zijp, J. C. M.; van Dijk, M. A.; Sevink, G. J. A. "Asymmetric block copolymers confined in a thin film" *J. Chem. Phys.* **2000**, *112*, 2452.
5. Konrad, M.; Knoll, A.; Krausch, G.; Maglerle, R. "Volume imaging of an ultrathin SBS triblock copolymer film" *Macromolecules* **2000**, *33*, 5518.
6. Fasolka, M. J.; Harris, D. J.; Mayes, A. M.; Yoon, M.; Mochrie, S. G. J. "Observed substrate topography mediated lateral patterning of diblock copolymer films" *Phys. Rev. Lett.* **1997**, *79*, 3018.
7. Fasolka, M. J.; Banerjee, P.; Mayes, A. M.; Pickett, G.; Balazs, A. C. "Morphology of ultrathin supported diblock copolymer films: Theory and experiment" *Macromolecules* **2000**, *33*, 5702.
8. Razumovskii, S. D.; Zailov, G. E. "Ozone and its Reactions with Organic Compounds" **1984**, Elsevier, NY, 300.
9. Lee, J. S.; Hirao, A.; Nakahama, S. "Polymerization of Monomers Containing Functional Silyl Groups. 7. Porous Membranes with Controlled Microstructures", *Macromolecules* **1980** *13*, 1602.
10. Harrison, C.; Park, M.; Chaikin, P. M.; Register, R. A.; Adamson, D. H. "Lithography with a mask of block copolymer microstructures" *J. Vac. Sci. Technol. B* **1998**, *16*, 544.

## BIOGRAPHICAL NOTE

### Education

**Massachusetts Institute of Technology Cambridge, MA** Fall 1996 – Spring 2001  
*Department of Materials Science and Engineering.*  
Thesis: Control of Block Copolymer Microdomain Patterns  
Conducted under supervision of Prof. Edwin L. Thomas

**M.S. Seoul National University Seoul, Korea** March 1992 – August 1995  
*Department of Fiber and Polymer Science and Engineering*  
Thesis: The Effect of PS/PI block copolymer as compatibilizing agent on Morphology and Gas Separation Properties of PPO/PI Blends.  
Conducted under supervision of Prof. Won Ho Jo

**B.S. Seoul National University, Seoul, Korea** March 1988 – February 1992  
*Department of Fiber Engineering, Magna Cum Laude*

### Research Experience

**Massachusetts Institute of Technology**  
September 1996 – February 2001  
Research Assistant in Department of Materials Science and Engineering,  
in the laboratory of Professor Edwin L. Thomas.

A new processing method was developed to control the micropattern structures of block copolymers for nanotechnologies. The method is based on the use of crystalline organic materials, which are solvents for the block copolymers above their melting temperatures, and when cooled and directionally crystallized, act as a substrate on which thin films of the block copolymers are formed. Various block copolymers and crystalline organic solvents such as benzoic acid and anthracene were applied to create controlled pattern structures. Topographically patterned substrate was combined with the current process for better control of microdomains. Moreover, one of microdomains of well aligned nano-scale pattern structures were selectively removed by exposing UV, Ozone and/or Oxygen Reactive Ion Etching for nanoscale templates

**National Synchrotron Light Source Brookhaven National Laboratory**  
September 1996 – February 2001  
In collaboration with Prof. Yachin Cohen (Technion, Israel), Dr. Yuanming Zhang (Cornell)

Proposals were written and granted for in-situ studies of deformation and phase behavior of liquid crystalline and semicrystalline block copolymers by synchrotron radiation at

NLS. Simultaneous small and wide angle x-ray scattering is performed during tensile stress deformation of various semicrystalline block copolymers.

**Institut Charles Sadron, CNRS, Strasbourg, France**

November 2000 – December 2000

In collaboration with: Prof. Bernard Lotz, Prof. Jean-Claude Wittman.

Semiconductor quantum dots were sequestered into the amorphous regions of the microstructure of a semi-crystalline block copolymer developed via epitaxy between anthracene (AN) crystal and polyethylene (PE) crystal. Oriented PE crystals on AN substrate was evidenced with dark field technique in transmission electron microscope and individual quantum dots were observed in bright field mode.

**Korea Institute of Science and Technology (KIST)**

**High Performance Membrane Laboratory, Seoul Korea**

August 1995 – August 1996

In collaboration with Dr. Yong Soo Kang

Gas separation membrane based on high performance poly(imide)s were prepared using phase conversion method to improve both chemical and thermal resistances. The controlled diffusion process, providing good mechanical properties avoided the formation of finger shape microstructure usually observed in phase conversion method.

**Seoul National University**

**Department of Fiber and Polymer Engineering, Seoul Korea**

March 1992 – August 1995

In collaboration with Prof. Won Ho Jo

The dependence of heterogeneous microdomain distribution and size on O<sub>2</sub>/N<sub>2</sub> separation properties was investigated using the polymeric blend system: poly(phenyleneoxide)(PPO)/poly(isoprene)(PI) with poly(styrene)/poly(isoprene)(PS/PI) diblock copolymer. The compatibilizing agent PS/PI block copolymer allowed controlling the size and distribution of PI microdomain in blends. The improved gas separation properties with the block copolymer were interpreted with percolation theory.

**Publications**

1. "Morphological effect of dispersed phase on gas permeation properties through heterophase polymer membrane: theoretical and experimental approaches" *Polymer* **2000**, 41, 1765. C. Park, W. H. Jo, H. C. Park, Y. S. Kang.
2. "Spherical to Cylindrical Microdomain Transformation by Application of a Flow Field" *Polymer* **2000**, 41 2971. C. Park, S. Simmons, F. Yeh, B. Hsiao, L. J. Fetters, E. L. Thomas.
3. "Microdomain Patterns via Directional Eutectic Solidification and Epitaxy" *Nature* **2000**, 405, 433. C. De Rosa, C. Park, B. Lotz, E. L. Thomas.

4. "Control of Molecular and Microdomain Orientation in a Semicrystalline Block Copolymer Thin Films by Epitaxy" *Macromolecules* **2000**, 33, 4791. C. De Rosa, C. Park, B. Lotz, L. J. Fetters, J. Wittmann, E. L. Thomas.
5. "Influence of an Oriented Glassy Cylindrical Microdomain Structure on the Morphology of Crystallizing Lamellae in a Semicrystalline Block Terpolymer" *Macromolecules* **2000**, 33, 7931. C. Park, C. De Rosa, L. J. Fetters, E. L. Thomas.
6. "Alteration of Classical Microdomain Patterns by Degenerate Epitaxy" *Advanced Materials* (in press) C. Park, C. De Rosa, B. Lotz, L. J. Fetters, E. L. Thomas.
7. "Large Area Orientation of Block Copolymer Microdomains in Thin Films via Directional Crystallization of a Solvent" *Macromolecules* **2001**, 34, 2602. C. Park, C. De Rosa, E. L. Thomas.
8. "Double Textured Cylindrical Block Copolymer Domains via Directional Solidification on a Topographically Patterned Substrate" C. Park, J. Y. Cheng, C. De Rosa, M. Fasolka, A. M. Mayes, C. A. Ross, E. L. Thomas submitted to *Appl. Phys. Lett.*
9. "Control of Molecular and Micropattern Orientation in Semicrystalline Block Copolymer Thin Films by Directional Solidification and Epitaxy" C. Park, C. De Rosa, B. Lotz, E. L. Thomas (in preparation).

## Meeting Presentations

1. "Development of Bulk and Surface Morphology in Semicrystalline Block Copolymers" C. Park, A. Avgeropoulos, L. J. Fetters, E. L. Thomas. American Physical Society Meeting, Division of High Polymer Physics. Los Angeles, March 1998.
2. "Influence of the Minority Phase Microdomain Structure on the Crystalline Block Morphology of a Terpolymer" C. Park, E. L. Thomas. American Physical Society Meeting, Division of High Polymer Physics. Atlanta, March 1999.
3. "Epitaxial Crystallization of Triblock Copolymers onto Benzoic Acid" C. De Rosa, C. Park, E. L. Thomas. American Physical Society Meeting, Division of High Polymer Physics. Atlanta, March 1999.
4. "Patterning of a Semicrystalline Block Copolymer Thin Film via Epitaxial Crystallization" C. Park, C. De Rosa, B. Lotz, L. J. Fetters, E. L. Thomas. American Physical Society Meeting, Division of High Polymer Physics. Minneapolis, March 2000.
5. "Selective Semiconductor Nanocluster Deposition on Epitaxially Patterned Semicrystalline Block Copolymer Film" C. Park, J. Lee, K. F. Jensen, M. G. Bawendi, E. L. Thomas. American Physical Society Meeting, Division of High Polymer Physics. Seattle, March 2001.